Developing Constrained p27 Peptides to Target the Oncogenic E3 Ubiquitin Ligase SCF^{Skp2}

Grasilda Zenkevičiūtė

Jesus College
University of Cambridge

This thesis is submitted for the degree of
Doctor of Philosophy

September, 2019

Declaration

This thesis is the result of my own work and includes nothing which is the outcome of work done in collaboration except as declared in the Preface and specified in the text. It is not substantially the same as any that I have submitted, or, is being concurrently submitted for a degree or diploma or other qualification at the University of Cambridge or any other University or similar institution except as declared in the Preface and specified in the text. I further state that no substantial part of my thesis has already been submitted, or, is being concurrently submitted for any such degree, diploma or other qualification at the University of Cambridge or any other University or similar institution except as declared in the Preface and specified in the text. It does not exceed the prescribed word limit for the relevant Degree Committee.

Abstract

Developing Constrained p27 Peptides to Target the Oncogenic E3 Ubiquitin Ligase SCF^{Skp2}

Grasilda Zenkevičiūtė

The ubiquitin-proteasome system (UPS) maintains homeostatic levels of proteins in normal cells and controls the levels of oncogenes and tumour suppressors by tagging proteins with ubiquitin for proteasomal degradation. The UPS is regulated by sequential action of three enzymes: E1 – ubiquitin activating enzyme, E2 - ubiquitin conjugating enzyme, and E3 - ubiquitin ligase. The SCF^{Skp2} complex is one of 600 E3s in the human genome, and Skp2 serves as a substrate recognition subunit. Skp2 is an oncoprotein that exerts its oncogenic functions through degradation of specific substrates. A major target of SCF^{Skp2} is the cyclin-dependent kinase inhibitor p27 which positively regulates cell cycle progression. Elevated levels of Skp2 and reduced levels of p27 are common in a variety of cancers, including lymphomas and breast and prostate carcinomas. A lack of suitable binding pockets in Skp2 and the intrinsically disordered nature of p27 make this protein-protein interaction (PPI) challenging for conventional small molecule approaches. We aim to develop instead a macrocyclic peptide inhibitor for this PPI.

We have designed and synthesised p27 peptides containing unnatural amino acids and successfully constrained them using 'click' chemistry. The dissociation constants show that the constrained peptides (CPs) have dramatically higher affinities for the Cks1-Skp2-Skp1 complex compared with the linear (unconstrained) p27 peptide. The 30 nM affinity of the tightest binding peptide is almost two orders of magnitude higher than that of the linear peptide (3 μM). We suggest that this large enhancement of affinity arises because

the binding-competent form of the peptide has a tight turn-like conformation, which is very effectively constrained by the macrocyclic linker. The CPs were also shown to inhibit p27 ubiquitination in vitro. Interestingly, the CPs also inhibited the ubiquitination of two other Skp2 substrates, p21 and N-myc, to varying degrees. A number of different approaches were taken to deliver the CPs into cells and investigate their effect on p27 protein levels and on cellular proliferation. CPs were able to restore p27 levels associated with Skp2 over-expression as well as reduce proliferation of breast cancer cell line MCF-7.

We additionally investigated a different route to constrain the p27 sequence by grafting it onto a loop of a small, stable protein scaffold. These grafted proteins were also able to inhibit p27 ubiquitination. Lastly, we constructed novel proteolysis-targeting proteins (polyproxins) that hijack SCF^{Skp2} and direct it to drive the destruction of disease-causing proteins. We generated a library of polyproxins, combining a module that binds a cancer-associated protein, β-catenin, with a module that binds Skp2. β-catenin ubiquitination and degradation in cells was successfully demonstrated using these polyproxins.

Acknowledgements

First and foremost I would like to thank Laura Itzhaki. It was such a pleasure to do my PhD in this lab. Your guidance and support was irreplaceable and kept me motivated and excited about research! I could not have asked for a better supervisor during my time here and I will always remember my first Christmas in Cambridge. I would like to thank everyone in the Itzhaki lab, Marie, Sian, Pam, Piyush, Harry, Zhen, Aurora, Juliane, Elin, Albert, Owen, Sarah and especially Wenshu who was such a great help in my first few months and taught me so many things about peptides. And of course Rohan, who was my partner in crime in Singapore and all the peptide conferences. I will never forget all the chats we had in Long Black and unfortunately I don't think I will ever forget the Bear Hike even if I wanted to.

I would also like to thank Heike Laman and all the Laman's lab members for teaching me new techniques during my first year. As well as David Spring and his lab members. I am especially happy to have met Lisa Kent who was a great part of my PhD experience and who has become a great friend for life.

Big thank you goes to David Lane and his lab for hosting me as a visiting student in A*STAR. I am especially grateful for Fernando Ferrer for teaching me all about the peptide chemistry and all the help of Tsz Ying in peptide purification.

Of course, the acknowledgments would not be complete without mentioning someone who is the biggest part of my Cambridge PhD experience. Nicolas Scirocco, my life partner, the forever bear, without whom I cannot imagine my time in Cambridge.

Contents

List of Figures **vi**

List of Tables **xii**

Abbreviations **xv**

1 Introduction **1**

1.1 The ubiquitin-proteasome system 1

1.2 E3 ubiquitin ligases 5

1.2.1 SCF^{Skp2} 7

1.3 Skp2-mediated p27 degradation 8

1.4 Development of UPS inhibitors 12

1.4.1 Inhibitors of E3 ligases 13

1.5 Peptide-based drugs 14

1.5.1 Stapled peptides 15

1.5.2 Non-helical constrained peptides 23

1.6 Intracellular peptide delivery 25

1.6.1 Cell-penetrating peptides 25

1.6.2 Other strategies for intracellular peptide delivery 28

1.7 Targeted protein degradation 30

1.8 Project aims 35

2 Materials and Methods **37**

2.1 Chemicals 37

2.1.1 Sterile procedure 37

2.1.2 LB plates 37

2.1.3 Culture media 37

2.1.4 Antibiotics 38

2.2 Molecular biology techniques 38

2.2.1 Plasmids 38

2.2.2 Polymerase chain reaction 38

2.2.3 Agarose gel electrophoresis 40

2.2.4 Digestion of destination vector and insert 40

2.2.5 Ligation protocol 41

2.2.6 Transformation 41

2.2.7 Purification of plasmid DNA 42

2.2.8 DNA quantification 42

2.2.9 Confirmation of construct integrity 42

2.3 Protein expression and purification in *E. coli* 42

2.3.1 Preparation of competent cells 43

2.3.2 Small-scale expression and solubility assay of Cks1 and Skp1-Skp2 proteins 43

2.3.3 Large-scale expression of Cks1 and Skp1-Skp2 proteins in *E. coli* . . 44

2.3.4 Bacterial cell lysis 44
2.3.5 Affinity purification of His_6-tagged Cks1 45
2.3.6 Affinity purification of GST-tagged Skp1-Skp2 complex 46
2.3.7 Size-exclusion chromatography 46
2.3.8 Purification of TPR proteins 47
2.3.9 Expression and purification of TPR proteins in pTriExMOD vector . 47
2.3.10 Evaluation of proteins by electrophoresis 48
2.3.11 Protein quantification 49
2.4 Peptide synthesis and characterisation 49
2.4.1 Manual peptide synthesis 50
2.4.2 Peptide macrocyclisation 51
2.4.3 Peptide purification using HPLC 51
2.5 Isothermal titration calorimetry 53
2.6 Fluorescence Polarisation assays 53
2.6.1 Direct FP 53
2.6.2 Competition FP 55
2.7 Western blot 56
2.8 Tissue culture 57
2.9 Mammalian cell transfection 57
2.10 Mammalian cell lysis 57
2.11 β-catenin levels western blot assay 58
2.12 General immunoprecipitation pull-down 58
2.13 Immunoprecipitation of HA-p21, HA-p27 and HA-β-catenin 58
2.14 Purification of SCF complexes 59

2.15 Quantification of SCF^{Skp2} ligase 59

2.16 *In vitro* ubiquitination assay 59

2.17 Ubiquitination assay in HEK293T cells 60

2.18 Production of Wnt-3A conditioned media 60

2.19 TOPFLASH dual-luciferase reporter assay of β-catenin activity 60

2.20 Live-cell imaging after treatment with peptides 61

2.21 Peptide electroporation 61

2.22 Liposomal peptide delivery 62

2.23 Treatment of MCF-7 with p27 peptides 63

2.24 Cell proliferation assay 63

3 Design and Synthesis of p27 Peptides 65

3.1 Introduction 65

3.2 Results and Discussion 66

3.2.1 Design of p27 peptides 66

3.2.2 Macrocyclisation of p27 peptides 68

3.2.3 Other p27 peptides synthesised 75

3.2.4 Cell permeable peptides 78

4 Biophysical Characterisation of Constrained p27 Peptides 81

4.1 Introduction 81

4.2 Results and Discussion 82

4.2.1 Production of Skp1-Skp2-Cks1 complex 82

4.2.2 Expression and purification of His-Cks1 from *E. coli* 82

4.2.3 Expression and purification of GST-Skp2-Skp1 from *E. coli* 84

4.2.4 Skp1-Skp2-Cks1 complex formation 87

4.2.5 Biophysical analysis of the interaction between p27 peptides and Skp1-Skp2-Cks1 88

5 Biological Activity of Constrained p27 Peptides 101

5.1 Introduction 101

5.2 Results and Discussion 102

5.2.1 Cloning of Skp2 mammalian expression constructs 102

5.2.2 Expression of Skp2 in HEK293T cells 103

5.2.3 Production of SCF^{Skp2} E3 ligase complex 103

5.2.4 Development of *in vitro* p27 ubiquitination assay 105

5.2.5 p27 ubiquitination inhibition assay 108

5.2.6 Constrained p27 peptides inhibit ubiquitination of other Skp2 substrates 113

5.2.7 Ubiquitination assay in HEK293T cells 119

5.2.8 Approaches of peptide cellular delivery 120

5.2.9 Effects of p27-peptides in cells 129

6 Constraining p27 in a Protein Scaffold 135

6.1 Introduction 135

6.2 Results and Discussion 136

6.2.1 p27- and p53-derived peptides grafted onto the TPR scaffold 136

6.2.2 p27 grafted onto the loop of a TPR protein inhibits p27 ubiquitination 139

6.2.3 Targeting β-catenin for degradation using bi-functional TPRs 141

6.2.4 Taking a step back: p27 sequence effects on TPR 154

6.2.5 Analysis of constrained phosphomimetic p27 peptides 159

7 Ongoing Work **165**

7.1 Crystallography 165

7.2 Mouse xenograft models using MCF-7 breast cancer cells 167

8 Final Conclusions and Future Work **169**

References **177**

List of Figures

1.1 Schematic of the ubiquitin-proteasome system 2

1.2 Schematic of the ubiquitin activation and the subsequent transfer from an E1 to an E2 enzymes. 2

1.3 Different outcomes of substrate ubiquitination 4

1.4 A schematic of the mechanisms of ubiquitin transfer by the three classes of E3 ligases 6

1.5 Schematic of the crystal structure of the Skp1-Skp2 complex (PDB: 1FQV) 7

1.6 Schematic of the crystal structure of the Cullin1-Rbx1-Skp1-F-box^{Skp2} SCF ubiquitin ligase complex (PDB: 1LDK) 8

1.7 Binding of p27 to Cdk2 inhibits kinase activity 9

1.8 Model of the SCF^{Skp2} E3 ligase in complex with Cks1, Cdk2/cyclin A and p27 10

1.9 A schematic of one-component peptide stapling. 16

1.10 Potential reaction pathways of the two-component CuACC stapling 20

1.11 Diversity oriented peptide stapling using a two-component CuACC method with tris-alkyne linker 21

1.12 A schematic of strain-promoted azide–alkyne cycloaddition (SPAAC) mechanism. 22

1.13 A schematic of constraining non-helical peptides using double-click chemistry 23

1.14 A schematic of electroporation and liposomal encapsulation delivery methods 28

1.15 Schematic illustration of the PROTAC mechanism of action 30

1.16 PROTAC-mediated ternary complex formation and the Hook effect 31

1.17 Positive and negative cooperativity of ternary complex formation 32

1.18 Project workflow 35

2.1 Chemical structures of lipids used to form liposomes for peptide delivery . . 62

3.1 Crystal structure of Cks1-Skp2-Skp1 in complex with p27 peptide 67

3.2 Chemical structure of aminohexanoic acid 68

3.3 Chemical structure of linear p27 peptide 68

3.4 Mechanism of copper(I) catalysed 'Click' reaction arrows 69

3.5 'Click' reaction set up in the hood 70

3.6 Design of constrained p27 peptides 71

3.7 Superimposed IR spectra of the unconstrained precursor peptide (blue) and the product after click reaction (red) 72

3.8 Chemical structure of CP1 peptide 73

3.9 Chemical structure of CP2 peptide 73

3.10 Chemical structure of CP3 peptide 74

3.11 Chemical structure of CP4 peptide 74

3.12 Chemical structure of CP5 peptide 74

3.13 Analytical HPLC of p27 peptide 76

3.14 Analytical HPLC of p27 peptide labelled with FAM 78

3.15 Analytical HPLC of antennapedia (CPP) labelled p27 peptide 80

4.1 Purification of His-Cks1 from *E. coli* 83

4.2 Purification of GST-Skp2-Skp1 from *E. coli* 85

4.3 Mass spectrometry of purified Skp2-Skp1 and Cks1 protein samples 86

4.4 Purification of Cks1-Skp2-Skp1 complex from *E. coli* 87

4.5 Principles of using fluorescence anisotropy to measure protein-ligand interactions 88

4.6 Direct FP traces of TAMRA-AGSVEQT(phos)PKK peptide binding to Skp1-Skp2-Cks1 complex and its components 90

4.7 Chemical structures of 5-TAMRA and 6-FAM fluorophores. 91

4.8 Direct FP traces showing the linear p27 peptide binding to Skp1-Skp2-Cks1, fitted to a one-site binding model. 91

4.9 Displacement of TAMRA-AGSVEQT(phos)PKK peptide from Cks1-Skp2-Skp1 by titration of unlabelled p27 peptides 92

4.10 Displacement of TAMRA-AGSVEQT(phos)PKK peptide from Cks1-Skp2-Skp1 by titration of CPs 94

4.11 Competitive fluorescence polarisation assays overlay of constrained p27 peptides 95

4.12 Displacement of TAMRA-AGSVEQT(phos)PKK peptide from Cks1-Skp2-Skp1 by titration of CPs with mutations introduced 96

4.13 ITC trace of linear p27 peptide being titrated into Skp1-Skp2-Cks1 complex in the cell 97

4.14 ITC traces showing p27 peptide titration into Skp1-Skp2-Cks1 complex . . 98

5.1 Restriction enzyme analysis of the Skp2 constructs using EcoRI and XhoI restriction enzymes 102

5.2 Western blot analysis of Skp2 expression in HEK293T 103

5.3 Crystal structure of the Cullin1-Rbx1-Skp1-F-box^{Skp2} SCF ubiquitin ligase complex. 104

5.4 Analysis of SCF^{Skp2} and $SCF^{Skp2\text{-}\Delta Fbox}$ production 105

5.5 *In vitro* p27 ubiquitination assay 107

5.6 Model of the SCF^{Skp2} E3 ligase in complex with Cks1, Cdk2/cyclin A and p27 108

5.7 SDS-PAGE and Western blot analysis of SCF^{Skp2}, p21 and p27 samples immunoprecipitated from HEK293T cells 109

5.8 Titration of linear control p27 peptide in a p27 ubiquitination assay 110

5.9 Titration of linear and constrained peptides in a p27 ubiquitination assay . 111

5.10 Titration of 1:10 dilution of CP1 peptide in a p27 ubiquitination assay . . . 112

5.11 Titration of linear and constrained peptides in a p21 ubiquitination assay . 114

5.12 Titration of linear and constrained peptides in a N-myc ubiquitination assay 116

5.13 Titration of linear and constrained peptides in a N-myc ubiquitination assay 117

5.14 p27 ubiquitination assay in HEK293T cells 119

5.15 Structural schematic of TAMRA and Antp labelled CP2 peptide used in cellular assay 120

5.16 Confocal microscope images of live U2OS cells after 4-hour treatment with TAMRA-CP2-Antp peptide 123

5.17 Confocal microscope images of live U2OS cells after electroporation of TAMRA-AGSVEQT(phos)PKK peptide 124

5.18 Comparison between peptide cellular delivery using either Antp CPP or electroporation methods 125

5.19 Confocal microscope images of live U2OS cells showing liposomal delivery of AGSVEQT(phos)PKK-K(FAM) peptide 126

5.20 Confocal microscope images of live MCF-7 cells showing liposomal delivery of AGSVEQT(phos)PKK-K(FAM) peptide 127

5.21 Confocal microscope images of live U2OS cells showing liposomal delivery of TAMRA-AGSVEQT(phos)PKK peptide 128

5.22 Treatment of Skp2/Cks1-transfected MCF-7 cells with constrained peptide 130

5.23 Schematic of p27 proteasomal degradation after ubiquitination by $SCF^{Skp2/Cks1}$ 131

5.24 Affects of doxorubicin in BrdU cellular proliferation assay of U2OS and HEK293T cells 131

5.25 BrdU cell proliferation assay of MCF-7 cells after treatment with peptides . 132

5.26 BrdU cell proliferation assay of MCF-7 cells after treatment with p27 peptides 133

6.1 Schematic of the 10-residue Skp2-binding sequence derived from p27 grafted onto an inter-repeat loop of a TPR protein (TPR-p27) 135

6.2 Schematic of immunoprecipitation principles 137

6.3 Analysis of immunoprecipitated HA-TPR with a ligase binding motif 138

6.4 Analysis of immunoprecipitated MDM2 ligase with HA-4TPR-p53 139

6.5 SDS-PAGE His-5TPR-p27 purification from *E. coli* 140

6.6 Titration of 5TPR-p27 protein in a p27 ubiquitination assay 141

6.7 Schematic of the bi-functional TPR design, wherein sequences are grafted onto the TPR scaffold 142

6.8 Binding of different β-catenin partner proteins 144

6.9 SDS-PAGE showing mini-purifications of His tagged TPR proteins 146

6.10 *In vitro* ubiquitination of β-catenin by SCF^{Skp2} by bi-functional TPRs . . . 147

6.11 Effect of bi-functional TPRs on β-catenin levels. 149

6.12 Effect of bi-functional TPRs on β-catenin levels using β-catenin-TPR-p27 . 150

6.13 β-catenin degradation assay using transfected bi-functional TPRs in HEK293T cells. 151

6.14 Effect of bi-functional TPRs on β-catenin levels using β-catenin-TPR-p53 . 152

6.15 Effect of transfected bi-functional TPRs on Wnt-activated HEK293T cells . 153

6.16 Cloning of 3TPR and 6TPR with the p27 loop grafted in. 155

6.17 HisTrap purification of 3TPR with no loops, p27 and p27 scramble loops grafted in. 156

6.18 HisTrap purification of 6TPR with no loops, p27 and p27 scramble loops grafted in. 157

6.19 ITC traces showing titration of 6TPR-p27 or 6TPR-p27-scramble purified proteins into Skp1-Skp2-Cks1 complex 157

6.20 Titration of TPR proteins in a p27 ubiquitination assay 158

6.21 Western blot analysis of TPR protein ubiqutination by SCF^{Skp2} ligase . . . 159

6.22 Displacement of TAMRA-AGSVEQT(phos)PKK peptide from Cks1-Skp2-Skp1 by titration of unlabelled phosphomimetic p27 peptides 160

6.23 ITC traces showing titration of linear p27 peptide containing either phospho threonine or glutamic acid reside into Skp1-Skp2-Cks1 complex 161

6.24 Titration of linear and constrained phosphomimetic peptides in a p27 ubiquitination assay 162

7.1 2D plate crystals formed in several screens 166

7.2 3D micro crystals 166

7.3 Workflow of mouse xenograft experiment 168

8.1 ProtoArrays Human Protein Microarrays v4.1 (Invitrogen) screen used to profile enzymatic activity of E3 ligases 171

List of Tables

1.1 Stapled α-helical peptides that target PPIs in diseases 17

1.2 Examples of CPPs and their sequences, origins, and physical–chemical properties 26

2.1 Plasmids containing *skp2* genes generated in this study 38

2.2 Primers used to amplify *skp2* genes 39

2.3 Typical PCR reaction setup 39

2.4 Thermal cycling conditions for PCR 40

2.5 Buffers used for purification of His-Cks1 and GST-Skp2-Skp1 45

2.6 Buffers used for purification of 3TPR and 6TPR constructs 48

2.7 Extinction coefficients of the most commonly used proteins in this study. . . 49

2.8 List of peptides synthesised and their molecular weight pre- and post-'click' reaction. 52

3.1 Peptides designed for the 'click' reaction 69

3.2 LC-MS data of macrocyclised peptides 72

3.3 Other p27 peptides synthesised 75

3.4 Amino acid sequences of common CPPs 78

3.5 Cell penetrating peptides synthesised 79

4.1 Dissociation constants determined by direct fluorescence polarisation 89

4.2 Dissociation constants for the binding of macrocyclised p27 peptides to Cks1-Skp2-Skp1 93

6.1 Mono- and bi-functional TPR constructs used for targeting β-catenin and SCF^{Skp2} 145

6.2 p27 sequences used in TPR loop 155

6.3 3TPR and 6TPR constructs in pTriExMOD vector. 156

Copyright

The publication attached is included without prior permission as authors are allowed to re-use their own work without seeking the Portland Press's permission for use in a thesis/dissertation.

Re-use licenses or permission have been obtained for the following figures:

Figure	**Publisher**	**License number**
1.7	National Academy of Sciences of the United States of America	Permission was granted for re-use of the material
1.8	Elsevier	4758740126168
1.10	John Wiley and Sons	Permission was granted for re-use of the material
1.12	John Wiley and Sons	4801990512990

Abbreviations

°C	Degrees Celsius
Å	Angstrom
Ahx	6-aminohexanoic acid
Amp	Ampicilin
APC/C	Anaphase promoting complex/cyclosome
APS	Ammonium peroxodisulphate
ATP	Adenosine triphosphate
BLAST	Basic local alignment search tool
β-ME	Beta-mercapthoethanol
bp	Base pair
BSA	Bovine serum albumin
Cam	Chloramphenicol
CD	Circular dichroism
Cdk	Cyclin dependent kinase
CKI	Cyclin dependent kinase inhibitor
Cks1	Cyclin-dependent kinases regulatory subunit 1
CuAAC	Copper-catalysed azide-alkyne cycloaddition
CV	Column volume
DCM	Dichloromethane

dH_2O	Distilled water
DIPEA	N,N-diisopropylethylamine
DMF	Dimethylformamide
dNTPs	Deoxyribonucleotides
DTT	Dithiothreitol
E.coli	*Escherichia coli*
EDTA	Ethylenediaminetetraacetic acid
Fmoc	Fluorenylmethyloxycarbonyl
FP	Fluorescence polarisation
FT	Flowthrough
HEPES	4-(2-hydroxyethyl)-1-piperazineethanesulfonic acid
His_6	Hexahistidine
HPLC	High-performance liquid chromatography
IMAC	Immobilised metal affinity chromatography
IPTG	Isopropyl β-D-1-thiogalactopyranoside
IR	Infrared spectroscopy
ITC	Isothermal titration calorimetry
K_a	Association constant
Kan	Kanamycin
kb	Kilobase
K_d	Dissociation constant
kDa	Kilo dalton
LB	Luria-Bertani Medium
LCMS	Liquid chromatography mass spectrometry
LRR	Leucine- rich repeat
mg	Miligram

min	Minute
mL	Mililitre
mmol	Milimole
MS	Mass spectrometry
MW	Molecular weight
MWCO	Molecular weight cut-off
NMR	Nuclear magnetic resonance
NTA	Nitrolotriacetic acid
OD_{600}	Optical density at 600 nm
PAGE	Polyacrylamide gel electrophoresis
PBS	Phosphate buffered saline
PCR	Polymerase chain reaction
PDB	Protein data bank
PPI	Protein-protein interaction
rpm	Rotations per minute
SAR	Structure activity relationship
SCF	Skp1-Cullin-F-box
SDS	Sodium dodecyl sulfate
SEC	Size exclusion chromatography
Skp1	S-phase associated protein 1
Skp2	S-phase associated protein 2
SOC	Super optimal catabolite repression medium
TAE	Tris-acetate-EDTA
TAMRA	5-carboxytetramethylrhodamine
TAT	Trans-activating transcriptional activator
TCEP	Tris-(2-carboxyethyl)-phosphine

TEMED	Tetramethylethylenediamine
TFA	Trifluoroacetic acid
TPR	Tetratricopeptide repeat
Tris	Tris(hydroxymethyl)aminomethane
Ub	Ubiquitin
v/v	Volume per volume
w/v	Weight per volume
WB	Western blot
WT	Wild type
µL	Microlitre
µM	Micromolar

Chapter 1

Introduction

1.1 The ubiquitin-proteasome system

Protein degradation or proteolysis is mediated by proteases which can vary from small proteins like trypsin to large, multi-component, multi-functional proteasomes. For a very long time proteins were believed to be long-lived despite some opposing evidence by Schoenheimer et al. 1942.[1] That is until 1980s when A. Hershko, his student A. Ciechanover, his collaborator I. Rose, and their colleagues discovered that certain proteins, when added to reticulocyte extract, became covalently tagged to a protein known as ubiquitin, and that these ubiquitinated proteins were gradually destroyed by an ATP-dependent protease present in the extract.[2–4] They then identified and characterised the enzymes, termed E1, E2, and E3, that carry out ubiquitin–protein conjugation.[5,6] For the discovery of ubiquitin-mediated protein degradation all three scientist were awarded the Nobel Prize in Chemistry in 2004. The ATP-dependent protease that mediates the degradation of ubiquitin-conjugated proteins was characterised later and is now known as the 26S proteasome.[7–12]

The E1, E2, E3, deubiquitinating enzymes (DUBs) and the 26S proteasome collectively constitute the ubiquitin-proteasome system (UPS) (see Figure 1.1). The majority of intracellular proteins are degraded via this pathway.[13] The UPS E1, E2 and E3 act sequentially. The E1 enzyme first activates the ubiquitin (Ub), a highly conserved, 76 amino acid (8.3 kDa) protein, in an ATP-dependent manner. A thioester bond is formed between the conserved cysteine residue in the active site of the E1 and the C-terminal glycine residue of ubiquitin. Ubiquitin is then transferred onto the E2 enzyme via a *trans*-thiolation reac-

tion. The mechanism is shown in Figure 1.2. Next, the E3 enzyme catalyses the formation of an isopeptide bond between the ε-amino group of the substrate lysine residue and the C-terminal glycine residue of ubiquitin and then between ubiquitin molecules to form a poly-ubiquitin chain.

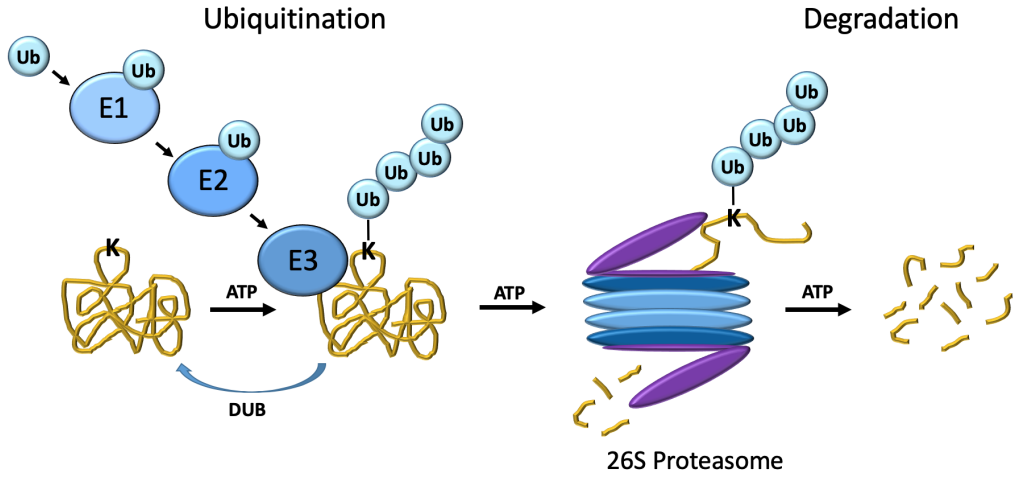

Figure 1.1: Schematic of the ubiquitin-proteasome system. Protein selected for ubiquitination and subsequent degradation is shown in yellow. First, E1 activates ubiquitin (Ub) which then is transferred onto an E2. E3 serves as a substrate recognition domain; it binds to the substrate protein and allows the Ub transfer from the E2 to the lysine (K) of the substrate protein. Once poly ubiqutin chain is added onto the protein, it is then recognised and degraded by the 26S proteasome. The ubiquitination process can be reversed by deubiquitinating enzymes (DUBs).

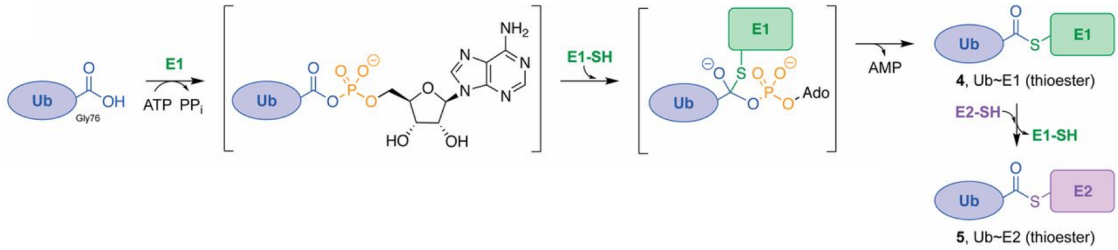

Figure 1.2: Schematic of the ubiquitin activation and the subsequent transfer from an E1 to an E2 enzymes. E1 binds ATP, Mg^{2+}, and Ub to catalyze adenylation of the Ub C-terminal glycine (1), forming a Ub-adenylate [Ub-adenosine 5'-monophosphate (Ub-AMP) (2)] and pyrophosphate (PP_i). After PP_i release, Ub is transferred to the E1 catalytic cysteine by nucleophilic attack on the Ub-AMP via a tetrahedral intermediate (3), forming a thioester bond (E1∼Ub (4)) with loss of AMP. The thioester from the E1 catalytic cysteine (E1∼Ub) is then transferred to an E2 catalytic cysteine (E2∼Ub (5)) via a trans-thiolation reaction.

The mammalian UPS has two E1 ubiquitin-activating enzymes and approximately 40 E2 ubiquitin-conjugating enzymes, which are sufficient to deliver ubiquitin to more than 600 E3 ubiquitin ligases.[14–17] The ubiquitinated substrates are then recognised by the 26S proteasome, stripped of the ubiquitin chains and threaded though the central pore of the proteasome where they undergo degradation.[4,18–20] Protein ubiquitination can be reversed by deubiquitinases (DUBs), protease enzymes that are able to hydrolyse the isopeptide bond.[21]

The ubiquitin is added onto a lysine residue of the protein, and the protein can be either mono-ubiquitinated (one ubiqutin molecule conjugated) or poly-ubiquitinated (several ubiquitins conjugated to form a polyubiquitin chains). Furthermore, ubiquitin contains seven lysine residues (Lys6, Lys11, Lys27, Lys29, Lys33, Lys48, Lys63) and a free N-terminus of Met1, all of which can undergo ubiquitination and resulting in formation of poly-ubiquitin chains with different linkage types.[22,23] To add to the complexity of the system, ubiquitination is not only a signal for protein degradation but can also mediate DNA repair, signaling, gene regulation, endocytosis and more (see Figure 1.3). The ubiquitin-mediated cellular responses determined by the protein ubiqutination stage as well as ubiqutination linkage type are reviewed in Komander[24] and Yau.[25]

Furthermore, in recent years several new modes of ubiquitin chain attachment have emerged. For instance, covalent modification of non-lysine sites in substrate proteins has been observed. For example, the hydroxyl group of serine and threonine residues and even the thiol groups of cysteine residues can all be employed as sites of ubiquitination, this is known as "non-canonical ubiquitination".[26] To date, this non-canonical ubiquitination is not well understood. It requires development of new methodologies to detect distinct non-canonical ubiquitination events which are difficult to study using current techniques. Understanding of ubiquitination of other amino acids than lysine could lead to a better understanding of the complexity of protein regulation by ubiquitination.

Here, we will focus on reviewing the mechanisms of E3 ubiquitin ligase and will not discuss in detail the ubiquitin activation by the E1 and transfer onto the E2. Recent studies, especially determination of the structure of a ubiquitin E1-E2 complex,[27] have contributed to making this process the best understood mechanism of the UPS.[28–33]

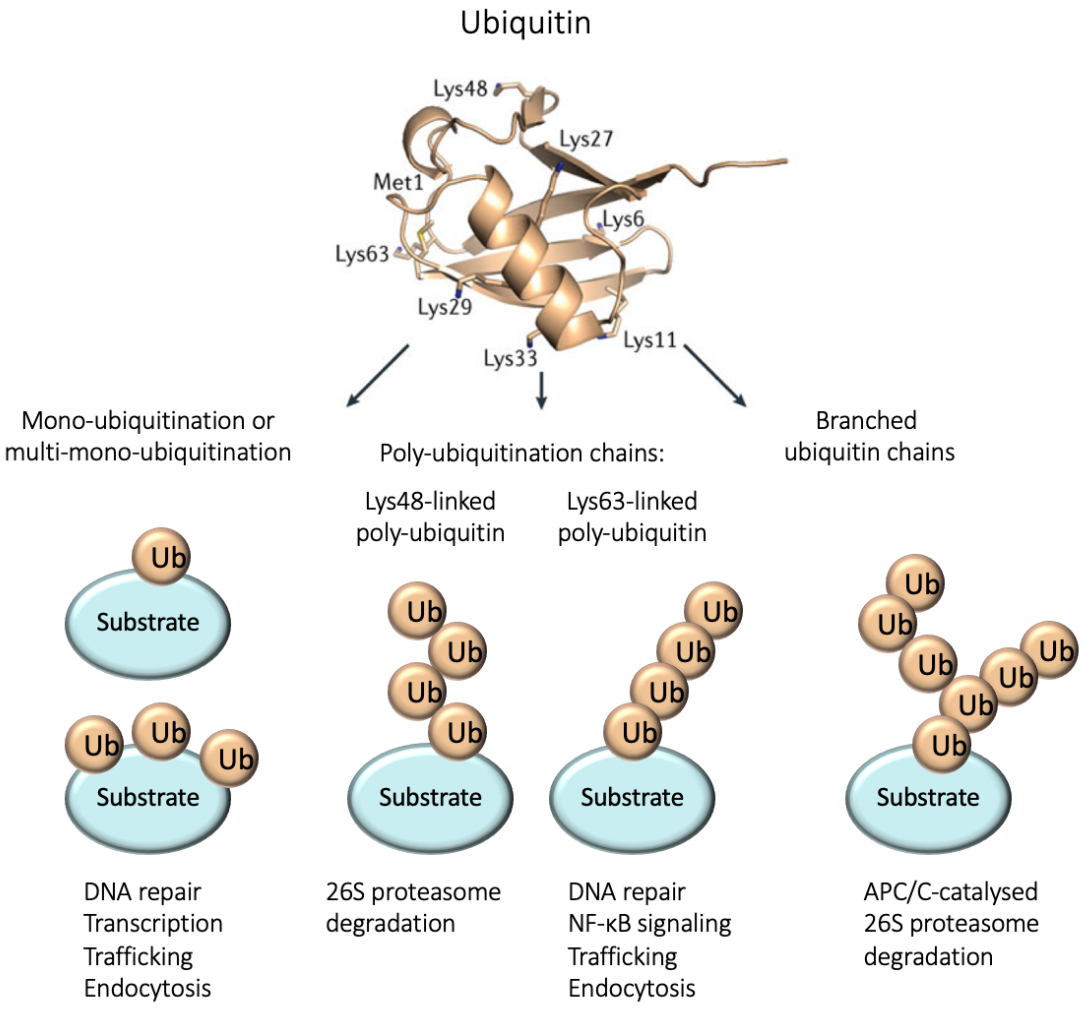

Figure 1.3: Different outcomes of substrate ubiquitination. The structure of ubiquitin protein is shown in yellow. Ubiquitin contains seven lysine residues and a free N-terminus of methionine, all of which can undergo ubiquitinations. Ubiquitination can occur as a mono-ubiquitination or a multi-mono-ubiquitination, it can also result in a formation of poly-ubiquitin chains with different linkage types. These different ubiquitination types are not only targeting proteins for degradation but can also mediate various cellular responses as shown in the schematic.

1.2 E3 ubiquitin ligases

The E3 ligases serve as the substrate-recognition component of the UPS, and the diversity needed is clearly reflected in the fact that there are more than 600 E3s currently identified compared to far fewer E2s and E1s. All E3 ligases have a domain to bind the E2∼ubiquitin conjugate and are classified by the structure of that domain and the mechanism of ubiquitin transfer. There are three classes of E3 ligases identified to date: RING (really interesting new gene), HECT (homologous to E6AP C-terminus) and RBR (RING-between-RING). RING E3s catalyse the direct transfer of ubiquitin from E2∼ubiquitin to the substrate.[17,34] HECT and RBR E3s first receive the ubiquitin from the E2∼ubiquitin conjugate onto a catalytic cysteine to form an E3∼ubiquitin intermediate before transferring the poly-ubiquitin chain to the substrate (see Figure 1.4).[35,36]

RING E3 ligases are diverse and by far the largest of the three E3 classes.[16] RING E3 ligases can be further subdivided into CRLs (Cullin-RING E3 ubiquitin ligases) and APC/C (anaphase promoting complex/cyclosome).[17] The CRL is the largest family of all E3 enzymes consisting of more than 200 members.[37] One type of ligases belonging to this family are the SCF-type ligases, consisting of Skp1, Cullin1, Rbx1 and the F-box protein (defined by its F-box motif). Cullin1 provides a rigid scaffold, whose C-terminal moiety binds to the RING protein Rbx1 (RING-box protein 1) that recruits the E2 enzyme, whereas its N-terminal moiety binds to an adaptor protein Skp1 (S phase kinase-associate protein 1). Skp1 binds to the F-box motif of the F-box proteins, which serve as a substrate recognition subunit of the E3 ligase. The F-box proteins bind to substrates using various domains. There are 69 known F-box proteins, and they are divided into three subgroups based on their structural features. The Fbxw proteins contain the WD40 domain (12 members), Fbxl proteins have leucine-rich repeats (LRRs) (21 members) and Fbxo F-box proteins have "other" domains (36 members).[38]

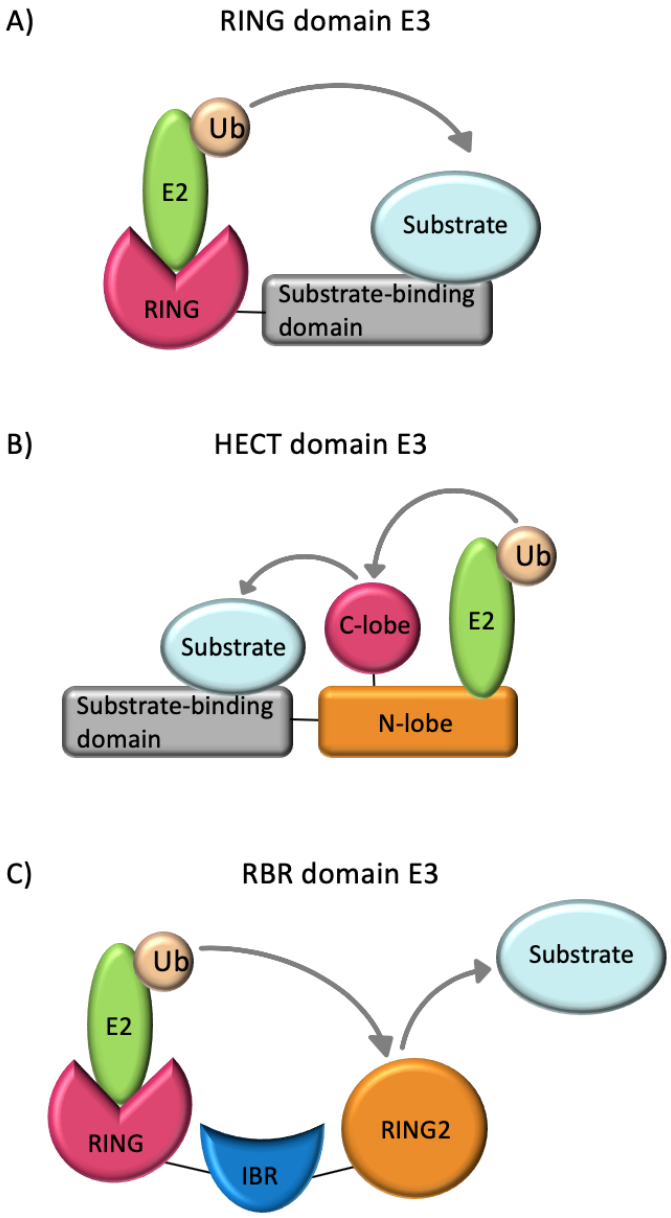

Figure 1.4: A schematic of the mechanisms of ubiquitin transfer by the three classes of E3 ligases. A) The RING domain binds E2∼ubiquitin conjugate whilst the substrate-binding domain recruits a substrate. Ubiquitin is then transferred directly from the E2 to the substrate. B) The N-lobe of the HECT domain recruits E2∼ubiquitin and the substrate-binding domain recruits a substrate. In contrast, the ubiquitin is first transferred onto the C-lobe of HECT E3 ligases, and only then is ubiquitin transferred to the substrate. C) In RBR E3 catalysis, the RING1 domain binds E2∼ubiquitin, and ubiquitin is transferred from E2 to the RING2 domain and then to the substrate. How RBR E3s recruit substrates is still unclear.

1.2.1 SCF^{Skp2}

My work focuses on a member of the CRL family, the SCF (Skp1-Cul1-Rbx1-F-box^{Skp2}) ubiquitin ligase. The F-box protein Skp2 (S phase associated protein 2) belongs to the leucin-rich repeat family of F-box proteins and consists of 10 LRRs. Most LRR domains consist of 2–45 leucine-rich repeats, with each repeat about 20–30 residues long. Structurally, LRR domains adopt an arc or horseshoe shape, with the concave face consisting of parallel β-strands, each usually three residues long, flanked by loops. And the convex face representing a more variable region of secondary structures, which are often helical.[39–41]

The structure of Skp1-Skp2 identified the extensive hydrophobic interface between the Skp1 and Skp2. The structure of the Skp2 F-box consists of three helices (Figure1.5), the F-box is followed by a 70-residue 'linker' that forms three non-canonical LRRs and a further seven LRRs predicted from the amino acid sequence.[42]

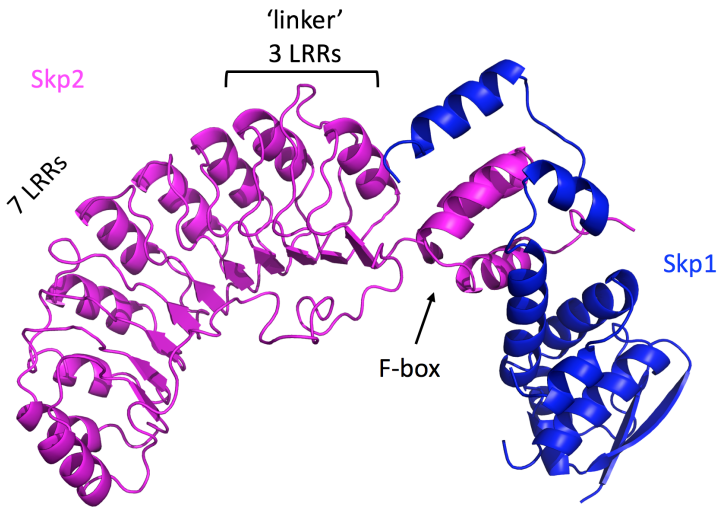

Figure 1.5: Schematic of the crystal structure of the Skp1-Skp2 complex (PDB: 1FQV). Skp2 in magenta, Skp1 in blue. The image was generated using PyMOL.

The crystal structure of the Cullin1-Rbx1-Skp1-F-box^{Skp2} ubiquitin ligase complex provided the first structural information on the Cullin scaffold and its interactions with the other components of the CRL ligase (see Figure 1.6).[43] The N-terminus of the Cullin scaffold binds to the adaptor protein Skp1, which in turn recruits the substrate-recognition protein (Skp2) via the F-box motif.[38] The C-terminus of Cul1 binds to Rbx1, which associates with the E2 bearing an activated ubiquitin. Thus, Cul1 scaffold facilitates the transfer of the ubiquitin molecule from the E2 enzyme onto the substrate by bringing the E2 and the substrate-recognition protein (Skp2) into close proximity.

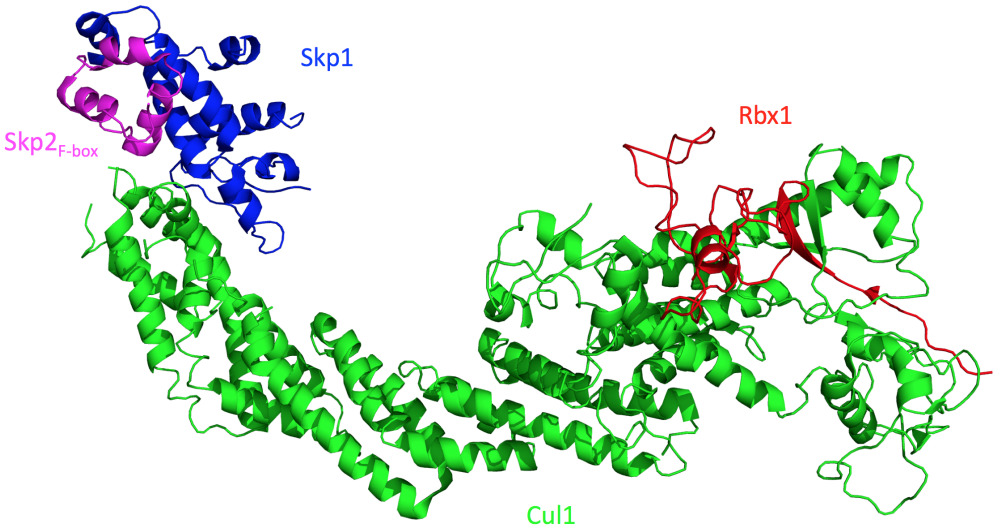

Figure 1.6: Schematic of the crystal structure of the Cullin1-Rbx1-Skp1-F-box^{Skp2} SCF ubiquitin ligase complex (PDB: 1LDK). Skp2$_{F\text{-}box}$ in magenta, Skp1 in blue, Cullin1 in green and Rbx1 in red. The image was generated using PyMOL.

Skp2 is an oncoprotein that is overexpressed in several different cancers, including lymphomas and prostate and breast carcinomas. Furthermore, it has been associated with tumour metastasis and poor prognosis.[44–46] SCF^{Skp2} targets tumour suppressor proteins for degradation including p21, p27, p57 and p300.[47] A major target of Skp2 is the cyclin-dependent kinase inhibitor p27, degradation of which positively regulates cell cycle progression.[48,49] Increased levels of Skp2 and reduced levels of p27 are common in many types of cancers.[50,51] Moreover, the Skp2/p27 pathway plays a central role in breast cancer initiation and metastasis.[45] The inverse relationship between Skp2 and p27 in breast cancer has been noted, and here we will investigate the effects of our stapled peptides as Skp2 inhibitors in the MCF-7 breast cancer cell line.[52–55]

1.3 Skp2-mediated p27 degradation

Interplay between cyclin-dependent kinases (Cdk), cyclins, and the Cip/Kip family of Cdk inhibitors drive the progression through the cell cycle.[56] Cdk inhibitor p27^{Kip1} plays a key role in the control of the proliferation of mammalian cells.[57] p27 is an intrinsically disordered protein (IDP), and binding to Cdk2/cyclin A induces structure formation in the N-terminal domain (p27$_{1\text{-}95}$).[58] This binding results in a complete inhibition of Ckd2/cyclin A kinase activity. Furthermore, the C-terminal domain (p27$_{96\text{-}198}$) remains

unstructured upon N-terminal binding and participates in a phosphorylation and subsequent ubiquitination signaling cascade.[59] Activation of nonreceptor tyrosine kinases by proliferative signals causes phosphorylation of p27 within the Cdk2-bound N-terminal at Tyr88. This occurs during G_1 phase of the cell cycle.[60] Phosphorylation at Tyr88 causes ejection of the p27 inhibitory loop from Cdk2 but without releasing p27, which results in partial restoration of Cdk2 kinase activity[60] (see Figure 1.7). Partially active Cdk2 is then able to phosphorylate Thr187 in the C-terminal domain of p27, creating a Skp2-recognition site.

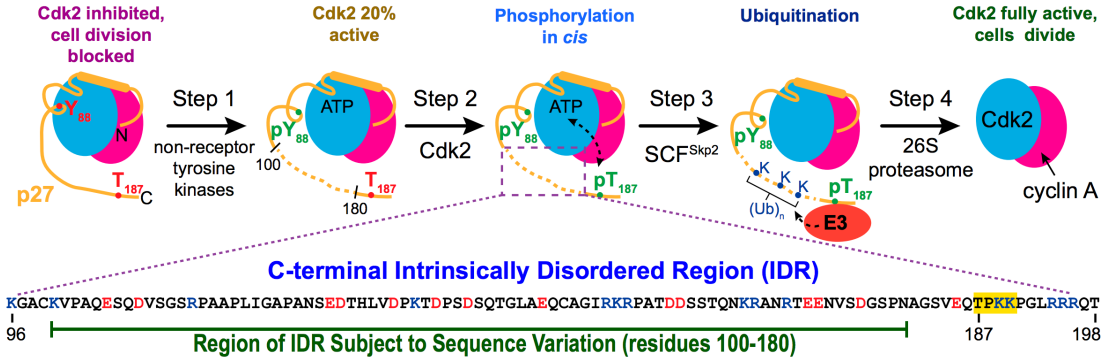

Figure 1.7: Binding of p27 to Cdk2 inhibits kinase activity resulting in a blocked cell division. Phosphorylation at Tyr88 by nonreceptor tyrosine kinases restores partial activity of Cdk2 (step 1) allowing intracomplex phosphorylation of p27 at Thr187 (step 2). In turn, this is recognised by SCF^{Skp2} E3 ligase resulting in ubiquitination of the lysines within the C-terminal domain of p27 (step 3). Subsequent degradation of p27 by the proteasome releases an active Cdk2 resulting in restoration of cell division and progression into the S phase (step 4). Image adapted from Das *et al.* 2016.[61]

p27 is a known substrate of the ubiquitin-proteasome pathway.[62] Skp2 is required for ubiquitinion and subsequent degradation of p27.[63] Furthermore, phosphorylation of p27 at Thr187 was shown to be essential for SCF^{Skp2}-dependent degradation.[64,65] Unlike other SCF substrates, ubiquitination of p27 requires an adapter protein, Cks1.

All Cks (Cyclin-dependent Kinase Subunit) proteins share a function in regulating Cdk (Cyclin-Dependent Kinase) activity by binding to substrates, as well as roles in targeting the cyclin subunit of Cdk2 for degradation via the APC (anaphase promoting complex).[66] Mammalian Cks1 plays an additional role in targeting p27 for degradation via SCF^{Skp2}.[67–69] This unique function of Cks1 was attributed to its ability to bind Skp2.[67] In addition, all three different binding sites (i.e. Cdk2, Skp2 and p27) of Cks1 are required for p27 ubiquitination.[70] Furthermore, it has been shown by the Itzhaki lab and

others that the Cks1-Skp1-Skp2 complex has more than 100-fold greater affinity for p27 phosphopeptide than does Skp1-Skp2 alone, and that Cks1-Skp1-Skp2 complexed with Cdk2 further increases the affinity for the p27 phosphopeptide.[71] The crystal structure of Cks1-Skp2-Skp1 revealed that the phosphorylated Thr187 of p27 peptide was binding to Cks1 rather than Skp2 as previously thought.[72]

Based on the previously published crystal structures of Skp1-Skp2[42] and of the Cullin1-Rbx1-Skp1-F-box^{Skp2} complex[43] a model of the SCF^{Skp2} E3 ligase in complex with Cks1, Cdk2/cyclin A and p27 has been proposed, as shown in Figure 1.8.[72]

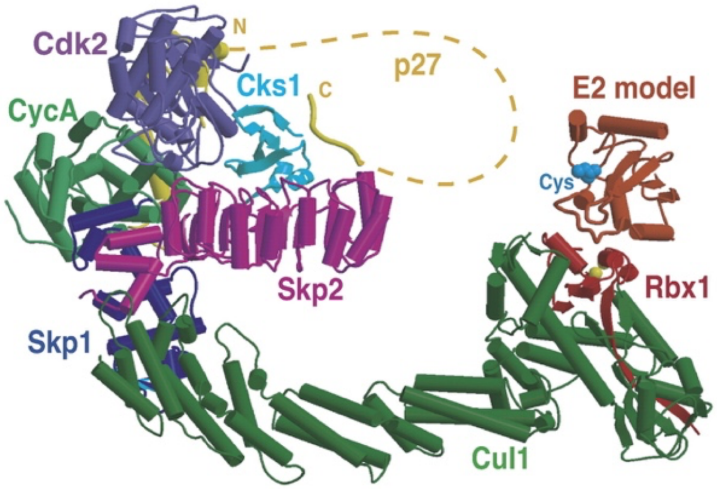

Figure 1.8: Model of the SCF^{Skp2} E3 ligase in complex with Cks1, Cdk2/cyclin A and p27, adapted from Hao et al. 2005.[72] This model suggests that all eight proteins can coexist in one complex without any significant steric hindrance.

The model suggests that all eight proteins co-exist in one complex, which was further confirmed by size-exclusion chromatography where all eight proteins co-eluted in the same peak.[72] This model agrees with previously established results that Cdk2/cyclin A facilitates the recruitment of p27 to SCF$^{Skp2\text{-}Cks1}$.[60,65] Overall, degradation of p27 results in the release of fully active Cdk2/cyclin A, thus promoting progression of the cell cycle into S phase.[60,73]

Mouse models have shown that the loss of *Cdkn1b* gene encoding p27 results in endocrine dysfunction and the development of cancer.[74] Furthermore, mice lacking p27 are larger in size and also exhibit abnormally enlarged organs compared to the wild type mice. These enlargements could be associated with an enhanced proliferation of cells. In addition, $p27^{-/-}$ mice spontaneously develop pituitary tumours.[50,74] Moreover, the absence of Skp2 in mice resulted in the accumulation of p27, and $Skp2^{-/-}$ mice were smaller in size than the wild type mice. Cellular phenotypes of $Skp2^{-/-}$ include nuclear enlargement, polyploidy in cells of the lung, kidney, liver and testis. All these phenotypes were reversed in the $Skp2^{-/-}$; $p27^{-/-}$ double-mutant mice, indicating that p27 is the key substrate of Skp2.[50] Thus Skp2/p27 presents a desirable therapeutic target for cancers with reduced levels of p27 due its Skp2-mediated degradation.

1.4 Development of UPS inhibitors

Ubiquitination of proteins has multiple effects on diverse biological processes including cell-cycle progression, apoptosis, oncogenesis, angiogenesis and protein quality control. Therefore, the inhibition of the UPS represents an attractive target for developing therapeutic agents for many diseases. Targeting of the ubiquitin enzymes, E1, E2 and E3, their multiple subunits and substrates have both advantages and disadvantages. Many factors should be considered when choosing a drug target such as its biological role, specificity of the drug, potential side effects, and druggability of the target.[75,76]

The first class of proteasome inhibitors discovered were the peptide aldehydes, including MG132. High potency and wide availability of peptide aldehydes made them attractive potential drugs. However, poor selectivity, rapid oxidation and rapid reversibility of binding to the proteasome resulted in this class of drugs being unsuitable as therapeutic agents. Nevertheless, MG132 is widely used in biological studies. Studies of peptide aldehydes led to the discovery of the peptidyl boronates with even higher potency, this further lead to the development of dipeptidyl boronic acid, such as Bortezomib which was the first FDA approved UPS inhibitor.[77]

Another class of proteasome inhibitors are epoxyketones. Epoxyketones not only irreversibly inhibit the proteasome but also have greater specificity as opposed to peptidyl boronates. The chemical structure of epoxytones was further improved and lead to the disocvery of Carfilzomib (Kyprolis, 2012), which is used for treating multiple myelomas in patients resistant to Bortezomib. It also shows reduced side effects and significantly improved rates of peripheral neuropathy compared to Bortezomib. Both drugs are not available orally; Bortezomib is administered intravenously or subcutaneously, and Carfilzomib is administered intravenously. Moreover, some patients develop resistance and painful side effects from both drugs, and therefore more specific means of targeting oncogenically activated pathways in the UPS is highly desirable.

1.4.1 Inhibitors of E3 ligases

Several inhibitors of the E1 and E2 enzymes are in development and were reviewed recently (Zhang *et al.* 2014).[76] This section will focus on the development of inhibitors to target E3 ligases. It is appealing to target this component of the UPS because this step is where substrate specificity lies. Many small molecules targeting interactions between ubiquitin ligases and their substrates are being developed. Targeting of Cullin-RING E3 ubiquitin ligases has been recently reviewed (Bulatov *et al.* 2015).[78] Recently, there have been a few reports of the identification of small molecules that target interactions between ubiquitin ligases and their substrates, including inhibitors of MDM2-p53,[79–82] SCF(Skp2)-p27,[83,84] CRL4(CRBN)-MEIS2,[85] SCF(Cdc4),[86] and SCF(Met30)[87] ubiquitin ligases.

The first E3 ligase successfully targeted was MDM2, which ubiquitinates the tumour suppressor protein p53. Nutlins, developed by Roche, are the first group of small molecule that can disrupt the MDM2-p53 interaction and thus stabilise p53.[79] Nutlins occupy the p53-binding pocket of MDM2, the leading compound, Nutlin-3a has been shown to inhibit the p53–MDM2 interaction in the cellular context with a high degree of specificity, leading to p53 stabilization and a non-genotoxic activation of the p53 pathway.[88]

Many other small molecule inhibitors were discovered that are able to stabilise p53. However further studies need to be carried out to determine whether these molecules could be used for human cancer treatment. Drugs stabilising p53 will be useful for tumours that retain wild-type p53 but show overexpression of MDM2. However they will have little effect on the large proportion of cancers with mutated p53.

Many E3 ligases are strongly implicated in cancer, and among these is SCF^{Skp2} whose substrate specificity is determined by the prototypical oncogenic F-box protein Skp2. Small molecule inhibitors of SCF^{Skp2} were recently identified with *in silico* screening and proposed to inhibit the enzyme via disrupting protein-protein interactions rather than targeting a catalytic site. But despite preventing p27 ubiquitination and causing an increase in p27 levels, they see only modest effects on cell cycle and only cell line-specific effects or required high concentrations to show effects and it was never determined that there was actual direct binding.[83,89,90] We propose a different approach, creating a competitive inhibitor, known as a 'stapled' peptide to prevent p27 binding to Skp2. The next sections will introduce peptides as emerging therapeutics and discuss their advantages over small molecule drugs as well as the potential challenges.

1.5 Peptide-based drugs

Compared to small molecules drugs (MW <500 Da), which are mainly designed to bind small well-defined pockets in the protein structure, usually in the catalytic site, peptides can be used to target protein-protein interaction interfaces, that previously were thought "undruggable". Signaling mechanisms that govern important physiopathalogical pathways are mostly regulated by protein-protein interactions (PPIs) that are characterised by shallow and undefined pockets.[91] More than 80% of proteins are considered to be undruggable with small molecules, based on the nature of their binding interfaces.[92,93] Despite some successes targeting PPIs using small molecules,[94,95] this remains the biggest challenge for small molecule drugs. This leaves a large portion of the human proteome "locked", and by being able to target these large and shallow surfaces, numerous diseases could potentially be treated.

Peptides offer an ideal intermediate between the small molecules and protein biologics (typically >5000 Da, such as insulin, growth factors and engineered antibodies). Peptides are able to mimic the endogenous part of the interacting proteins thus are able to bind large and flat target surfaces offering superior efficacy and selectivity.[93,96,97] Currently, there are more than 400 peptide drugs that are under global clinical development, with over 60 already approved for clinical use in the United States, Europe and Japan.[98,99] Peptide drugs are mainly for metabolic diseases, oncology and cardiovascular diseases.[99] It should be noted that the major targets of both protein- and peptide-based therapeutics are extracellular, due to challenges of their cellular uptake. Compared to traditional small molecules, peptides exhibit very high specificity towards their targets, and have been found to be safe, well-tolerated and efficacious in humans. Furthermore, compared to protein-based biopharmaceuticals the production cost is lower and similar to that of small molecules.[100,101] Unfortunately, naturally occurring peptides exhibit poor chemical and physical stability, since they are sensitive to enzymatic degradation as well as short circulating plasma life, thus are not directly suitable for use as convenient therapeutics.[102] This has spurred numerous studies aimed at overcoming these intrinsic limitations of peptides and has led to the discovery of new methods to improve the stability of peptides and aid peptide intracellular delivery. Most of these issues have been addressed by engineering diastereoisomeric peptides, or by performing cyclisation (N- to C-terminus), macrocyclisation (not termini) or "stapling" (chemical crosslinking) of the peptides for the target protein by comparison with the unconstrained peptide. Currently, most peptide drugs

are administered parenterally, but alternative administration routes, including oral and intranasal, are being investigated.[100,101]

1.5.1 Stapled peptides

The term macrocyclic peptide encompasses all peptides that have at least two amino acid residues linked together to form a macrocycle. These include cyclic peptides, stapled α-helical peptides, constrained β-hairpins and cysteine-rich peptides (to allow disulfide bridge formation[103–106]).[107] Cyclisation is the most widely used methods to improve peptide stability and recent report showed that at least 125 cyclic peptides are orally absorbed.[108] Cyclic peptides can be achieved in several ways - for example, joining head-to-tail or side chain-to-side chain and these are reviewed extensively.[109–111] Here, we will focus on the stapling methods used to achieve peptide cyclisation.

Stapling of peptides serves a key purpose of constraining it in its bioactive (i.e. binding-component) conformation thereby potentially dramatically improving the binding affinity. This arises from conformational rigidity and thus the entropic contributions upon binding to the protein. For example, when binding ligands are not flexible they do not sample different structural conformations and therefore it reduces the entropic penalty upon binding which then subsequently increases their affinity.[112,113] Furthermore, stapling of peptides has been shown to be particularly successful in enhancing the proteolytic stability of peptides.[114,115]

One-component stapling

There is a variety of different stapling methodologies reported. The first method involved the intramolecular linkage between the side chains of the natural amino acids, for example a lactamisation reaction between either aspartic or glutamic acid and lysine.[116–118] This is known as one-component stapling method. Currently, the "gold standard" of the one-component stapling method is the hydrocarbon staple. Two amino acid residues bearing alkene functionalities forms a staple during a Grubbs catalysed ring-closing metathesis (RCM).[119] In fact, the first peptide to ever progress to the clinical trials was stapled using RCM (the Aileron drug, known as ALRN-5281, for rare endocrine disorders).[120] In addition, copper(I)-catalysed azide-alkyne cycloaddition (CuAAC) were used to staple peptides containing amino acid residues functionalised with alkyne and azide.[121–127] A

schematic of a one-component peptide stapling using and RCM or CuACC is shown in Figure 1.9.

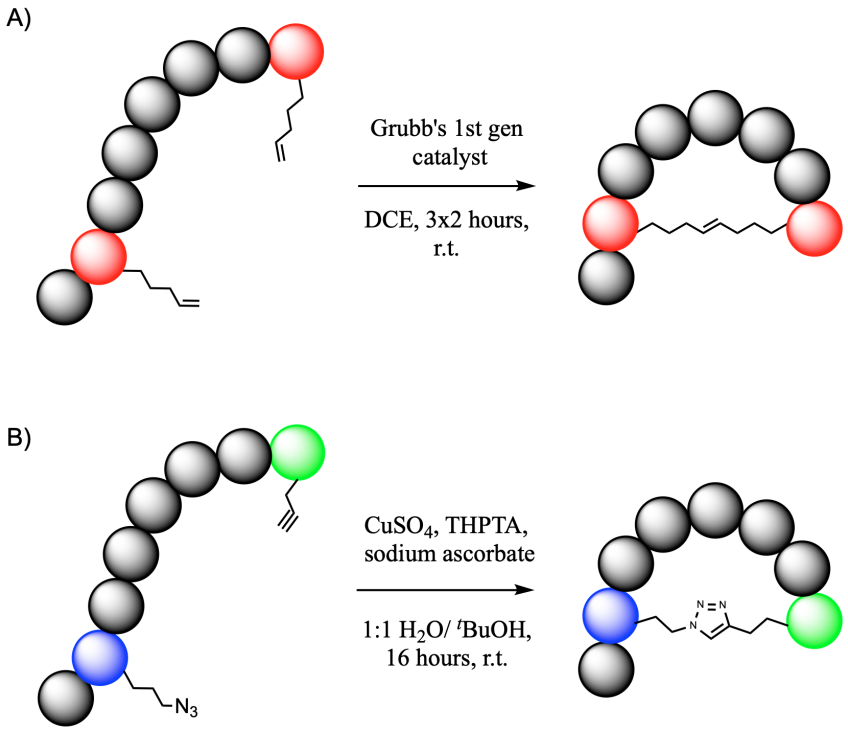

Figure 1.9: A schematic of one-component peptide stapling. A) Two amino acid residues within the peptide are changed to amino acids containing alkene functionalities which then can form a staple during Grubbs catalysed ring-closing metathesis. B) Copper(I)-catalysed cycloaddition reaction between the amino acids containing azide and alkyne functionalities forms a staple within the peptide.

Another recently developed stapled peptide is one that acts as a dual inhibitor of MDM2 and MDMX for p53-dependent cancers.[128] Aileron Therapeutics has emerged as a new biopharmaceutical company that specialises in the development of stapled peptides and is carrying out a Phase II clinical trial of this p53 stapled peptide.[129] Furthermore, the p53 stapled peptide is able to penetrate cell membrane without addition of any cell penetrating moieties.[128] Several studies have shown that some hydrocarbon-cross-linked peptides, including the p53 peptide, are able to permeate through lipid bilayers of the cell membrane as opposed to native, non-cross-linked peptides. Stapled peptides were able to bind to the lipid bilayer resulting in membrane thinning and finally causing pore formation.[130] Table 1.1 shows a list of stapled α-helical that target PPIs in diseases.

Table 1.1: Stapled α-helical peptides that target PPIs in diseases (not a comprehensive list). CRF: corticotropin- releasing factor. PTH: parathyroid hormone. Bcl-2: B-cell lymphoma 2. RSV: respiratory syncitial virus. MC1: melanocotin-1.

Stapling method	**Target**	**Literature**
RCM	MDM2/p53	Bernal & Verdine et al. 2007[131]
RCM	Notch/MAML-1	Moellering & Bradner et al. 2009[132]
RCM	MCL-1/BH3	Stewart & Walensky et al. 2011[133]
RCM	IRAP	Andersson & Hallberg et al. 2011[134]
RCM	β-catenin/axin	Grossmann & Verdine et al. 2012[135]
CuAAC	β-catenin/BCL9	Kawamoto & Wang et al. 2012[136]
CuAAC	HIV-1 gp41	Ingale & Dawson 2011[137]
Lactam bridge	CRF receptors	Rivier & Vale et al. 1998[138]
Lactam bridge	PTH receptors	Condon & Labaudiniere et al. 2000[116]
Lactam bridge	Bcl-2 proteins	Yang & Huang et al. 2004[139]
Lactam bridge	RSV infection	Shepherd & Fairlie et al. 2006[118]
Lactam bridge	MC1 receptors	Guo & Miao et al. 2013[140]

Two-component stapling

The one-component stapling approach for peptide macrocyclisation poses a few challenges. It is difficult to build a large library of peptides where several modifications and functionalities are varied to achieve the optimal peptide. For example, the position of the staple, the length of the staple linkage, modifications to improve solubility and cell permeability, as well as attachments of affinity tags and fluorophores for biophysical studies, all need to be varied. If any of these parameters is changed it requires re-synthesis and re-stapling of the peptide, making this process extremely time-consuming and resource-intensive. Furthermore, the newly introduced changes in the original peptide sequence could have a detrimental effect on their binding to the target.[141]

This is where the two-component stapling approach allows scientists to overcome these issues. In a two-component stapling reaction the two side chains on the linear peptide are stapled with a bifunctional linker to produce a stabilised peptide. In contrast to one-component stapling, large libraries of diverse peptides can be rapidly generated using the same linear peptide whilst modifying the linker. Furthermore, linkers can be designed to increase the binding affinity to the desired PPI as well.[142] Most of the two-components stapling methods were derived directly from their one-component counterparts and are briefly discussed below mainly focusing on a CuAAC methodology, as it was used to staple p27 peptides in this study.

Using natural amino acids

Using natural amino acids offers great benefits since they are cheap and widely available. Furthermore, the changes introduced in the wild type peptide can be kept to a minimum, thus reducing any adverse affects on binding. The most reactive amino acids, lysine and cysteine are commonly used for two components stapling. Phelan et al. successfully stabilised α-helical peptides using bis-lactimisation reaction at i and $i + 7$ positions.[143] Several methods are established to cross-link cysteine residues and are reviewed by Fairlie et al.[144] However, the abundance of lysine and cysteine resides in natural proteins posses problems with orthogonality and chemoselectivity. To a small extent tryptophan residues can be stapled as well but this is far less explored. For example, Johannes et al. 2018 developed a method to constrain two tryptophan residues, at i and $i+4$, via acid-mediated condensation with an aldehyde. Even though the constraint did not impart any α-helicity

to the peptide, and therefore did not enhance binding it nevertheless greatly improved its proteolytic stability as compared to the linear analogue.[145] Since tryptophan residues are not abundant in natural proteins it can minimise the risks of chemoselectivity issues. Thus, tryptophan stapling could be a great potential avenue to explore peptide macrocyclisation especially for stabilising non-helical peptides.

Using CuAAC

The Cu(I)-catalysed azide-alkyne cycloaddition (CuACC) reaction is based on the 1,3-dipolar cycloaddition chemistry developed by Huisgen in the 1960.[146] First, one-component intramolecular CuACC stapling was used by D'Ursi[125] and Wang[136] to stabilise α-helical peptides.

In the two-component stapling approach, two amino acids in the linear peptide are changed to azido-containing unnatural amino acids to produce a di-azido peptide which then can be stapled using dialkynyl linker under Cu(I) catalyst. This reaction was first used to stabilise α-helix peptides (azido amino acids positioned at i, $i+4$) by Bong,[147] and have been widely used thereafter (Pedersen,[148] Thurber,[149] Spring[150]). A schematic of possible double-click reaction pathways is shown in Figure 1.10. It is important to note that once the intermolecular coupling between one azide group and a linker alkyne occurs (Figure 1.10a) the next reaction has several potential pathways that could either lead to the formation of the double-click'ed desired product (Figure 1.10c), or intermolecular reactions between another peptide or linker (Figure 1.10b,d). This was further investigated by Spring and coworkers and the optimal reaction conditions to produce the desired product were found to be when the peptide is present at relatively low concentrations and one equivalent of the linker is used.[151]

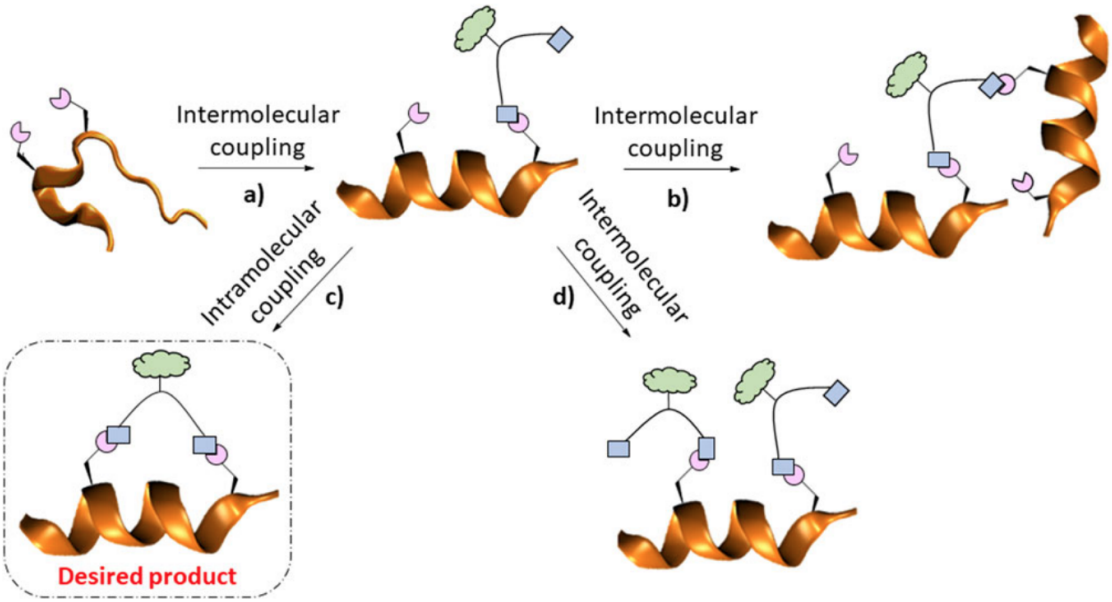

Figure 1.10: Potential reaction pathways of the two-component CuAAC stapling. a) once the first intermolecular reaction between the peptide and an alkyne occurs it then either: c) leads to the intramolecular coupling to form the desired product, or an intermolecular coupling between b) another peptide; d) another linker. Image adapted from Iegre *et al.* 2018.[152]

Moreover, Spring has successfully stabilised α-helix peptides by substituting azido amino acids at positions i, $i + 7$ which indicates that the double-click reaction may be used in different spacing of the non-native amino acids.[151] In addition, the reaction has been reported to perform well in mild conditions thereby allowing the use of stapling linkers containing high range of functionalities that otherwise might be unstable. Azide containing unnatural amino acids were reported to be compatible with solid phase peptide synthesis methods and simple to synthesise.[153] Furthermore, the azido amino acids are not prone to cross-reactivity with other unprotected functional groups. This is in contrast to the stapling of the natural amino acids like lysine and cysteine that may cross-react if unprotected.

However, CuAAC stapling efforts on-resin are so far unsuccessful and thus requires the peptide purification step prior to the stapling reaction.[154] This then has to be followed by another purification step to remove any by-products and leftover catalyst to minimise the risk of toxicity arising from any residual copper in the final stapled peptides. Furthermore, the reaction is air sensitive must be carried out using degassed solvents as Cu(I) catalyst is susceptible to oxidation.[151]

A recent study by Pedersen et al. 2017 introduced an iteration on a two-component CuAAC stapling.[148] Termed as a diversity-oriented peptide stapling (DOPS), this strategy introduces a triyne linker that after stapling reaction leaves a free alkyne. This alkyne can be functionalised further when required (see Figure 1.11). This might be advantageous compared to previously discussed double-click reaction as it addresses the issue of synthesis of unique linkers and re-stapling of the peptide afterwards.

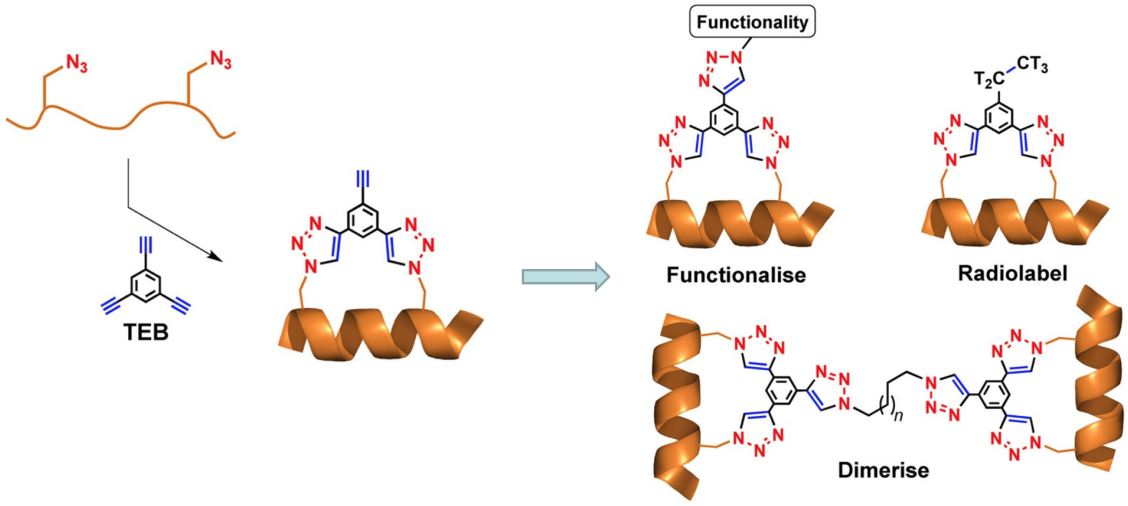

Figure 1.11: Diversity oriented peptide stapling using a two-component CuACC method with tris-alkyne linker (1,3,5-triethynylbenzene (TEB)). The reactions leaves a free alkyne positioned on the staple, which can be further conjugated or dimerised. Free alkyne can be radiolabelled by catalytic tritiation. Image modified from Tran *et al.* 2017.[148]

Using SPAAC

Recently a variation of CuAAC, strain-promoted azide–alkyne cycloaddition (SPAAC), was used by Spring and coworkers to produce α-helical p53 peptides.[155] Reaction mechanism is shown in Figure 1.12. In this study they had modified strain promoted alkyne-azide cycloaddition (Figure 1.12a) pioneered by Bertozzi)[156,157] and CuAAC method to develop a new SPAAC method for peptide stapling. They reported that the SPAAC method does not require any catalyst, thus reducing the possible effects of toxicity of peptides due to residual catalyst. Furthermore, unlike CuAAC this reaction is not air sensitive and peptide stapling was achieved *in situ*.[155]

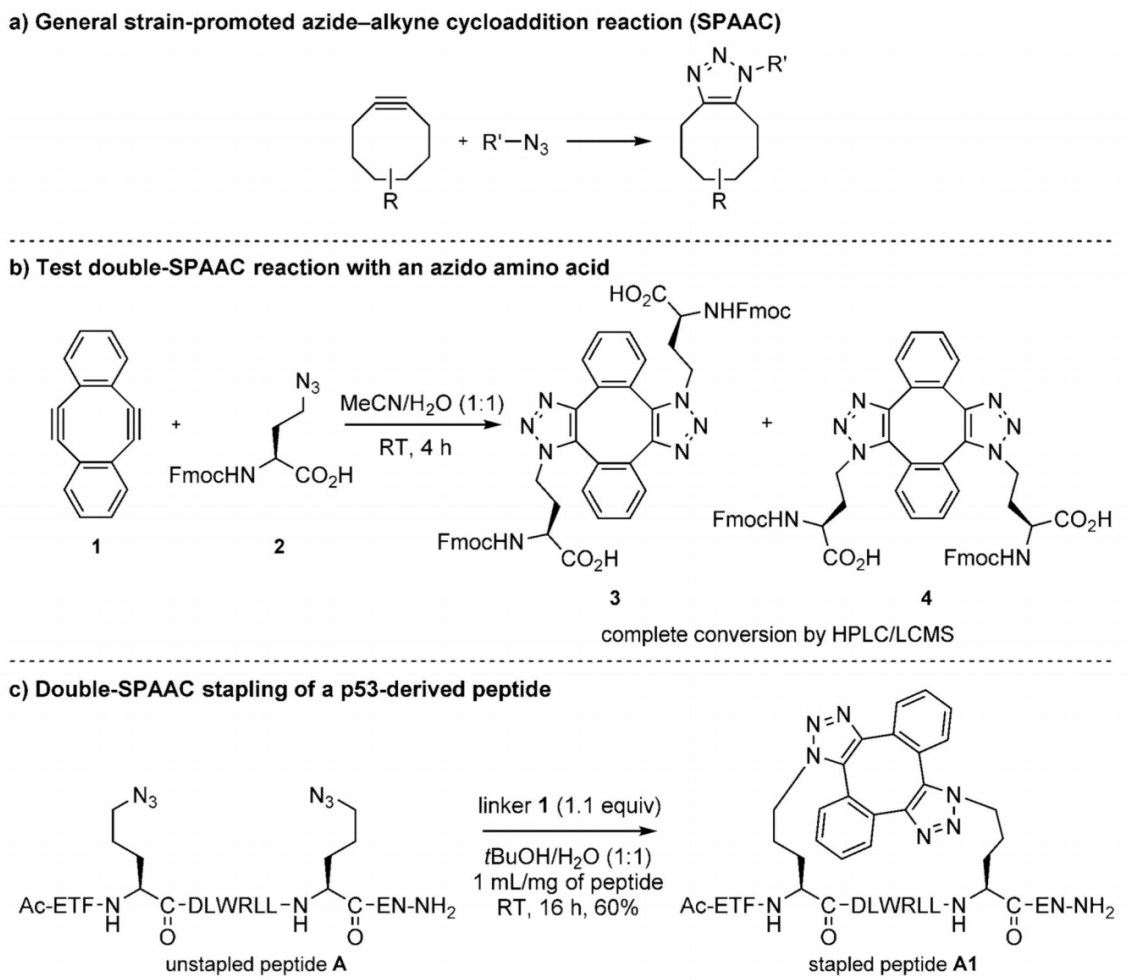

Figure 1.12: a) Strain-promoted azide–alkyne cycloaddition (SPAAC).[156] b) Test double SPAAC on Fmoc-Aha-OH. c) Double-SPAAC stapling of p53-derived diazidopeptide A. Image adapted from Lau *et al.* 2015.[155]

This could further improve the timescale of peptide synthesis, since CuAAC method requires multiple purification steps to achieve the desired constrained peptide. However, the linkers used in SPAAC are not yet functionalised and thus the peptide libraries produced are still not comparable to the diversity of peptides that can be achieved using CuAAC two-component peptide stapling method.

Currently, there are not many studies that investigate the effects of different stapling techniques on the same linear peptide sequence. Although one-component stapling approaches have been compared in several studies,[158–160] only one study (by Fairlie's lab) has looked at the effects of different two-component stapling methods.[161] Due to the lack of the comparison studies, it is difficult to chose the best approach of peptide stapling. This would help scientists to choose the method that allows easy and quick functionalisation

and modification of peptides for their use in the biophysical and biological assays.

1.5.2 Non-helical constrained peptides

Most peptide-derived PPI inhibitors are stabilised α-helices. As summarised above, the design is relatively straightforward and various methodologies can be employed to achieve desired features. Moreover, the success of stapling can be validated using circular dichroism to evaluate its helicity. However, up to 50% of all PPIs involve interactions of proteins with an unstructured peptide motif, such as a loop or a turn.[162] Therefore, a large majority of PPIs are unaddressed using helical peptides.

Irregular-structured peptide inhibitors are much more difficult to design, and so far there is no rational approach to designing constrained non-helical peptides with high affinities for desired PPIs.[162,163] Furthermore, chemical stabilisation may be less efficient due to high conformational flexibility in irregular peptides compared to helical peptides in which the intrinsic helicity can greatly reduce the entropic cost and drive the cyclisation process.[114,119] Grossmann et al. demonstrated the application of all-hydrocarbon crosslinking to irregularly structured peptides via intramolecular side chain-to-side chain macrocyclisation.[163] In addition, the recent advances in two-component peptide macrocyclisation developed by the Spring group have utilised click chemistry and separate functionalised linkers to allow one-step transformation of stapled α-helical peptides coupled with diverse functions. Using this double-click approach the Spring and Itzhaki groups were also successful in constraining non-helical peptides. A schematic of constraining non-helical peptides using double-click chemistry is shown in Figure 1.13.

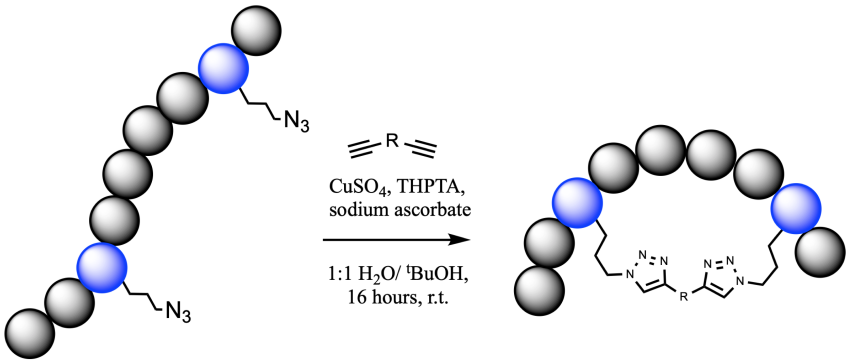

Figure 1.13: A schematic of constraining non-helical peptides using double-click chemistry. Two amino acid residues within the peptide are changed to amino acids containing azido functionalities which then can be stapled using a bis-alkynyl linker.

Dr Wenshu Xu (Spring and Itzhaki groups) developed macrocyclised peptide inhibitor for tankyrase-axin PPI.[164] In this study a combinatorial approach was used to screen for the optimal length of azido-containing unnatural amino acids (incorporated in the peptide) and alkynyl linkers. They were able to develop peptides with a sub-micromolar affinities and also obtain a crystal structure of tankyrase bound to the constrained peptide. In a similar manner, the Spring lab designed a peptide inhibitor targeting the PPI between HNF1β transcription factor and nuclear transport protein transportin-α.[165] The best constrained peptide had a 2.5-fold increase in binding affinity compared to the wild-type linear peptide. In addition, constrained peptides displayed cell-permeability.[165] Both of these studies indicate that it is possible to achieve constrainment of irregular peptide structure and use them successfully to inhibit PPIs. These macrocyclised peptides exhibited only a small affinity increase compared to their linear counterparts, likely because the bioactive conformations are relatively extended so "constraining" them cannot "improve" their structures. Nevertheless, the macrocyclisation process confers stability on them, meaning that it is a valuable approach.

1.6 Intracellular peptide delivery

1.6.1 Cell-penetrating peptides

It is essential that p27 stapled peptides are able to enter cells with high efficiency. During this study we have investigated peptide conjugation to the cell penetrating peptide (CPP) to aid cellular delivery. This section will describe some commonly used CPPs, their benefits and associated drawbacks. CPPs are short cationic peptide sequences that are widely used and are able to transport various cargos inside living cells, such as small molecules, proteins, peptides, DNA and biopolymers.[166–173] Several CPPs have been identified, including TAT (Trans-Activator of Transcription) protein of HIV, penetratin (antennapedia), transporton and polyarginines.[174,175] A repository of experimentally validated cell-penetrating peptides was created by Agrawal in 2016 and contains more than 1700 CPPs.[176] A non-exhaustive list of well-known CPPs is shown in Table 3.4.

Two major classes of CPPs are the cationic CPPs, in which positively charged residues mediate interactions with the negatively charged plasma membrane, and the amphipathic helical CPPs such as transportan, where the non-polar, hydrophobic amino acids are responsible for internalisation.[177,178] The actual translocation mechanism is not yet fully understood. However, many studies suggest that CPPs from different families are likely to translocate via different uptake pathways, and many can take two or more routes.

Studies have shown the ability of antennapedia and TAT to deliver biologically active proteins and peptides *in vitro* and *in vivo*.[179,180] A cellular uptake and toxicity examination of these CPPs indicated that polyarginine conjugates were taken-up by cells most efficiently, however they also had the greatest toxicity. In comparison, antennapedia-peptide conjugates showed no significant toxicity even at 100 μM.[174] Antennapedia and TAT mediated peptide delivery was observed to occur via lipid raft-dependent endocytosis, more detailed mechanisms of cellular uptake of different CPPs have been reviewed in Madani *et al.* 2011.[177]

Table 1.2: Examples of CPPs and their sequences, origins, and physical–chemical properties.

Peptide	Sequence	Class	Literature
Antennapedia Penetratin (43-58)	RQIKIWFQNRRMKWKK	Cationic and amphipatic	Derossi et al. 1994[181]
HIV-1 TAT protein (48-60)	GRKKRRQRRRPPQ	Cationic	Green et al. 1988[182] and Frankel et al. 1988[182]
Transportan Galanine/Mastoparan	GWTLNSAGYLLGKINLK ALAALAKKIL	Amphipatic	Pooga et al. 1998[183] and Langel et al. 1996[184]
Polyarginines	$(R)_n$; <n<12	Cationic	Wender et al. 2000[185]
pVEC Cadherin (615-632)	LLIILRRRIRKQAHAHSK	Amphipatic	Elmquist et al. 2001[186]
MAP	KLALKLALKALKAALKLA	Amphipatic	Oehlke et al. 1998[187]
ARF (1-22)	MVRRFLVTLRIRRACGPP RVRV	Amphipatic	Johansson et al. 2008[188]
8-lysines	KKKKKKKK	Cationic	Mai et al. 2002[189]

High concentrations (> 10 μM) of CPP-conjugated peptides, sometimes even up to 200 μM, are required for cellular activity even though their dissociation constants to the target protein can be in the submicromolar range.[180,190] This has raised a question of how efficient the CPP-mediated delivery is, and how much of the peptide is actually present intracellularly. Gomez et al. performed quantitative analysis on the cell-penetrating pentapeptides activity (sequence: VPTLK), and showed a striking difference in the intracellular and extracellular concentrations of the CPP.[191] Several other studies investigated the efficiency of the cytoplasmic delivery of bioactive cargos by CPPs. They also observed the endosomal entrapment of CPP conjugates following endocytosis and that only a small fraction being released into the cytosolic space of the cell.[192,193]

A very detailed review about CPP development and their use in clinical trial is published by Guidotti 2017.[194] However, to date there are still no FDA approved CPP-conjugated drugs. The main reasons for that are poor *in vivo* stability due to proteolytic degradation, immunogenicity issues, poor efficiency caused by the cargo's inability to escape endosomes, toxicity due to the CPP's lack of specificity. Similar to linear peptides, CPPs are susceptible to proteolytic degradation and thereby exhibit poor stability *in vivo*. Surprisingly not many studies are yet carried out to improve the CPP stability. One study showed that CPPs synthesised using D-amino acids are fully protease resistant.[195] So far only two studies had looked into stapling the CPPs using hydro-carbon and lactam-stapled methods.[196,197] Dose-dependent cell penetration assays showed that stapling strategy greatly improves the cellular uptake of Antp and poly-Arg_8 peptides.[197] These stapled CPPs could potentially be used to not only deliver the peptide of interest but potentially enhance the stability of it as well.

1.6.2 Other strategies for intracellular peptide delivery

In our study of stapled p27 peptides we also explored electroporation and liposomal encapsulation delivery methods. These methods are currently more extensively explored for delivery of proteins.[198,199] We pursued this to overcome the poor cytosolic delivery efficiencies encountered using p27 peptides conjugated to the CPP (Antp). A schematic of electroporation and liposomal encapsulation delivery methods is shown in Figure 1.14, and the two methods are briefly discussed below.

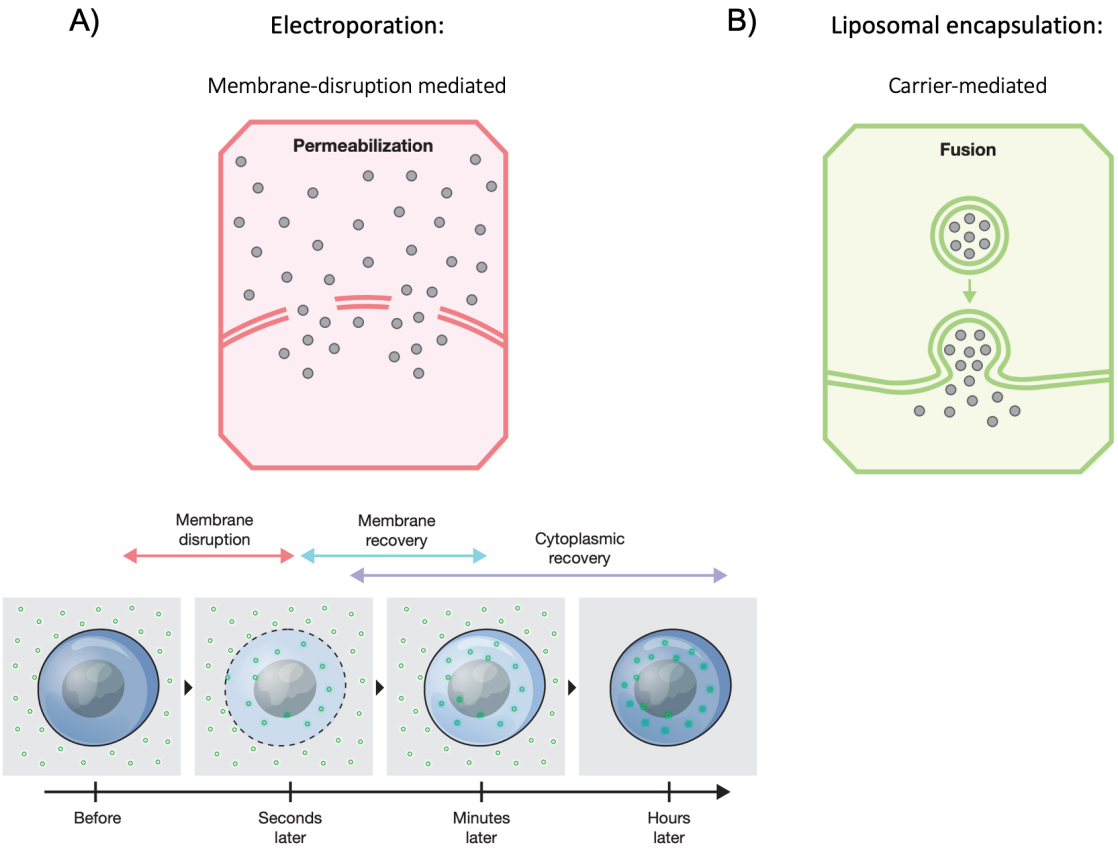

Figure 1.14: A schematic of electroporation and liposomal encapsulation delivery methods. A) Electroporation permeabilises the membrane to allow the entry of peptides into cells whilst B) liposomes have fusogenic potential and the peptide enters cells through membrane fusion. Image modified from Stewart et al. 2016.[198]

As shown in Figure 1.14, the cargo is encapsulated within the liposome and is released into the cell as liposome fuses with the cellular membrane. Liposomes are one of the more traditional nanocarriers, with strengths that include modularity and ease of preparation. Liposomal carriers have been used to effectively deliver a wide variety of proteins into cells, including albumin, antibodies, enzymes, and cytokines.[200,201] For example, lysine-

based cationic liposomes effectively delivered albumin and antibodies into cytoplasm via endocytosis, and the delivery efficiency of the liposome/albumin complexes can reach 99% at 37°C.[200]

Although encapsulation of protein in liposomes has high cellular transport efficiency, the amount of encapsulated protein remains a challenge. An interesting study investigated the efficiency of liposomal encapsulation of various peptides based on their theoretical pI and hydrophobicity. They showed that encapsulation efficiency varied drastically from 9% to 79% between the peptides tested.[202] This indicates the need of more studies on endosomal encapsulation before it can be used as a robust peptide delivery method.

Electroporation is mostly used to transfect primary cell lines, which are not susceptible to lipid-mediated transfection methods.[203] It utilises high-voltage electrical pulses to transiently disrupt the cell membrane. The resulting formation of nanopores allows a rapid uptake of exogenous materials. Freund et al. 2013 showed that monoclonal antibodies can be successfully delivered into a cytoplasm.[204] The delivered antibodies were extremely effective for targeting endogenous nuclear proteins. Furthermore, they showed that by optimising the electropration protocol they were able to retain a high degree of cell viability. More recently, electroporation was used to deliver various antibodies into cells to rapidly deplete cellular proteins using the Trim-Away technique.[205] However, electroporation is a low-throughput technique, and several groups are working on designing microfluidic approach which can also be used to localise the electric field to the scale of the cell.[206–209]

1.7 Targeted protein degradation

The majority of traditional therapeutics are small molecules, in which protein function is modulated by binding a functional site. As discussed previously, efforts are being made to develop peptide- and protein-based drugs to allow targeting of more proteins in the human proteome. Nevertheless, these therapeutics are aimed to occupy a functional PPI site. This requires the drug to retain a high target occupancy whereby high doses are needed and often lead to undesired side effects due to off-target binding.[210] Furthermore, patients with cancer and bacterial infections can develop resistance to these drugs.[211,212]

PROteolysis TArgeting Chimeras (PROTACs) have emerged recently as a novel therapeutic modality in drug discovery, whereby target function is inhibited by PROTAC-induced degradation.[213,214] PROTACs are hetero-bifunctional molecules consisting of two binding motifs connected by a linker. One motif is capable of binding protein of interest (POI) and the other motif recruits an E3 ligase.[215–219] PROTACs work by bringing the POI and E3 ligase into close proximity and thus allowing ubiquitination and subsequent degradation of the POI. Since the PROTAC is not degraded in this process, it can promote degradation of multiple equivalents of the POI, thus performing substoichiometrically (the first study of catalytic mechanism for PROTAC-mediated protein degradation was reported by Bondeson et al. 2015).[220] The schematic of the PROTAC mechanism of action is shown in Figure 1.15.

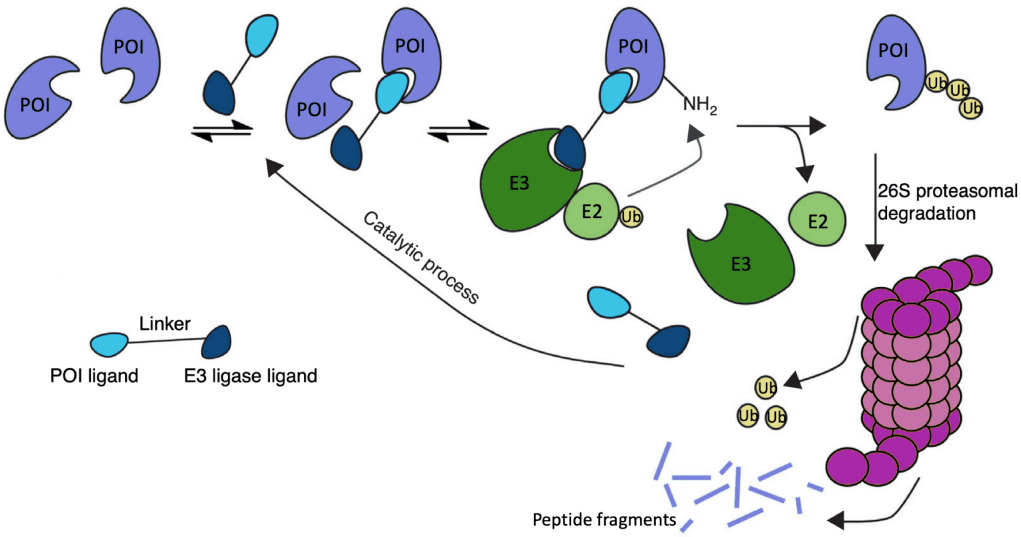

Figure 1.15: Schematic illustration of the PROTAC mechanism of action. The PROTACs bind the POI and the E3 ligase and initiates ubiquitination followed by subsequent degradation of the POI via the 26S proteasome.

The first PROTAC was developed by the Crews and Deshaies laboratories in 2001.[215] They were able to induce degradation of methionine aminopeptidase-2 (MetAp-2) by recruiting $SCF^{\beta\text{-}TRCP}$ E3 using a peptide ligand. Since then, small molecule ligands have been mostly used to recruit E3s: VHL, CRBN, cIAP and MDM2. PROTACs were shown to successfully degrade a myriad of proteins and to date, there are more than 100 reports describing the use of PROTACs for targeted protein degradation.[221] For example, PROTACs have been able to induce the degradation of a membrane-bound protein.[222] Furthermore, PROTACs were successfully used to selectively degrade highly homologous members of the kinase protein family.[223,224] Additionally, in 2017, Arvinas (Crew's PROTACs spin-out company) reported the first orally available PROTAC targeting androgen receptor that was able to induce 90% degradation in mouse xenograft studies.[225] Nevertheless, PROTACs remain limited to targets that already have small molecule ligands and have therefore not allowed us to expand the druggable proteome.

The mechanism of PROTAC-induced degradation is not yet fully understood but is known to be dependent on the formation of a ternary complex (POI-PROTAC-E3). Mathematical equations describing ternary complex formation[226,227] have been applied to the PROTAC-mediated ternary complex. These models predicted a bell-shape dependency on PROTAC concentration[228] (see Figure 1.16).

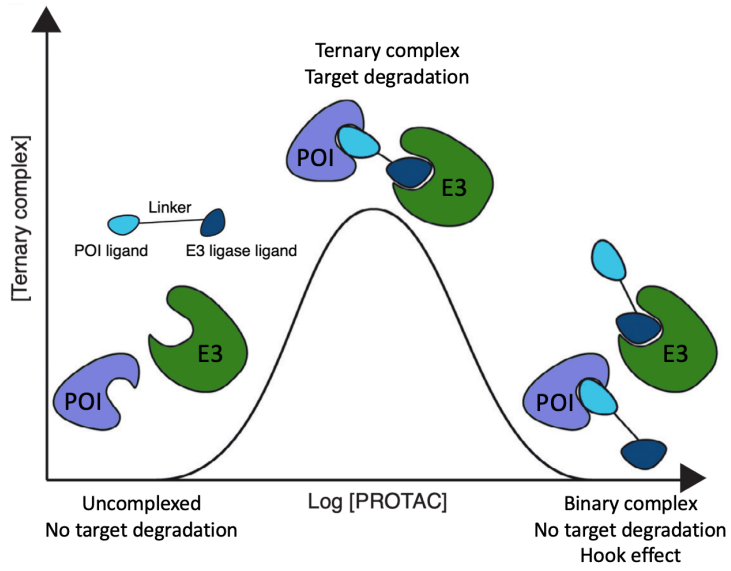

Figure 1.16: PROTAC-mediated ternary complex formation and the Hook effect. The optimal concentration of the PROTAC results in formation of the ternary complex and target degradation. However, at high concentrations of the PROTAC the Hook effect is observed where the formation of unproductive binary complexes result in no target degradation.

The optimal concentration of the PROTAC is one in which ternary complex formation is favored over the two binary complexes resulting in effective target degradation. In contrast, too high PROTAC concentrations lead to the formation of unproductive binary complexes of the PROTAC-E3 and/or POI-PROTAC, which is known as the Hook effect.[229] The Hook effect caused by high concentration of the PROTAC results in no target degradation and is widely documented in PROTACs studies.[230–234]

The first crystal structure of a ternary complex (BRD4-PROTAC-VHL) was reported by the Ciulli lab.[232] The structure revealed that the PROTAC promotes additional interactions between the E3 and POI and this positive cooperativity of the ternary complex has been shown to result in the higher PROTAC potency (see Figure 1.17). Furthermore, the Hook effect is reduced in the presence of stabilising interactions between POI and E3 due to favorable formation of the ternary complex.[231]

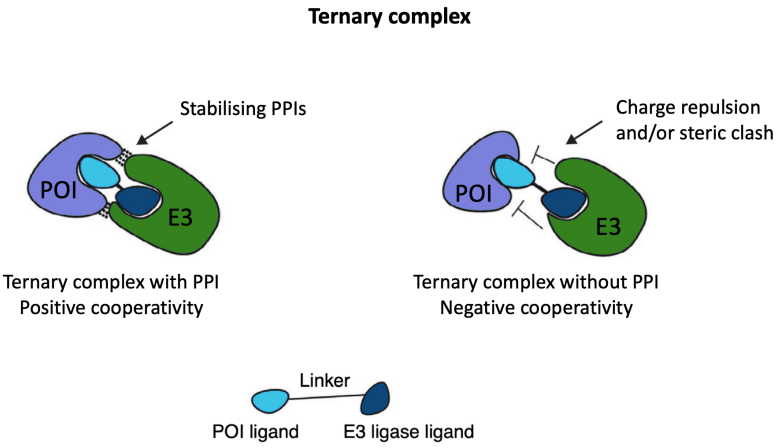

Figure 1.17: Positive and negative cooperativity of ternary complex formation. Stabilising PPIs between the POI and E3 ligase promote ternary complex formation. In contrast, charge repulsion and/or steric clash negatively affect the formation of the ternary complex.

Several studies have reported that PROTACs with relatively low binary binding affinities for the POI could nonetheless induce degradation because of favorable ternary complex formation.[224,235] For example, 11 μM ligand binding affinity for the kinase p38α was sufficient for degradation.[224] Another study reported that a higher affinity ligand for BRD4 (K_d=4 nM) was less effective than a weaker ligand (K_d=100 nM) at promoting BRD4 degradation.[235] Both studies found that this is caused by the positive cooperativity of the ternary complex formation. Similarly, Crew et al. 2018 showed that a high E3-binding affinity is not necessary for efficient PROTAC-mediated degradation.[236] This further in-

dicated that ternary complex formation might be more important than the affinity of the POI or E3 ligand. In contrast to the mentioned studies, efficient POI degradation was achieved for a selection of CRBN-based PROTAC with no or even negative cooperativity.[237] Based on current data, it is difficult to determine general principles underlying ternary complex formation. Other factors, such as the orientation of the recruited ligase and the positioning of the ubiquitin chains on the POI can determine if the POI will be degraded effectively by the 26S proteasome.

The PROTAC technology can be applied to broad scope of potential targets since a 'non-functional' ligand can be used as the POI-recruiting element in PROTAC design.[223,238] As mentioned previously, even low affinity binders (11 μM) resulted in a successful POI degradation. Thereby, small molecule based drugs previously abandoned in drug discovery programs because of low efficacy could be explored as potential POI ligands.[239] Additionally, it has been shown that the PROTAC linker length, chemical composition and attachment points can affect the selectivity and degradation profiles.[237] This means that there is a diverse library of potential PROTAC molecules to be explored.

However, with such a large scope available of potential targets it is important to choose the POI that would be receptive to protein degradation. Currently, the design and optimisation of PROTACs is laborious and time consuming. This is mostly because the techniques used to study PROTAC activity are usually measuring protein levels using end-point techniques (e.g. immunoblotting, mass spectroscopy) and are not high-throughput. Therefore, early validation of selected POIs is extremely important.

Several methods exist that can validate potential drug targets as well as aid the design of effective PROTACs. The dTAG system can be used to validate the PROTAC-mediated POI degradation and study the biological effects of its degradation without the need for a POI ligand.[240] In this study, POIs are fused to the dTag that is selectively tagged for degradation by CRBN E3. This approach was recently used to validate preclinical targets.[241] However, dTAG and similar style approaches do not offer insights into real-time PROTAC-mediated ternary complex formation and POI degradation. A new approach was developed by Promega that allows real-time monitoring for each of the steps involved in PROTAC-mediated degradation *in cellulo* from cell permeability, ternary complex formation, ubiquitination, and degradation.[242] This offers a far more high-throughput approach for PROTAC screening compared to previously used methods.

To date relatively few E3 ligases have been used for PROTACs, specifically only those belonging to the RING family (VHL, CRBN, XIAP and cIAP, Keap1, RNF4,RNF114 and MDM2).[221] This corresponds to <1% of the putative E3 ligases in the human proteome. The small number is due to the limited number of small molecule binders known to date. More studies need to be carried out to expand the scope of E3s that can be harnessed by PROTACs and that can be used in different disease conditions. In our study, instead of a linker that joins the E3- and POI-binding moieties we are exploring the use of a modular protein scaffold. This allows us to graft peptides motifs for POIs and for E3s (taking advantage of Nature's way to engage E3s) that cannot be addressed using small molecules.

1.8 Project aims

We aim to develop a macrocyclic peptide inhibitor for the SCF^{Skp2}-p27 protein interaction. Peptide therapeutics have the potential to be highly specific and potent, thus resulting in fewer side effects than small molecule drugs. Most peptide therapeutics are however used to target extracellular proteins, but a recently developed stapled peptide inhibitor of the MDM2-p53 interaction has demonstrated that they can be used to disrupt intracellular protein-protein interactions.

The workflow of this study is outlined in Figure 1.18. We are presenting here the development process of potentially therapeutic p27 peptides for biological study, from virtual design, synthesis, and their biophysical characterisation to evaluating their cellular effects in breast cancer cell lines.

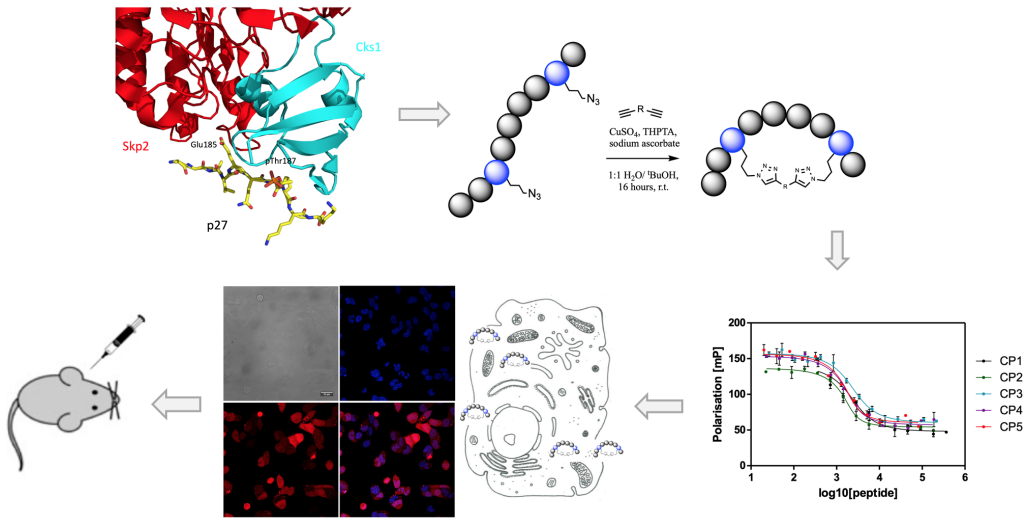

Figure 1.18: Project workflow. Based on the structure of Skp1-Skp2-Cks1-p27 we have designed 10-residue p27 peptides. Peptides were made using solid phase peptide synthesis and incorporating azido-containing unnatural amino acids. The peptides were then stapled using "Click" chemistry. The constrained peptides were then tested for binding to Skp1-Skp2-Cks1 complex using fluorescence polarisation and isothermal titration calorimetry. Peptides were also tested in a p27 *in vitro* ubiquitination assay to evaluate their effectiveness for inhibiting the activity of SCF^{Skp2} E3 ligase. Next, the highest affinity peptide was functionalised with a cell-penetrating peptide for intracellular delivery. Peptides were evaluated in the appropriate cellular assays before proceeding to establish the mouse xenograft model experiments.

Chapter 3 discusses the design process of p27 peptides, synthesis and macrocyclisation

approach. Based on the crystal structure of Skp1-Skp2-Cks1-p27$^{175\text{-}197}$ (PDB: 2AST) we designed 10-residue p27 peptides for stapling/macrocyclisation. Within the peptide, two amino acids were substituted by non-natural residues bearing azide functionalities on the side chains. These peptides were macrocyclised using a staple linker containing two alkyne functionalities via a double-click reaction recently developed by the Spring group and applied to inhibit MDM2-p53, tankyrase-axin, as well as other protein-protein interactions.[151,164,165] These macrocyclisation modifications will constrain the p27 peptide and potentially enhance its stability, binding affinity and pharmacokinetics.

In Chapter 4 we discuss the biophysical analysis of the stapled p27 peptide binding to the Skp1-Skp2-Cks1 complex. This was mainly carried out using an FP assay previously established for this interaction by the Itzhaki group.[71] Here we also present protein expression and purification protocols established to produce the Skp1-Skp2-Cks1 complex for biophysical and biochemical studies.

In Chapter 5 we explore the biological effects of p27 peptides. First, we discuss the development of an *in vitro* p27 ubiquitination assay using SCF^{Skp2} purified from mammalian cells. We then tested the ability of constrained p27 peptides to inhibit p27 ubiquitination. In addition, we also evaluated p27 peptide effects on ubiquitination of other SCF^{Skp2} substrates, p21 and N-myc. Secondly, we present three approaches for the intracellular peptide delivery: CPP attachment, electroporation and liposomal encapsulation. Finally, we show that CPP-conjugated p27 peptides are able to restore p27 levels associated with Skp2 over-expression as well as reduce proliferation of breast cancer cell line MCF-7.

In Chapter 6 we examine an alternative route to constrain the p27 peptide by grafting it onto a loop in a small stable protein scaffold. We showed that the protein containing a grafted p27 loop can inhibit SCF^{Skp2} activity in the ubiquitination assay and thereby could be used as a ligase-recruiting motif of a protein-based PROTAC. To this end, we grafted several β-catenin binding peptides onto the scaffold and pursued to examine ubiquitination and degradation of β-catenin using hetero-bifunctional proteins.

Finally, we present the ongoing efforts to crystallise the Skp1-Skp2-Cks1 complex with our constrained p27 peptides as well as the experimental outline for the future mouse xenograft experiments. Overall, these studies test whether a constrained p27 peptide can effectively target the oncogenic E3 ubiquitin ligase SCF^{Skp2} both as a direct ligase inhibitor and as a ligase-recruiting motif of a protein-based PROTAC.

Chapter 2

Materials and Methods

2.1 Chemicals

All chemicals used in this study were of analytical grade and were purchased from Sigma-Aldrich, Bio-Rad or Thermo Fisher Scientific unless otherwise stated.

2.1.1 Sterile procedure

All microbiological techniques were carried out using sterile apparatus and media under strict aseptic conditions. All media, agar, flasks, eppendorfs and tips were autoclaved (120 °C, 1 atm, 20 min) prior to use.

2.1.2 LB plates

Agar plates were prepared using Luria Bertani broth (10 g/L tryptone, 5 g/L yeast extract, 5 g/L sodium chloride) with 1.5 % w/v agar. Plates were stored at 4°C and used within 1 week of preparation.

2.1.3 Culture media

Luria Bertani (10 g/L tryptone, 5 g/L yeast extract, 10 g/L sodium chloride) growth media was dissolved in distilled water and pH adjusted to pH 7.5.

2.1.4 Antibiotics

Antibiotic stocks were prepared using distilled water and sterilised with 0.22 μm filter (Sartorins). Antibiotics were included in agar and growth media at the following concentrations: 100 μg/mL of ampicilin (Amp), 30 μg/mL of kanamycin (Kan).

2.2 Molecular biology techniques

2.2.1 Plasmids

Constructs containing *Skp2* genes

Plasmids containing *skp2* full length, *skp2* with F-box deleted and *skp2* with a deleted N_{term} and F-box genes for mammalian expression generated in this study are listed in Table 2.1.

Table 2.1: Plasmids containing *skp2* genes generated in this study.

Construct	Vector	Insert length (aa)	Source DNA
Skp2WT-Flag	pcDNA3	1-424	human
Skp2-ΔFbox-Flag	pcDNA3	Δ93-144	human
Skp2-ΔN_{term}-Flag	pcDNA3	144-424	human

2.2.2 Polymerase chain reaction

Primers used to amplify *skp2* genes are listed in Table 2.2 and were synthesised by Sigma Aldrich. PCR reactions were set up on ice in autoclaved PCR tubes using VENT DNA polymerase (NEB). A typical PCR reaction is summarised in Table 2.3.

Table 2.2: Primers used to amplify *skp2* genes. F - forward primer, R - reverse primer, red - restriction enzyme recognition site.

Primer	Primer sequence 5'-3'	Restriction Enzyme
2 Step Skp2 aa141 F	GAGAACTTTCCAGACCTCACAGGTAA AAATCTGCAC	N/A
2 Step Skp2 aa93 R	ACCTGTGAGGTCTGGAAAGTTCTCTC GATTTAGCTT	N/A
Skp2 aa1 F	GTATAGAATTCTGATGCACAGGAA GCACCTC	EcoRI
Skp2 aa141 F	GCAATGAATTCTGATGGACCTCA CAGGTAAAAAT	EcoRI
Skp2 aa424 R	GTATCTCGAGTCATAGACAACTG GGCTTTTG	XhoI

Table 2.3: Reaction setup for PCR using VENT DNA polymerase.

Component	Final Concentration
10X VENT Reaction Buffer	1X
10 mM dNTPs	0.4 mM
Forward Primer	50 pM
Reverse Primer	50 pM
Template DNA	$<$ 1,000 ng
VENT DNA Polymerase	0.02 U/µL
Nuclease-Free Water	to 50 µL

Thermocycling conditions for a typical PCR are represented in Table 2.4. NEB T_m calculator was used to determine the optimal annealing temperature of the primers. PCR was carried out in PTC-225 Thermal Cycler (MJ Research).

Table 2.4: Thermal cycling conditions for PCR using VENT DNA polymerase.

Step	Temperature	Time
Initial Denaturation	95°C	3 minutes
30 Cycles	95°C	60 sec
	50°C	60 sec
	72°C	60 sec/kb
Final Extension	72°C	10 minutes
Hold	4°C	

After amplification, 5 µL of the PCR reaction were loaded on 0.75 % agarose gel (Section 2.2.3) to verify PCR product. The amplified DNA was then cleaned up using QIAquick® gel extraction kit (Qiagen) following the manufacturer's instructions and eluted with 30 µL nuclease-free water.

2.2.3 Agarose gel electrophoresis

Agarose gel electrophoresis was used to separate DNA fragments and to purify DNA. Agarose (0.75 to 1% (w/v) agarose) was dissolved in TAE (40 mM Tris pH 7.5, 0.114 % (v/v) acetic acid, 2 mM $Na_2EDTA.2H_2O$). SYBR® Safe DNA gel stain (Invitrogen) was added to a final concentration of 1X to visualise the DNA. The agarose solution was poured into a gel cast and left to solidify. 6X DNA loading buffer (Thermo Fisher Scientific) was added to the DNA samples before loading on the gel. 1kb DNA ladder (Thermo Fisher Scientific) was loaded alongside the samples to identify sizes of the DNA fragments. The gel was run at 100 V for approximately 1 h.

2.2.4 Digestion of destination vector and insert

PCR products were subjected to a double digest using appropriate restriction enzymes and recommended buffers by the manufacturer (NEB). Destination vectors were digested in parallel. In the digest mixture the final amount of restriction enzymes was less than 10 % of the total reaction volume. NEB buffer at 1X final concentration, restriction enzyme 1 and restriction enzyme 2 were added to the 50 µL of PCR product (insert). For the

vector digest, 2 units of restriction enzyme 1, 2 units of restriction enzyme 2 and NEB buffer at 1X were added to 1 to 2 µg of DNA. Nuclease free water was added to achieve a final volume of 30 µL. Double digestions were carried out at 37°C for 2 to 3 h.

After the double digest, samples were mixed with DNA loading dye at 1X final concentration and run on the 0.75 % agarose gel (Section 2.2.3). Single DNA bands corresponding to the double digested insert were cut under UV light. DNA was extracted from the gel and purified using a QIAquick® gel extraction kit (Qiagen) following the manufacturer's instructions and eluted with 30 µL nuclease-free water.

2.2.5 Ligation protocol

Gel purified double-digested insert and vector were ligated using the Rapid Ligation kit (Thermo Fisher Scientific) according to the manufacturer's instructions.

The amount of vector and insert to be ligated was calculated using the formula:

$$ng\ of\ insert\ =\ \frac{ng\ of\ vector \times kb\ size\ of\ insert}{kb\ size\ of\ vector} \times molar\ ration\ of\ \frac{insert}{vector} \qquad (2.1)$$

The vector and insert DNA were mixed together in a ratio of 1:3 to maximise the chances of successful ligation. Ligation reactions were setup on ice by mixing 100 ng of vector, the calculated ng of insert, rapid ligation buffer at 1X final concentration, 2 units of T4 DNA Ligase, and nuclease free water to 10 µL. After incubation for 15 min at room temperature, 10 µL were transformed into competent DH5α cells (Invitrogen) as described (Section 2.2.6) and plated out on LB agar plates containing appropriate antibiotic(s).

2.2.6 Transformation

Between 50 ng and 150 ng of plasmid DNA or 10 µL of ligation reaction (Section 2.2.5) were added to 50 µL of ice-thawed *E. coli* competent cells (DH5α only for cloning and propagation purposes, other strains used for protein expression (C41, FB810, BLR)) and left to incubate on ice for 30 min. Bacteria were subjected to a heat-shock for 30 sec in a 42°C water bath and immediately placed on ice for 5 min prior to the addition of 80 µL of SOC. Bacteria were incubated at 37°C with shaking for 1 h. 100 µL of bacteria cells were plated on the LB-agar plate containing appropriate antibiotic(s) and incubated at 37°C

overnight. After colony growth, plates were wrapped with parafilm and stored at 4°C for no longer than 1 month.

2.2.7 Purification of plasmid DNA

A single colony was picked from the transformed bacteria plates with an inoculation loop and transferred into a 50 mL falcon tube containing 5 mL of LB with appropriate antibiotic(s). The tube was incubated in a shaker at 37°C at 220 rpm overnight and then cells were pelleted at 3,220 g at 4°C for 15 min and the supernatant was discarded carefully. Plasmid DNA was extracted and purified using a QIAprep® Spin Miniprep Kit (Qiagen) as per manufacturer's instructions and eluted with 30 to 50 µL of nuclease-free water and stored at -20°C.

2.2.8 DNA quantification

The concentration of DNA was measured using a NanoDrop 2000 (Thermo Scientific) by measuring light absorption at 260 nm.

2.2.9 Confirmation of construct integrity

Purified plasmid DNA was digested with appropriate endonucleases to confirm insertion of the gene into the vector. Control digest was set up as follows: 250 ng of plasmid DNA was mixed with 1 unit of restriction enzyme 1, 1 unit of restriction enzyme 2, NEB buffer (1X) and nuclease free water to 10 µL. After 1 h incubation at 37°C, reaction mixture was loaded on an agarose gel to identify sizes of DNA fragments (Section 2.2.3). One positive clone after control digest of each construct were sent for sequencing. The study was proceeded with 100 % verified clones.

2.3 Protein expression and purification in *E. coli*

Plasmids containing His-Cks1 and GST-Skp2-Skp1 proteins were kindly passed on by Dr Kelly (Itzhaki's Lab).

2.3.1 Preparation of competent cells

Protein production was carried out using chemically competent *E. coli* C41 cells prepared in the lab (derived from BL21 cells). C41 cultures were grown in 5mL LB media in 50 mL falcon tube overnight at 37°C shaking at 220 rpm. The following day the pre-culture was diluted in a 1:100 ratio with fresh autoclaved LB media and grown for 2-3 h at 37°C at 220rpm until OD_{600} of 0.3 was reached. Cultures were incubated on ice for 5 min and then centrifuged at 3000 g for 10 min at 4°C. The pellet was resuspended in 50 mL of transformation buffer I (30 mM KOAc pH 5.8, 100 mM RbCl, 10 mM $CaCl_2$, 50 mM $MnCl_2$, 3 mM hexamine cobalt Cl, 15% glycerol). The resuspended mix was incubated on ice for 5 min and then centrifuged at 3000 g for 10 min at 4°C. The pellet was resuspended in 5 mL of transformation buffer II (10 mM MOPS pH 6.5, 10 mM RbCl, 75 mM $CaCl_2$, 15% glycerol). The mixture was incubated on ice for 15 min. Finally, aliquots (50 µL) were frozen in dry ice and stored at -80°C.

2.3.2 Small-scale expression and solubility assay of Cks1 and Skp1-Skp2 proteins

For each protein, different IPTG induction concentrations, growth temperature and times were tested for best protein expression and solubility using C41, Rosetta 2 and BLR *E. coli* strains.

For a starter culture, a single colony was inoculated in 5 mL LB in a 50 mL falcon tube containing appropriate antibiotic(s) and grown overnight at 37°C at 220 rpm. The following day the pre-culture was diluted 1:100 in fresh 5 mL of LB with antibiotic(s) and grown at 37 °C at 220 rpm until OD_{600} of around 0.6 and then induced with either 0.1 mM, 0.2 mM or 0.5 mM of IPTG. After induction with IPTG, the temperature was reduced to 16°C, 20°C or 30°C and the cultures were grown for 3 h, 5 h or overnight at 220 rpm.

Cultures were centrifuged for 15 min at 3,220 g at 4°C. The supernatant was carefully removed, and the pellet was resuspended in 1 mL binding buffer (Table 2.5). Cells were incubated on ice for 20 min followed by sonication for 5 min using a 30 sec on/off cycle. 10 µL were taken for analysis of the total protein sample before being centrifuged at 10,600 g at 4°C for 10 min to remove insoluble proteins. Total protein sample and supernatant, containing soluble proteins, were analysed by SDS-PAGE (Section 2.3.10) to evaluate

protein expression and solubility levels.

After identification of the best expression strain and media conditions in a small scale approach, protein purification was then carried out on a large scale.

2.3.3 Large-scale expression of Cks1 and Skp1-Skp2 proteins in *E. coli*

Plasmids were transformed into C41 *E. coli* strain and cultured in 5 mL LB medium with antibiotic(s). Overnight starter culture was then diluted 1:100 in a fresh LB medium with antibiotic(s) and grown for 4-5 h. This culture was used to inoculate 500 mL LB medium with antibiotic(s) (1:100) for large scale expression in a 2 L erlenmeyer flask. Cultures were grown at 37°C at 220 rpm until OD_{600} reached 0.6 and then induced with 0.2 mM IPTG and grown overnight at 16°C for His-Cks1, or induced with 0.5 mM IPTG and grown overnight at 25°C for GST-Skp2-Skp1. Cells were harvested by centrifuging at 4,500 g at 4°C for 20 min (Bechman-Coulter). Supernatant was carefully removed and cells were resuspended in a small amount of phosphate buffered saline (PBS) followed by further centrifugation at 4,500 g at 4°C for 10 min. Supernatant was discarded and pellets were stored at -20°C until needed.

2.3.4 Bacterial cell lysis

Pellets were resuspended in binding buffer (Table 2.5), (approximately 3 mL of binding buffer per gram of cell pellet) with a protease inhibitor cocktail tablet (Roche) prepared following the manufacturer's guidelines. Resuspended cells were incubated on ice with frequent shaking for 30 min. Cells were lysed by high pressure homogenisation, sample was passed several times (Avestin Emulsiflex C5). The cell lysate was cleared by centrifugation (43,150 g, 50 min, 4°C). The supernatant, containing soluble proteins, was filtered through a 0.45 μm filter (Sartorius).

Proteins were purified using two different chromatography techniques - affinity and size exclusion. All purification steps were carried out at 4-10°C to ensure protein stability. Buffers used for protein purifications are listed in Table 2.5.

Table 2.5: Buffers used for purification of His-Cks1 and GST-Skp2-Skp1.

Buffer	Buffer Composition
Binding (His-Cks1)	50 mM Tris-HCl pH 7.5, 150 mM NaCl, 30 mM imidazole, 1 mM DTT
Binding (GST-Skp2-Skp1)	50 mM Tris-HCl pH 7.5, 150 mM NaCl, 10% w/v glycerol, 1 mM DTT
Elution (His-Cks1)	50 mM Tris-HCl pH 7.5, 150 mM NaCl, 350 mM imidazole, 1 mM DTT
Elution (GST-Skp2-Skp1)	50 mM Tris-HCl pH 7.5, 150 mM NaCl, 10% w/v glycerol 10 mM glutathione, 1 mM DTT
SEC/Dialysis	50 mM Tris-HCl pH 7.5, 150 mM NaCl, 1 mM DTT

2.3.5 Affinity purification of His_6-tagged Cks1

Cleared lysate was loaded onto 1 - 3 mL of Ni-NTA resin (Qiagen) pre-equilibrated with the binding buffer in a poly-prep chromatography tube (Bio-Rad). The resin was allowed to spin gently on a rotating wheel for 2 h to allow efficient binding of the 6-histidine tagged protein. After incubation with the resin, unbound proteins were allowed to flow through. The resin with the bound protein was washed with 40 column volumes (CV) of lysis buffer and then eluted in 1 mL fractions in elution buffer. Protein concentration was measured by the UV-Vis absorbance at 280 nm with NanoDrop 2000 (Thermo Scientific) and the purity was analysed by SDS-PAGE (Section 2.3.10).

Affinity chromatography allows the separation of molecules based on reversible interactions of the target protein with the ligand in a column matrix. In this work, proteins were expressed as hexahistidine tagged fusions and purified using immobilised metal affinity chromatography (IMAC). In IMAC, a solid matrix is coupled with divalent metal cations e.g. Ni^{2+} immobilised with nitrolotriacetic acid (NTA) on agarose beads. The technique takes advantage of His and Cys side-chain interactions with divalent transition metal cations.[243] After cell lysis, the soluble protein fraction is loaded on an IMAC column. The bound protein is subsequently eluted using buffer containing a high concentration of

imidazole. Imidazole is a competitive inhibitor for histidine-tagged protein and displaces the bound protein.

2.3.6 Affinity purification of GST-tagged Skp1-Skp2 complex

Cleared lysate was loaded onto 0.5 to 2 mL of Glutathione Sepharose beads (GE Healthcare) pre-equilibrated with the binding buffer in a poly-prep chromatography tube (Bio-Rad). The resin was allowed to spin gently on a rotating wheel for 2 h (at 4°C) to allow efficient binding of GST-Skp2-Skp1. After incubation with the resin, unbound proteins were let to flow through. The resin with the bound protein was washed with 40 CV of lysis buffer and then eluted in 5-10 mL fractions in elution buffer (each elution was incubated on beads for 5 min). Protein concentration was measured by the UV-Vis absorbance at 280 nm with NanoDrop (Varian) and the purity was analysed by SDS-PAGE (Section 2.3.10).

2.3.7 Size-exclusion chromatography

SEC purifications were carried out on an AKTA Purifier (GE Healthcare) following manufacturer's guidelines. Concentrated protein was passed through 0.45 μm filter (Sartorins) and then injected onto HiLoad^{TM} 26/60 Superdex^{TM} 75 column or HiLoad^{TM} 16/60 Superdex^{TM} S75 column pre-equilibrated with SEC buffer (Table 2.5). The protein was eluted from the column isocratically. The elute was collected in 1 or 2 mL fractions which were further analysed by SDS-PAGE (Section 2.3.10). Fractions containing pure protein of interest were pooled together and concentrated. Aliquots of 0.5 to 1 mL of concentrated protein (60 μM for His-Cks1 and 130 μM for GST-Skp2-Skp1) were flash-frozen using liquid nitrogen and stored at -80°C until further studies.

Size exclusion chromatography (SEC) is a method used to separate molecules according to differences in size.[244] The column is packed with a gel filtration resin, a porous matrix composed of spherical particles. Unlike affinity chromatography, molecules should not bind the chromatography medium. As the sample moves through the column, molecules diffuse in and out of the pores of the matrix. Smaller molecules move further into the pores than larger molecules and take longer to pass through the column. Larger molecules elute from the column first, followed by molecules with a smaller hydrodynamic radius.

2.3.8 Purification of TPR proteins

Plasmids containing mono- or bi-functional or non-functionilised TPRs were transformed into C41 *E. coli* cells and plated overnight. 2xTY media (15 mL) was aliquoted into 50 mL tubes with appropriate antibiotics. Several colonies were picked and inoculated. Cells were grown at 37°C at 220 rpm. When 0.6 of OD_{600} was reached protein production was induced with 0.5 mM IPTG. After 3-5 h cells were pelleted and resuspended in 1 mL of BugBuster Mastermix (Novagen) solution. After 20 min of incubation with agitation at room temperature transparent solution was achieved. This clear solution indicates that cell pellet has been successfully solubilised. The lysate was then centrifuged at 19,000 g for 1 min at room temperature. Supernatant was added into 100 µL of pre-equilibrated Ni-NTA agarose beads and incubated for 1-2 h. The beads were washed 4 times with 1 mL of each buffer. First wash contains 10% BugBuster solution and 30 mM imidazole in the purification buffer. Here we used 50 mM Tris-HCl pH 7.5, 150 mM NaCl. The three following washes contained purification buffer with 30 mM imidazole. Extensive wash needed to remove detergent present in the BugBuster solution. Protein was eluted with a single step of 1 mL of purification buffer containing 350 mM imidazole. Imidazole was then removed with a NAP-5 column (GE healthcare).

2.3.9 Expression and purification of TPR proteins in pTriExMOD vector

E. coli C41 cells were transformed with nonfunctionalised, mono- or bi- functional 3TPR or 6TPR containing plasmid and plated overnight. Several colonies were picked and inoculated and cells were grown at 37°C at 220 rpm. When 0.6 of OD_{600} was reached protein production was induced with 0.2 mM IPTG overnight at 18°C. Cells were pelleted by centrifugation at 5000 g at 4°C for 15 min. Pellets were resuspended in binding buffer (Table 2.6), (approximately 3 mL of binding buffer per gram of cell pellet) with a protease inhibitor cocktail tablet (Roche) prepared following the manufacturer's guidelines. Resuspended cells were incubated on ice with frequent shaking for 30 min. Cells were lysed by high pressure homogenisation, sample was passed through several times (Avestin Emulsiflex C5). The cell lysate was cleared by centrifugation (43,150 g, 50 min, 4°C). The supernatant, containing soluble proteins, was filtered through a 0.45 µm filter (Sartorins). Cell lysate was loaded on HisTrap Excel (5 mL) column using ÄKTA pure purification system (GE Healthcare), washed with wash buffer until UV stabilised (no more protein

was coming off) and then eluted step-wise with the elution buffer. Eluted protein was passed through a HiLoad 16/600 Superdex 75 PG size exclusion column. Peak fractions were pooled and concentrated using Amicon Ultra-4 centrifugal filter units (Millipore). Protein aliquots were frozen and stored at -80°C.

Table 2.6: Buffers used for purification of 3TPR and 6TPR constructs.

Buffer	**Buffer Composition**
Binding	50 mM Tris-HCl pH 7.5, 300 mM NaCl, 10 mM imidazole, 5% glycerol
Wash	50 mM Tris-HCl pH 7.5, 300 mM NaCl, 60 mM imidazole, 5% glycerol
Elution	50 mM Tris-HCl pH 7.5, 300 mM NaCl, 350 mM imidazole, 5% glycerol
SEC	50 mM Tris-HCl pH 7.5, 150 mM NaCl

2.3.10 Evaluation of proteins by electrophoresis

SDS-PAGE was used to monitor expression levels and purity of the proteins throughout the purification procedure. Samples were mixed with 2X LaemmLi loading buffer and heated at 95 °C for 5 min prior to loading onto polyacrylamide gel. Proteins were then separated by electrophoresis in running buffer at 200 V for Coomassie staining and 120 V for immunoblotting in a vertical protein electrophoresis system (Bio-Rad). 3 µL of Precision Plus Protein^{TM} Standards Dual Color marker (Bio-Rad) was run alongside samples. The gels were run for approximately 1 h 45 min until the bromophenol dye reached the end of the gel and stained using InstantBlue Coomassie stain (Expedeon) as per manufacturer's instructions. Gels were casted in a Bio-Rad casting system using ProtoGel buffers (National Diagnostics) following manufacturer's guidelines.

Sodium dodecyl sulfate polyacrylamide gel electrophoresis (SDS-PAGE) is used to separate and analyse proteins based on their ability to move within an electric current. Migration of the proteins through the gel depends on the length of their polypeptide chains and their molecular weights. SDS detergent is added to denature the secondary and tertiary protein

structures. SDS coats the protein and imparts negative charge across the polypeptide chain. Therefore, proteins can be separated based mainly on the molecular weight. Larger proteins migrate across the gel more slowly than the smaller proteins.

2.3.11 Protein quantification

Concentration of the protein was determined using NanoDrop 2000 (Thermo Scientific) by measuring light absorption at 280 nm. Concentration of the protein was calculated using the Beer-Lambert law:

$$c = \frac{A}{\epsilon d} \tag{2.2}$$

where c is molar concentration (mol L^{-1}), A is the absorption, d is the path length of light (cm) and ϵ is the molar extinction coefficient of the protein (L mol^{-1} cm^{-1}). For the proteins, ϵ is the sum of the extinction coefficients of the absorbing species: tyrosine, tryptophan and disulphides and was calculated in ExPASy. Extinction coefficients of the most commonly used proteins in this study are summarised in Table 2.7.

Table 2.7: Extinction coefficients of the most commonly used proteins in this study.

Protein	**Extinction coefficient ($M^{-1}\times$ cm^{-1})**
His-Cks1	15,930
Cks1	15,930
GST-Skp2-Skp1	96,830
Skp2-Skp1	53,970
GST-Skp2-Skp1-Cks1	112,760
Skp2-Skp1-Cks1	69,900

2.4 Peptide synthesis and characterisation

p27-binding peptides were synthesised manually on H-Ramage ChemMatrix resin (Sigma-Aldrich). This resin allows loading of 0.49 mmol/g. Peptide synthesis was carried out on

0.125 mmol scale with 255 mg of resin using a Vac-Man Laboratory Vacuum Manifold (Promega) according to Fmoc-based solid-phase peptide synthesis (SPPS) methods.[245] Cell penetrating peptide and p27 with cell penetrating peptide sequence attached were synthesised on H-Ramage ChemMatrix resin (Sigma Aldrich), on a CEM Liberty Blue Peptide Synthesiser (p53 lab, A*STAR) following manufacturer's instructions.

The following peptides were purchased from Cambridge Peptides Ltd: Pep1: AGS(X2)EQ T(phos)P(X4)-K, Pep2: AGS(X2)EQT(phos)P(X3)K, Pep3: AGSVE(X3)T(phos)P(X4)K, Pep4: AGSVE(X2)T(phos)-P(X3)K, Pep5: AGSVE(X2)T(phos)P(X2)K, where X2: L-azidohomoalanine; X3: L-azidoornithine; X4: L-azidolysine.

2.4.1 Manual peptide synthesis

Before the first coupling, resin was left swelling in dimethylformamide (DMF) for 10 min. Fluorenylmethoxycarbonyl (Fmoc) protected amino acid (5 equiv.) was dissolved in N-methyl-2-pyrrolidone (NMP) and mixed with 1-[bis(dimethylamino)methylene]-1H-1,2,3-triazolo[4,5-b]pyridinium 3-oxide hexafluorophosphate, also known as hexafluorophosphate azabenzotriazole tetramethyl uronium (HATU) (5 equiv.) and 1-hydroxy-7-azabenzotriazole (HOAt) (5 equiv.) and N,N-diisopropylethylamine (DIPEA) (1.7 equiv.). The mix was incubated for 7 min before adding it onto the resin. After 1 h of coupling reaction the resin was drained and washed 3 times with DMF. Fmoc was deprotected with 20% piperidine in DMF for 10 min and then the resin was washed 5 times with DMF. Steps were repeated for the addition of amino acids from $C_{terminus}$ to the $N_{terminus}$ until full sequence was achieved. When methoxy trityl (Mtt) lysine was used for 6-carboxyfluorescein (FAM) attachment, lysine was deprotected with 5% v/v trifluoroacetic acid (TFA) in dichloromethane (DCM) for 5 min. Deprotection was repeated 3 times with three DCM washes in between. Before continuing with FAM attachment, any excess TFA was neutralised with DIPEA (4 equiv. in DCM). FAM was then coupled using the same protocol as amino acid coupling but the step was extended to overnight. Reaction tube containing FAM labelled peptide was wrapped in foil in all steps following FAM addition to avoid degradation of the fluorophore. $N_{terminus}$ was acetylated as the last step leaving the resin in acetic anhydride (10 equiv.) and DIPEA (10 equiv.) mix in DMF for 1 h. Peptides were cleaved from the resin by shaking the resin in a mix of TFA (92.5%, v/v), triisopropylsilane (2.5% v/v), DCM (2.5% v/v) and water (2.5% v/v) for 2 h. The eluate was then collected and peptide precipitated with diethylether. Peptide was dissolved in a mix of water and acetonitrile

and the mass of the peptide was confirmed by liquid chromatography–mass spectrometry (LC-MS). The crude mixture was lyophilised (Labconco Freezone Plus 4.5 L) and purified on a preparative high-performance liquid chromatography (HPLC) Shimadzu LC-20AP using Phenomenex Gemini-NX 5u, C18 110 Å, AXIA packed (250 x 30 mm) column, eluting with a linear gradient system (solvent A: 0.05% v/v TFA in water, solvent B: 0.05% v/v TFA in acetonitrile).

2.4.2 Peptide macrocyclisation

All solvents were degassed for 1 h prior to use. A solution of copper sulfate ($CuSO_4$, 1 equiv.), sodium ascorbate (NaAs, 3 equiv.) and tris(3-hydroxypropyltriazolylmethyl)amine (THPTA, 1 equiv.) in H_2O was added to a sealed reaction flask containing diazido-peptide (1 equiv.) and dialkynyl linker (1.1 equiv.) in 1:1 water/*t*-butanol (2 mL). The mixture was stirred at room temperature for 16 h. Progress of the reaction was monitored on LC-MS. Another portion of the linker and catalysts was added if the reaction was not completed after 16 h. The mass of the macrocyclised peptide was confirmed by LC-MS, and the crude was lyophilised. No IR absorption associated with the azido group was found. Peptide used in this study, including sequences and their molecular weights pre- and post-'click' reaction, are summarised in Table 2.8.

2.4.3 Peptide purification using HPLC

HPLC was performed on semi-preparative HPLC Agilent 1260 Infinity using a Supelcosil ABZ+PLUS column (250 mm × 21.2 mm, 5 μm). Samples were run at the flow rate of 20 mL per min, at 25°C. Gradient method was as follows: MeCN/H_2O (0.01% TFA) 5% - 50% for 20 min, 50% for 1 min, 5% for 1 min. Absorbance was monitored at 254 nm and 220 nm. Mass of the macrocyclised peptides was confirmed by LC-MS.

Table 2.8: List of peptides synthesised and their molecular weight (MW) pre- and post-'click' reaction. Where X2: L-azidohomoalanine; X3: L-azidoornithine; X4: L-azidolysine; Ahx: amino hexanoic acid; T(phos): phosphothreonine; FAM: 6-carboxyfluorescein; TAMRA: 5-carboxytetramethylrhodamine; PM: phospho mimetic, where glutamic acid, E is used instead of phosphothreonine.

Name	Sequence	MW pre-'click' (g/mol)	MW post-'click' (g/mol)
CP1	AGS(X2)EQT(phos)P(X4)K	1219.4	1383.4
CP2	AGS(X2)EQT(phos)P(X3)K	1205.4	1369.4
CP3	AGSVE(X3)T(phos)P(X4)K	1204.4	1296.4
CP4	AGSVE(X2)T(phos)P(X3)K	1176.6	1268.6
CP5	AGSVE(X2)T(phos)P(X2)K	1162.6	1254.6
Ala variant	Ac-AGSVAQAPKA-NH_2	939.51	N/A
Linear	Ac-AGSVEQT(phos)PKK-NH_2	1164.55	N/A
D linear	Ac-DGSVEQT(phos)PKK-NH_2	1208.54	N/A
D CP2	Ac-DGS(X2)EQT(phos)P(X3)K-NH_2	1247.50	1411.50
DR CP2	Ac-DGR(X2)EQT(phos)P(X3)K-NH_2	1316.57	1480.57
PM linear	Ac-AGSVEQEPKK-NH_2	1070.57	N/A
D PM linear	Ac-DGSVEQEPKK-NH_2	1128.58	N/A
R PM linear	Ac-AGRVEQEPKK-NH_2	1139.64	N/A
DR PM linear	Ac-DGRVEQEPKK-NH_2	1197.65	N/A
PM CP2	Ac-AGS(X2)EQEP(X3)K-NH_2	1151.54	1315.54
PM CP1	Ac-AGS(X2)EQEP(X4)K-NH_2	1165.56	1329.56
FAM linear	Ac-AGSVEQT(phos)PKK-Ahx-K(FAM)-NH_2	1763.78	N/A
FAM CP2	Ac-AGS(X2)EQT(phos)P(X3)K-Ahx-K(FAM)-NH_2	1802.74	1966.74
CPP (Antp)	Ac-RQIKIWFQNRR-Nle-KWKK-NH_2	2267.79	N/A
CP2-CPP	TAMRA-Ahx-AGS(X2)EQT(phos)P(X3)K-Ahx-RQIKIWFQNRR-Nle-KWKK-NH_2	3838.50	4002.50

2.5 Isothermal titration calorimetry

Isothermal titration calorimetry (ITC) was used to monitor binding of peptides and TPR-p27 proteins to Skp1-Skp2-Cks1 complex. The binding affinities were determined at 10 °C. The release of heat upon binding to the complex was monitor using MicroCal VP instrument (MicroCal, Northampton, USA). Protein complex was formed on the day of measurement by mixing Cks1 and Skp1-Skp2 in 1:2 molar ratio. The complex was then further purified using SEC so that excess Cks1 was removed. The buffer used in complex purification was 50 mM Tris-HCl, pH 7.5, 150 mM NaCl and 2 mM DTT. Protein complex and peptides solutions were degassed prior to the titration experiment at 10 °C. The sample chamber and syringe were washed with water followed by buffer prior to sample loading. 3 μL of peptides or TPR-p27 (40 - 100 μM concentrations) were injected followed by 46 injection steps at 6 μL into Skp1-Skp2-Cks1 (4 - 10 μM). The concentration of Skp1-Skp2-Cks1 was determined from an aliquot of the sample chamber to account for residual buffer after a wash that might have diluted the sample. The instrument was operated as per manufacturer's instructions and data was analysed by MicroCal Origin software.

2.6 Fluorescence Polarisation assays

Fluorescence polarisation (FP) assays were performed in 96-well black microplates (Corning) on a CLARIOstar microplate reader (BMG Labtech). Excitation filter 540-20 nm, emission filter 590-20 nm and dichroic mirror LP 566 nm were used. TAMRA-labelled peptide was dissolved in water as a stock solution and the concentration determined using NanoDrop 2000 (Thermo Scientifc). Absorption was measured at 556 nm and the extinction coefficient of 5-TAMRA of 8900 L mol^{-1} cm^{-1} was used.

2.6.1 Direct FP

For direct binding assays, Cks1, Skp2-Skp1 and Cks1-Skp2-Skp1 were serially diluted 1:2 in the SEC buffer containing 0.01 % v/v Tween 20 for a 12-point titration curve in triplicate. In each well, TAMRA-labelled peptide (20 nM, 50 μL) was mixed with the serially diluted protein (for Cks1 (130 μM - 0 μM, 50 μL), for Skp2-Skp1 (60 μM - 0 μM, 50 μL), for Cks1-Skp2-Skp1 (40 μM - 0 μM, 50 μL), and incubated for 30 min at room temperature before the measurements. The data was analysed using GraphPad Prism 5.0

and the dissociation constant, K_d, was determined using the following equation assuming the ratio between the concentration of the bound and that of the total TAMRA-labelled peptide is proportional to the polarisation change:

$$FP = FP_{\min} + (FP_{\max} - FP_{\min}) \frac{L_0 + P_0 + K_d - \sqrt{(L_0 + P_0 + K_d)^2 - 4L_0P_0}}{2L_0} \quad (2.3)$$

where FP is the fluorescence polarisation, FP_{min} is the minimum FP, FP_{max} is the maximum FP, P_0 is the total concentration of protein, L_0 is the total concentration of TAMRA-labelled peptide, and K_d is the dissociation constant.

The equation was derived as follows:

$$[P][L] = K_d[PL] \quad (2.4)$$

where [P] is the concentration of the free protein in solution and thus $[P]=[P]_0$-[PL], [L] is the concentration of free TAMRA-ligand in solution $[L]=[L]_0$-[PL], and [PL] is the concentration of the bound protein and ligand, therefore equation can be rewritten:

$$([P]_0 - [PL])([L]_0 - [PL]) = K_d[PL] \quad (2.5)$$

This is then further rearranged to:

$$[PL]^2 - (K_d + [P]_0 + [L]_0)[PL] + [P]_0[L]_0 = 0 \quad (2.6)$$

Solving the quadratic equation to give the concentration of the bound [PL]:

$$[PL] = \frac{L_0 + P_0 + K_d - \sqrt{(L_0 + P_0 + K_d)^2 - 4L_0P_0}}{2} \quad (2.7)$$

Therefore the ratio between bound L ([PL]) and total L (L_0) is:

$$\frac{[PL]}{L_0} = \frac{L_0 + P_0 + K_d - \sqrt{(L_0 + P_0 + K_d)^2 - 4L_0P_0}}{2L_0} \quad (2.8)$$

Assuming the FP signal is proportional to the percentage of ligand bound Equation 2.8 is used in Equation 2.3.

2.6.2 Competition FP

For the competition FP assays, the top concentration of the macrocyclic peptide or non-phosphorylated peptide was prepared up to 5 mM in water, and serially diluted 2-fold for a 12 or 16-point titration curve in triplicate. TAMRA-AGSVEQT(phos)PKK peptide (20 nM) and Cks1-Skp2-Skp1 (4 μM) were incubated in a SEC buffer containing 0.01 % v/v Tween 20. In each well, the unlabelled macrocyclic peptide (up to 5 mM, 50 μL) was mixed with the Cks1-Skp2-Skp1-TAMRA-AGSVEQT(phos)PKK solution (50 μL), and incubated for 30 min at room temperature before the measurement was taken. The data was analysed using GraphPad Prism 5.0 using Equation 2.9 previously described by Wang.[246]

$$FP = FP_0 + (FP_{\max} - FP_0)\frac{2\sqrt{(a^2 - 3b)}cos(\frac{\theta}{3}) - a}{3K_{\mathrm{d}} + 2\sqrt{(a^2 - 3b)}cos(\frac{\theta}{3}) - a} \tag{2.9}$$

where:

$$a = K_{\mathrm{i}} + K_{\mathrm{d}} + L_0 + (x - P_0) \tag{2.10}$$

$$b = K_{\mathrm{i}}(L_0 - P_0) + K_{\mathrm{d}}(x - P_0) + K_{\mathrm{i}}K_{\mathrm{d}} \tag{2.11}$$

$$c = -K_{\mathrm{i}}K_{\mathrm{d}}P_0 \tag{2.12}$$

$$\theta = arccos\frac{-2a^3 + 9ab - 27c}{2\sqrt{(a^2 - 3b)^3}} \tag{2.13}$$

where FP is fluorescence polarisation, K_{d} is the known dissociation constant of the TAMRA-labelled peptide, K_{i} is the dissociation constant of the unlabelled macrocyclic peptide, L_0 is the total concentration of the TAMRA-labelled peptide, P_0 is the total concentration of Cks1-Skp2-Skp1 complex, x is the concentration of the unlabelled macrocyclic peptide, FP_0 is the fluorescence polarisation when no TAMRA-labelled peptide is bound to Cks1-Skp2-Skp1, and $FP_{\max}$ is the fluorescence polarisation when all TAMRA-labelled peptide is bound.

2.7 Western blot

Samples were resolved by SDS-PAGE and then transferred to PDVF membrane (Immobilon-P Membrane, 0.45 μm, Millipore) using a Pierce Power Blotter semi-dry transfer cell (Thermo Scientific). Membranes were blocked in 5% cow's milk (Marvel) in PBS-T (PBS with 0.05% Tween 20) for 1 h at room temperature. Membranes were incubated in primary antibodies (diluted in 5% milk) at 4°C overnight. Membranes were washed 3 × 5 min in PBS-T and then incubated in HRP-conjugated secondary antibody (diluted in 5% milk) for 1 h at room temperature. Membranes were washed again for 3 × 5 min in PBS-T and then developed using an enhanced chemiluminescence detection reagent (ECL low) (Amersham ECL, GE Healthcare) and exposed on X-ray film (Konica). If higher signal was required, membranes were developed using an enhanced chemiluminescence detection reagent with higher sensitivity (ECL high) (WBKLS0100, Merck Millipore). Once dark room was nonoperational western blots were developed and analysed using UVP BioSpectrum system.

2.8 Tissue culture

HEK293T, U2OS, MCF-7 and SW480 cells were cultured in Dulbecco's Modified Eagle's Medium (SigmaAldrich) supplemented with 10 % fetal bovine serum and 1 % penicillin/streptomycin (LifeTech); DLD1 were cultured in RPMI-1640 Medium (SigmaAldrich) supplemented with 10 % fetal bovine serum at 37°C with 5 % CO_2 supply.

2.9 Mammalian cell transfection

HEK293T cells were seeded in 10 cm tissue culture plates and grown to 50-80 % confluency before transfection. PEI (polyethylenimine), GeneJuice (Novagen) or Lipofectamine 2000 (Thermo Fisher Scientific) transfection reagents were used. DNA was diluted in OptiMEM (serum free media), 3 µl of transfection reagents were used per 1 µg of DNA. The mix was vortexed for 10 sec and incubated for 15 min at room temperature prior to drop-wise addition on plates. Plates were gently rocked to ensure even distribution of the transfection mix throughout the plate surface. Plates were incubated at 37°C with 5 % CO_2 supply for 36-48 h.

For preparation of p27, p21 and β-catenin, 3-5 µg of DNA were used for 10 cm dish transfection. When making SCF^{Skp2} or $SCF^{Skp2\Delta Fbox}$ 5 µg of Skp2 or Skp2ΔFbox together with 1.7 µg of each of Cks1, Skp1, Cullin1 and Rbx1 were used for one 10 cm dish.

Degradation experiments using unfunctionalised, mono- and bi- functional TPRs were carried out using HEK293T, DLD1 and SW40 cells. Cells were seeded in 6-well tissue culture plates (500,000 cells per well) and transfected the next day using the Lipofectamine2000 transfection reagent and 1- 2 µg of DNA was used per well.

2.10 Mammalian cell lysis

Cells were washed with PBS, lysis buffer added and then cells taken using cell scraper. All buffers were supplemented with 1 mM Na_3VO_4, 10 mM NaF, 1 mM phenylmethylsulfonyl fluoride (PMSF) and 1× protease inhibitors (P8340, Sigma). Cells were incubated on ice for 20-30 min with occasional vortexing and then centrifuged at 19,000 × g at 4°C for 25 min. Supernatant was transferred to a fresh tube and, where indicated, protein

concentration was quantified using a BCA protein assay kit (Pierce).

2.11 β-catenin levels western blot assay

3HA-β-catenin (1 μg) alone and with various unfunctionalised, mono- and bi- functional TPRs (1 μg) were transfected in HEK293T cells in 6-well plates using Lipofectamine2000. After 48 h post-transfection, the cells were lysed in 200 μL of 2× Laemmli buffer (128 mM Tris pH 6.8, 4 % SDS, 19.2 % glycerol, 0.02 % bromophenol blue, 10 % β-mercaptoethanol). After sample was boiled at 95°C for 20 min proteins were resolved by SDS-PAGE and immunoblotting was performed using anti-HA (C29F4, Cell Signaling Technologies) and anti-actin (A2066, Sigma-Aldrich) antibodies. Change in β-catenin levels were evaluated by the densitometry of the bands corresponding to HA-β-catenin normalised to actin levels using ImageJ.

2.12 General immunoprecipitation pull-down

Cells were transfected with HA-tagged nonfunctionalised, mono- or bi- functional TPRs. After 48 h post-transfection (as described in 2.9), the cells were lysed in KCl lysis buffer (25 mM Tris-HCl pH 7.5, 225 nM KCl and 1% NP-40) supplemented with protease inhibitors (Sigma-Aldrich) and phosphatase inhibitors (1mM Na_3VO_4 and 10 mM NaF). Cell lysate was cleared by a 14,000 g centrifugation at 4°C for 20 min. The lysates were incubated with agarose anti-HA beads (Sigma-Aldrich) for 4 h at 4°C with rocking. Beads were washed five times with lysis buffer and eluted in 2× Laemmli buffer. After sample was boiled at 95°C for 3 min proteins, were resolved by SDS-PAGE and immunoblotting was performed using appropriate antibodies

2.13 Immunoprecipitation of HA-p21, HA-p27 and HA-β-catenin

After 48 h post-transfection (as described in 2.9), the cells were lysed in lysis buffer (25 mM Tris-HCl pH 7.5, 225 nM KCl and 1% NP-40) supplemented with protease inhibitors (Sigma-Aldrich) and phosphatase inhibitors (1mM Na_3VO_4 and 10 mM NaF). Cell lysate was cleared by a 14,000 g centrifugation at 4°C for 20 min. The lysates were incubated with agarose anti-HA beads (Sigma-Aldrich) for 4 h at 4°C with rocking. Beads were

washed with lysis buffer and eluted with elution buffer (500 µg/mL of HA peptide, 10 mM HEPES pH 7.9, 225 mM KCl, 1.5 mM $MgCl_2$ and 0.1% NP-40) for 2 h at 4°C. Eluates were stored at -20°C in 5-10 µL aliquots. To evaluate the purification of SCF complexes, immunoblotting was performed and probed for anti-HA (C29F4, Cell Signaling Technologies).

2.14 Purification of SCF complexes

The SCF components Skp1, myc-Rbx1, Cullin1 and FLAG-Skp2WT or FLAG-Skp2ΔFbox were transfected in HEK293T cells using PEI. After 48 h post-transfection, the cells were lysed in lysis buffer (LB) (25 mM Tris-HCl pH 7.5, 225 nM KCl and 1% NP-40) supplemented with protease inhibitors (Sigma-Aldrich) and phosphatase inhibitors (1mM Na_3VO_4 and 10 mM NaF). Cell lysate was cleared by a 10,600 g centrifugation at 4°C for 20 min. The lysates were incubated with agarose anti-FLAG beads (Sigma-Aldrich) for 4 h at 4°C with rocking. Beads were washed with lysis buffer and eluted with FLAG elution buffer (500 µg/mL of FLAG peptide, 10 mM HEPES pH 7.9, 225 mM KCl, 1.5 mM $MgCl_2$ and 0.1% NP-40) for 2 h at 4°C. Glycerol was added to the final concentration of 15% and eluates were stored at -20°C. To evaluate the purification of SCF complexes immunoblotting was performed and probed for anti-FLAG (Sigma), anti-myc (Cell Signaling Technologies), anti-Skp1 (BD Transduction Laboratories) and anti-Cullin1 (Cell Signaling Technologies).

2.15 Quantification of SCF^{Skp2} ligase

The concentration of SCF complexes were determined against known concentrations of BSA standards by Coomassie blue staining. The densitometry of the bands corresponding to Cullin1 and Skp2WT or Skp2ΔFbox was determined using ImageJ.

2.16 *In vitro* ubiquitination assay

For the ubiquitination reactions, purified SCF complexes were used at the indicated concentrations in combination with ubiquitin mix (1X ubiquitination buffer, E1 (100 nM), E2 UBE2DE1 (UbcH5a) (500 nM), ubiquitin (20 µM), Mg-ATP (2 mM)) (Boston Biochem)

and substrate and then incubated for 90 min at 30°C water bath. Substrates were prepared as follows: HA-p27 purified from HEK293T cells or produced by *in vitro* transcription/translation (IVT), HA-p21 and 3HA-β-catenin purified from HEK293T cells (see Section 2.13). Proteins were resolved by SDS-PAGE and immunoblotting was performed using anti-HA (C29F4, Cell Signaling Technologies) or anti-p27 (C-19) (Santa Cruz Biotechnologies).

2.17 Ubiquitination assay in HEK293T cells

HEK293T cells were transfected with FLAG-Skp2 or FLAG-Skp2ΔFbox in combination with p27-HA and ubiquitin-6xHis-myc. Cells were treated with 10 μM of MG132 for 4 h prior to harvesting and cell lysis. Cells were lysed in LB buffer for 30 min on ice and then centrifuged at 10,600 g at 4°C for 20 min. Supernatants were subjected to IP with agarose-anti-HA (Sigma-Aldrich) for 4 h at 4°C. The proteins were eluted by Laemmli buffer and the eluates were resolved by SDS-PAGE and immunoblotting was performed using anti-HA or anti-p27 (C-19).

2.18 Production of Wnt-3A conditioned media

L-cells, grown to 90-95% confluence, were split 1:10 and grown in Dulbecco's Modified Eagle?s Medium (Sigma-Aldrich) supplemented with 10% fetal bovine serum and penicillin/streptomycin (LifeTech) at 37°C with 5% CO_2 supply. After 4 days medium was removed, sterile filtered (0.2 μm) and stored at 4°C. Fresh medium was added, and cells were grown for a further 3 days. Medium was removed and sterile filtered (0.2 μm). Media after 4 days and 7 days was mixed 1:1 and used as Wnt-3A conditioned media. The media was stored at 4°C.

2.19 TOPFLASH dual-luciferase reporter assay of β-catenin activity

The Wnt pathway was activated by treating HEK293T cells with Wnt-conditioned media obtained from L-cells expressing Wnt3A for 8 days. To perform the TOPFLASH assay, 10^5 HEK293T cells/well were seeded on a 24-well plate Nunclon Delta Surface plate (NUNC) and incubated overnight at 37°C, 5% CO_2. The following day, cells were transfected with

100 ng of TOPFLASH TCF7L2-firefly luciferase plasmid, 10 ng of CMV-Renilla plasmid (as internal control) and 100 ng of the TPR construct. Plasmids were mixed with 0.5 μL of Lipofectamine 2000 transfection reagent according to the manufacturer's protocol (Invitrogen). Transfected cells were allowed to recover for 8 h, then they were treated with Wnt-conditioned media (1:2 final concentration) for a further 16 h. The TOPFLASH assay was performed using the Promega Dual-Luciferase Reporter Assay System (Promega) according to the manufacturer's instructions. The activities of firefly and Renilla luciferases were measured sequentially from a single sample, using the CLARIOstar plate reader. Relative luciferase values were obtained from triplicate samples by dividing the firefly luminescence activity by the CMV-induced Renilla activity, and standard deviation was calculated.

2.20 Live-cell imaging after treatment with peptides

U2OS or MCF-7 cells were grown to 8-100 % confluency before use in all assays. Cells (10^6) were seeded in individual glass-bottom dishes (35 mm diameter, MatTek Corporation) and grown for 16 h at 37 °C, 5% CO_2 in 2 mL of DMEM (1x)+GlutaMAX-1 (Life Technologies) supplemented with 10 % v/v fetal bovine serum and 1 % penicillin-streptomycin. Cells were then incubated with TAMRA-labelled peptides (10 - 100 μM) for 4 h, and a further 0.5 hr with Hoechst 33342 nucleic acid stain (5 μg / mL) at 37 °C, 5 % CO_2, before being washed with PBS (3-5 × 1 mL) and replenished with 1 mL of HBSS (1x) (Life Technologies). Confocal images of live cells were taken at 37°C on a Leica TCS SP5 Confocal Microscope with sequential excitation at 405 nm (for Hoechst nuclear stain) and 543 nm (for TAMRA-peptide) respectively, and a differential interference contrast (DIC) channel. Images were captured at a single focal point adjusted to the nucleus, objective 60× and 40× zoom.

2.21 Peptide electroporation

All peptides were diluted to 0.5-1 mg/mL in PBS prior to electroporation. Peptide electroporation was performed using the Neon 9000 Transfection System (Thermo Fisher). U2OS or MCF-7 cells were washed with PBS and resuspended in Buffer R (Thermo Fisher) at a concentration of 8×10^7 cells/mL. For each electroporation reaction 8×10^5 cells (10 μL)

were mixed with 2 µL of peptide or PBS. The mixture was taken up into a 10 µL Neon Pipette Tip (Thermo Fisher) and electroporated using the following settings: 1400 V, 20 ms, 2 pulses. Electroporated cells were transferred to DMEM medium supplemented with 10% BSA without antibiotics. Then, cells were gently resuspended and seeded in individual glass-bottom dishes (35 mm diameter, MatTek Corporation) and grown for 3-4 h at 37 °C, 5% CO_2 until adhered to the dish. Cells then were washed 3-5 times with PBS and replinished with HBSS medium for imaging.

2.22 Liposomal peptide delivery

Liposomes were prepared by dissolving DOPE/DOTAP/DiR in chloroform in a ratio of 1/1/0.1. Chemical structures of these lipids are shown in Figure 2.1. The solution was then dried overnight inside a vacuum desiccator. The resulting lipid film was resuspended in 10 mM HEPES pH 7.4 containing p27 peptides to a 4 mg/mL lipid concentration and 1 mM peptide concentration. This dispersion was first vortexed for 1-2 min and then sonicated for 20 min at room temperature. Liposomes formed were stored at 4°C until further use.

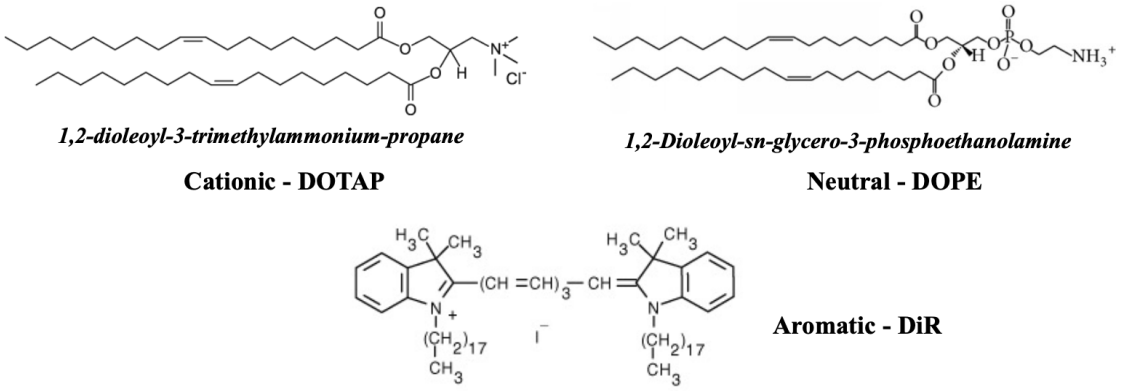

Figure 2.1: Chemical structures of lipids used to form liposomes for peptide delivery.

U2OS or MCF-7 cells were grown to 8-100 % confluency before use in all assays. Cells (10^6) were seeded in individual glass-bottom dishes (35 mm diameter, MatTek Corporation) and grown for 16 h at 37 °C, 5% CO_2 in 2 mL of DMEM (1x)+GlutaMAX-1 (Life Technologies) supplemented with 10 % v/v fetal bovine serum and 1 % penicillin-streptomycin. Cell were then incubated for 15 min with lipsome-peptide mix diluted in the DMEM media to a final concentration of 40 µM of peptide. Cells then were washed 3-5 times with PBS and replenished with HBSS medium for imaging.

2.23 Treatment of MCF-7 with p27 peptides

MCF-7 cells were seeded in 24-well plates (1×10^5/well). After 12 h, cells were transfected with 0.5 μg of either empty vector (pcDNA3.1) control or Skp2-WT and Cks1 using Lipofectamine 2000 (see Section 2.9). After another 24 h, cells were treated with TAMRA-CP2-Antp peptide for 16 h at 20 μM, and the levels of the $SCF^{Skp2/Cks1}$ substrates p21 and p27 were then determined by western blot. When MG132 treatment was carried out it was done at 10 μM for 6 h prior cell harvesting.

2.24 Cell proliferation assay

HEK293T or MCF-7 cells were seeded 4×10^5 cells/well in a 96-well plate and incubated overnight. Cell were then treated with various p27 peptides for 16 h. Finally, 10 μM BrdU was added to the plate and cells were incubated for another 4 h. Media was then removed and manufacturer's protocol of BrdU Cell Proliferation Assay Kit #6813 (Cell Signaling Technologies) followed. Briefly, fixing/denaturing solution was added (100 μL) to each well and the plate was incubated at room temperature for 30 min. Solution was then removed and anti-BrdU primary antibody was added (100 μL). After 1 h, antibody was removed and wells were washed three times with a wash buffer (100 μL each wash). HRP-conjugated secondary antibody was added (100 μL/well) and plate was incubated for 30 min at room temperature following three washes with a wash buffer. 100 μL of TMB substrate was added to each well and the reaction was stopped with an addition of 100 μL of STOP solution after 15-30 min. Absorbance was read at 450 nm on CLARIOstar microplate reader (BMG Labtech) immediately and within 30 min of adding STOP solution.

Chapter 3

Design and Synthesis of p27 Peptides

3.1 Introduction

The ubiquitin-proteasome system (UPS) is regulated by the sequential action of three enzymes (E1, E2 and E3), of which the E3 ubiquitin ligase confers substrate specificity to the reaction. Following poly-ubiquitination, substrates may be recognized and targeted for degradation by the 26S proteasome.[4] The SCF^{Skp2} E3 ligase, a member of the family of SCF ubiquitin ligases, comprises four subunits, Skp1, Cullin1, Rbx1 and F-box protein Skp2, of which Skp2 is the substrate-recognition subunit.[42] A subset of SCF^{Skp2} substrates additionally require the small adapter protein Cks1, which has been shown to form a bimolecular interface together with Skp2 for substrate recognition.[71] Skp2 is overexpressed in a range of cancers, including lymphomas, prostate and breast carcinomas, and is associated with tumor metastasis and poor prognosis.[44–46] Several $SCF^{Skp2/Cks1}$ substrates are tumor suppressor proteins, including the cyclin-dependent kinase 2 inhibitors p21, p27 and p57,[47] degradation of which positively regulate cell cycle progression.[48,49] Thus, increased levels of Skp2 and reduced levels of p27 are common in many types of cancers,[50,51] and the Skp2-p27 pathway plays a central role in breast cancer initiation and metastasis.[45] There is consequently much interest in developing inhibitors of the Skp2/Cks1-p27 interaction. Given the large bimolecular surface involved in binding p27, we chose macrocyclic peptides rather than small molecules for our inhibitor design.

Constrained peptides have been used very successfully to mimic and thereby inhibit protein-protein interactions (PPIs), and some of these peptides are already in clinical trials.[116,118,131–133,136,137,163,247] It is now well understood that constraining peptides in

their bioactive helical conformations results in greatly enhanced binding affinities relative to their unconstrained counterparts, and furthermore these so-called 'stapled' peptides also possess high stabilities and in some instance cell permeability. There are, however, very few examples of constrained non-helical peptides, in part because the design process is harder compared with helical peptides, which can be reliably constrained between i,i+4, i,i+7 or i, i+11 sites with predictable distance requirements.[164,165] Here, we used the natural p27 peptide sequence and the crystal structure of the quaternary Skp1-Skp2-Cks1-p27 complex as the starting point for our designs,[72] and we employed a two-component macrocyclization approach,[151,152,154] in which the peptide and the linker are independent variables in the design process, thereby enabling the assembly of structurally diverse peptides from a relatively small number of synthesised peptides. Such diversity is likely to be important for finding the best constraint for non-helical peptides, as the design process is not readily predictable in contrast to that of α-helical peptides.

3.2 Results and Discussion

3.2.1 Design of p27 peptides

From the published crystallographic data[72] it can be seen that the phospho-p27 peptide interacts with both Cks1 and Skp2 in a bipartite fashion (see Figure 3.1). pThr187 of p27 forms charged stabilised hydrogen bonds with Lys11, Arg20, Ser51 and Trp54 in Cks1. The side chain of Glu185 interacts with both Skp2 and Cks1. It forms hydrogen bonds with the side chains of Arg294 and Tyr346 in Skp2, and also inserts into a Cks1 pocket. The crystal structure of this complex revealed that the key post-translation modification of p27 required for recognition by the ligase, in this case threonine phosphorylation is actually interacting with Cks1 and not Skp2 itself as previously thought.

Only 10 amino acids of the phosphorylated p27 peptide are resolved in the crystal structure (amino acids 181 - 190 of p27), although a longer 24 amino acid peptide was used (175 - 198 aa of p27). The other 14 amino acids did not have interpretable electron density and are likely to be disordered.[72]

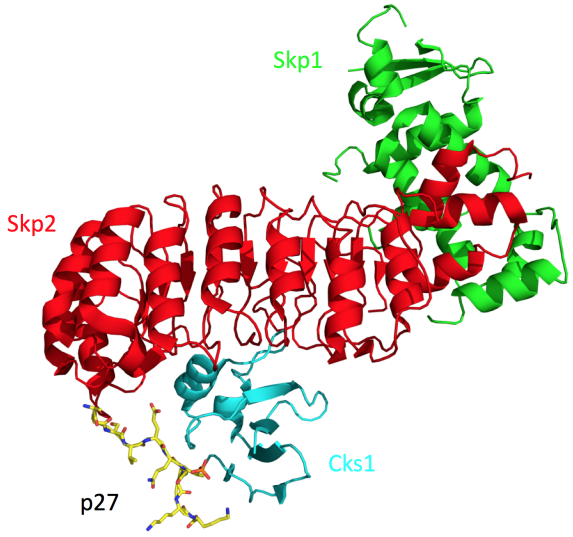

(a)

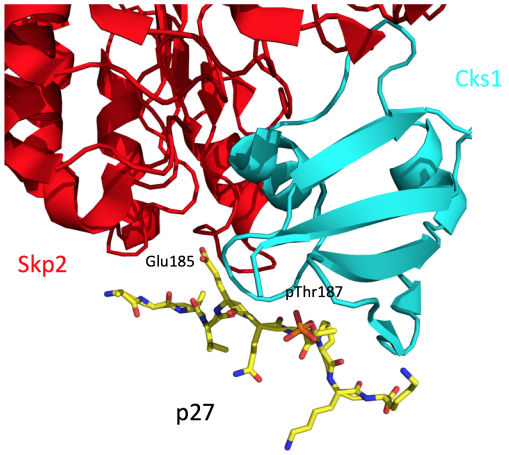

(b)

Figure 3.1: (a) Crystal structure of Cks1-Skp2-Skp1 in complex with p27 peptide. Cks1 is in cyan, Skp2 in red, and Skp1 in green. (b) Closeup of the p27-binding interface with Cks1 and Skp2. Structures were generated in PyMOL using PDB: 2AST.

Previous solution binding studies of the interaction have used this 24-residue peptide and dissociation constants of 7 μM were observed for the interaction with Cks1-Skp2-Skp1 complex.[72] This binding affinity is the same as that of full-length phosphorylated p27.[72] Based on the crystal structure we decided to synthesize a shorter 10-residue peptide and test its affinity. To start off the project quickly, we initially ordered several peptides from Cambridge Peptides Ltd so that I could focus on establishing Cks1-Skp2-Skp1 protein complex purification. First, a 10-residue peptide conjugated with a TAMRA fluorophore (TAMRA-Ahx-AGSVEQT(phos)PKK) was designed and purchased. We included the

aminohexanoic acid (Ahx) spacer (Figure 3.2) to separate the fluorophore from the binding sequence to avoid disruption of binding or unwanted interactions.

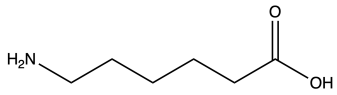

Figure 3.2: Chemical structure of aminohexanoic acid.

The fluorophore was added for use of this peptide in fluorescence polarisation (FP) assays. We then measured its binding affinity for Cks1-Skp2-Skp1 using direct FP. The observed dissociation constant (K_d) of 2.78 ± 0.19 μM indicates that this short peptide can effectively mimic the full-length protein (see Chapter Biophysical characterisation of peptides for all biophysical analysis). Based on this data we decided to only work with short 10-residue peptides since the binding affinity was as tight as the 24-residue peptide indicating that the unresolved amino acids in crystal structure are in fact not interacting with the Cks1-Skp2-Skp1 complex.

3.2.2 Macrocyclisation of p27 peptides

To constrain the 10-residue p27 peptide to potentially enhance its binding affinity, stability and pharmacokinetics, we performed macrocyclisation using 'click' chemistry. Based on the structure of the linear p27 peptide shown in Figure 3.3 and its interactions with Cks1 and Skp2 in the crystal structure (Figure 3.1) we identified positions on the peptide that are not involved in binding and that could therefore be substituted by unnatural amino acids (UAA) for cross-linking. These were found to be valine, glutamine and lysine.

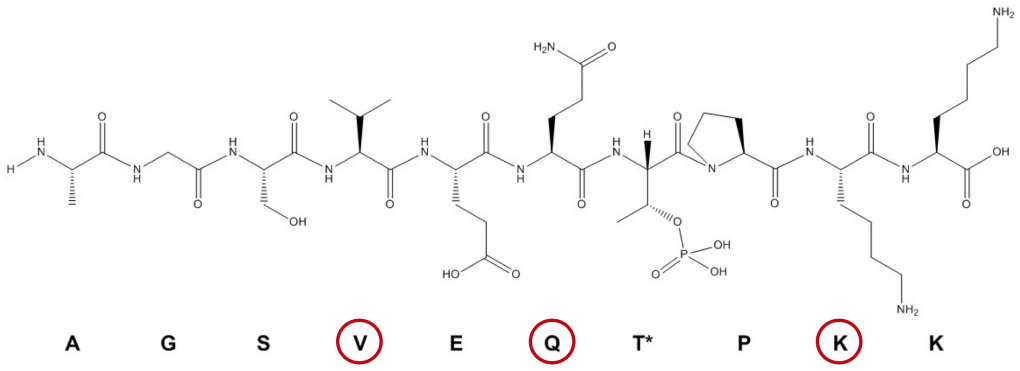

Figure 3.3: Chemical structure of linear p27 peptide. Residues likely to be substituted to UAAs are V,Q and K and are highlighted in red. These were chosen as from the crystal structure they do not appear to interact with Skp2 or Cks1.

The aim was to constrain the peptide in the turn-like conformation that it adopts in its bound form, and the sites for cross-linking, the UAA side-chain lengths and the linker were chosen accordingly. Amino acids that point away from the binding interface were chosen so as not to disrupt the binding. Sequences of the designed peptides are summarised in Table 3.1, and these peptides were ordered from Cambridge Peptides Ltd.

Table 3.1: Peptides designed for the 'click' reaction. Where X are the unnatural amino acids bearing azide functionality. X2: L-azidohomoalanine; X3: L-azidoornithine; X4: L-azidolysine.

	Peptide sequence
Pep1	AGS(X2)EQT(phos)P(X4)K
Pep2	AGS(X2)EQT(phos)P(X3)K
Pep3	AGSVE(X3)T(phos)P(X4)K
Pep4	AGSVE(X2)T(phos)P(X3)K
Pep5	AGSVE(X2)T(phos)P(X2)K

Two different pairs of residues were selected for cross-linking, one of which was five and the other three amino acids apart. The side chains of the UAAs at these sites are of varying lengths comprising between two and four methylene groups, and all have an azide group at the end to enable macrocyclisation with one of two different alkyne-containing linkers using 'Click' chemistry.[150,151] The copper(I)-catalyzed azide alkyne cycloaddition (CuAAC), the 'click' reaction, mechanism between an azide and an alkyne is shown in Figure 3.4.

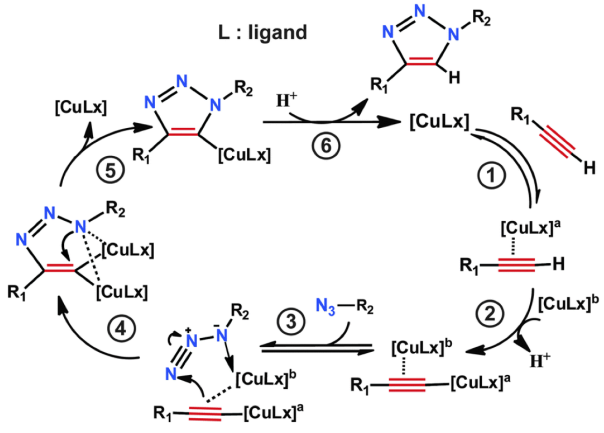

Figure 3.4: Mechanism of copper(I) catalysed 'Click' reaction.

'Click' reaction is catalysed by copper(I) and thus it is important to perform this reaction under conditions where no oxygen is present to avoid copper oxidation. Macrocyclisation of the peptides was performed using 'click' chemistry and the reaction was set up under nitrogen pressure with all oxygen removed from solutions and vials as shown in Figure 3.5 (see Materials and Methods for a full protocol).

Figure 3.5: 'Click' reaction set up in the hood. To ensure no presence of the oxygen the reaction was performed under nitrogen. This protects copper(I) from oxidation which is crucial for the reaction.

Pep1 and pep2 were macrocyclised using the longer m7N linker. The shorter m3 linker was used for pep3, pep4 and pep5 peptides. Each linker was chosen based on the modeled distance between the azide functionalities of the unnatural amino acids in the peptide. Design of the two types of constrained p27 peptides is shown in Figure 3.6.

Completion of 'click' reactions were monitored by LC-MS. m/z values of expected and observed molecular weights of the macrocyclised peptides are summarised in Table 3.2. These values indicate the correct sizes of the product corresponding to the singly 'clicked' peptides. Completion of the 'click' reaction was also evaluated using IR spectroscopy. Un-reacted peptides have a unique azide peak on the IR spectrum which can be seen prior reaction. After reaction goes to full completion and azide reacts with alkyne to form a triazole ring this peak disappears (see a representative IR spectrum in Figure 3.7).

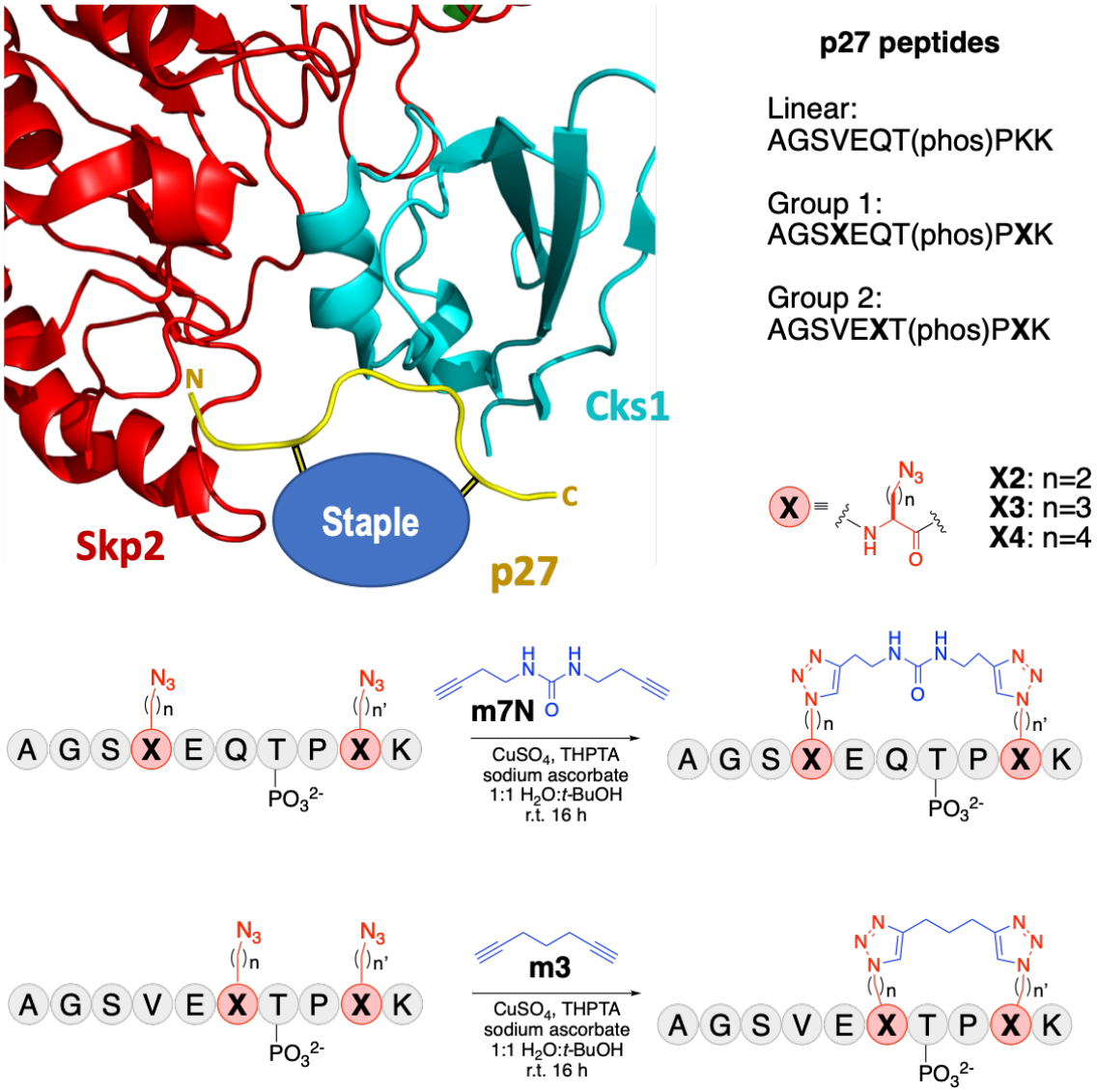

Figure 3.6: Design of constrained p27 peptides. Two groups of peptides were designed for macrocyclisation at different sites and with different linkers. "X" indicates the positions of the azido-containing unnatural amino acids. Group 1 peptides were constrained with the longer alkyne-containing m7N linker and Group 2 with the shorter alkyne-containing m3 linker. Click chemistry was used to conjugate the azido-containing unnatural amino acids of the peptide to the alkyne-containing linker to constrain it in the same bioactive conformation as observed in the crystal structure.

Table 3.2: LC-MS data of macrocyclised peptides after the 'click' reaction. Calculated m/z ratios are for $[M+2H]^{2+}$.

Peptide	Linker	m/z calculated	m/z observed
CP1	m7N	692.7	692.3
CP2	m7N	685.7	685.4
CP3	m3	649.2	648.9
CP4	m3	635.3	634.9
CP5	m3	628.3	627.9

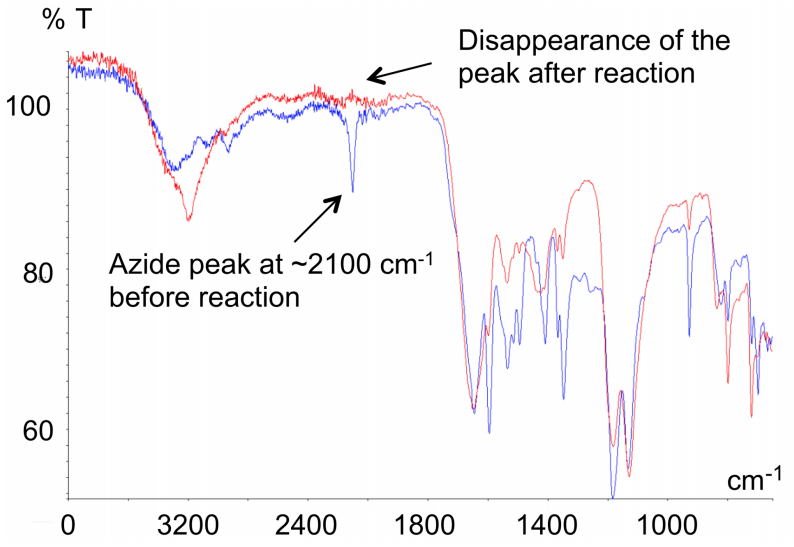

Figure 3.7: Superimposed IR spectra of the unconstrained precursor peptide (blue) and the product after click reaction (red).

After confirmation of the completion of the reaction, all peptides were freeze-dried, dissolved in water-acetonitrile mix and purified using HPLC in order to remove excess reagents of the 'click' reaction and any starting materials left. Purified fractions were further tested on LC-MS and freeze-dried. Dried peptides were dissolved in water to a final concentration of 10 mM and sent for Amino Acid Analysis (AAA) in the Department of Biochemistry to ensure correct peptide sequence and determine accurate concentrations. Predicted structures of macrocyclised peptides were drawn using ChemDraw 15.1 and are shown in Figures 3.8, 3.9, 3.10, 3.11 and 3.12. Throughout my PhD I mainly focused on investigating the effects of CP1-CP5 peptides.

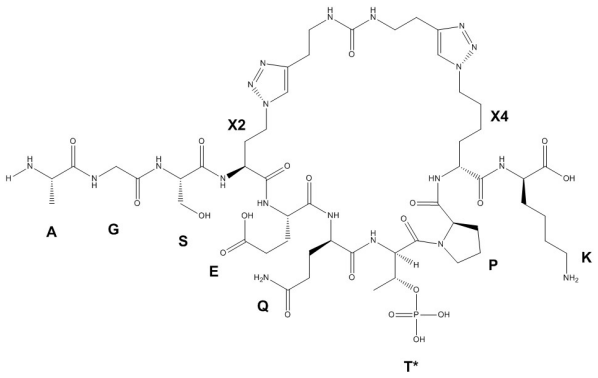

Figure 3.8: Chemical structure of CP1 peptide.

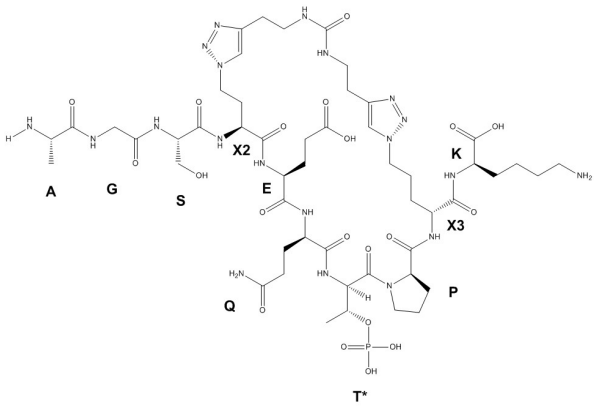

Figure 3.9: Chemical structure of CP2 peptide.

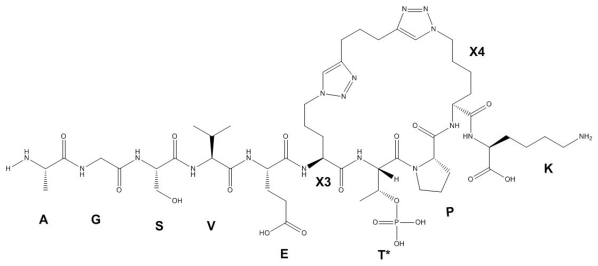

Figure 3.10: Chemical structure of CP3 peptide.

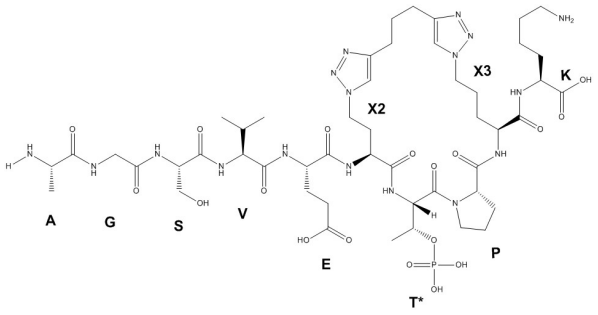

Figure 3.11: Chemical structure of CP4 peptide.

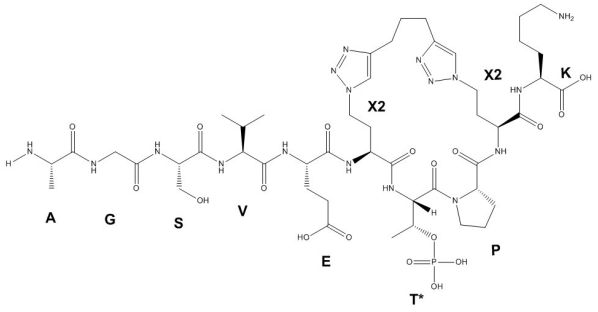

Figure 3.12: Chemical structure of CP5 peptide.

3.2.3 Other p27 peptides synthesised

During my PhD I had the opportunity to work in David Lane's p53 lab at A*STAR in Singapore. I spent 3 months there working with Dr Fernando Ferrer, who taught me manual and automated peptide synthesis. Dr Tsz Ying has taught me peptide purification using Shimadzu LC-20AP, which allowed me to purify large amounts of peptides on a fast timescale. Because I went to Singapore at the end of my second year, after already designing several high affinity peptide sequences of p27, I used these peptides as a starting point for further development during my stay at A*STAR. I was able to make around 14 peptides in large quantities, which allowed investigation of various mutations and their effects on Cks1-Skp2-Skp1 binding as well as in cells.

Table 3.3: Other p27 peptides synthesised. X2: L-azidohomoalanine; X3: L-azidoornithine; X4: L-azidolysine; Ahx: amino hexanoic acid; T(phos): phosphorylated threonine; FAM: 6-carboxyfluorescein.

Peptide	**Sequence**
Controls:	Ac-AGSVAQAPKA-NH_2
	Ac-AGSVEQT(phos)PKK-NH_2
Variations:	Ac-DGSVEQT(phos)PKK-NH_2
	Ac-DGS(X2)EQT(phos)P(X3)K-NH_2
	Ac-DGR(X2)EQT(phos)P(X3)K-NH_2
Phosphomimetic series:	Ac-AGSVEQEPKK-NH_2
	Ac-DGSVEQEPKK-NH_2
	Ac-AGRVEQEPKK-NH_2
	Ac-DGRVEQEPKK-NH_2
	Ac-AGS(X2)EQEP(X3)K-NH_2
	Ac-AGS(X2)EQEP(X4)K-NH_2
FAM peptides:	Ac-AGSVEQT(phos)PKK-Ahx-K(FAM)-NH_2
	Ac-AGS(X2)EQT(phos)P(X3)K-Ahx-K(FAM)-NH_2

All peptides listed in Table 3.3 were made using manual peptide synthesis. A peptide, in which all of the Cks1-Skp2-Skp1 contacting residues are mutated to alanines, was made as a non-binding control for the biophysical assays. The linear 10-residue peptide containing no fluorophore was synthesised to test any effects arising from the presence of the fluorophore.

All peptides were made using Ramage resin, which leaves an amide group on the $C_{terminus}$ of the peptide and also were acetylated on the $N_{terminus}$ to avoid any reactivity from the amine group. The manual peptide synthesis method is described in the Materials and Methods. Each amino acid was coupled for one hour, with the exception of amino acids following phosphorylated threonine coupling which required an additional coupling step. The bulky nature of the phosphorylated threonine side-chain sterically hindered the coupling of the next amino acid, indicated via Kaiser test. Kaiser test was used to monitor the completeness of the amino acid coupling step (yellow colour) and the presence of free amine after deprotection (dark blue colour). The presence of free primary amines results in an intensive blue colour which is generated by reaction of ninhydrin. It is of interest to note that a year later Spring and coworkers found that 10 min coupling reactions were as efficient as the one hour or even longer times that were used previously across the labs.

After cleavage from the resin, the peptides were further analysed using LC-MS and analytical HPLC to determine if the peptides were made correctly and its purity as well as acetonitrile gradient conditions needed for its further purification. A typical analytical HPLC chromatogram of p27 peptide after cleavage from the resin is shown in Figure 3.13.

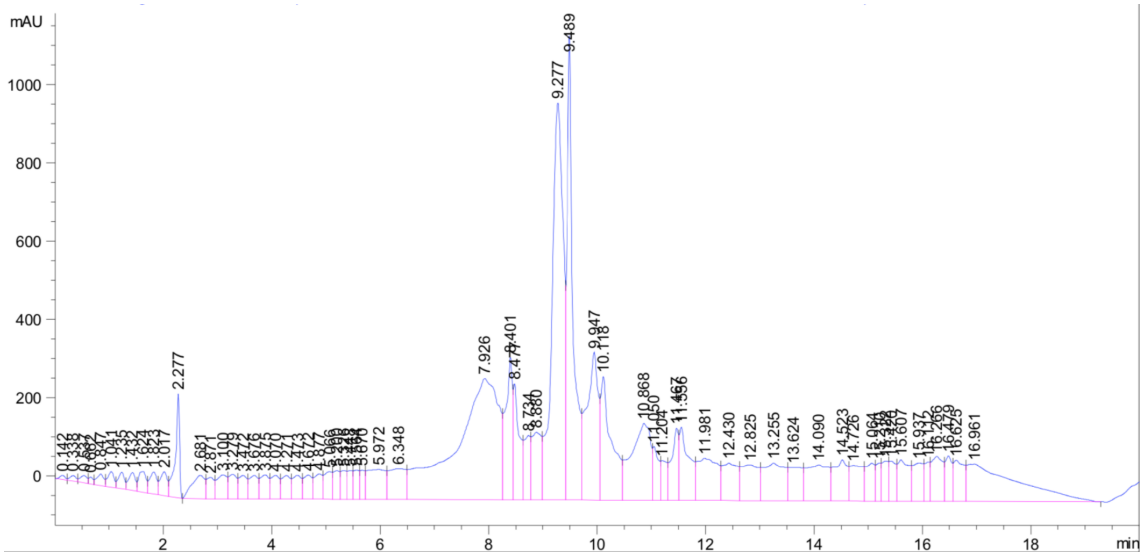

Figure 3.13: Analytical HPLC of the linear p27 peptide.

All of the p27 peptides showed a double peak (9.277 and 9.489 min in Figure 3.13), although mass spectrometry analysis indicated a clean sample. This may arise from the amino-acid composition of the p27 peptide, which has several charged residues that may affect the conformation and consequently cause different retention times. All peptides were purified to >95% purity.

We also synthesised several variants of p27 peptides introducing mutation of alanine to aspartic acid and serine to arginine (see Table 3.3). These mutations were selected after the *in silico* analysis by Dr Chandra Verma (A*STAR) to potentially increase p27 peptide binding affinity to Cks1-Skp2-Skp1 complex by creating additional charge-charge interactions. The peptides synthesised for constraining were designed based on the CP2 peptide, which was shown to have the tightest affinity for the ligase complex (see Chapter on biophysical analysis of p27 peptides).

Furthermore, peptides containing FAM fluorophore were made in order to test whether fluorophore or its position has any effect on binding. Previously purchased peptide was designed to have a TAMRA label on the $N_{terminus}$. Here we attached FAM on the $C_{terminus}$ to test if there will be any differences observed. We have also synthesised CP2-FAM labelled peptide to investigate the ability of constrained p27 peptide to enter cells without any delivery aid. This will be further monitored using confocal microscopy (see Chapter on biological effects for cellular delivery). These FAM-labelled peptides were also made manually with FAM attachment as the last step. Orthogonal chemistry was used were lysine for FAM attachment was protected with Mtt (methyltrityl), which can be cleaved using 5% TFA. The 5% acid does not affect any other protecting groups present on the peptide and only exposes lysine side chain amine for further reaction with FAM. A typical FAM labelled HPLC is shown in Figure 3.14. Due to the additional steps required to synthesise these peptides they were less pure and produced lower yields. Peptides were purified to >95% purity.

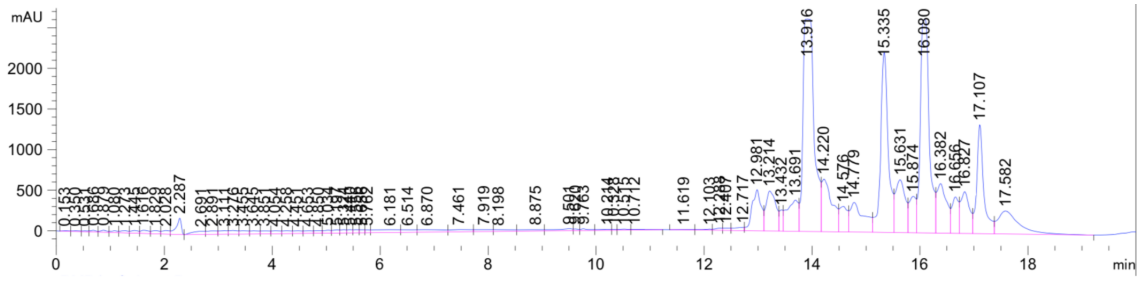

Figure 3.14: Analytical HPLC of p27 peptide labelled with FAM.

Initial data of peptide binding to the ligase complex and their performance in the *in vitro* ubiquitination assays indicated that p27 peptides could potentially be strong binders even with a glutamic acid in place of phosphorylated threonine. This potentially could be due to gaining sufficient affinity by constraining the peptide in its bio-active state (see Chapter on constraining p27 peptide in the protein scaffold). It could potentially be a very interesting discovery, since Skp2 is know to recognise p27 by its phospho motif. To investigate this further we synthesised several phosphomimetic variants to compare them to the linear and stapled phosphothreonine peptides (see Table 3.3).

3.2.4 Cell permeable peptides

It is essential that the p27 stapled peptides are able to enter cells with high efficiency. We decided to investigate conjugation to cell-penetrating peptides (CPPs) for cellular delivery. CPPs are short cationic peptide sequences that are able to transport various cargos, including proteins and peptides, into living cells. Several natural CPPs have been identified, including TAT (Trans-Activator of Transcription) protein of HIV, penetratin (antennapedia) or Antp, transporton and polyarginines (see Table 3.4).[174,175]

Table 3.4: Amino acid sequences of common CPPs.

CPP	Sequence
Penetratin (Antp)	RQIKIWFQNRRMKWKK
TAT	GRKKRRQRRRPPQ
Transporton	AGYLLGKINLKALAALAKKIL
Polyarginines	$(R)_n$; <n<12

Studies have shown that the antennapedia and TAT peptides can deliver biologically active proteins and peptides *in vitro* and *in vivo*.[179,180] A cellular uptake and toxicity examination of these CPPs indicated that polyarginine conjugates were taken up by cells most efficiently, but they also had the greatest toxicity. In comparison, Antp conjugates showed no significant toxicity even at 100 μM.[174] Antp- and TAT- mediated delivery was observed to occur via lipid raft-dependent endocytosis. More detailed mechanisms of cellular uptake of different CPPs are reviewed in Madani *et al*. 2011.[177]

In out study, Antp peptide was chosen as the preferred CPP due to these favorable properties. We have synthesisted several p27 peptides containing antp CPP sequence using automated peptide synthesiser (Liberty Blue). This was preferred over the manual synthesis because of the length of the peptide. All peptides containing CPP used in further studies are listed in Table 3.5. Antp CPP was made by itself to serve as a control in cellular assay to investigate any effects arising from CPP sequence alone as compared to CPP-labelled peptides. CP2-CPP was purchased from Cambridge Peptides Ltd, and the others were synthesised in Singapore. All these peptides have methionine amino acid exchanged for nor-leucine to avoid issues associated with methionine oxidation, which leads to formation of methionine sulfoxide and further to methionine sulfone, both of which are almost impossible to reverse. Nor-leucine has the same side-chain length as methionine and is widely used as a methionine substitute in peptide synthesis.[248]

Table 3.5: Cell penetrating peptides synthesised. X2: L-azidohomoalanine; X3: L-azidoornithine; X4: L-azidolysine; Nle: L-norleucine; Ahx: amino hexanoic acid; T(phos): phosphorylated threonine

Peptide	**Sequence**
CPP (Antp)	Ac-RQIKIWFQNRR-Nle-KWKK-NH_2
CP2-CPP	TAMRA-Ahx-AGS(X2)EQT(phos)P(X3)K-Ahx-RQIKIWFQNRR-Nle-KWKK-NH_2
CP2 D-CPP	Ac-DGS(X2)EQT(phos)P(X3)K-Ahx-RQIKIWFQNRR-Nle-KWKK-NH_2
CP2 DR-CPP	Ac-DGR(X2)EQT(phos)P(X3)K-Ahx-RQIKIWFQNRR-Nle-KWKK-NH_2

Unfortunately due to the length of these peptides they seemed to be quite tricky to synthesise. Analytical HPLC of CP2 D-CPP is shown in Figure 3.15. Both HPLC and LC-MS indicated that synthesis produced several other peptides along with peptide of interest. These CPP conjugated peptides had to undergo several HPLC purification steps to achieve >90% sample purity.

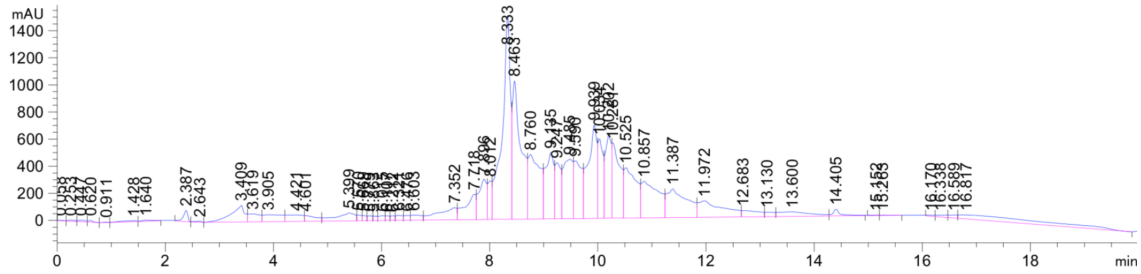

Figure 3.15: Analytical HPLC of antennapedia (CPP) labelled p27 peptide.

Peptides containing azido amino acids were then constrained using 'double-click' chemistry as described previously (see Materials and Methods). Unfortunately, very low amounts of purified CP2 D-CPP and CP2 DR-CPP were produced which hindered subsequent purification after 'click' reaction, and these peptides were not tested further due to extremely low yields. All cellular assays were performed using CP2-CPP peptide.

Chapter 4

Biophysical Characterisation of Constrained p27 Peptides

4.1 Introduction

Following the synthesis and cross-linking of the p27 peptides, we investigated their binding affinities using biophysical techniques in order to evaluate the effectiveness of stapling and of mutations introduced. p27 is known to bind to Skp2 in the presence of Cks1, and we will investigate the binding of these peptides after forming Skp2-Cks1 complex. As previously discussed in the Introduction chapter, Skp2 is a leucine rich repeat protein and the expression of Skp2 on its own is problematic. To circumvent this we have used a dual cistronic vector expressing both Skp2-Skp1 proteins together kindly donated by Prof. Brenda Schulman (Max Planck Institute of Biochemistry).

The 10-residue p27 peptides were shown to have very similar Skp1-Skp2-Cks1 binding affinity as the full-length p27 protein as well as longer p27 peptides previously published in several papers. Our approach of constraining these shortened peptides using 'double-click' method resulted in more than 10-fold increase in binding affinity, with one peptide having an almost 100-fold increase in binding affinity. This result indicates that the turn-like conformation of the bioactive state of p27 is efficiently established by the constraint.

4.2 Results and Discussion

4.2.1 Production of Skp1-Skp2-Cks1 complex

In order to investigate the binding of macrocyclic p27 peptides to Cks1-Skp1-Skp2 complex we used a fluorescence polarisation assay developed previously by the Itzhaki lab (see Materials and Methods) and isothermal titration calorimetry (ITC). It requires relatively large amounts of pure proteins, and thus the Cks1-Skp1-Skp2 complex was produced using a bacterial expression system.

Expression and solubility of His-tagged Cks1 and GST-tagged Skp2-Skp1 proteins were first trialled on small-scale conditions. Protein expression was induced with IPTG. A number of *E. coli* strains were tested (Rosetta2, BL21 (DE3), C41 (DE3), C43 (DE3)), these strains are certain codon optimised and C41 and C43 cells are designed for toxic protein expression. By testing different *E.coli* strains it allowed us to fine tune the protein expression. This was particularly important for Skp2-Skp1 proteins where slow expression allowed correct folding and resulted in much greater yields than previously seen in the Itzhaki lab. Different IPTG concentrations, induction temperature and incubation times were also tested. After determination of the best conditions, protein expression was scaled up, and the optimised protocols for large-scale purification of the proteins are summarised in Materials and Methods. After proteins were produced separately the Skp1-Skp2-Cks1 complex was made and purified each time on the day of binding assays performed.

4.2.2 Expression and purification of His-Cks1 from *E. coli*

Small-scale trials identified that over night induction at 16°C with 0.2 mM IPTG yielded the best results. His-Cks1 was expressed in C41 *E. coli* strain and purified using immobilised metal affinity chromatography (IMAC). The detailed protocol can be found in Materials and Methods. Expression, solubility and purity after the IMAC purification step was evaluated by SDS-PAGE (see Figure 4.1a). His-Cks1 has a molecular weight of just over 12 kDa and is seen clearly on the gel following its purification. From the total protein and soluble protein fractions it can be concluded that the protein is mostly soluble and elutions contain mainly the protein of interest.

Size-exclusion chromatography (SEC) was performed to further purify Cks1 and remove high molecular weight contaminants seen on the gel. Based on the amounts of protein produced, either the 300 mL or the 120 mL S75 Superdex column was used. A chromatogram of SEC purification of His-Cks1 is shown in Figure 4.1c. Finally, pure His-Cks1 protein was concentrated, aliquoted, snap frozen in liquid nitrogen and stored at -80°C until further use. The purity of the Cks1 sample was evaluated by SDS-PAGE (see Figure 4.1d). His-Cks1 purification yielded 20 mg of protein per liter of bacterial culture.

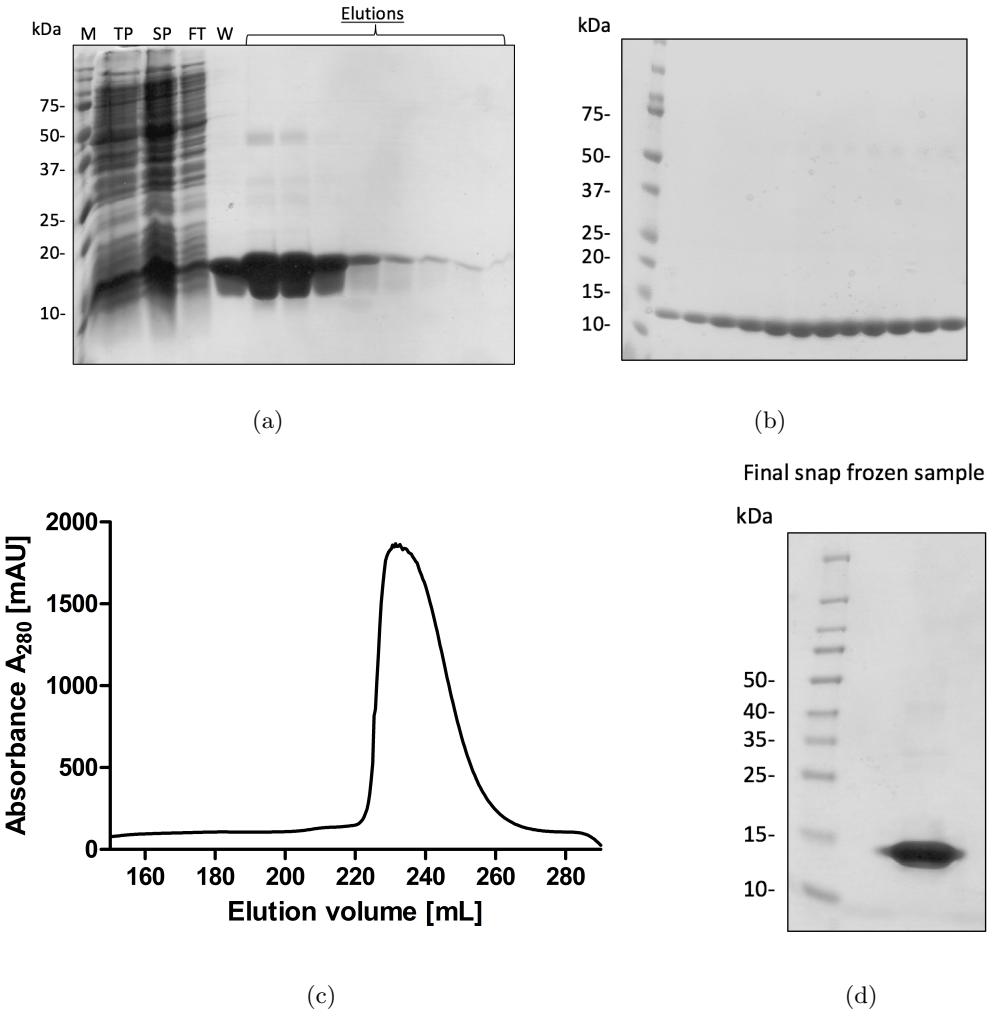

Figure 4.1: Purification of His-Cks1 from *E. coli*. (a) SDS-PAGE of IMAC purification step of His-Cks1. M - marker, TP - total protein, SP - soluble protein, FT - flow through, W - wash. Protein was eluted in 1 mL fractions with a buffer containing 250 mM imidazole. (b) SDS-PAGE of the elution fractions of Cks1 from HiLoad^{TM} 26/60 Superdex^{TM} 75 column. (c) Chromatogram showing elution of HiLoad^{TM} 26/60 Superdex^{TM} 75 column. The protein was concentrated, aliquoted and flash-frozen in liquid nitrogen until further biochemical analysis. (d) SDS-PAGE of the final frozen Cks1 sample.

4.2.3 Expression and purification of GST-Skp2-Skp1 from *E. coli*

GST-Skp2-Skp1 expression required more optimisation than did His-Cks1. The best conditions identified on a small scale did not convert well to large scale, and therefore expression was optimised using 0.5 l cultures. GST-Skp2-Skp1 were expressed using C41 *E. coli* strain with 0.15 mM IPTG, overnight at 16°C. Similar to His-Cks1, the first step of GST-Skp2-Skp1 purification was affinity chromatography. Purity of the GST-Skp2-Skp1 was then evaluated by SDS-PAGE (Figure 4.2a). The two major bands correspond to GST-Skp2 at around 60 kDa and Skp1 at 18 kDa. However several contaminant protein bands are present. SEC was performed to further purify GST-Skp2-Skp1. The chromatogram is shown in Figure 4.2c. Fractions corresponding to peaks in the chromatogram were evaluated by SDS-PAGE (see Figure 4.2b). Peak 1 eluted at the void volume corresponding to a high molecular weight species that could be attributed to GST-Skp2-Skp1 aggregates based on SDS-PAGE analysis. Peak 2 corresponds to the complex of Skp2-Skp1; it was then concentrated, snap frozen in liquid nitrogen and stored at -80°C.

Purified protein samples were tested using mass spectroscopy analysis to ensure the correct mass of the sample protein and evaluate any impurities present. Mass spec was performed by Ewan McCaully, former PhD student in Itzhaki's lab. Both Skp2-Skp1 and Cks1 samples showed correct molecular mass of these proteins and no other impurities present (see Figure 4.3. The two peaks of 26 kDa and 13 kDa in the Skp2-Skp1 sample correspond to the GST tag in +1 and +2 charged states respectively.

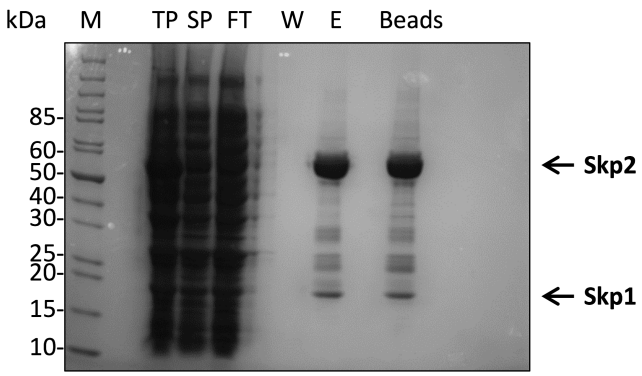

(a)

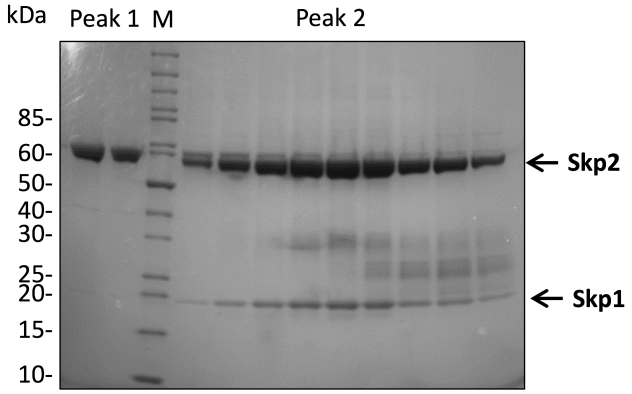

(b)

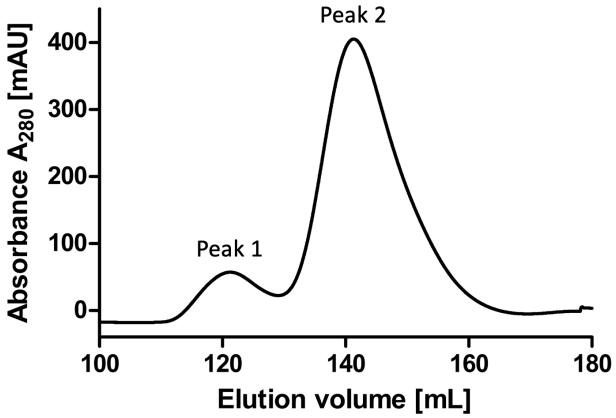

(c)

Figure 4.2: Purification of GST-Skp2-Skp1 from *E. coli*. (a) SDS-PAGE of affinity purification step of GST-Skp2-Skp1. TP - total protein, SP - soluble protein, FT - flow through, W - wash, E - elution. Protein was eluted in 0.5 mL fractions with a buffer containing 10 mM glutathione. (b) SDS-PAGE of fractions corresponding to peak 1 and peak 2 eluted from HiLoad^{TM} 16/60 Superdex^{TM} S75 column. (c) Size exclusion chromatogram showing elution of HiLoad^{TM} 16/60 Superdex^{TM} S75 column. The protein was concentrated, aliquoted and flash-frozen in liquid nitrogen until further use.

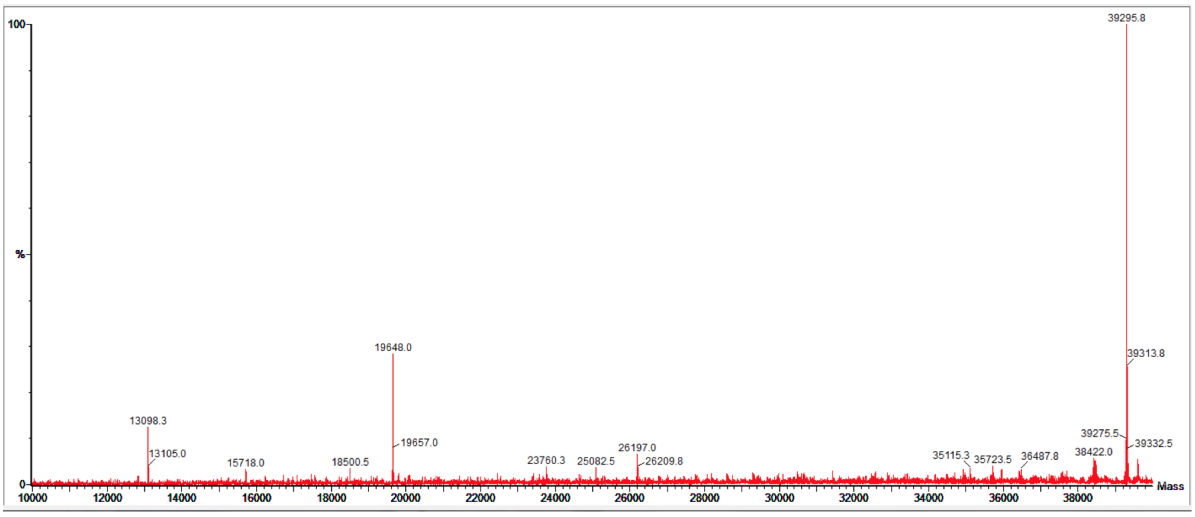

(a) Mass spectrum of purified Skp2-Skp1 protein sample

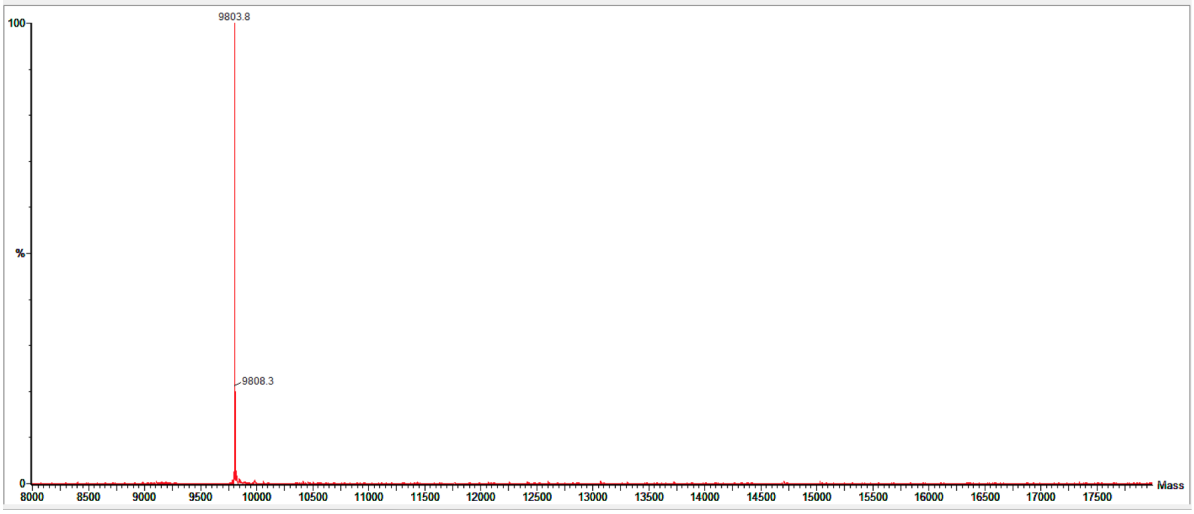

(b) Mass spectrum of purified Cks1 protein sample

Figure 4.3: Mass spec analysis of purified Skp2-Skp1 and Cks1 samples. (a) MS of Skp2 and Skp1 with mass traces 39295.8 and 19648.0 Da respectively. (b) MS of Cks1 with a mass of 9803.8 Da.

4.2.4 Skp1-Skp2-Cks1 complex formation

Previously published dissociation constant for Skp2-Skp1 with Cks1 was determined to be K_d=6 nM using ITC methodology.[72] Since the affinity is very high, the Cks1-Skp2-Skp1 complex was made by mixing purified GST-Skp2-Skp1 and His-Cks1 1:2 molar ratio and incubated at room temperature for 1-2 hours prior to SEC purification to remove excess Cks1 (as described in the publication). The SEC chromatogram and associated SDS-PAGE of the peaks are shown in Figure 4.4.

Peak 1 correspond to the Cks1-Skp2-Skp1 protein complex which can be seen on SDS-PAGE. Peak 2 is the uncomplexed Cks1, which was used in 2x molar excess to ensure efficient/complete complex formation. From these data it can be concluded that Cks1-Skp2-Skp1 complex was made successfully and is sufficiently pure for the subsequent fluorescence polarisation assays. This complex was used straight away for biophysical characterisation of p27 peptides. I have also tried using this complex the next day, however it either crashed out overnight (stored -4°C), if stored at concentrated form, or the complex couldn't be concentrated to high enough concentrations the next day if stored in the dilute form (stored -4°C). Due to this instability issue, the complex was always prepared fresh on the day before performing each biophysical assays.

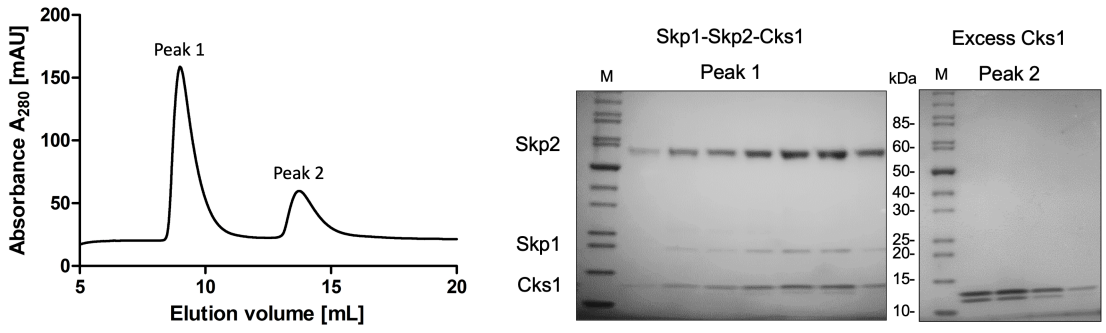

(a) (b)

Figure 4.4: Purification of Cks1-Skp2-Skp1 complex from *E. coli*. (a) Chromatogram showing elution of the complex from Superdex^{TM} S200 10/300 GL column. (b) SDS-PAGE of fractions corresponding to peak 1 and peak 2 eluted from Superdex^{TM} S200 10/300 GL column. The protein complex was concentrated and used immediately for FP assays.

4.2.5 Biophysical analysis of the interaction between p27 peptides and Skp1-Skp2-Cks1

Direct FP assays of labelled p27 peptides

First, fluorescence polarisation (FP) assay was chosen as a primary tool to measure peptide binding because of its high sensitivity and low amounts of samples needed for the very small volumes of a 384-well plate format. In the system comprising Skp1-Skp2-Cks1 and peptide, we have a large molecular weight complex (around 90 kDa) interacting with a small molecular weight peptide which makes this system ideal for FP. In Figure 4.5 the principals of FP binding measurements are shown. It can be seen that fluorescently labelled protein in solution tumbles quickly and thus produces a low fluorescence anisotropy. Upon binding to the large complex the peptide tumbles slower relative to its unbound state and produces higher fluoresence anisotropy signal as more peptide binds to the protein complex (Figure 4.5A).

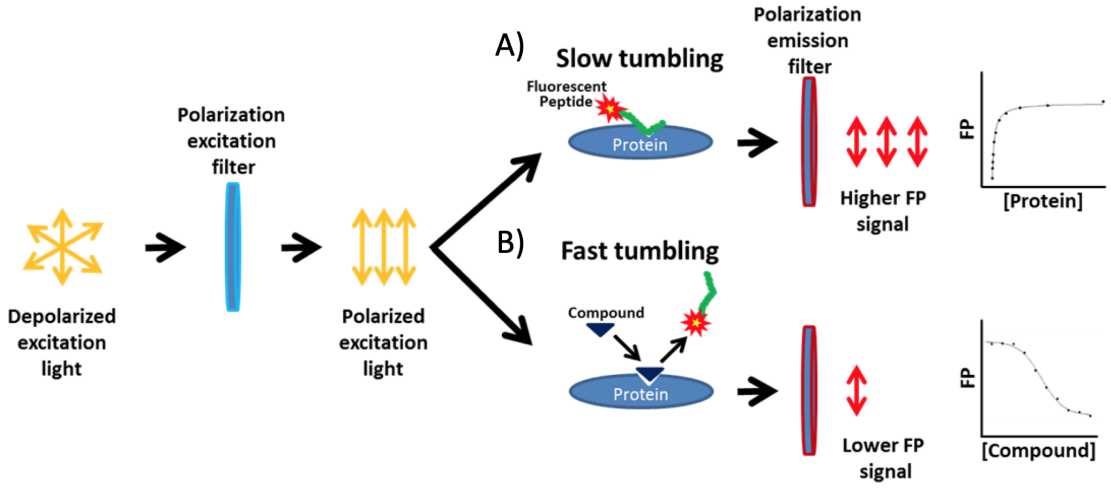

Figure 4.5: Principles of using fluorescence anisotropy to measure protein-ligand interactions. Free fluorescent ligands (peptides) irradiated with plane-polarized light rotate quickly and emit light in a depolarized manner. Fluorescent ligands bound to larger proteins tumble slowly and emit polarized light. The degree of molecular binding can be inferred by measuring the amount of polarized emission.

The phosphorylated p27 peptide resolved in the crystal structure is 10 amino acids in length (amino acids 181-190 of p27). Previous solution binding studies of the interaction have used much longer 24-residue peptides (175-198 of p27) and dissociation constants of 7 μM were observed for the interaction with Cks1-Skp2-Skp1.[72] This binding affinity is the same as that of full-length phosphorylated p27.[72] We synthesized the 10-residue

peptide, conjugated with a TAMRA fluorophore (TAMRA-Ahx-AGSVEQT(phos)PKK), and measured its binding affinity for Cks1-Skp2-Skp1 using fluorescence polarisation (FP). 10 amino acids of p27 peptide that were resolved in the crystal structure were selected. We have reasoned that unresolved amino acids are not interacting sufficiently with Skp2-Cks1 and thus are flexible in the structure and could not be resolved. In addition, an amino hexanoic acid (Ahx) spacer was used to allow adequate distance between the binding sequence of the peptide and the introduced fluorophore.

At first, binding of this peptide was used in the direct FP assay with Cks1 alone, Skp2-Skp1 alone and the complex of Skp1-Skp2-Cks1. Direct fluorescence polarisation traces are shown in Figure 4.6. The data indicate that even though p27 interacts with both Cks1 and Skp2, tight binding was only observed with Cks1-Skp2-Skp1 complex. K_{d} values obtained are listed in Table 4.1. Interestingly, Cks1, without Skp2-Skp1, showed only weak affinity for the peptide, even though pThr187 of p27 interacts predominantly with Cks1. These data further confirm that presence of Cks1-Skp2 complex is necessary for high-affinity binding to p27.[71] The observed dissociation constant (Kd) of 2.78 ± 0.19 μM indicates that this short peptide can effectively mimic the full-length protein (that of 7 μM).

Table 4.1: Dissociation constants of labelled 10 amino acid linear (unconstrained) p27 peptides determined by direct FP. The experiments were conducted in triplicate.

	$K_{\mathbf{d}}$ **(μM)**
Cks1 + TAMRA-AGSVEQT(phos)PKK	268 ± 403
Skp2-Skp1 + TAMRA-AGSVEQT(phos)PKK	15 ± 8
Cks1-Skp2-Skp1 + TAMRA-AGSVEQT(phos)PKK	2.7 ± 0.2

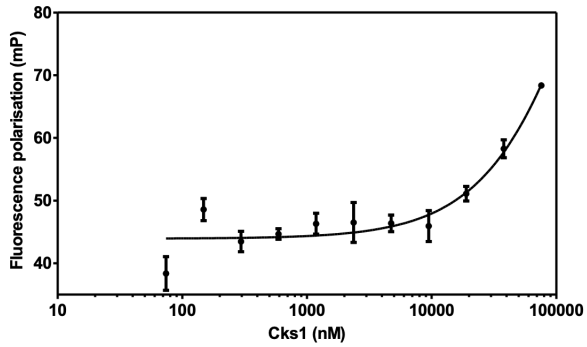

(a) Binding to Cks1

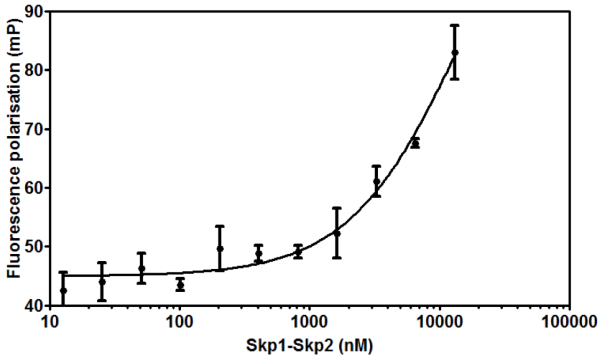

(b) Binding to Skp1-Skp2

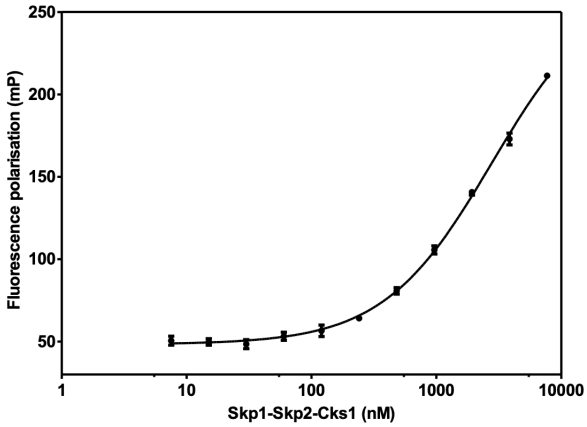

(c) Binding to Skp1-Skp2-Cks1 complex

Figure 4.6: Direct FP traces of TAMRA-AGSVEQT(phos)PKK peptide binding to Skp1-Skp2-Cks1 complex and its components. (a) TAMRA-AGSVEQT(phos)PKK peptide binding to Cks1 only. (b) TAMRA-AGSVEQT(phos)PKK peptide binding to Skp2-Skp1 only. (c) TAMRA-AGSVEQT(phos)PKK peptide binding to Cks1-Skp2-Skp1 complex. The experiments were conducted in triplicate.

Placement of the fluoresecent tag on the peptide was also evaluated by comparing two fluorescently labelled p27 peptides with fluorophores either on the N- or C-terminus of the peptide. Peptides were TAMRA-AGSVEQT(phos)PKK and AGSVEQT(phos)PKK-Ahx-K-FAM respectively. Different tags were used since TAMRA-labelled peptide was synthesised by Cambridge Peptides whereas FAM-labelled protein was synthesised later on in the study during my p53 laboratory visit as described previously. Structures of the dyes are shown in Figure 4.7.

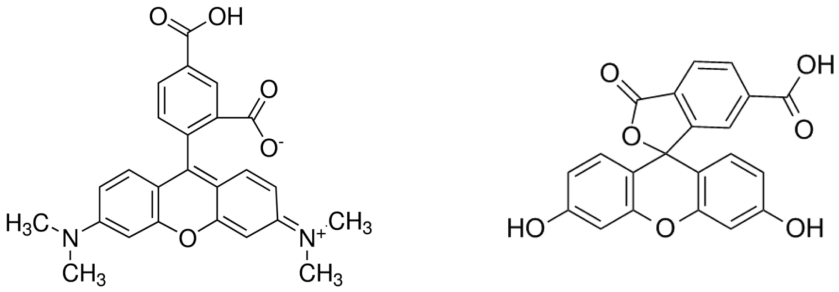

Figure 4.7: Chemical structures of 5-TAMRA and 6-FAM fluorophores.

Direct FP traces of these peptides binding to Skp1-Skp2-Cks1 complex are shown in Figure 4.8. The TAMRA-labelled peptide had a K_{d} of 2.78 ± 0.19 μM, whereas the FAM-labelled peptide had a K_{d} of 3.34 ± 0.14 μM. This indicated that the placement of fluorophore did not have a significant influence on the peptide binding and most likely Ahx is a long enough spacer to avoid any interactions of fluorophore to the protein complex.

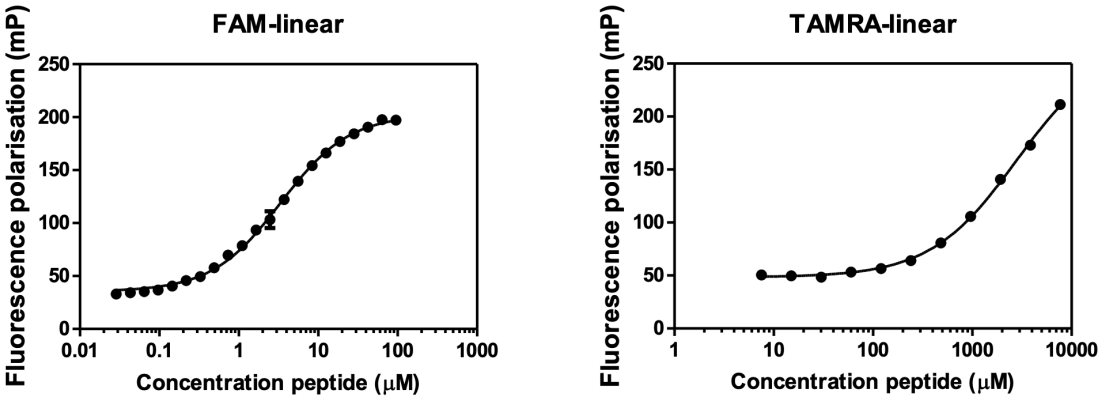

Figure 4.8: Direct FP traces showing the the linear p27 peptide binding to Skp1-Skp2-Cks1, fitted to a one-site binding model. TAMRA was attached to the $\mathrm{N}_{\mathrm{terminus}}$ and FAM to the $\mathrm{C}_{\mathrm{terminus}}$ of the p27 peptide.

Competition FP analysis of unlabelled peptides

Next, the effect of macrocyclisation on p27 peptide binding to Cks1-Skp2-Skp1 complex was investigated using competition FP. First, a competition FP assay was performed using control peptides. Three key amino acid residues interacting with Skp2 and Cks1 were replaced with alanine residues to abolish any binding to the complex. From competition FP traces no binding can be seen (see Figure 4.9a). Similarly the binding of unlabelled p27 peptide was also measured to evaluate any effect that the fluorophore and spacers could have any contributions to the binding (see Figure 4.9b). The K_{d} of 3.0 ± 0.2 μM indicated that unlabelled and labelled p27 peptides bind to the complex with the same affinity.

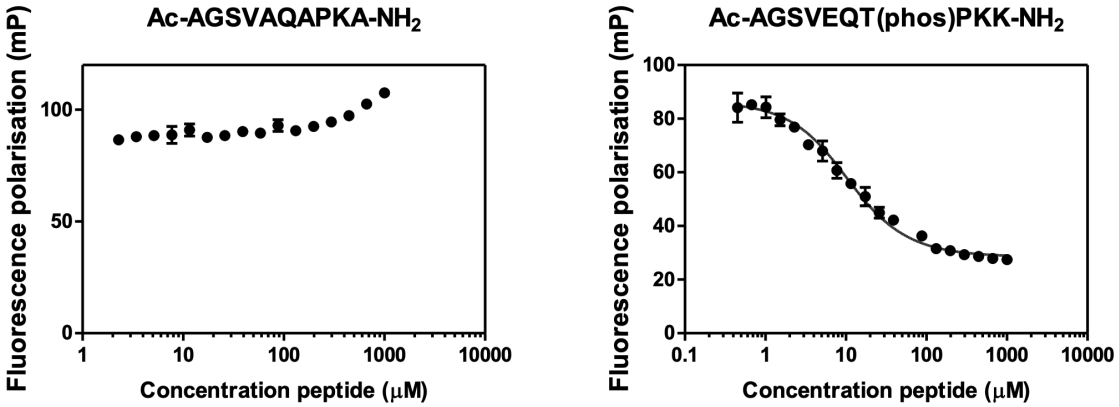

Figure 4.9: Competition FP of displacement of TAMRA-AGSVEQT(phos)PKK peptide from Cks1-Skp2-Skp1 by titration of unlablled p27 peptides. TAMRA-AGSVEQT(phos)PKK peptide (10 nM) and Cks1-Skp2-Skp1 (4 μM) were incubated for 15 min followed by addition of displacement peptide at varying concentrations and read after 30 min. The experiments were conducted in triplicate in a final volume of 25 μl. (a) Control p27 peptide with key amino acids mutated to alanines. (b) Unlabelled p27 linear peptide.

As described previously the aim was to constrain the peptide in the turn-like conformation that it adopts in its bound form and thereby increase its affinity for the Cks1-Skp2-Skp1 complex due to reduced entropy. For this, preformed Cks1-Skp2-Skp1 was mixed with labelled peptide TAMRA-AGSVEQT(phos)PKK so that half of the complex binding sites were occupied. The concentration of the labelled peptide required to occupy half of the binding sites was determined from the direct FP assay (see Figure 4.6) and was determined to be 3 μM. Constrained (unlabelled) peptide (CP) was then added to the mixture

and fluorescence reading was taken after 30 min. The initial fluorescence polarisation reading is high corresponding to protein-bound TAMRA-AGSVEQT(phos)PKK peptide, as in the complex the peptide is tumbling more slowly and thus the fluorescence signal is anisotropic. With increasing concentration of the unlabelled competitive ligand, in this case CP, TAMRA peptide is displaced and thus the FP signal decreases, as the labelled peptide now tumbles freely in solution and polarisation is more isotropic. All CPs were tested using competitive FP assay, and data are shown in Figure 4.10.

K_{d} values determined for CPs are summarised in Table 4.2. Compared to the K_{d} of 2.78 ± 0.19 μM of linear p27, all macrocyclised peptides bind Cks1-Skp2-Skp1 complex with higher affinities. CP2 and CP4 showed greater than 50-fold increases in affinity, CP3 and CP5 $\sim$ 30-fold increase. These data indicate that macrocyclisation of the linear p27 peptide has a large positive impact on its binding affinity. Macrocyclisation constrains the p27 peptide in it bioactive conformation thereby dramatically improving the binding affinity. Competition FP data for these peptides is shown in Figure 4.10.

Table 4.2: Dissociation constants for the binding of macrocyclised p27 peptides to Cks1-Skp2-Skp1, as measured by competition FP. The fold increase in binding affinity relative to the linear p27 peptide is also listed. No binding (N.B.) could be detected for the control peptide in which the three key contacting residues are mutated to Ala.

Peptide	**Sequence**	K_{d} **(nM)**	**Fold increase**
Control	AGSV**A**Q**A**PK**A**	N.B.	N/A
Linear	TAMRA-Ahx-AGSVEQT(phos)PKK	2,777 ± 190	N/A
CP1	AGS(X2)EQT(phos)P(X4)K	356 ± 95	8
CP2	AGS(X2)EQT(phos)P(X3)K	32 ± 8	86
CP3	AGSVE(X3)T(phos)P(X4)K	81 ± 4	34
CP4	AGSVE(X2)T(phos)P(X3)K	46 ± 9	60
CP5	AGSVE(X2)T(phos)P(X2)K	72 ± 7	38

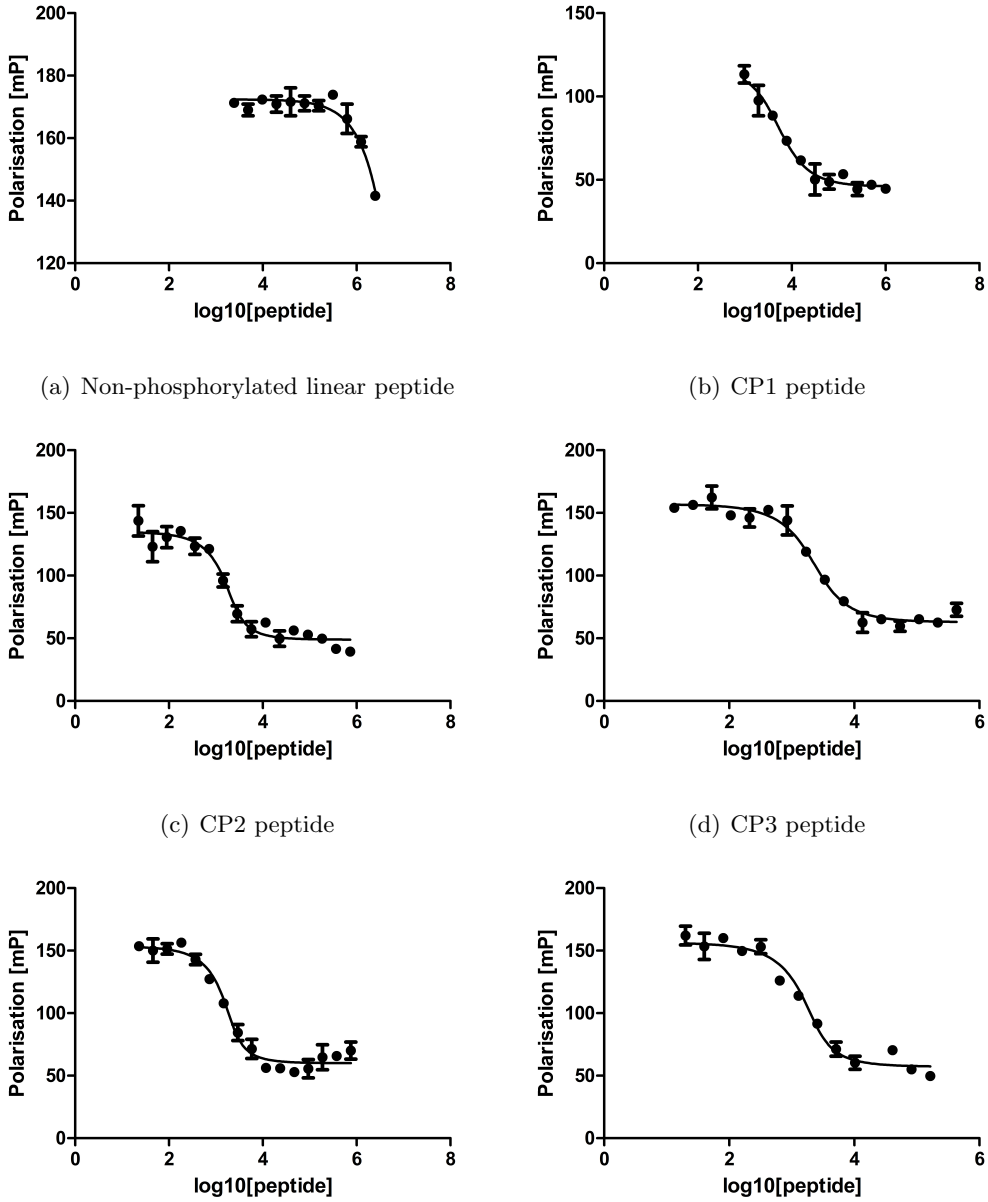

(a) Non-phosphorylated linear peptide

(b) CP1 peptide

(c) CP2 peptide

(d) CP3 peptide

(e) CP4 peptide

(f) CP5 peptide

Figure 4.10: Competition FP of displacement of TAMRA-AGSVEQT(phos)PKK peptide from Cks1-Skp2-Skp1 by titration of unlablled peptides. TAMRA-AGSVEQT(phos)PKK peptide (10 nM) and Cks1-Skp2-Skp1 (4 µM) were incubated for 15 min followed by addition of displacement peptide at varying concentrations and read after 30 min. The experiments were conducted in triplicate in a final volume of 50 µl. (a) AGSVEQEPKK peptide. (b) CP1 peptide. (c) CP2 peptide. (d) CP3 peptide. (e) CP4 peptide. (f) CP5 peptide.

From Figure 4.10 it can be seen that CP1 curve was not complete and thus the affinity of CP1 for Skp1-Skp2-Cks1 could be higher than the value obtained from the fit. Since CP1 performed as well as CP2 in the biochemical studies (see further chapter on ubiquitination assays) we believe that the true K_d is similar to other CPs. Figure 4.11 shows CP1-CP5 overlayed and it can be seen that all traces are very similar and that CP1 binds to Skp1-Skp2-Cks1 complex with a similar affinity as other constrained peptides. Unfortunately due to peptide degradation over time, it was not possible to repeat this experiment and obtain a full data set for CP1 binding.

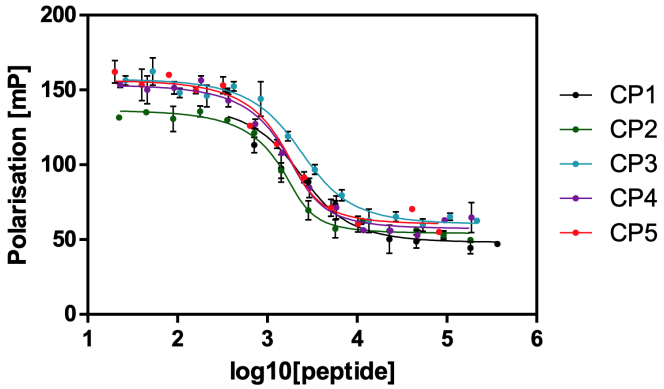

Figure 4.11: Competitive fluorescence polarisation assays overlay of constrained p27 peptides titrated into the complex of Cks1-Skp2-Skp1 with TAMRA-labelled unconstrained p27 peptide.

Next, peptides with mutations introduced were also evaluated using competition FP. Two constrained peptides with either one mutation of alanine to aspartic acid or two mutations introduced where alanine was mutated to aspartic acid and serine to arginine were tested. These mutations were introduced after an analysis of charge distribution on the crystal structure of Skp1-Skp2-Cks1-p27 by Dr Chandra Verma (A*STAR). The results show that the mutations did not further increase the binding affinity of the constrained peptides (see Figure 4.12).

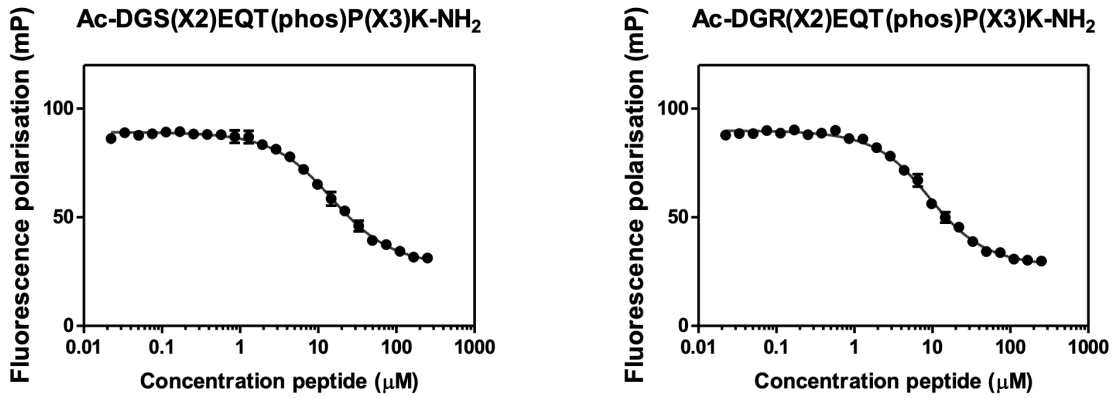

Figure 4.12: Competitive fluorescence polarisation performed on the microplate reader for measuring displacement of TAMRA-AGSVEQT(phos)PKK peptide from Cks1-Skp2-Skp1 by titration of unlablled CPs with mutations introduced. TAMRA-AGSVEQT(phos)PKK peptide (10 nM) and Cks1-Skp2-Skp1 (4 μM) were incubated for 15 min followed by addition of displacement peptide at varying concentrations and read after 30 min. The experiments were conducted in triplicate in a final volume of 25 μl. (a) Ala was mutated to Asp, (b) Ala was mutated to Asp and Ser to Arg.

Isothermal titration calorimetry of complex and peptide interactions

In order to obtain further thermodynamic data on peptide binding to the complex an isothermal titration calorimetry was performed. It was of a particular interest to investigate the nature of this binding in terms of its entropic and enthalpic contributions. Most literature of stapled peptides focus on the entropic effect however almost two order of magnitude increase in binding of p27 peptides could also arise due to additional interactions of the linker or triazole rings themselves with Skp2-Cks1 interface.

First, the ITC experiment required some optimisation. The Skp1-Skp2-Cks1 complex was chosen to be in the cell since it can only be concentrated to a certain concentration before precipitating whilst peptides of much higher concentration were titrated in. The ITC trace of linear p27 peptide titrated into Skp1-Skp2-Cks1 complex in the cell is shown in Figure 4.13. At first this was performed at 25°C (left) and showed noisy and weak signal. For subsequent experiments several conditions were optimised and titration was carried out at 10°C after thorough degassing (at least 15 min) of the complex and peptide solutions and using higher complex concentration, this resulted in tremendous improvement as can be seen on the (right).

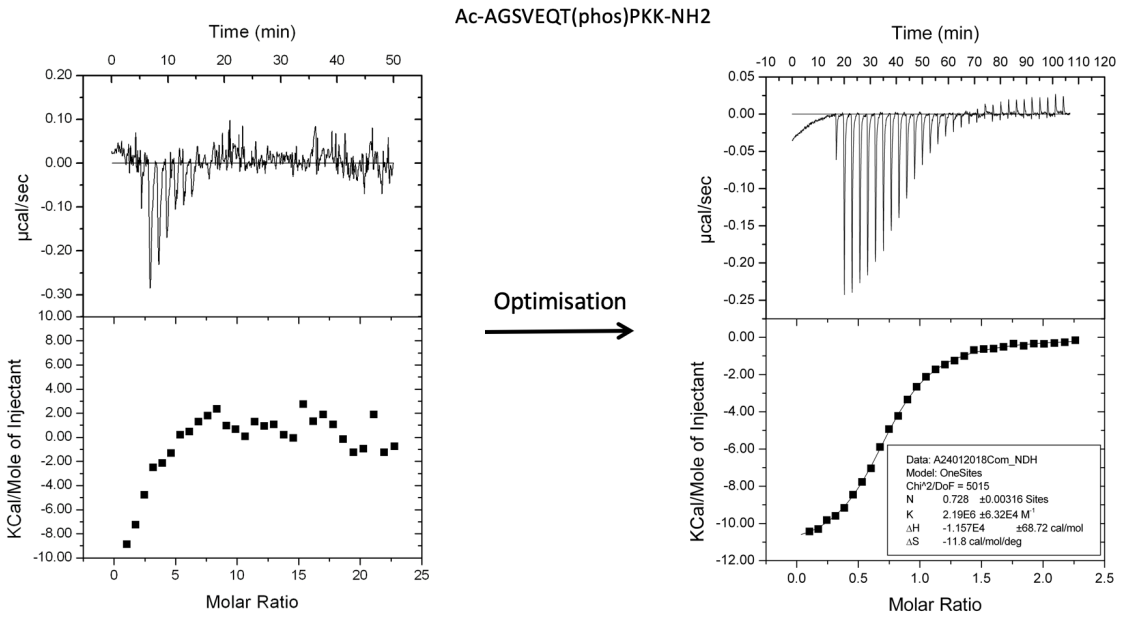

Figure 4.13: ITC trace of linear p27 peptide being titrated into Skp1-Skp2-Cks1 complex in the cell. Prior optimisation ITC was performed at 25°C, $left$ and showed weak and noisy signal. The optimised trace is shown on the $right$ where the experiment was performed at 10°C and all solutions degassed for 15 min, fitted to a one-site binding model.

Once suitable ITC experimental conditions had been established the peptides were tested. First, linear p27 peptide and control Ala peptides were tested to prove the reliability of the set up. Control Ala peptide resulted in no binding as expected and a linear peptide produced good heat responses (see Figure 4.14 top). A few constrained peptides were then tested, and ITC traces of CP1 and CP2 titration are shown in Figure 4.14 bottom. Unfortunately this resulted in binding affinities similar to that of the linear p27 peptide, unlike the FP results. We speculated that constrained peptides could have degraded over the period of 2.5 years. Potentially a triazole ring formation is not very stable. This was then further proven by LC/MS. The linear peptide appeared to be stable and had similar binding affinity to that obtained previously. At this point, no more ITC experiments were carried out using stapled peptides due to the lack of precursor peptide for stapling.

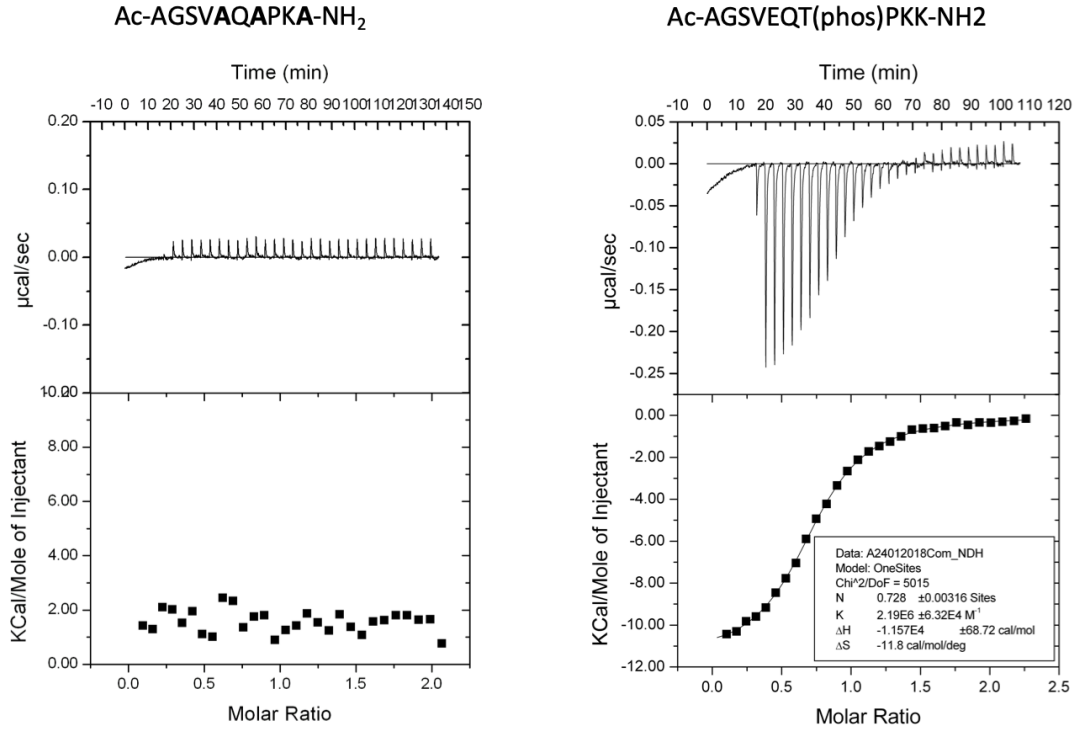

(a) ITC traces showing titration of control peptide (Ala variant) or linear peptide

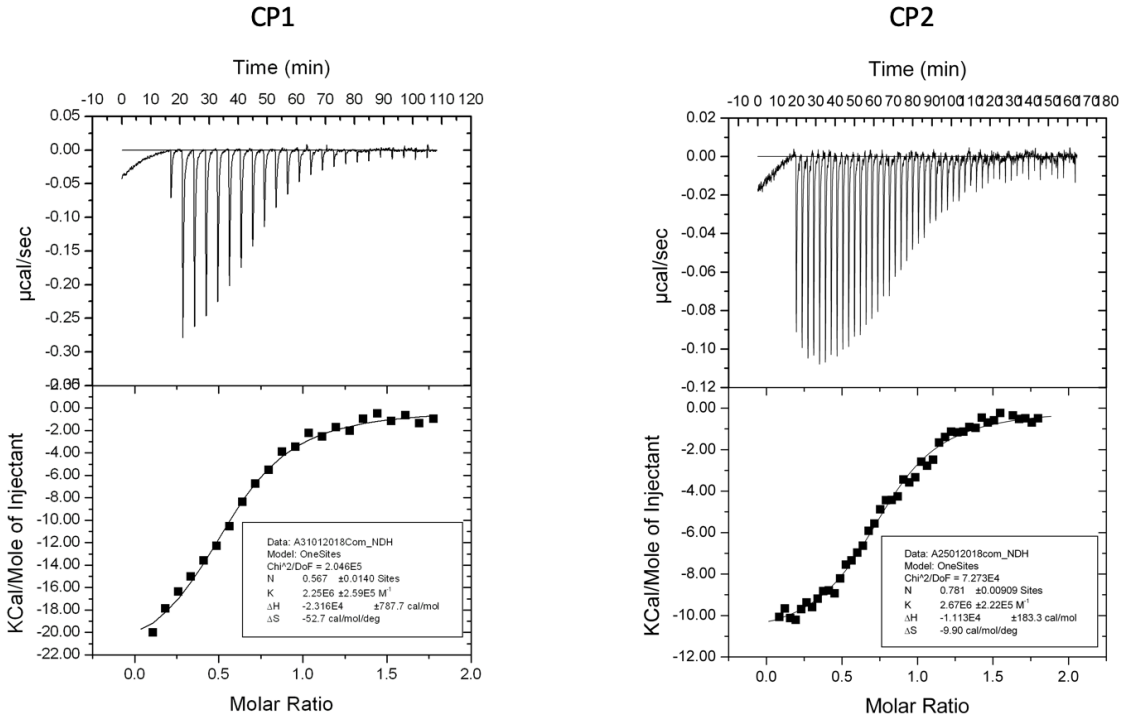

(b) ITC traces showing titration of CP1 or CP2 peptide

Figure 4.14: ITC traces showing p27 peptide titration into Skp1-Skp2-Cks1 complex. (a) ITC traces showing titration of control (Ala variant) or linear peptide into Skp1-Skp2-Cks1 complex. (b) ITC traces showing titration of CP1 or CP2 peptide into Skp1-Skp2-Cks1 complex. Fitted to a one-site binding model.

There are many examples in the literature of constrained α-helical peptide inhibitors. There are far fewer constrained non-helical peptide inhibitors, and their affinities have generally only been marginally improved relative to their linear counterparts.[164,165] Significantly, this is the first time that the constraint of a non-helical peptide has induced such a dramatic enhancement of binding affinity. It is possible that the process of macrocyclisation introduces new binding interactions, for example from the m7N linker or the triazole rings of the peptides effectively creating a triple-constrained peptide structure. However, we suggest that the main reason for the dramatic effect of macrocyclisation on binding affinity arises because the bioactive conformation of the p27 peptide is an entropically unfavourable tight turn, which is very effectively induced by the macrocyclic constraint. In contrast, many of the non-helical peptides constrained in previous studies have extended bioactive conformations that are very similar to those sampled when unconstrained and therefore cannot be dramatically improved by constraining them.

Chapter 5

Biological Activity of Constrained p27 Peptides

5.1 Introduction

As previously described in the Introduction, the interactions between p27 and SCF^{Skp2} ubiquitin ligase are widely characterised. SCF^{Skp2} is an E3 ubiquitin ligase that tags p27 with a polyubiquitin chain that then directs p27 for degradation by the proteasome. In order to study the relationship between a ligase and its substrate in more detail and investigate the p27 constrained peptides ability to disrupt this interaction we first had to develop a p27 ubiquitination assay.

In this Chapter we show that full-length Skp2 protein and its truncated variants can be produced in mammalian cells. Furthermore, the SCF^{Skp2} complex containing full-length Skp2, Skp1, Cks1, Cullin1 and Rbx1 was successfully purified from HEK293T cells using FLAG-tagged Skp2 for co-immunoprecipitation. Additionally, a Δ Fbox Skp2 variant was cloned and showed no interaction with Skp1 (and thereby with the SCF ligase complex), allowing production of a 'dead' (inactive) ligase sample. These ligases were further used for setting up p27, p21 and N-myc ubiquitination experiments. Linear and constrained p27 peptides were then assayed for their ability to inhibit ubiquitination of p27 and other SCF^{Skp2} substrates. CPs were shown to be much more effective than the linear peptide as expected from their binding. Furthermore, CPs were able to inhibit ubiquitination of several other substrates of SCF^{Skp2} ligase, namely p21 and N-myc, to various extent.

Furthermore, we investigated intra-cellular delivery of the peptides using cell-penetrating peptide tags, electroporation and liposomal encapsulational methods. CPs were able to restore p27 levels associated with Skp2 over-expression as well as reduce proliferation of breast cancer cell line MCF-7.

5.2 Results and Discussion

5.2.1 Cloning of Skp2 mammalian expression constructs

Skp2 wild type (WT) (1-424), Skp2-ΔFbox (Δ93-141) and Skp2 with the $N_{terminus}$ truncation including deletion of Fbox Skp2-ΔN_{term} (141-424) were PCR amplified and cloned into a pcDNA3 mammalian expression vector in frame with a double FLAG tag at the $N_{terminus}$. All constructs contain a FLAG tag to enable immunoprecipitation of Skp2. To confirm insertion of Skp2 genes, plasmid DNA was isolated from several independent colonies and digested with appropriate enzymes (see Materials and Methods). The inserts and vectors were resolved by agarose gel electrophoresis and visualised under UV light. Two bands on the gel of each of the constructs in Figure 5.1 correspond to pcDNA3 vector and the Skp2 insert. One clone for each construct was sent for sequencing, and all further work was carried out with verified clones.

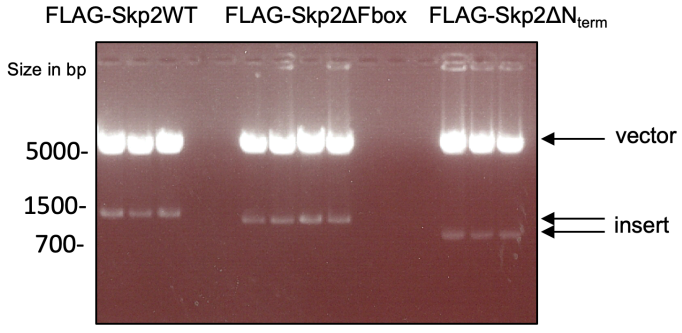

Figure 5.1: Restriction enzyme analysis of the Skp2 constructs using EcoRI and XhoI restriction enzymes. Samples were separated using 1% agarose gel. Two bands in lanes correspond to cut pcDNA3 vector and *skp*2 genes.

5.2.2 Expression of Skp2 in HEK293T cells

To evaluate expression of different Skp2 constructs and thus their suitability for producing the SCF^{Skp2} complex, HEK293T cells were transfected with the three different Skp2 constructs. After 48 hours post-transfection cells were lysed and FLAG tagged Skp2 constructs were immunoprecipitated with anti-FLAG agarose beads. Total lysate and immunoprecipitated (IP) samples were then resolved by gel electrophoresis and then further subjected to Western blot analysis using anti-FLAG antibody (see Figure 5.2). Red arrow indicates the possible mouse antibody heavy chain from the anti-FLAG antibody coupled agarose beads. This could be confirmed by probing the blot with anti-mouse secondary antibody prior to the primary anti-FLAG antibody. The analysis showed that all Skp2 constructs were well expressed, with Skp2-ΔN_{term} showing the lowest expression levels of the three.

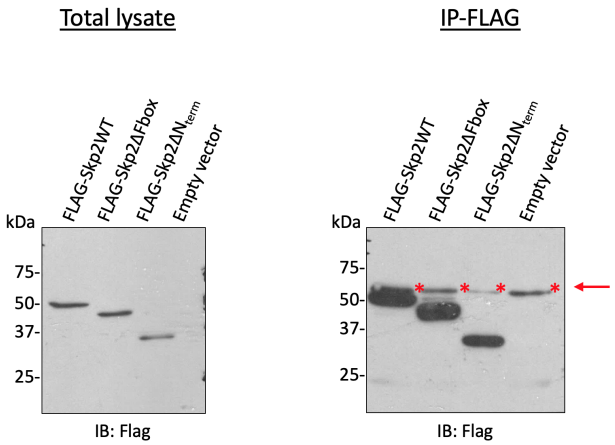

Figure 5.2: Western blot analysis of Skp2 expression in HEK293T. Anti-FLAG antibody was used to detect FLAG-tagged Skp2 constructs in total lysate and IP samples. Cells transfected with an empty vector were used as control. Red arrow indicates the possible mouse antibody heavy chain from the anti-FLAG antibody coupled agarose beads.

5.2.3 Production of SCF^{Skp2} E3 ligase complex

FLAG-Skp2-WT and FLAG-Skp2-ΔFbox ligases were used for SCF^{Skp2} complex production to represent the active ligase, which would be able to ubiquitinate its substrates, and inactive ligase, which would be used for control experiments. Since the Fbox of Skp2 is the main component which interacts with Skp1 the Fbox-deletion variant would be expected to be unable to co-immunoprecipitate all SCF ligase components. From the crystal struc-

ture of $Skp2^{Fbox}$-Skp1-Cullin1-Rbx1 complex (see Figure 5.3), can be seen that the Fbox interacts with Skp1 only, and the Skp1 is interacting with Cullin1 which binds to Rbx1. Rbx1 in turn interacts with E2 enzyme that carries ubiquitin, and the elongated and flexible Cullin 1 scaffold moves to bring substrate bound Skp2 and ubiquitin-conjugated E2 in close priximity to allow substrate ubiquitination. The ligase lacking Skp1, Cullin1 and Rbx1 proteins will not be able to bind to the E2 enzyme and thus will have no activity. This ligase will be referred as an inactive or 'dead' ligase.

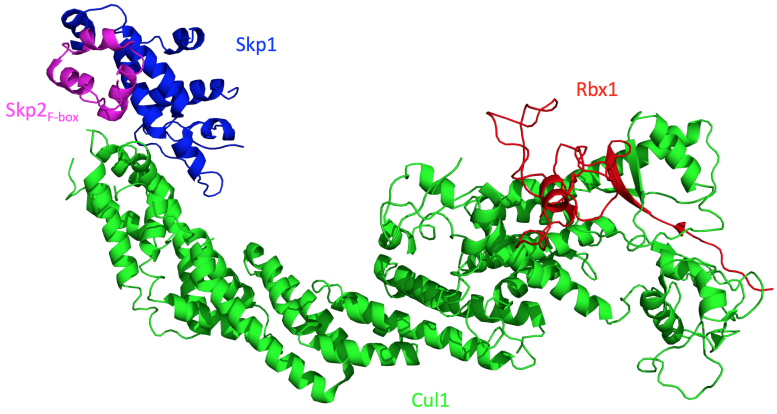

Figure 5.3: Crystal structure of the Cullin1-Rbx1-Skp1-F-box^{Skp2} SCF ubiquitin ligase complex. Structures were generated in PyMOL using PDB: 1LDK.[43]

FLAG-Skp2-WT and FLAG-Skp2-ΔFbox were transfected together with Skp1, Cullin1 and Rbx1 into HEK293T cells to make a SCF^{Skp2} and $SCF^{Skp2\text{-}\Delta Fbox}$ E3 ligase complexes. 48 hours post-transfection cells were lysed and the ligase was immunoprecipitated using anti-FLAG agarose beads as described in Material and Methods. Samples were resolved by gel electrophoreses and stained using Coomasie Blue (see Figure 5.4A). BSA standards were loaded on the same gel to allow quantification of the ligase using ImageJ based on the densitometry values of the bands corresponding to Skp2 and Cullin1 (see Materials and Methods). The red star in Figure 5.4A represent unknown contaminant in the $SCF^{Skp2\text{-}\Delta Fbox}$ sample lane. It could be mistaken for the presence of Cullin1 and full length Skp2 proteins indicating insufficient deletion of the F-box. However, from the western blot analysis in Figure 5.4B, it can be seen that the $SCF^{Skp2\text{-}\Delta Fbox}$ sample does not contain Cullin1 or full length Skp2 proteins, thus confirming a successful deletion of F-box motif.

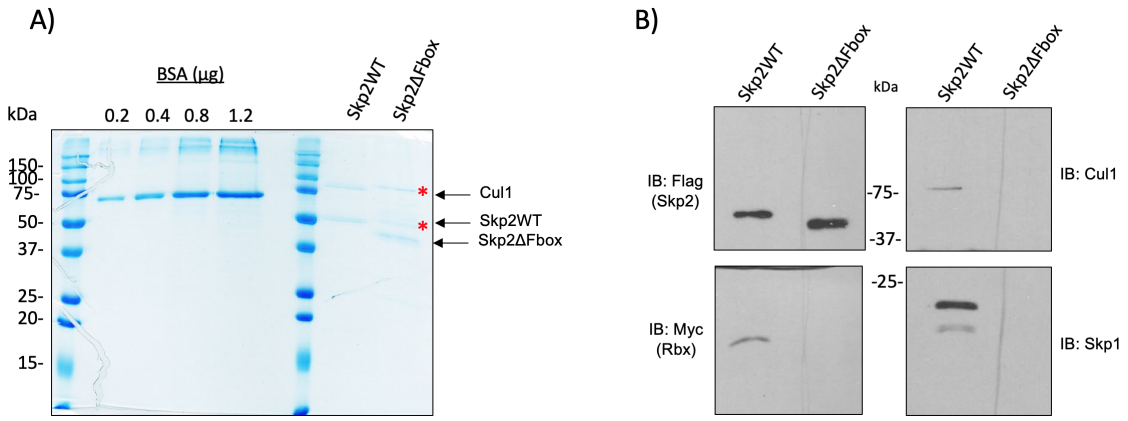

Figure 5.4: Analysis of immunoprecipitated SCF^{Skp2} and $SCF^{Skp2\text{-}\Delta Fbox}$ E3 ligase complexes. (a) SDS-PAGE gel of SCF^{Skp2} and $SCF^{Skp2\text{-}\Delta Fbox}$ and BSA standards. BSA = bovine serum albumin. Red start represent an unknown contaminant. (b) SCF^{Skp2} and $SCF^{Skp2\text{-}\Delta Fbox}$ samples were tested for the presence of Skp2, Cullin1, Skp1 and Rbx1 proteins using specific antibodies. Skp1, Cullin1, and Rbx1 are absent in $SCF^{Skp2\text{-}\Delta Fbox}$ ligase sample, thus indicating successful deletion of the Fbox and production of inactive ligase.

To validate if FLAG-tagged Skp2 co-immunoprecipitated all of the E3 ligase components, including Skp1, Cullin1 and Rbx1, samples of SCF^{Skp2} and $SCF^{Skp2\text{-}\Delta Fbox}$ were immunoblotted to assay for the presence of each of the component using specific antibodies (see Figure 5.4B). As can be seen in Figure 5.4B, Skp2-WT ligase was able to pull down all the component proteins (Skp1, Cul1, Rbx1), whereas the Skp2ΔFbox variant fails to immunoprecipitate the other subunits of the SCF^{Skp2} required for enzyme activity. This inactive ligase will be used as a negative control in subsequent ubiquitination experiments.

5.2.4 Development of *in vitro* p27 ubiquitination assay

p27 ubiquitination is a complex process and relies on a multi-protein complex play. To test whether the samples had functional ligase activity *in vitro* p27 ubiquitination assays were performed. To develop a working assay I have used an approach established in Dr Laman's lab (Pathology Department) for making other E3, SCF^{Fbxo7}. First, E1, E2, ATP, ubiquitination buffer and ubiquitin were purchased and SCF^{Skp2} was prepared as described above. Ubiquitin mix (Ub-mix) was made by mixing E1, E2, ATP and ubiquitin together. In this mix, E1 activates ubiquitin using ATP which is then conjugated onto the E2 enzyme. Once the E2 binds to the substrate-bound E3 the ubiquitin is transferred onto the substrate. p27 used in these assays was either prepared using *in vitro*

transcription/translation (IVT) or purified from HEK293T cells. It is important to note that p27 made by IVT will not be phosphorylated on Thr187, and thus it is expected to not be recognised by SCF^{Skp2} and subsequently not be ubiquitinated. The lack of p27 ubiquitination when using IVT p27 can be seen in Figure 5.5a. Further work was carried out only with p27 immunoprecipitated from HEK293T cells.

To assess the activity and find the optimal concentration of the prepared SCF^{Skp2} ligase complex, a Skp2 titration was performed keeping the amount of p27 constant. The extent of p27 ubiquitination was evaluated by Western blot (see Figure 5.5b). This produced a characteristic smear of poly-ubiquitinated p27. SCF^{Skp2} is able to ubiquitinate p27 even at low concentrations, as can be seen by the presence of the high molecular-weight bands corresponding to p27 of different polyubiquitinated forms. Furthermore, and as expected, $SCF^{Skp2\text{-}\Delta Fbox}$ was unable to ubiqutinate p27. Throughout ubiquitination assays, antibodies to the substrate were used to detect its post-translational modification with ubiquitin. It is worth noting that it is common to probe for ubiquitin in these type of assays. However in this case it could potentially result in false positives (or too strong of the ubiquitination signal) due to Skp2 ability to autobiquitinate. To further understand the results of this assay it would important to include more controls. Experiments should be performed lacking added ubiquitin, this would further confirm the smear is due to ubiquitination and not any other modification. Also, samples lacking E1 and/or E2 enzymes would serve as good controls, where in the absence we should not observe any ubiquitination. To understand the smearing pattern even more, an anti-secondary antibody blot should be used to make sure that there is no signal from the secondary antibody alone which could be mistaken for the ubiquitination of the protein.

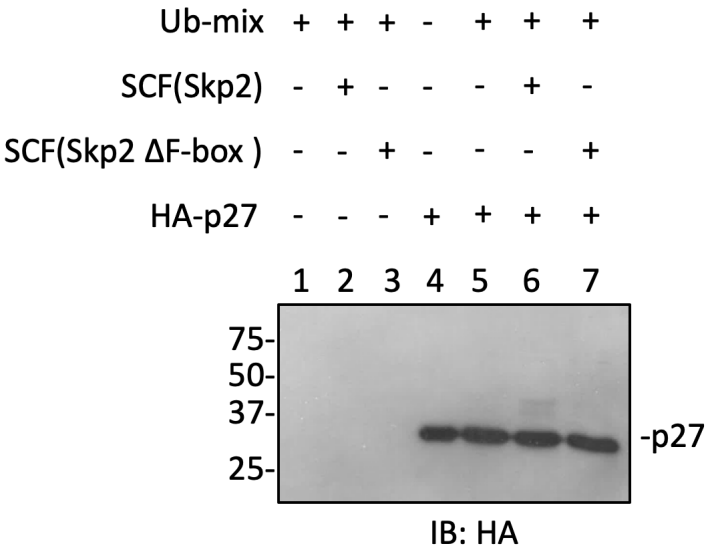

(a)

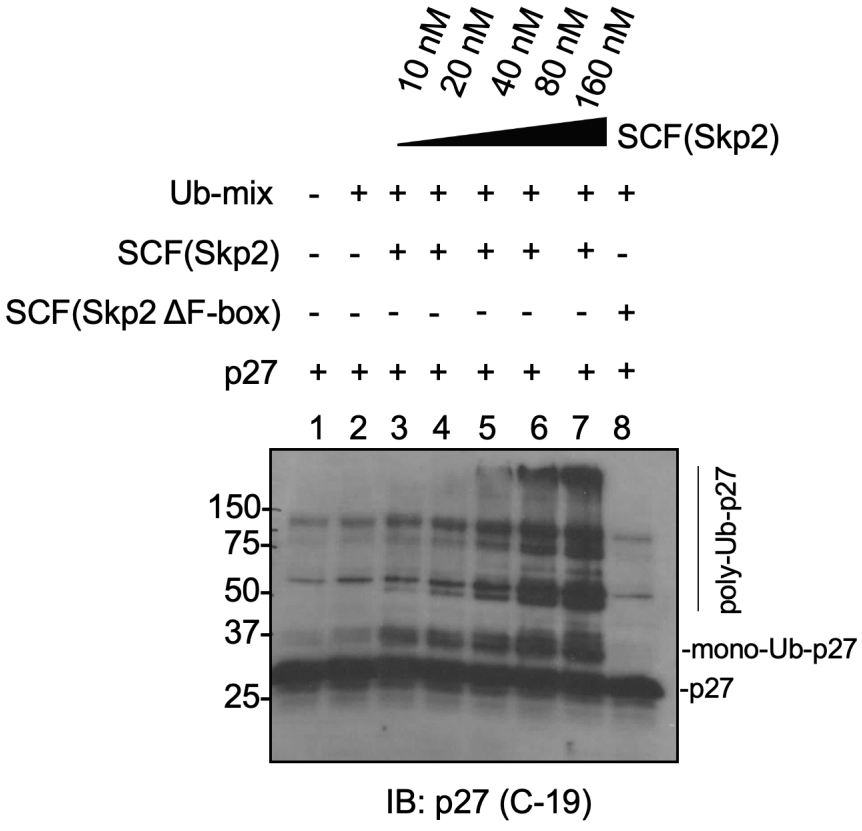

(b)

Figure 5.5: *In vitro* p27 ubiquitination assay performed using p27 prepared by: (a) *in vitro* translation and (b) immunoprecipitation from HEK293T cells.

5.2.5 p27 ubiquitination inhibition assay

Unlike other SCF substrates, ubiquitination of p27 requires an adapter protein, Cks1.[67–69] In addition, all three different binding sites (i.e. binding Cdk2, Skp2 and p27) of Cks1 are required for p27 ubiquitination.[70] Furthermore, it has been shown by the Itzhaki lab and others that the Cks1-Skp1-Skp2 complex has more than 100-fold greater affinity for p27 phosphopeptide than does Skp1-Skp2 alone, and that Cks1-Skp1-Skp2 complexed with Cdk2 further increases the affinity for the p27 phosphopeptide.[71] The crystal structure of Cks1-Skp2-Skp1 revealed subsequently that the phosphorylated Thr187 of p27 peptide makes key contacts with Cks1.[72] Based on the previously published crystal structures of Skp1-Skp2[42] and of the $SCF^{Skp2(F\text{-}box)}$ ubiquitin ligase complex[43] a model of the SCF^{Skp2} E3 ligase in complex with Cks1, Cdk2/cyclin A and p27 has been built as shown in Figure 5.6.[72]

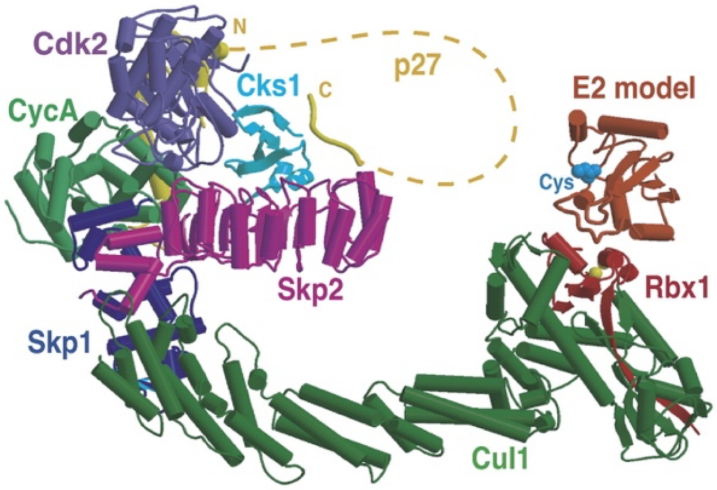

Figure 5.6: Model of the SCF^{Skp2} E3 ligase in complex with Cks1, Cdk2/cyclin A and p27.[72]

Based on this information the ligase production protocol was altered to include additional (i.e. exogenous) Cks1. We believe that the previously prepared ligase, lacking exogenous Cks1, was active due to Skp2's ability to bind to endogenous Cks1 but addition of Cks1 could result in a more active ligase towards p27 binding. To test various peptides a large amount of SCF^{Skp2} ligase and p27 had to be made to avoid batch to batch variations and to test all peptides using the same ligase and substrate. Samples of prepared ligase and p27 were analysed by SDS-PAGE and western blot shown in Figure 5.7. p21-HA was also made for further testing to evaluate ubiquitination of other SCF^{Skp2} substrates.

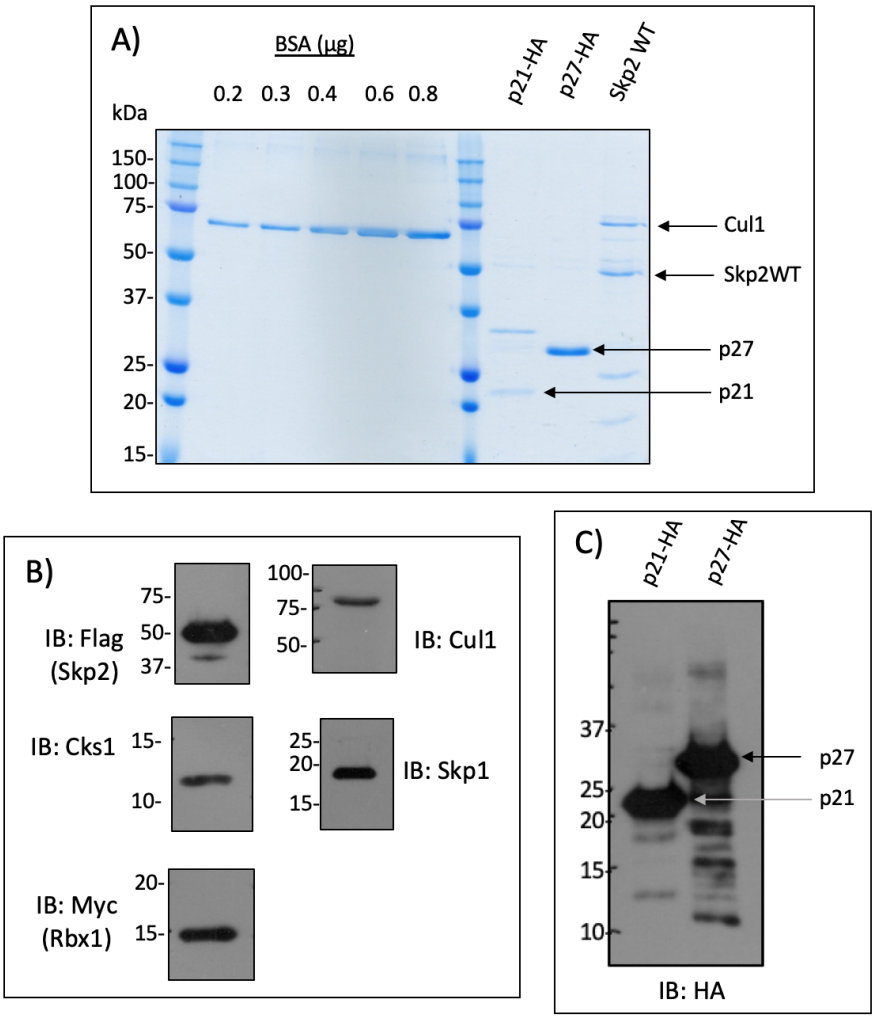

Figure 5.7: SDS-PAGE and Western blot analysis of SCF^{Skp2}, p21 and p27 samples immunoprecipitated from HEK293T cells 48 post-transfection. A) SDS-PAGE showing the purity of immunoprecipitated samples of SCF^{Skp2} containing 2xFLAG-Skp2, Cks1, Skp1, Cullin1 and Rbx1 which was immunoprecipitated using anti-FLAG agarose beads and p21-HA and p27-HA which were immonoprecipitated using anti-HA beads. The samples were quantified using densitometry values against the loaded BSA standards on ImageJ. B) Western blot analysis of SCF^{Skp2} immnoprecipitated sample showing successful co-immunoprecipitation of all components of the E3. C) Western blot analysis of immunoprecipitated p21-HA and p27-HA using anti-HA agarose beads.

First, the control peptide containing no ligase binding residues was tested. Concentrations of p27 and SCF^{Skp2} were kept constant whilst peptide was titrated in using serial 1:2 dilutions from 600 µM to 18.75 µM concentrations. As can be seen from Figure 5.8, this control peptide had no effect on p27 ubiquitination inhibition.

Interestingly, high concentrations of control peptide seemed to cause an increase in p27 ubiquitination as can be seen when comparing lanes 8 and 9 to lane 3. The experiment should be repeated several times to confirm that this is a true effect. Further experiments could be done to investigate the ability of this peptides to 'activate' the E3 or potentially the E1 or E2 enzymes. Using biophysical techniques we have shown in the previous chapter that this control peptide is unable to bind to Skp2-Cks1 complex, however it could be potentially interacting with other proteins of the E3 ligase, like Cullin1.

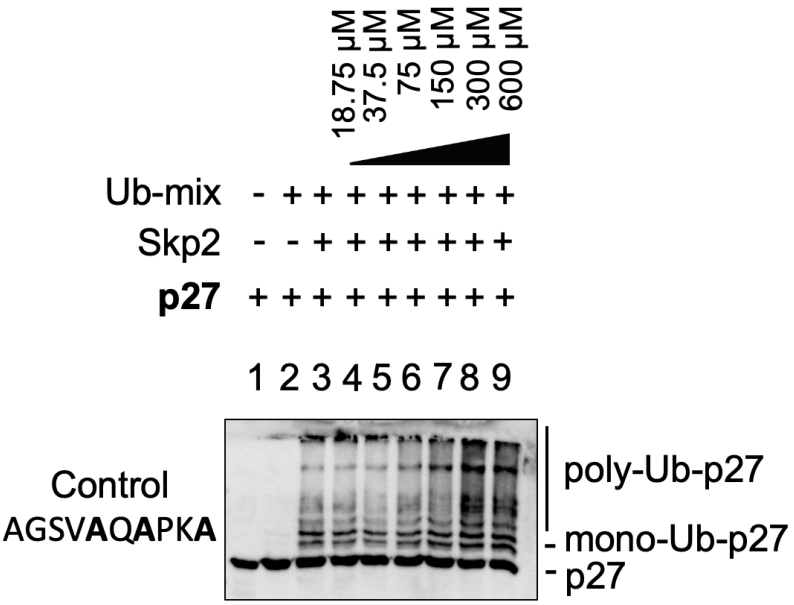

Figure 5.8: Titration of linear control p27 peptide in a p27 ubiquitination assay. This peptides has all the Skp2-binding residues changed to alanine and is unable to bind to Skp2. As expected, this peptide has no effect on p27 ubiquitination even at the highest concentration of 600 µM.

Linear and constrained p27 peptides were further used to study their ability to inhibit p27 ubiquitination *in vitro*. Assay was performed as described for the control peptide and western blot analysis of the levels of p27 ubiqutination are shown in Figures 5.9. Linear TAMRA-AGSVEQT(phos)PKK peptide was used as a control to evaluate the difference between linear and constrained peptides. All peptides were used at the same concentrations to allow comparison between them.

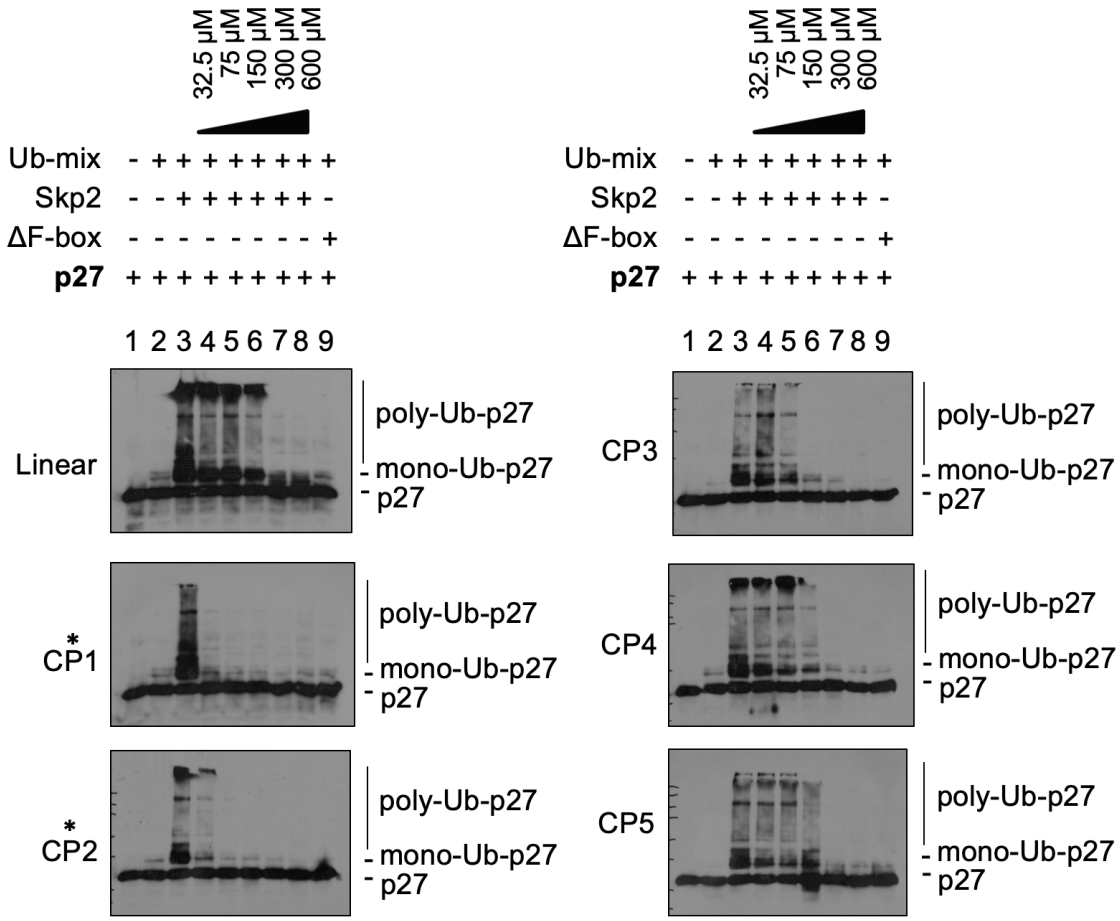

Figure 5.9: Titration of linear and constrained peptides in a p27 ubiquitination assay. "ΔF-box" is a truncated variant of Skp2, which lacks the F-box domain and is therefore unable to bind Skp1 and the other SCF subunits resulting in no ligase activity. All experiments were repeated twice, and representative data are shown. The extent of ubiquitination was estimated from the intensity of the poly-ubiquitinated p27 bands. The linear p27 peptide never achieves full inhibition of p27 ubiquitination even at the highest concentration used. 150 µM of CP1 and CP2 (Group 1 peptides; labelled with $*$) and of CP3 is sufficient for full inhibition. 300 µM of CP4 and CP5 is required for full inhibition.

All of the constrained peptides inhibited p27 poly-ubiquitination to a greater extent than did the linear peptide, consistent with their enhanced Skp1-Skp2-Cks1-binding affinities. All CPs appear to inhibit p27 ubiquitination more effectively than a linear peptide. AGSVEQT(phos)PKK linear peptide had the weakest effect on p27 ubiquitination and required concentration of 300 μM to have an effect. CP1 and CP2 showed greatest inhibition in comparison to other CPs. It inhibited more than 50% ubiqutitination at concentrations as low as 32.5 μM. Although CP2 and CP4 bind the most tightly of all the peptide to Cks1-Skp2-Skp1 (K_d of 32 ± 8 nM and 46 ± 9 nM respectively), CP4 only inhibited ubiquitination in the *in vitro* assay at 300 μM concentration.

Since CP1 seemed to inhibit p27 ubiquitination at the lowest concentration used in the previous assay and a good titration response was not achieved using those concentration this was then repeated using 1:10 dilution of CP1. This is shown in Figure 5.10. Similarly to CP2 peptide it was able to inhibit p27 ubiquitination at concentrations as low as 30 μM.

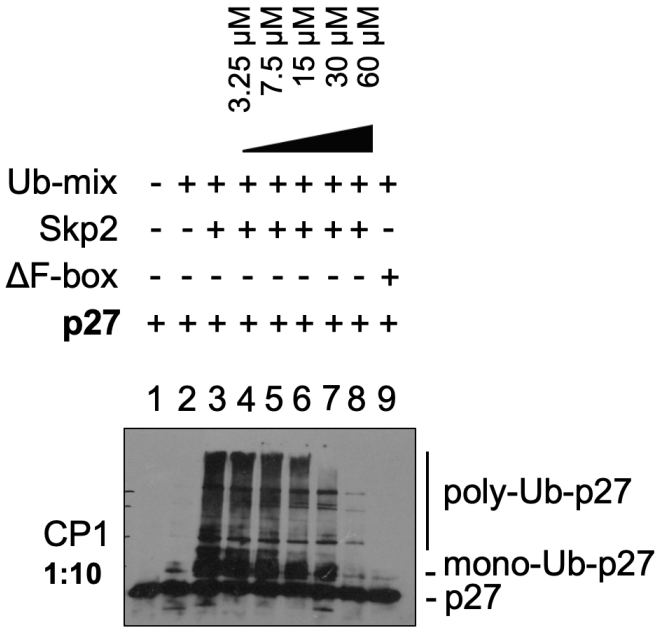

Figure 5.10: Titration of 1:10 dilution of CP1 peptide in a p27 ubiquitination assay. 'ΔF-box' indicates a truncated Skp2 that results in no ligase activity.

The results of the ubiquitination assay do not directly correlate perfectly with K_d values determined using FP where all stapled peptides had similar affinities for the Skp1-Skp2-Cks1 complex. Both CP1 and CP2 peptides belong to Group 1 peptides (see Chapter on peptide design and synthesis) which had 'click' performed between azido amino acids

spaced 4 amino acids apart and using a longer linker of urea origin. In comparison, CP3-CP5 belong to Group 2 peptides where 'click'ed' residues were only 2 amino acids apart. These ubiquitination inhibition data represent that Group 1 peptides are better at inhibiting SCF^{Skp2} ligase activity compared to Group 2. We speculate it could potentially arise from some interactions of the urea-origin linker and the ligase complex. Even though all peptides had similar K_d values it could be speculated that CP1 and CP2 binding kinetics are somewhat different in order to account for the differences in the ubiquitination inhibition assay. Further biophysical testing like surface plasmon resonance (SPR) and stopped-flow methods should be used to characterize the association rate constants (k_{on}) and the dissociation rate constants (k_{off}) to investigate these binding differences. For example, a peptide that does not dissociate rapidly from the ligase complex could potentially be more effective in the *in vitro* ubiquitination inhibition assay due to its ability to stay bound to the ligase for longer. Although the reason for this lack of close correlation between binding and inhibition is not clear at present, the results demonstrate the importance of using several techniques to functionally characterise macrocyclic peptide activity to increase the likelihood of inhibiting Skp2-mediated ubiquitination of p27 in cells.

5.2.6 Constrained p27 peptides inhibit ubiquitination of other Skp2 substrates

To further investigate peptide binding to SCF^{Skp2} we decided to test the ability of p27 peptides to inihibit ubiquitination of other Skp2 substrates. Since p21 is known to require Cks1 for its binding to Skp2 in the same manner as $p27^{249}$ it was chosen as one of the substrates to be tested. p21-HA was made by immunoprecipitation from cells to maintain any post-translational modifications needed for its ubiquitination. p27 peptides were then tested for their ability to inhibit ubiquitination of p21. The ubiquitination inhibition assay was performed in the same way as previously where p21 and Skp2 concentrations were kept constants and selected p27 peptides were titrated in. Western blots from these assays are shown in Figure 5.11. From lane 3 it can be seen that ubiquitinion assay of p21 by Skp2 worked well using previously established method for p27. The linear peptide had no effect whilst CP1 and CP2 were more effective at inhibiting p21 ubiquitination as compared to CP4. This follows a similar trend as in the p27 ubiquitination inhibition assay, which was as expected due to close similarities of p21 and p27 binding to Cks1-Skp2 interface.

For comparison, Skp2 substrate MYC was also tested which does not require Cks1 for its recognition. Skp2 is one of several proteins involved in the regulation of MYC protein

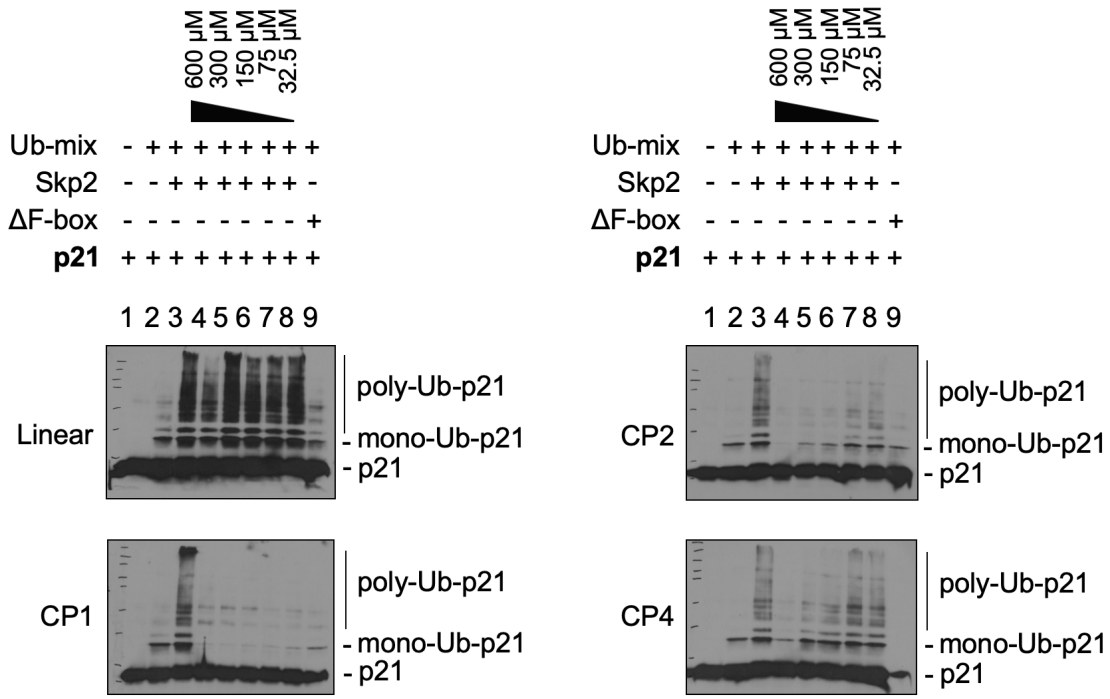

Figure 5.11: Titration of linear and constrained peptides in a p21 ubiquitination assay. 'ΔF-box' indicates a truncated Skp2 that results in no ligase activity. All experiments were repeated twice, and representative data are shown. The extent of ubiquitination was estimated from the intensity of the poly-ubiquitinated p21 bands. Linear p27 peptide did not inhibit p21 ubiquitination even at the highest concentration. CP1 and CP2 inhibited p21 ubiquitination at 32.5 µM and 75 µM respectively whereas 300 µM of CP4 was required for full inhibition.

stability. Skp2 recognizes MYC through both MBII and HLH-LZ motifs (amino acids 367 - 439) and promotes MYC poly-ubiquitination and degradation.[250,251] In addition, Skp2-mediated regulation of MYC degradation does not appear to be phosphorylation dependent. Furthermore, Skp2 expression stimulates MYC-induced S-phase entry.[251] Thus, unlike SCF^{Fbw7}, which stimulates MYC degradation and inhibits MYC activity, Skp2 promotes MYC transcriptional activity, acting as a transcriptional co-activator.[250,251] In addition, Skp2 was found to be associated with MYC target gene promoters, along with proteasome subunits, suggesting a link between SCF^{Skp2}-mediated ubiquitination, MYC transcriptional activation, and degradation.[252]

An additional layer of complexity exists here because Skp2 is a direct MYC target gene.[253] Thus, MYC can augment expression of Skp2, possibly contributing to oncogenesis by both increasing MYC transcriptional activity, while controlling its level, and inducing the degradation of p27. SCF component Skp2 not only signals Myc ubiquitylation and

destruction but is also a potent stimulator of Myc's transcriptional activity. These data suggest that Skp2 acts to couple the activity of Myc to its destruction by the proteasome and that activation of Myc by Skp2 is an important event in the control of mammalian cell growth.[252]

To test whether the p27 peptides are able to inhibit MYC ubiquitination and potentially blocking Myc's transcriptional activity, we decided to tested their inhibitory abilities in myc ubiquitination assay. *E. coli* purified N-terminus of N-myc (372-464 aa) was kindly provided by Dr Lisa Kent from Laman's lab. Firstly, the SCF^{Skp2} ligase containing Cks1 was used in the N-myc ubiquitination inhibition assay and results are shown in Figure 5.12. From lane 3 it can be seen that N-myc ubiquitination can also be successfully achieved using developed p27 ubiquitination assay. Furthermore, peptides seemed to be less active towards inhibiting N-myc ubiquitination as compared to p21 and p27. For comparison, the same assay was performed using SCF^{Skp2} ligase containing no additional Cks1 (see Figure 5.13). Interestingly, p27 peptides were much more potent in this setting. Myc does not require Cks1 for Skp2 binding, and potentially the absence of Cks1 in the reaction mix allows for more natural myc binding and subsequent ubiquitination.

The development of the p27 ubiquitination assay allowed for testing of peptides in a more biological setting. The assay was robust enough to allow testing ubiquitination of several other Skp2 substrates which could be a great tool in deciphering peptide specificity and further drug development.

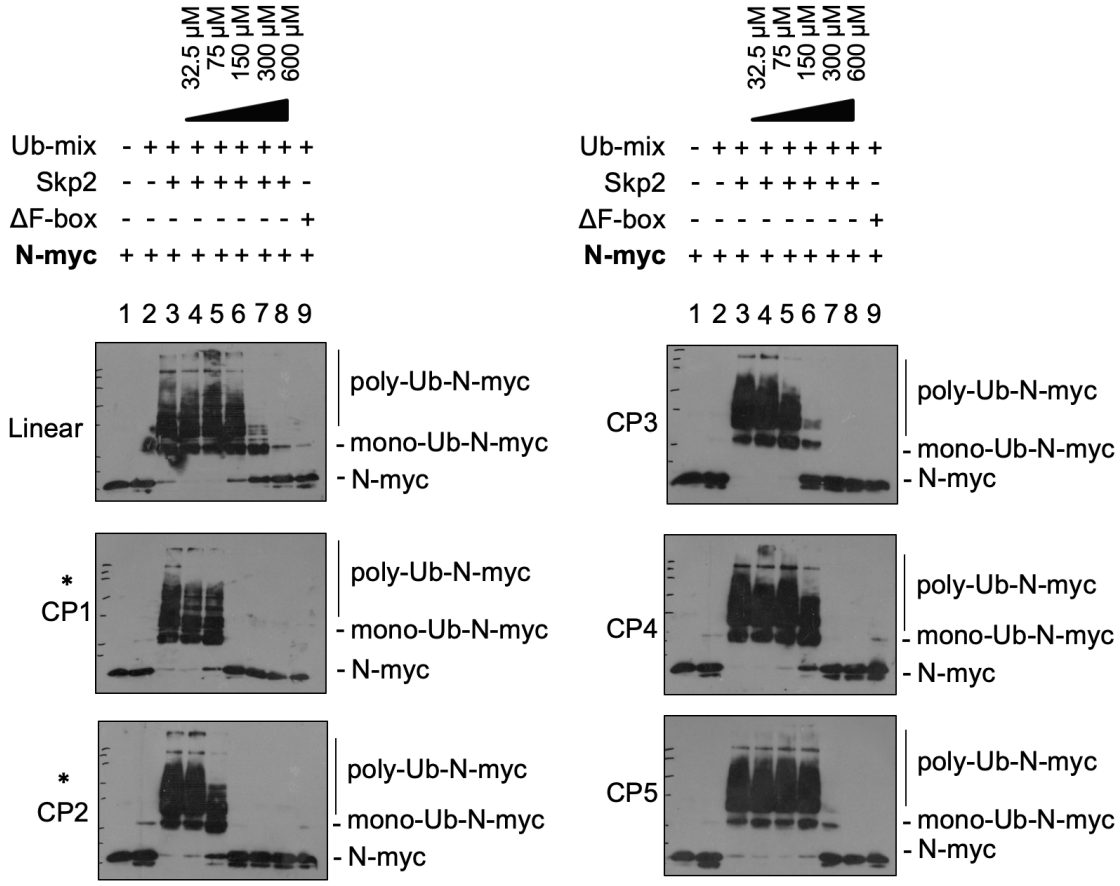

Figure 5.12: Titration of linear and constrained peptides in a N-myc ubiquitination assay. 'ΔF-box' indicates a truncated Skp2 that results in no ligase activity. All experiments were repeated twice, and representative data are shown. The extent of ubiquitination was estimated from the intensity of the poly-ubiquitinated N-myc bands. In this experiment SCF^{Skp2} ligase complex containing Cks1 was used. In comparison to the ligase lacking Cks1 here we can see that p27 peptides are less effective at inhibiting N-Myc ubiquitination. Peptides required far greater concentrations to achieve similar results. Linear, CP4 and CP5 peptide at 300 µM inhibited ubiquitination, and CP1 and CP2 at 150 µM.

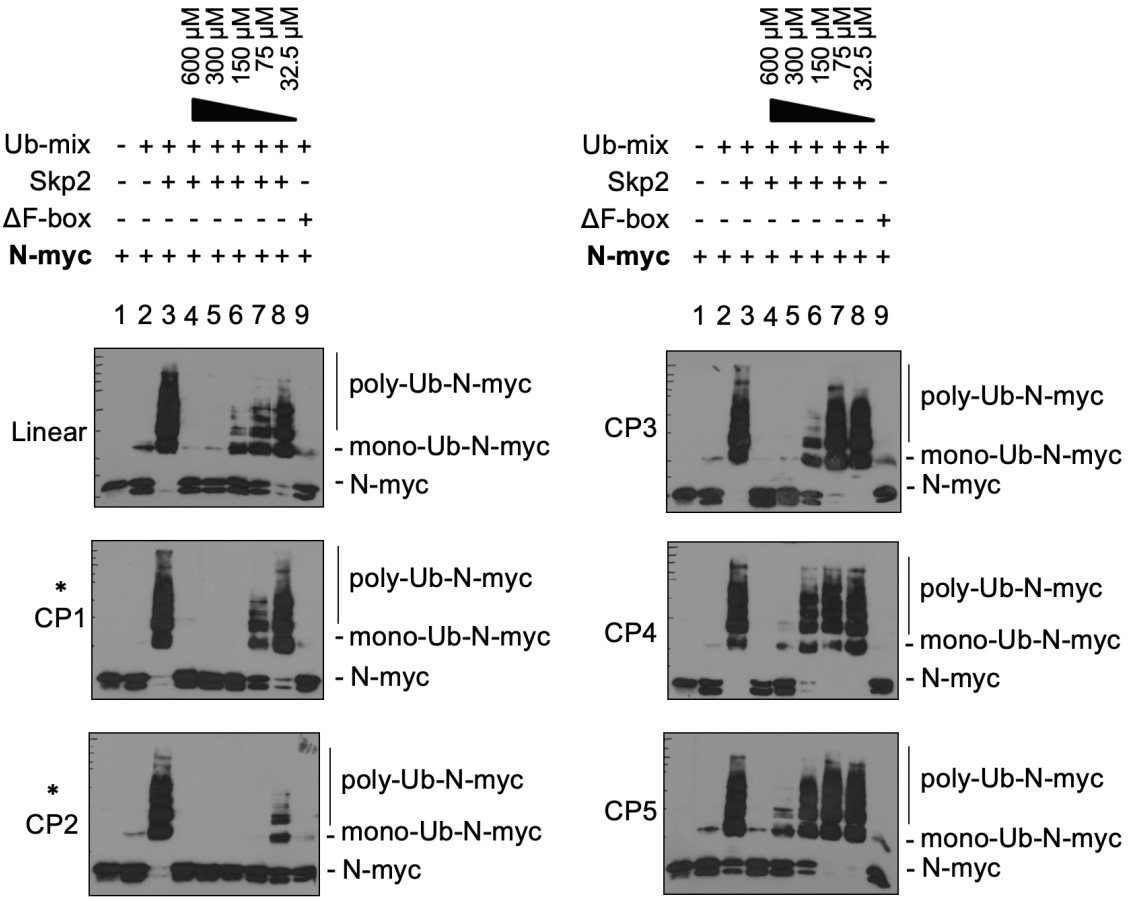

Figure 5.13: Titration of linear and constrained peptides in a N-myc ubiquitination assay. 'ΔF-box' indicates a truncated Skp2 that results in no ligase activity. All experiments were repeated twice, and representative data are shown. The extent of ubiquitination was estimated from the intensity of the poly-ubiquitinated N-myc bands. In this experiment SCF^{Skp2} ligase complex lacking Cks1 was used. The linear p27 peptide as well as CP3, CP4 and CP5 are all able to inhibit ubiquitination at around 150-300 µM concentration range. CP1 and CP2 were far more effective and caused inhibition of ubiquitination at 32.5 µM and 75 µM, respectively.

The ubiquitination assay has been a valuable tool to evaluate the more biological effects of various p27 peptides in the *in vitro* setting. Interestingly, after testing several SCF^{Skp2} substrates, we can determine that in this particular assay set up, the N-myc was ubiquitinated most efficiently. This can be seen then comparing the amounts of non-ubiquitinated substrate present after the ubiquitination reaction has taken place. For example, in the p27 and p21 assays, we observe only some conversion to ubiquitinated species whilst with N-myc we can see 100% conversion, and no unmodified substrate present in the sample. As discussed previously, p27 requires phosphorylation of the threonine to be recognised by the SCF^{Skp2} ligase. The poor ubiquitination could potentially be improved by using an alternative substrate preparation method to ensure maximum substrate recognition by the E3. In this case, p27 could be purified from the *E. coli*, to achieve higher yields as compared to cellular IP, and then threonine could be phosphorylated in the presence of the kinase. Subsequently, only phosphorylated p27 could be used in the ubiquitination assay which could greatly improve the reaction efficiency and could potentially result in total conversion to Ub-p27.

Furthermore, to avoid any data misinterpretation, all peptides should be tested in the control assay set up where instead of the SCF^{Skp2} E3 an alternative E3 ligase is used. This would further investigate if the inhibition effects observed are truly E3 specific and are not arising from the peptide interacting with other ubiquitination assay components. Lastly, it must be stated that all ubiqituination blots shown should be repeated and probed using poly-ubiquitin chain specific antibodies. This would determine the nature of the substrate ubiquitination as either poly-ubiquitination or multi-mono ubiquitination. However, by probing for the substrate, as done in this study, we have avoided any false positives associated with the ubiquitination of other reaction components, especially the auto-ubiquitination of the SCF^{Skp2}. Moreover, given the depth and breadth of literature on the p27 ubiquitination by the SCF^{Skp2}, the poly-ubiquitination of p27 is the most likely outcome and thus the ubiquitination observed was interpreted as a poly-ubiquitination in this study.

5.2.7 Ubiquitination assay in HEK293T cells

In parallel to *in vitro* ubiquitination assays we have been working on developing a ubiquitination assay in HEK293T cells. In order to avoid the degradation of ubiquitinated p27, which would prevent detection of ubiquitinated p27, cells were treated with 10 μM proteasome inhibitor MG132 for 4 hours prior the cell lysis and immunoprecipitation of p27 with anti-HA beads. The results of p27 ubiquitination by SCF^{Skp2} ligase in HEK293T cells are shown in Figure 5.14.

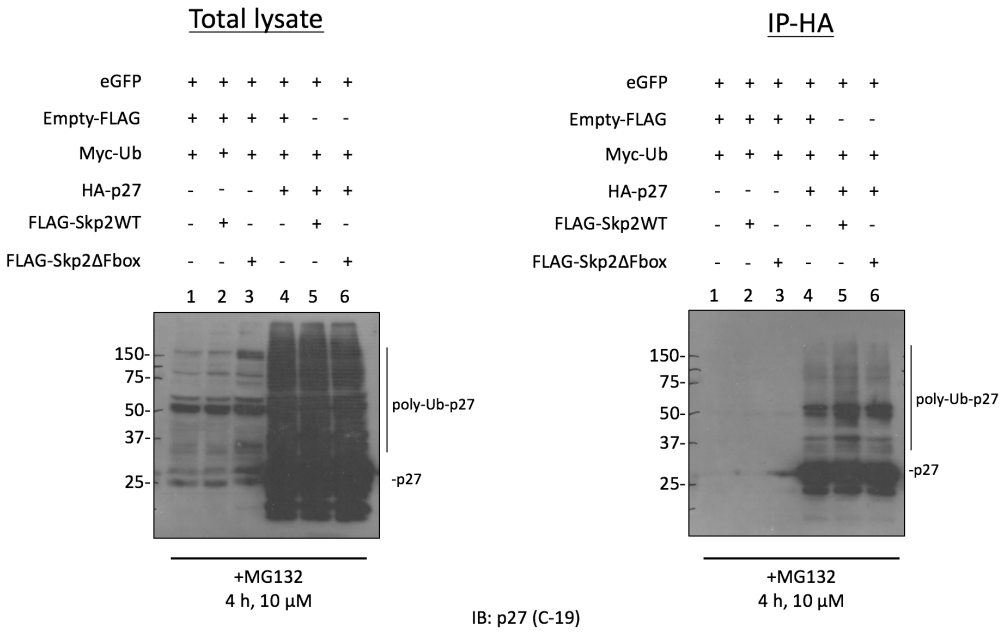

Figure 5.14: p27 ubiquitination assay in HEK293T cells. Cells were transfected with FLAG-Skp2WT or FLAG-Skp2-ΔFbox, Myc-Ubiquitin, HA-p27. HA-p27 was immunoprecipitated and the presence of high molecular weight bands corresponding to poly-ubiquitinated p27 were detected with anti-p27 antibody.

From western blot it can be seen that p27 is ubiquitinated in the absence of Skp2WT ligase as well as with Skp2-ΔFbox. This might be due to endogenous ligase available in the cell. In cells transfected with Skp2-WT, p27 ubiquitination does not seem to be significantly increased. This could be due to low amounts of phosphorylated p27 present in cells which could lead to a very small increase in ubiquitination as p27 needs to be phosphorylated in order to be recognised by SCF^{Skp2}. Further experiments could be done in G_1 arrested cells which would have higher amounts of phopshorylated p27. The work of p27 ubiqutination assays in cells was not proceeded any further during this study.

5.2.8 Approaches of peptide cellular delivery

To further investigate the effects of p27 peptides in a more biological environment we have set out to evaluate the effects of the peptides in live cells. First, we synthesised CP2 peptide fused to antennapedia (Antp) cell penetrating peptide (CPP) and a TAMRA fluorophore to monitor peptide cellular uptake using tandem confocal microscopy. Antp was attached at the $C_{terminus}$ of the p27 peptide, as the $C_{terminus}$ is further away than the $N_{terminus}$ from the Skp2/Cks1-binding site thereby minimising the risk of the Antp peptide affecting the interaction. We also added a 5TAMRA fluorophore for microscopy studies, and we included an amino hexanoic acid (Ahx) linker to provide an adequate spacing between the p27 binding sequence and 5TAMRA dye. As discussed previously Antp tag was used due its lower toxicity when compared to poly-arginine tags and fairly high cellular uptake profile (see chapter Design and Synthesis of p27 Peptides). In this Chapter, peptides referred to as CPP peptides have Antp peptide attached. CP2 peptide was chosen for cellular assays because it had the tightest affinity for Skp1-Skp2-Cks1 complex purified from bacterial cells as determined using FP. Furthermore, it was able to inhibit p27 ubiquitination *in vitro* at one of the lowest concentrations showing high affinity for the SCF^{Skp2} complex purified from mammalian cells also. These experiments indicated that CP2 would be expected to be the potent in cellular assays. The peptide synthesised is shown in Figure 5.15.

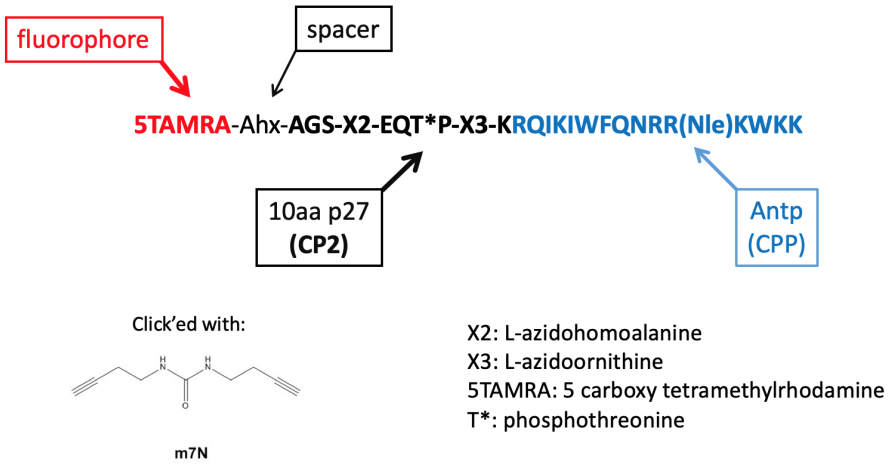

Figure 5.15: Structural schematic of TAMRA and Antp labelled CP2 peptide used in cellular assay. TAMRA was attached at the $N_{terminus}$ whilst Antp CPP was attached on the $C_{terminus}$ of the peptide. Norleucine (Nle) was used instead of the original methionine in the Antp sequence. Azido containing unnatural amino acids were macrocyclised using m7N linker.

All imaging was done using live cells. First, U2OS cells were treated with TAMRA-CP2-CPP peptide for 4 hours (at 37°C, 5% CO_2) at 40 μM concentration of the peptide in cell medium. And 30 min with Hoechst 33342 for nuclear staining. After that cells were washed 3 times with PBS and replenished with of HBSS media for imaging. Cells were imaged using a tandem confocal microscope (Leica) and images acquired are shown in Figure 5.16. Confocal microscopy shows that TAMRA-CP2-Antp was able to cross the cell membrane. A proportion of the peptide is localised to the cytosol (and not trapped in endosomes), as indicated by the diffuse cellular distribution rather than localised endosomal dots. However, a majority of the peptide appeared to be encapsulated in endosomes. Potentially, peptides might be able to be released in the cytosol after certain time, but more testing needs to be done.

To circumvent this issue, we tested electroporation as an alternative means to delivery peptides. This could allow us to study the whole array of already synthesised peptides since there is no need for CPP attachment. We used U2OS cells to have a direct comparison to Antp mediated delivery. Peptide was electroporated into U2OS cells using Neon 9000 (see full protocol in Materials and Methods). Cells then were seeded to 6-well imaging plates and incubated for at least 4 hours or until fully attached to the dish (4 - 6 hours). Once attached, cells were washed five times with PBS to remove any excess peptide and replenished with HBSS media for imaging. Images are shown in Figure 5.17. All cells contained peptide distributed extremely well through the cytoplasm. Figure 5.18 shows side-by-side comparison of Antp versus electroporation delivery of p27 peptide. These results are in agreement with other published data that suggest CPP-mediated delivery results in some endosomal encapsulation. The data indicated that electroporation could be a superior method to CPP delivery. However, due to its mode of action of mechanically disrupting a lipid bilayer it could pose issues in the downstream biological assays.

Simultaneously, Dr Piyush Chaturbedy a postdoc in Itzhaki's lab was working on a fusogenic liposome delivery system. He has shown that liposomes were able to deliver proteins of more than 10-20 kDa into the cells and thus we decided to explore this delivery method for peptides as well. See Materials and Methods for details on lipsome preparation. Liposomal delivery was tested using linear p27 peptides labelled with either TAMRA or FAM fluorophore. We also tested U2OS and MCF-7 cell lines. Acquired images are shown in Figures 5.19, 5.21 and 5.20. Liposomes are lipophilic carbocyanine DiOC18 (DiR) labeled which is near IR fluorescent (red staining in confocal images). DiR is weakly fluorescent in water but highly fluorescent and quite photostable when incorporated into membranes which allowed us to track its fusion with the cellular membrane. Liposomal delivery of peptides was found to be very dependent of the nature of peptides and the cell line. Compare U2OS vs MCF-7 cells using 40 μM of AGSVEQT(phos)PKK-K(FAM) peptide (Figures 5.19 and 5.20). Peptide was delivered very well to U2OS cells whilst MCF-7 cells did not fuse well with liposomes and thus resulted in little delivery. Interestingly, the confocal images in Figure 5.19 potentially show some co-localisation of the membrane-fused liposomes and the peptide. This could indicate that peptides might be sticking or unable to escape liposomes upon membrane fusion which further complicates evaluation of peptide delivery into cells using this method. Furthermore, TAMRA-labelled peptide had much less cell entry compared to FAM labelled peptide (compare Figures 5.19 and 5.21). This was attributed to different charges of these peptides since it affects formation of the liposomes.

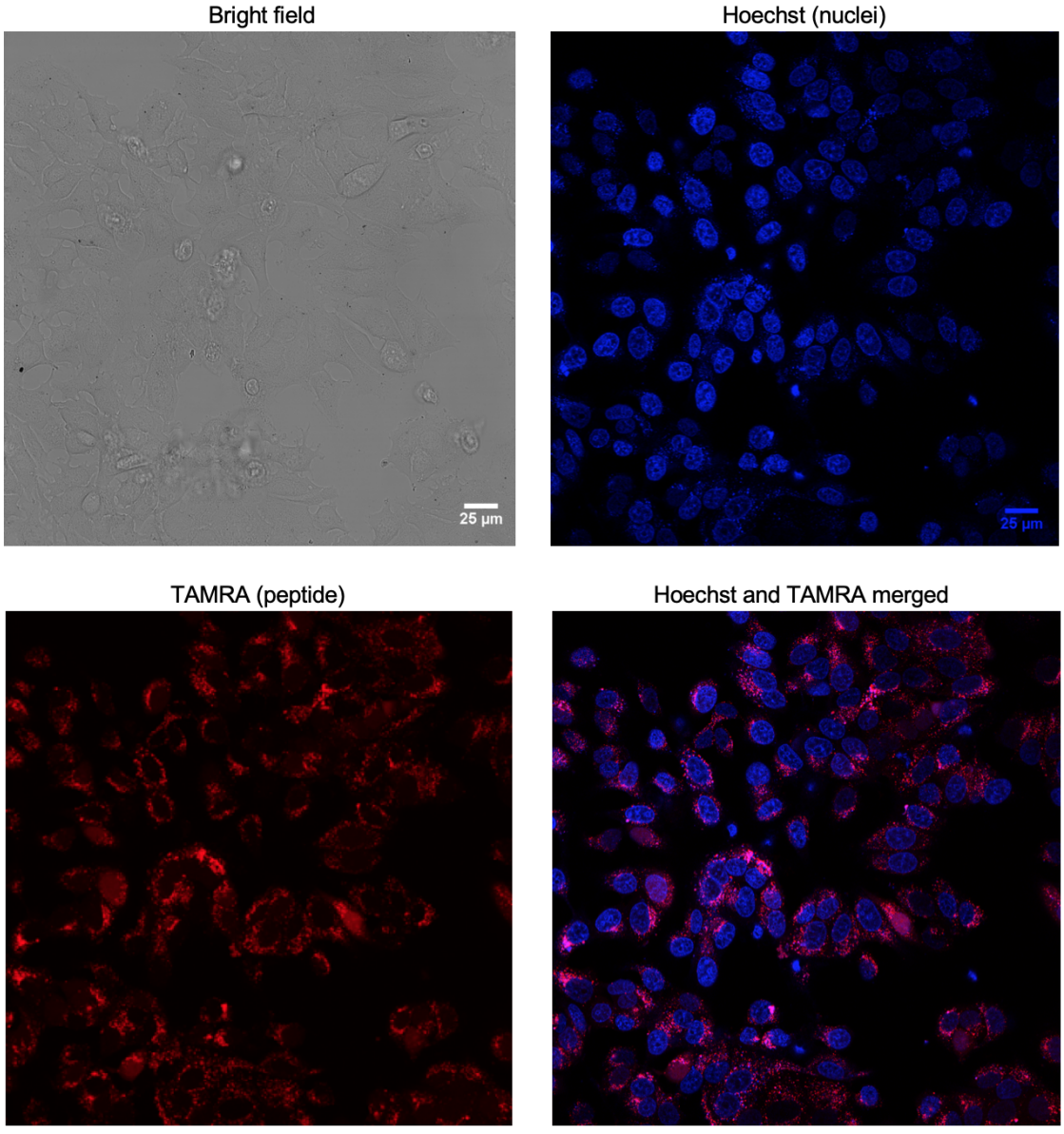

Figure 5.16: Confocal microscope images of live U2OS cells after 4-hour treatment with TAMRA-CP2-Antp peptide. Cells were treated with 40 µM of peptides following extensive wash prior to imaging. Images were taken on a Leica tandem confocal microscope using 40X objective. Blue dye shows nuclei staining with Hoechst 33342 and red corresponds to TAMRA-labelled peptide. The intensity of Hoechst 33342 was increased post data collection to allow clearer visualisation of cell nuclei.

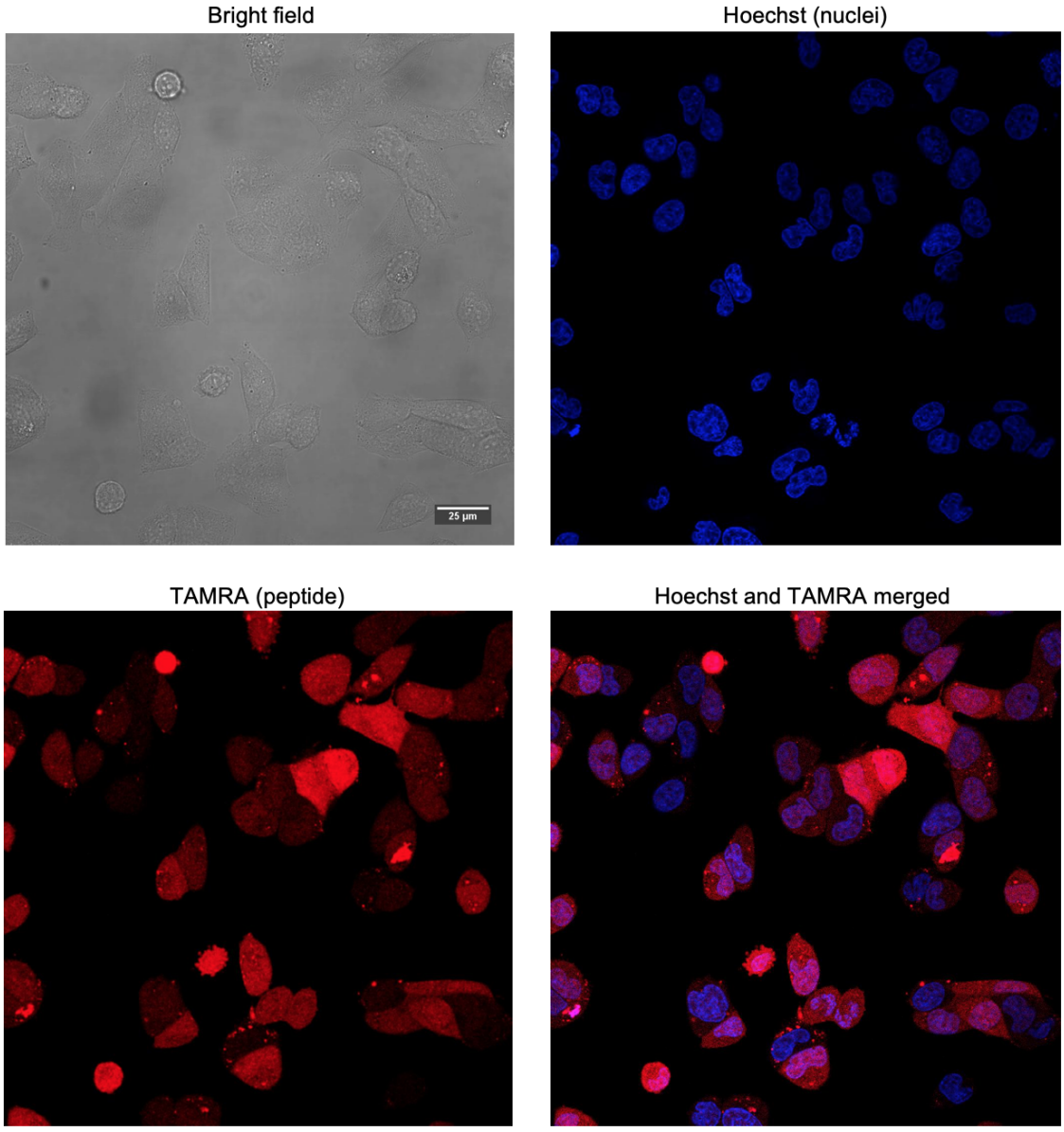

Figure 5.17: Confocal microscope images of live U2OS cells after electroporation of TAMRA-AGSVEQT(phos)PKK peptide. After electroporation performed uing Neon 9000, cells were plated in 6-well plates and recovered for 4 hours until fully attached and then washed extensively prior to imaging. Images were taken on a Leica tandem confocal microscope using 40X objective. Blue dye shows nuclei staining with Hoechst 33342 and red corresponds to TAMRA-labelled peptide.

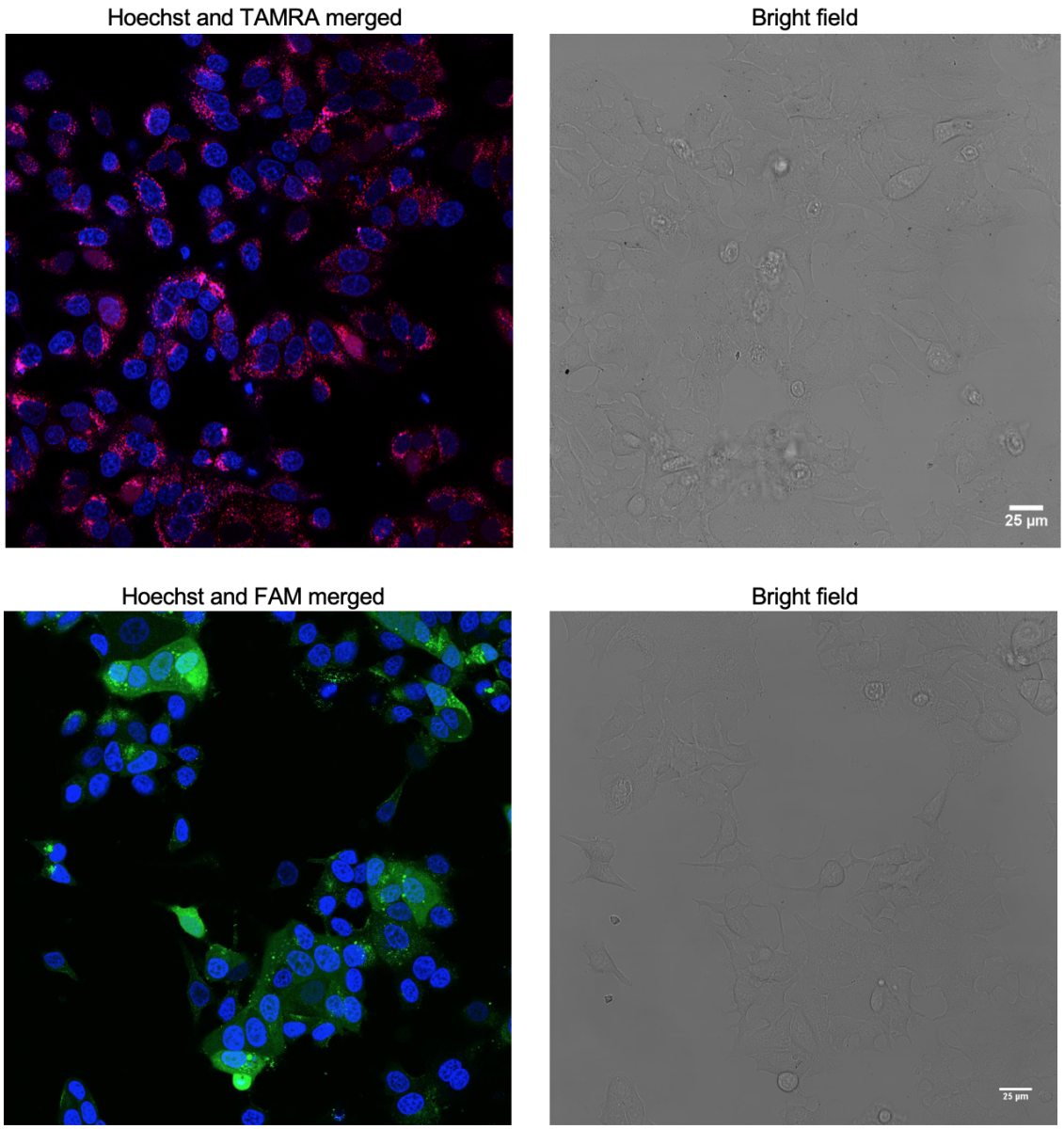

Figure 5.18: Comparison between peptide cellular delivery using either Antp CPP or electroporation methods. Top shows U2OS cellular uptake of TAMRA-CP2-CPP, bottom shows U2OS cells after AGSVEQT(phos)PKK-K(FAM) peptide electroporation. Cellular permeability achieved with Antp results in very little cytosolic dispersion and mostly show potential endosomal encapsulation of the peptide. In contrast, electroporated peptide (without Antp CPP) shows dispersion across cytosol. Images were taken on a Leica tandem confocal microscope using 40X objective. Blue dye shows nuclei staining with Hoechst 33342, red corresponds to TAMRA-labelled peptide, and green corresponds to FAM-labelled peptide.

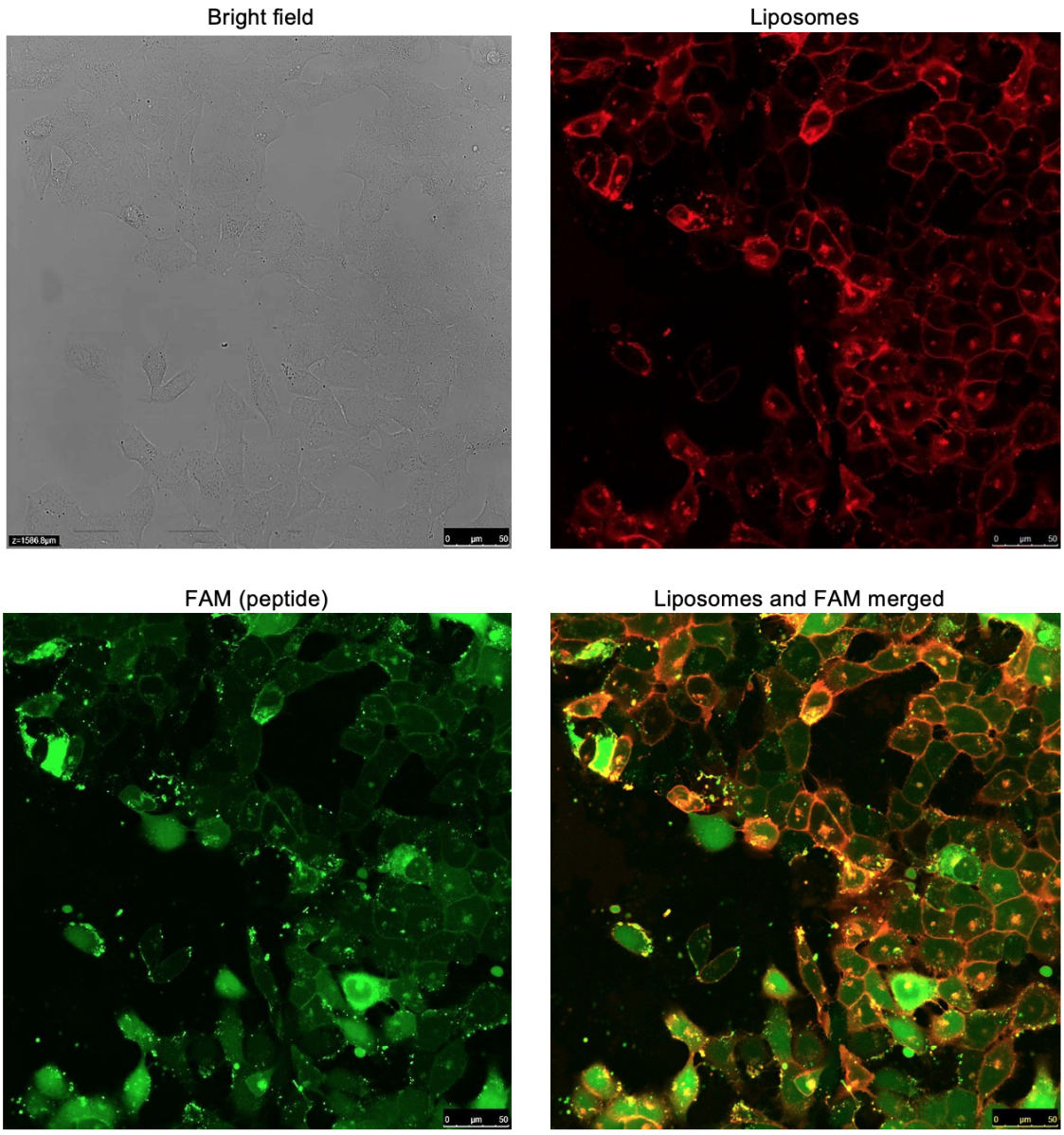

Figure 5.19: Confocal microscope images of live U2OS cells showing liposomal delivery of AGSVEQT(phos)PKK-K(FAM) peptide. Cells were treated with liposome-peptide mix containing 40 μM concentration of the peptide for 15 minutes and then washed extensively prior to imaging. Images were taken on a Leica tandem confocal microscope using 40X objective. Red dye shows liposome staining (liposomes are inherently fluorescent due to aromatic DiR component) and green corresponds to FAM-labelled peptide.

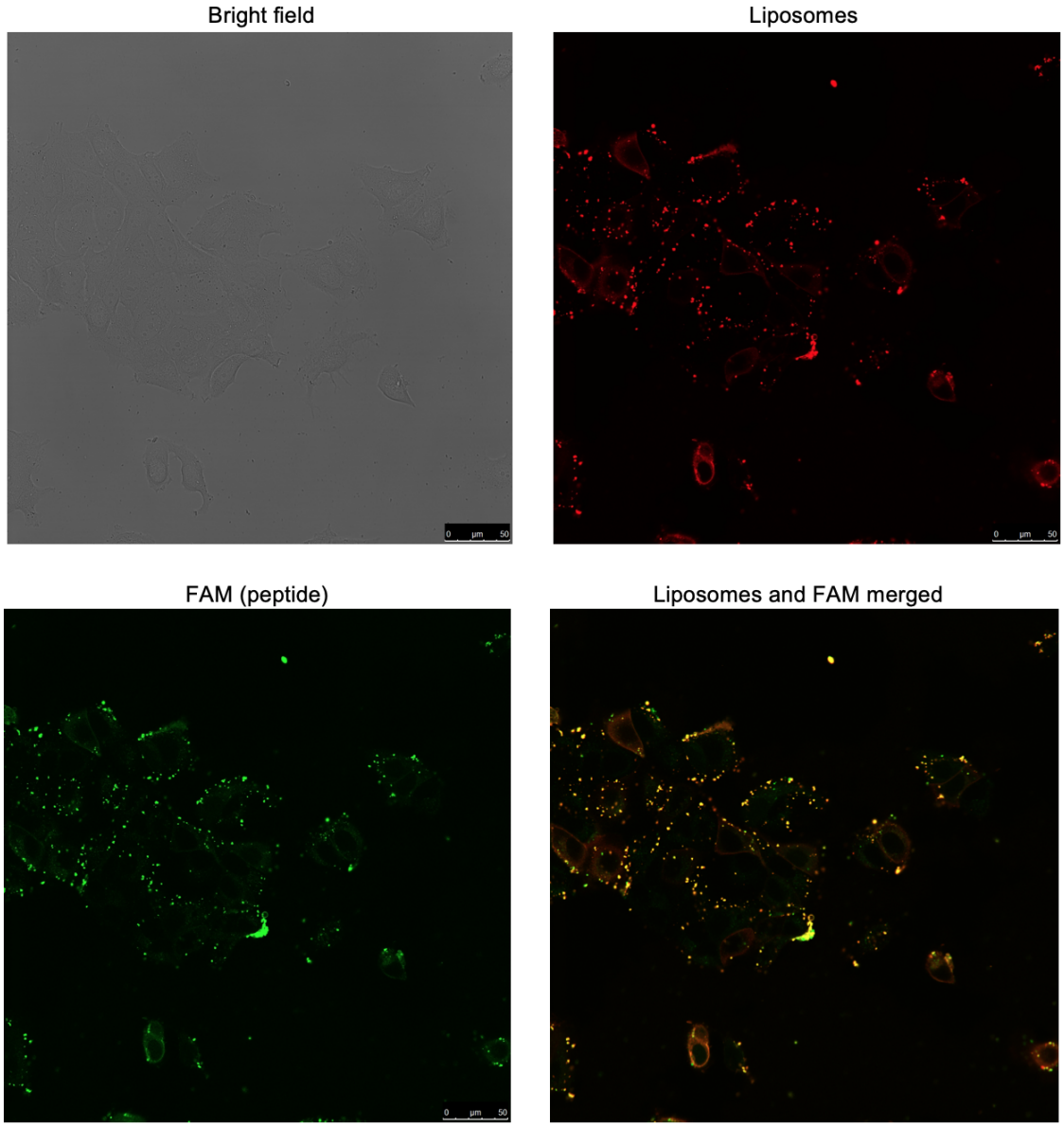

Figure 5.20: Confocal microscope images of live MCF-7 cells showing liposomal delivery of AGSVEQT(phos)PKK-K(FAM) peptide. Cells were treated with liposome-peptide mix containing 40 µM concentration of the peptide for 15 minutes and then washed extensively prior to imaging. Images were taken on a Leica tandem confocal microscope using 40X objective. Red dye shows liposome staining and green corresponds to FAM-labelled peptide.

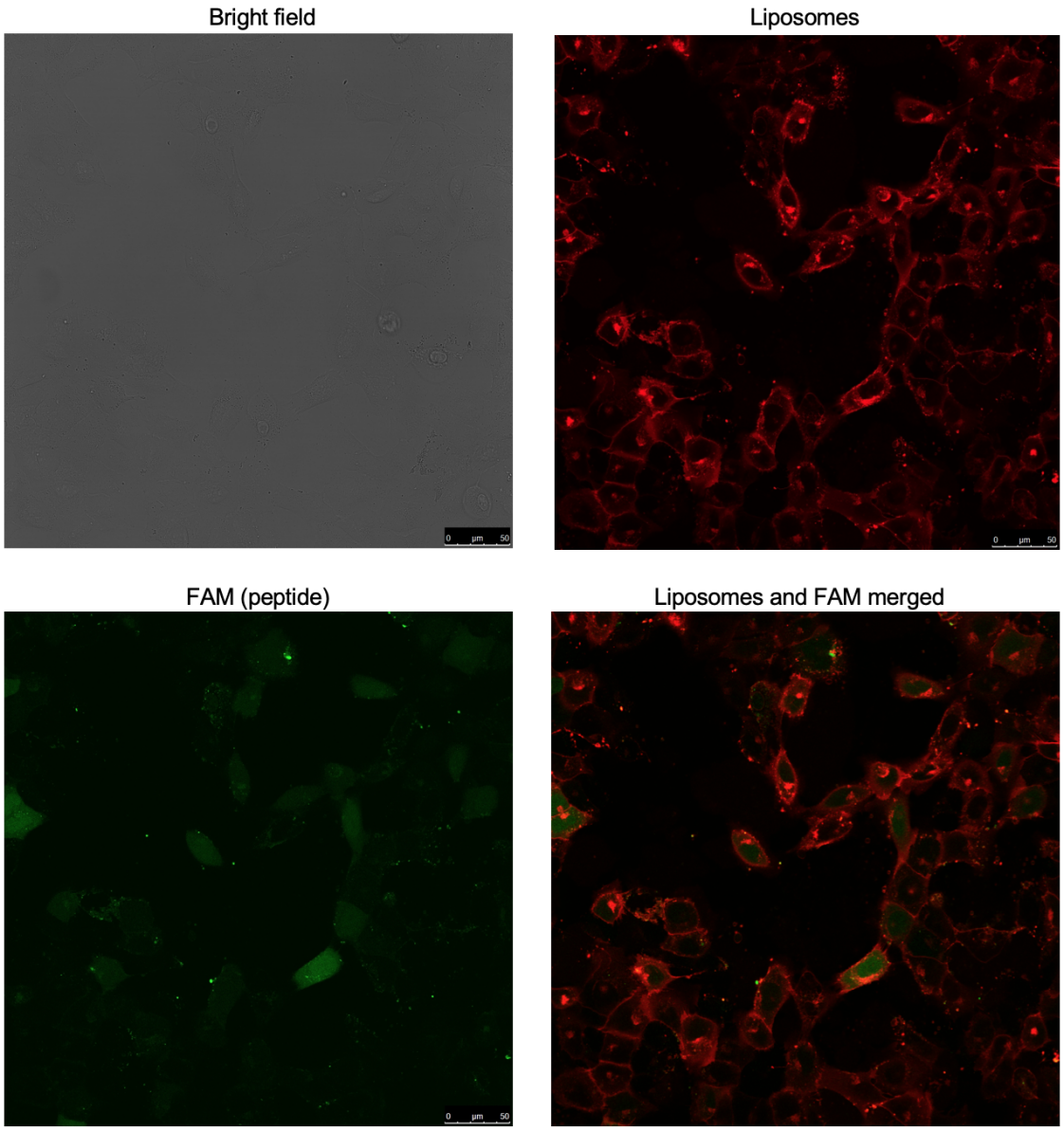

Figure 5.21: Confocal microscope images of live U2OS cells showing liposomal delivery of TAMRA-AGSVEQT(phos)PKK peptide. Cells were treated with liposome-peptide mix containing 40 μM concentration of the peptide for 15 minutes and then washed extensively prior to imaging. Images were taken on a Leica tandem confocal microscope using 40X objective. Red dye shows liposome staining and green corresponds to TAMRA-labelled peptide.

5.2.9 Effects of p27-peptides in cells

It was important to find a cell line that would have a direct response on p27 levels upon introduction of excess Skp2/Cks1. Several cancer cell lines (breast cancer, melanoma and prostate cancer cell lines) were transfected with FLAG-Skp2-WT and Cks1 constructs, and levels of p27 were compared to non-transfected cells. We have found that the best p27 response (the largest reduction in p27 levels upon Skp2/Cks1 overexpression) was observed in MCF-7 cell line which was then chosen to further study the effects of constrained peptides (data not shown).

We looked at the effects of the peptides on the cellular levels of p27 using the MCF-7 breast cancer cell line. First, we determined whether p27 levels were dependent on Skp2 expression. p27 is almost completely depleted in MCF-7 cells transfected with Skp2 and Cks1 compared with non-transfected cells (compare Lanes 1 and 4 in Figure 5.22). This result shows that p27 is targeted by $SCF^{Skp2/Cks1}$ for ubiquitination and subsequent degradation. Treatment with proteasome inhibitor MG132 resulted in an increase in p27 levels (compare lanes 1 and 2), consistent with p27 degradation occurring via the proteasome. However, it was not fully rescued by the MG132 treatment which could potentially mean that the rate of p27 synthesis is slower than the MG132 treatment time. The difference in protein synthesis rates can be observed by comparing lane 2 in the p21 and p27 blots as p21 is fully rescued my MG132 (compare lanes 1 and 2).

We then investigated whether treatment with a constrained p27 peptide could counteract the reduced p27 levels associated with increased Skp2/Cks1 expression. We found that a 16-hour treatment with TAMRA-CP2-Antp of cells that had been first transfected with Skp2 and Cks1 restored p27 levels to the control level (no Skp2/Cks1 transfected) (compare lanes 3 and 4). This result shows that the constrained p27 peptides have the desired inhibitory effect on p27 ubiquitination and subsequent degradation in cells. The same MCF-7 samples were also blotted for p21 since it is degraded via SCF^{Skp2} in a very similar fashion and requires Cks1 accessory protein. Here we also observed the same effect on p21 levels which were restored upon treatment with TAMRA-CP2-Antp. In the future, this assay should be repeated using varying peptide concentrations to produce a dose response curve, as well as varying treatment duration to evaluate how long the peptide effects last within the cell.

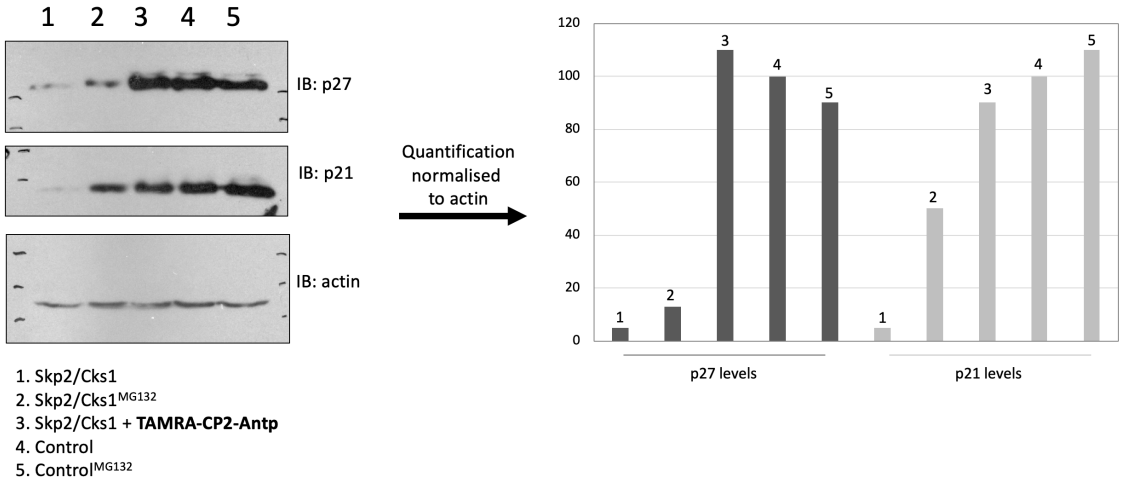

Figure 5.22: Treatment of Skp2/Cks1-transfected MCF-7 cells with constrained peptide TAMRA-CP2-Antp restores the levels of p27 and p21. 1×10^5 MCF-7 cells were seeded in 24-well plates and transfected after 12h with either empty vector control or Skp2 and Cks1. After another 24 hours, cells were treated with 20 μM of the TAMRA-CP2-Antp peptide for 16 hours, and the levels of the $SCF^{Skp2/Cks1}$ substrates p21 and p27 were then determined by western blot. Treatment with TAMRA-CP2-Antp restores p21 and p27 levels to approximately those observed in the control (empty vector transfected) (Lanes 3 and 4).

Since p27 is a key cell cycle inhibitor (see Figure 5.23), we next decided to look at the effects of the highest binding-affinity peptide (CP2) on cell proliferation. We chose to use the BrdU (5-bromo-2'-deoxyuridine) assay, as it can be performed in a 96-well plate that requires only relatively small amounts of peptides and perform experiments in triplicate. The luminescent nature of this assay also provided sensitivity. BrdU is an analog of the nucleotide thymidine and is incorporated into cellular DNA in place of thymidine during DNA replication. BrdU is detected with primary anti-BrdU antibody, and then HRP-linked secondary antibody is used. Once HRP is activated, BrdU levels can then be determined by measuring the absorbance at 450 nm.

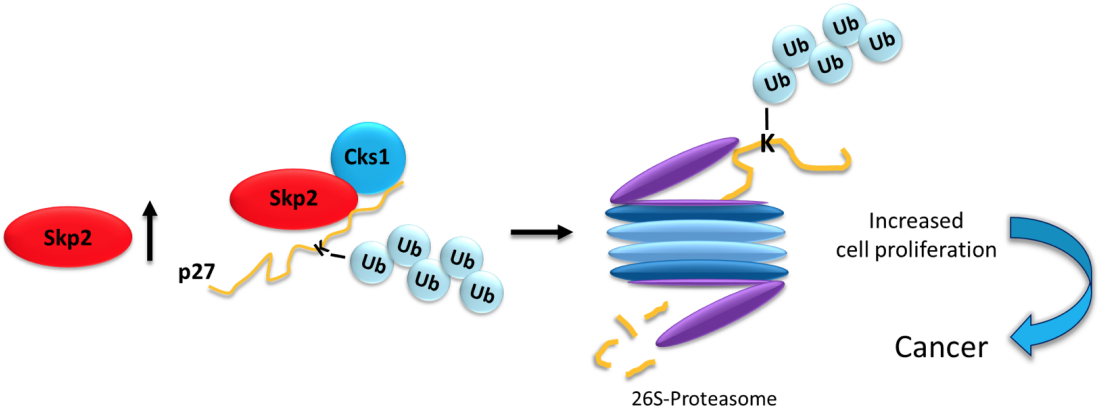

Figure 5.23: Schematic of p27 proteasomal degradation after ubiquitination by $SCF^{Skp2/Cks1}$. Reduced levels of p27 protein lead to increased cellular proliferation.

First, several BrdU assays were performed on HEK293T and MCF-7 cell lines to establish a working assay for the peptides. We have used doxorubicin in these experiments since it is a known chemotherapy drug which block proliferation of cancer cells. Results of doxorubicin treatment on cell proliferation is shown in Figure 5.24. As expected, the data showed a dependence of both cell line on doxorubicin. Also, the error bars were low indicating good reproducibility. We decided to use this assay to further study the effects of various p27 peptides on cell proliferation using MCF-7 breast cancer cell line.

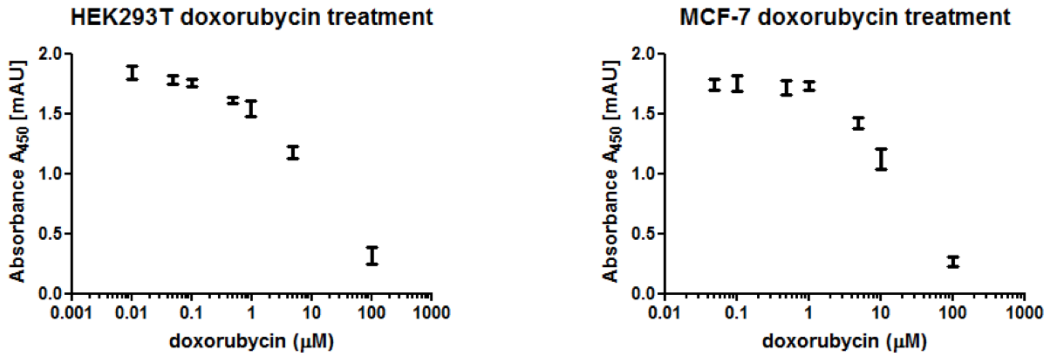

Figure 5.24: Affects of doxorubicin in BrdU cellular proliferation assay of U2OS and HEK293T cells. Cells were seeded at 4×10^5 cells/well in a 96-well plate and incubated overnight. Cell were then treated with various concentrations for 2 hours. Finally, 10 µM BrdU was added to the plate and cells were incubated for 4 hours. Doxorubicin decreases cell proliferation of U2OS and HEK293T cells as detected by BrdU Cell Proliferation Assay Kit #6813 (Cell Signaling Technologies). Error bars are those obtained from triplicate sample measurements.

MCF-7 cells were treated with peptides at a concentration of 20 μM for 16 hours and then cell proliferation tested using a BrdU assay. Data are shown in Figure 5.25. Control (Ala variant), linear and linear-FAM tagged peptides had no effects on cellular proliferation. Constrained peptide CP2-FAM that did not have a conjugated CPP had a small effect on cell proliferation, as well as the CPP alone, caused ∼10% decrease on proliferation. The inhibitory effect was much larger for the CPP-conjugated TAMRA-CP2 (35% decrease). We also tested the CPP for binding to the Cks1-Skp2-Skp1 complex using ITC, and no interaction could be detected (see Biophysical characterisation of constrained peptides). Thus, the small effect of the CPP on cell proliferation is not Skp2-dependent. We have also investigated the effects of phosphomimetic p27 peptides where the phosphothreonine residue is mutated to glutamic acid. Both linear and constrained phosphomimetic peptides had no effects on proliferation (see a section on phosphomimetic peptides in the chapter on Constraining p27 in the protein scaffold). In summary, the results show that constrained CP2 p27 peptide inhibits the ubiquitin ligase activity of oncogenic $SCF^{Skp2/Cks1}$ and reduce cell proliferation.

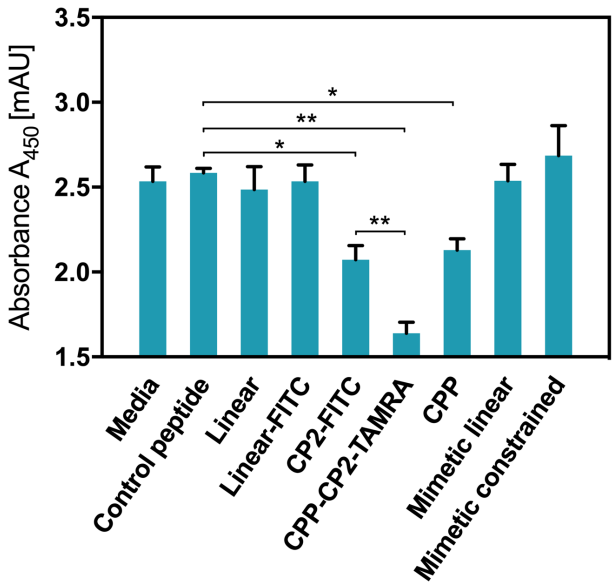

Figure 5.25: BrdU cell proliferation assay of MCF-7 cells after treatment with various p27 peptides. 10^4/well MCF-7 cells were seeded in a 96-well plate. After 24 hours cells were treated with peptides at 20 μM for 16 hours and the BrdU assay subsequently performed. Error bars are those obtained from triplicate sample measurements. Student t-test was performed using GraphPad Prism to evaluate significance of the differences between peptides (* for P≤0.05, ** for P≤0.01 and *** for P≤0.001).

We also performed the cell proliferation assay at different peptide concentrations. Unfortunately, due to a lack of TAMRA-CP2-CPP this particular experiment was only performed once and only at 10 μM of the peptide, whilst other peptides were tested at 10 μM, 25 μM and 50 μM concentrations. The data is shown in Figure 5.26.

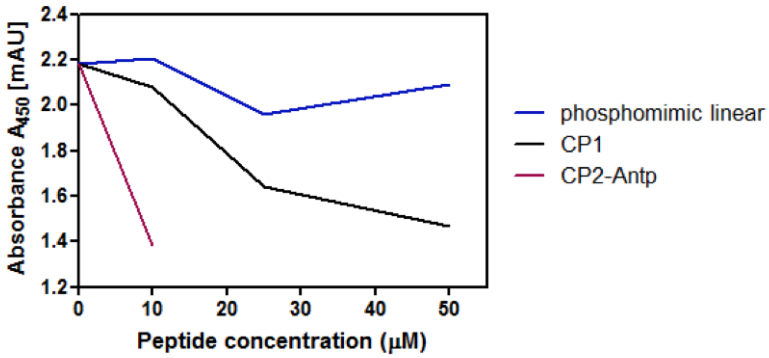

Figure 5.26: BrdU cell proliferation assay of MCF-7 cells after treatment with p27 peptides. 10^4/well MCF-7 cells were seeded in a 96-well plate. After 24 hours cells were treated with p27 peptides at 10 μM, 25 μM and 50 μM for 16 hours and the BrdU assay subsequently performed. Due to low amounts of CP2-Antp peptide only 10 μM concentration was used. The experiment was performed once.

Antp conjugated CP2 caused 35% in proliferation even at 10 μM concentrations whilst CP1 and phosphomimetic had almost no effect at 10 μM. CP1 shows a concentration dependent proliferation response and achieved 30% decrease in proliferation at 50 μM. However, that is a five-fold decrease in activity when compared to Antp conjugated CP2. This could be explained by small amount of CP1 being able to cross the cell membrane and elicit a response at higher concentrations. In contrast, a linear phosphomimetic peptide does not cause any reduction in cell proliferation even at 50 μM. This is in line with no binding observed of linear phosphomimetic peptide to Skp1-Skp2-Cks1 using competition FP and ITC.

We are working on repeating this assay with additional controls. We will perform titrations of several new peptides (linear-Antp, control-Antp and unlabelled CP2-Antp), in the BrdU proliferation assay as well as in the western blot assay of p27 levels. These experiments will allow us to study in more detail the effects of macrocyclisation in the cellular environment. In addition, the Skp2 knockout cell line, preferably an MCF-7 knockout, could be used as a control. This would indicated if the observed effects are Skp2 specific and not arising from the peptide interaction to other SCF components.

Furthermore, based on our previous data, we believe that a higher reduction of cellular proliferation can be achieved. From cellular delivery images using Antp conjugated peptide we observed that only a small amount entered cytoplasm whilst a majority of the peptide was potentially trapped in endosomes and thus inactive as it is unable to get to the target ligase. This could result in a need for much higher concentrations to see a large reduction in cellular proliferation. For example, 100 μM doxorubicin caused ∼90% reduction of MCF-7 cell proliferation. We believe, this could be achieved through the use of different peptide delivery methods or solving the endosomal encapsulation problem. Even though peptide delivery using CPPs is often associated with cytosolic distribution problems, other methods may pose other obstacles as well. We plan to explore electroporation and liposomal delivery methods in the future since, based on confocal images they both achieved a high cytoplasmic uptake. However, due to the nature of electroporation (physically creating holes in the membranes for the peptide to pass through), it might have detrimental effects on cellular proliferation which could be potentially mistakenly attributed to the peptide action, and therefore the experimental work must be carefully designed. In addition, liposomal delivery appeared to be extremely dependent on the cargo (peptide chemical composition), which could make comparing biological effects of different peptides difficult due to their varying levels of delivery.

Chapter 6

Constraining p27 in a Protein Scaffold

6.1 Introduction

This chapter will discuss the use of tetratricopeptide repeat (TPR) proteins as a scaffold for developing mono- and bi-functional proteins and their ability to drive targeted protein degradation. This scaffold was developed by Dr Albert Perez-Riba and Dr Pam Rowling in the Itzhaki lab. We have then grafted p27 sequences in to the loop between adjacent repeats of a TPR protein (Figure 6.1) based on the peptide work carried out in Chapters 3-5.

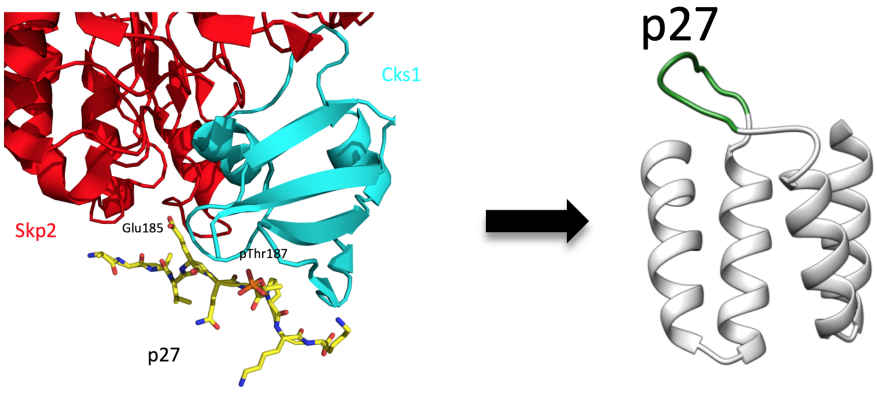

Figure 6.1: Schematic of the 10-residue Skp2-binding sequence derived from p27 grafted onto an inter-repeat loop of a TPR protein (TPR-p27).

TPRs containing an MDM2-binding p53 helix were also tested. Pull-down experiments were performed to evaluate whether p27- and p53- grafted sequences are capable of binding to SCF^{Skp2} and MDM2 ligases in cells. Further testing was carried out to investigate

whether we can target a non-native ligase substrate for degradation using bi-functional proteins. This work was mainly focused on targeting β-catenin.

We have shown that p27-TPR and β-catenin-TPR-p27 proteins can be expressed in *E. coli* and in mammalian cells. Furthermore, β-catenin-TPR-p27 was able to drive β-catenin ubiquitination in an *in vitro* ubiquitination assay. We were able to show reduction of β-catenin levels in HEK293T cells as well as functional Wnt assay using bi-functional TPRs. However, some data proved to be difficult to replicate, and therefore a more focused approach was used to evaluate the effects of p27 loop insertion. We have shown that TPR proteins containing a p27 loop can undergo ubiquitination by SCF^{Skp2} *in vitro* which could potentially result in its rapid degradation in cells. Due to this it was difficult to deconvolute the data of p27 ubiquitination assay.

Furthermore, the grafted p27 loops contain glutamic acid as a mimetic of the phosphothreonine. It is well documented that p27 phospho-threonine is a key residue for Skp2-Cks1 recognition. After seeing positive effects of the TPR with a grafted p27 loop we have further synthesised constrained peptides with glutamic acid instead of phosphothreonine to further investigate the effects of this amino acid substitution. Peptides were designed based on the tightest binding peptide sequences (CP1 and CP2).

6.2 Results and Discussion

This project was a collaborative effort, but here I will mainly discuss data that I have generated. Several mono- and bi-fucntional TPR proteins were designed and cloned by Dr Albert Perez-Riba and Dr Pam Rowling (Itzhaki lab). I have further investigated their ability to either bind MDM2 or SCF^{Skp2} E3 ligases and target β-catenin for ubiquitination and degradation.

6.2.1 p27- and p53-derived peptides grafted onto the TPR scaffold

First, we have investigated if the SCF^{Skp2} and MDM2 ligase binding sequences grafted on the TPR scaffold are able to bind these ligases in cells. Since these TPR proteins are relatively large molecules (over 10 kDa) it is challenging to deliver them across the cell membrane. A postdoc in the Itzhaki lab, Dr Piyush Chaturbedy, is working on the liposomal delivery of these proteins. Here, we have used transient transfection methods

to deliver the DNA of these constructs (in the pcDNA3.1(-) vector) for their expression within mammalian cells. These constructs were designed with a $C_{terminal}$ HA tag to allow immunoprecipitation experiments and their identification by Western blotting. First, immunoprecipitation experiment was used to determine if these ligase-binding TPR constructs are able to pull down the respective ligases present in cells. Schematic of immunoprecipitation was acquired from ThermoFisher website and is shown in Figure 6.2.

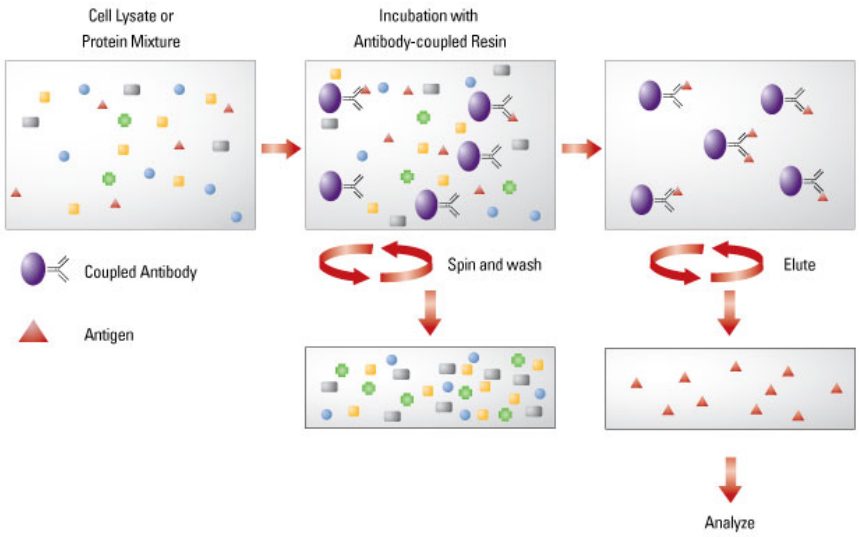

Figure 6.2: Schematic of immunoprecipitation principles (acquired from ThermoFisher website). Cell lysate is incubated with the protein of interest specific antibody-coupled resin. This allows the protein of interest and any other interacting proteins to bind. The resin is then washed multiple times to remove unbound proteins. Bound fraction is then eluted and further analysed using western blot to detect interacting proteins.

This method allows a pull-down of proteins associated with the protein of interest (for the full protocol see Materials and Methods). Briefly, HEK293T cells were transfected with HA-TPR-p53 or HA-TPR-p27, and after 48 hours they were lysed and incubated with HA-agarose beads for at least 4 hours to allow optimum binding of expressed proteins to the beads. The beads were then washed to remove any unbound protein, and Laemmli loading dye was added. Samples were then boiled and analysed using western blot, and the results are shown in Figure 6.3. Pull down samples were blotted for Skp2 and MDM2 ligases to evaluate if TPR proteins containing p27 and p53 binding peptides are able to pull-down these ligases. Samples were also blotted for HA to ensure that the transfected TPR proteins were expressed. In this experiment, the control sample is cells transfected with empty pcDNA3.1(-) vector. In Figure 6.3 A, we can see that HA-3TPR-p27 was

expressed in cells (IB: HA) and was able to pull-down Skp2 ligase (IB: Skp2) but not the control sample. This could indicate that p27 constrained in the loop within TPR scaffold is able to bind to Skp2. Similarly, HA-4TPR-p53 was expressed in cells (IB:HA). However, both control and HA-4TPR-p53 samples pulled down E3 ligase MDM2. This is most likely due to MDM2 'sticking' to the HA-agarose beads, and it therefore can not be concluded that the p53 helix grafted on the TPR scaffold is able to bind MDM2 ligase.

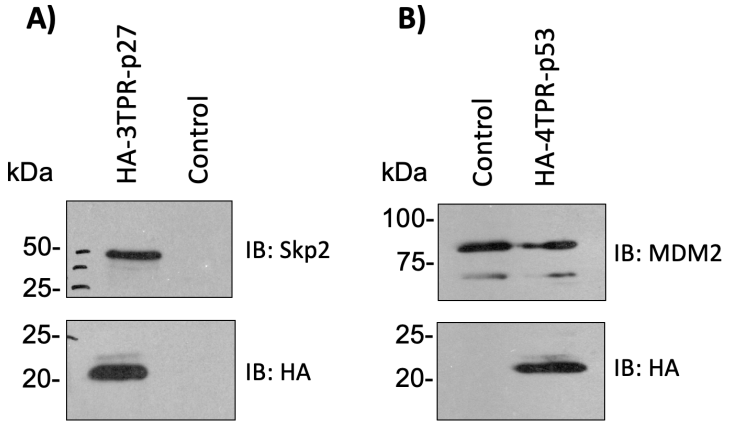

Figure 6.3: Analysis of immunoprecipitated HA-TPR with a ligase binding motif. A) HA-3TPR-p27 pulled down Skp2 ligase whilst control did not. B) HA-4TPR-p53 and control both pulled-down MDM2 ligase indicated that MDM2 is interacting non-specifically with the HA-beads used in the assay.

To potentially circumvent the issue of MDM2 binding to HA-agarose beads we performed a reversed immunoprecipitation. Instead of HA beads, we attached an MDM2 antibody on the agarose beads and tried to pull-down HA-4TPR-p53 instead. Ligase KCl and NET2 buffers were tested with both endogenous and exogenous (transfected) MDM2 (ligase KCl buffer was developed in the Laman lab to use in ligase purification experiments, see Materials and Methods for the buffer information.). Results are shown in Figure 6.4.

Both ligase KCl and NET2 buffers lysed cells efficiently and the transfected proteins (HA-tagged TPRs and MDM2) are detected in total lysate samples. Endogenous MDM2 was not detected at this stage indicating low levels in the dilute lysate samples. IgG beads were used to pre-clear the lysate and eliminate any nonspecific binding to the MDM2 antibodies at the later stage. It can be seen that when using ligase KCl buffer there is some binding of endogenous MDM2 to IgG beads but less of transfected MDM2 (see IB: MDM2). When using NET2 buffer this nonspecific interaction appears to be diminished. This could be due to NET2 buffer having additional detergent (0.1% SDS) and thus stronger ability to disrupt any nonspecific interactions. MDM2 antibody was able to bind to transfected

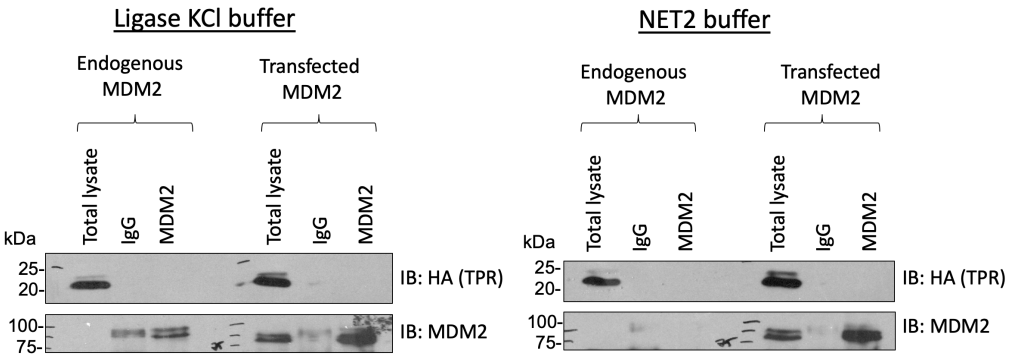

Figure 6.4: Analysis of immunoprecipitated MDM2 ligase with HA-4TPR-p53. Either endogenous or transfected MDM2 was tested using ligase KCl and NET2 buffers. Total lysate prior incubation with beads was loaded to ensure expression of transfected proteins. IgG sample is a pre-clear step indicating any unspecific interactions with the IgG beads prior antibody loading. All samples were blotted for MDM2 (the immunoprecipitated protein) and HA, which would indicate if MDM2 was interacting with HA-4TPR-p53 and thus able to pull it down.

MDM2, but it did not pull down the HA-TPR-p53 (evident from the lack of the band in the IB:HA blot). This result indicated that the p53 helix grafted onto the TPR might not be able to bind to MDM2. However, we do have ITC data demonstrating binding of the purified proteins from *E. coli* (TPR-p53 and the N-terminal domain of MDM2). Thereby we believe that no binding observed in the pull-down assays could be caused by either incorrect folding of the TPR-p53 protein in mammalian cells, and thus the lack of correctly folded p53-helix, or suboptimal buffer conditions used in the assay.

6.2.2 p27 grafted onto the loop of a TPR protein inhibits p27 ubiquitination

To further investigate the TPR-p27 proteins we have decided to test it in the previously established p27 ubiquitination assay. First, I purified a His-5TPR-p27 protein in *E. coli* using a clone provided by Dr Albert Perez-Riba. p27 sequence was inserted between the third and fourth repeat, as previously he had found that the loop insertion after several repeats results in a more stable protein than inserting a loop between the first and second repeats. Protein purification from *E. coli* was carried out as described in Material and Methods, and the purification SDS-PAGE is shown in Figure 6.5.

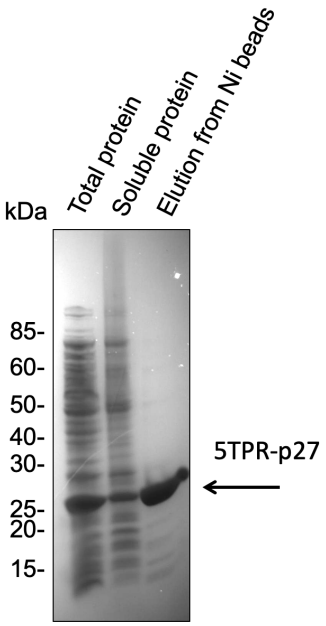

Figure 6.5: SDS-PAGE of one-step Ni-affinity purification of His-5TPR-p27 from *E. coli*. The protein was concentrated, aliquoted and flash-frozen in liquid nitrogen until further biochemical analysis.

From the data it can be seen that 5TPR-p27 is well expressed and soluble and results in pure protein after a single-step affinity purification using His-tag. 5TPR-p27 was concentrated, buffer exchanged to the ubiquitination buffer and titrated into p27 ubiquitination reaction in same manner as constrained peptides discussed in previous chapters. Its effects on ubiquitination were evaluated by western blot and are shown in Figure 6.6.

p27 peptide constrained in the TPR protein scaffold loop was able to fully inhibit p27 ubiquitination at 150 μM concentration. The effect is similar to that of the chemically constrained p27 peptides. The best performing constrained peptides, CP1 and CP2, fully inhibited ubiquitination at 75 μM concentration, whilst 300 μM of CP4 and CP5 was required for full inhibition.

It is important to note that there are two amino acid substitutions in the p27 peptide sequences used in the peptide studies and in the protein scaffold. The linear p27 peptide sequence is AGSVEQT(phos)PKK whilst the one grafted into TPR is AGS**N**EQ**E**PKK. First, since *E. coli* cannot perform post-translational modifications like phosphorylation, phosphothreonine was changed to glutamic acid which is widely used as phosphomimetic. Additionally, valine was changed to asparagine as we thought it would aid solubility of the protein. From Skp1-Skp2-Cks1-p27 crystal structure (PDB: 2AST) we have seen that

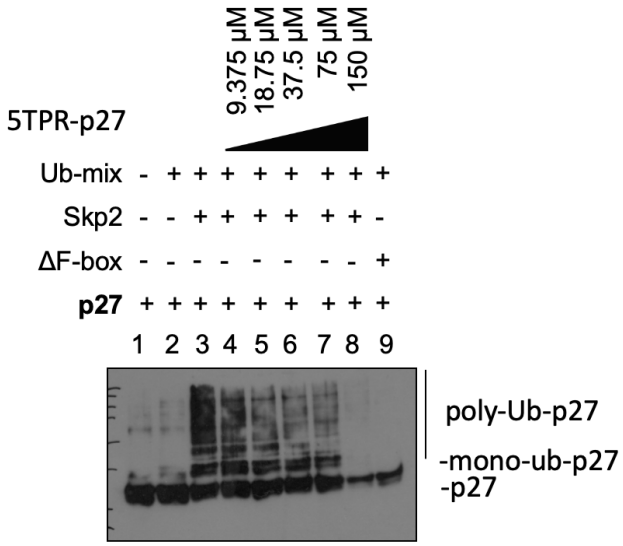

Figure 6.6: Titration of 5TPR-p27 protein in a p27 ubiquitination assay. 'ΔF-box' indicates a truncated Skp2 that results in no ligase activity. The extent of ubiquitination was estimated from the intensity of the poly-ubiquitinated p27 bands. Some effects on p27 ubiquitination can be seen at as low concentrations of 5TPR-p27 as 18.75 µM of 5TPR-p27 (compare lane 3 to lane 5), and it was able to fully inhibit p27 ubiquitination at 150 µM concentration.

valine is pointing away from the binding interface and therefore is not essential for the ligase binding. Furthermore, in our constrained peptide studies it was also changed to the azido unnatural amino acid. This ubiquitination data led us to hypothesise that the phosphothreonine may not be essential for SCF^{Skp2} binding, and possibly the bioactive conformation achieved in the TPR loop is enough to result in a strong SCF^{Skp2} binder. To validate this hypothesis, several phosphomimetic (glutamic acid)-containing constrained peptides were synthesised and tested (see last section of this chapter).

6.2.3 Targeting β-catenin for degradation using bi-functional TPRs

Based on the TPR-p27 pull-down and ubiquitination assay we were confident that p27 grafted on the TPR protein loop is able to bind SCF^{Skp2}. We further focused on developing bi-functional TPRs to bring this E3 ligase and a target protein of interest in to close proximity to facilitate the target's ubiquitination and subsequent degradation. To date, this approach is mostly known as PROteolysis TArgeting Chimeras (PROTAC) and has been widely documented (see Introduction chapter). PROTACs consist of a linker region

that connects two distinct binding moieties, one that binds the ligase and another one that binds protein of interest.

Instead, we have used a TPR scaffold developed in the Itzhaki lab to attach both ligase- and target-binding motifs. We grafted short binding sequences, either loops or helices, to bind various different targets and ligases. This approach allows much wider ranges of ligases and targets to be tested compared to a small molecule PROTACs. This should give us access to the so called 'undruggable' targets, which have extended binding interfaces and no small molecule binders available. Binding sequences can be easily grafted on the TPR scaffold. This modular TPR scaffold allows a mix and match combinatorial use of two peptides. Furthermore, grafting ligase in between different repeats in the TPR scaffold allows us to explore different orientations of the recruited ligase. This is advantegous, since it has recently been shown by C. Crews et al. 2019 that the PROTAC substrate specificity is dictated by the orientation of the recruited E3 ligase.[254] A schematic of bi-functional TPR which was later named as Polyproxin molecules is shown in Figure 6.7.

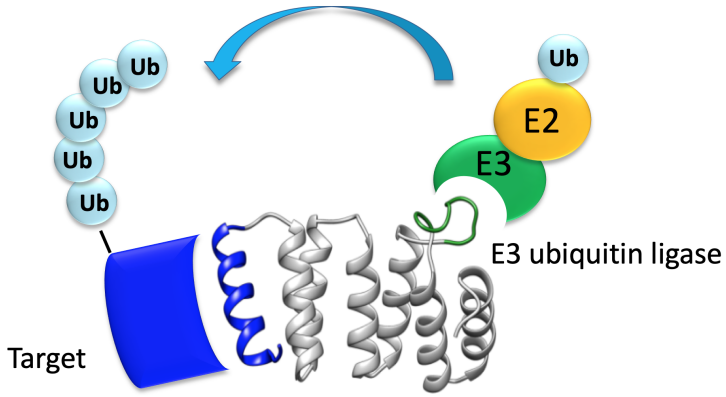

Figure 6.7: Schematic of the bi-functional TPR design, wherein sequences are grafted onto the TPR scaffold. By bringing the target protein and the E3 ligase into close proximity we could potentially facilitate ubiquitination and subsequent proteasomal degradation of the target protein.

My work mainly focused on exploring hetero-bifunctional TPR proteins designed to bind β-catenin and Skp2 ligase. Here we tested their ability to target β-catenin for its ubiquitination and subsequent degradation. Dr Pam Rowling has designed a library of motifs that are potentially able to bind β-catenin. These motifs are shown in Figure 6.8 and were grafted onto TPR helices and loops. Binding peptides from LRH1, axin, bcl9 and ICAT were grafted onto TPR scaffold as helices whilst APC and groove were grafted as loops. Groove peptide refers to a positively charged groove formed between the armadillo repeats

5–9 and is involved in the binding of several β-catenin ligands.[255] Constructs cloned and investigated in this study are summarised in Table 6.1.

It is important to note that the PROTAC project was at a very early stage. At that point Dr Pam Rowling was working on assembling a very large library consisting of a number of different ligase- and substrate-binding peptides to be put together combinatorially. However, not all clones had been successfully produced at the time I came into the project, so we started testing on the ones that we already had. Therefore we did not have a set of hetero-bifunctional proteins where all the various parameters (including number of repeats) were systematically varied. This is reflected in variability in the number of TPR repeats between constructs, grafted peptide positioning within the TPR scaffold as well as variable affinity tag placement within the protein. It was important to validate the grafted peptide sequences so that the library could be adjusted to rule out the sequences that did not bind their targets.

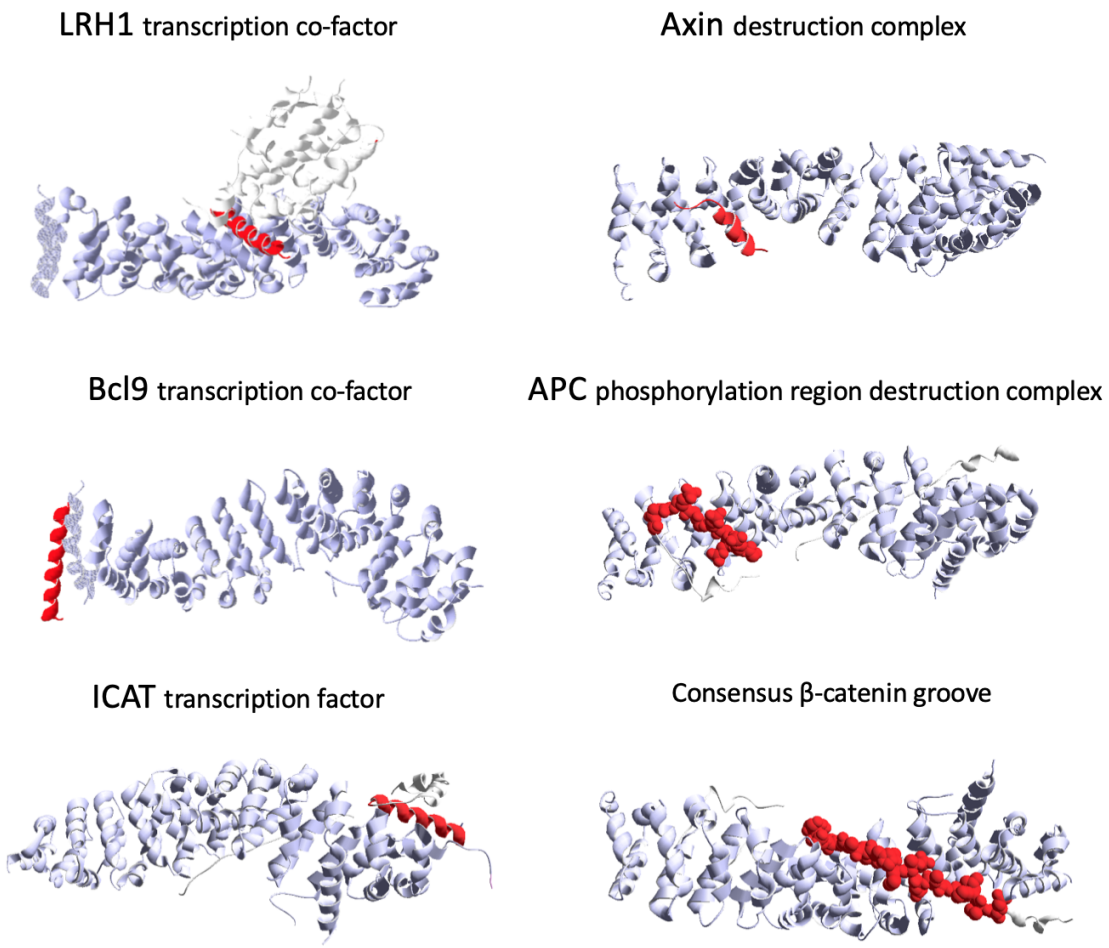

Figure 6.8: Binding of various β-catenin partner proteins that were used to develop bi-functional TPR proteins to target β-catenin degradation.

Table 6.1: Mono- and bi-functional TPR constructs used for targeting β-catenin and SCF^{Skp2}. Bacterial constructs were cloned into pRSET vector, and mammalian constructs were in pcDNA3.1(-) vector.

Expression system	Name	Positions of binding peptides within the TPR scaffold
Bacterial	2TPR	2TPR-His
Bacterial	3TPR-p27	2TPR-p27-TPR-His
Bacterial	axin-2TPR	axin-2TPR-His
Bacterial	bcl9-2TPR	bcl9-2TPR-His
Bacterial	LRH-2TPR	LRH-2TPR-His
Bacterial	phospho-4TPR	TPR-phospho-3TPR-His
Bacterial	axin-3TPR-p27	axin-2TPR-p27-TPR-His
Bacterial	bcl9-3TPR-p27	bcl9-2TPR-p27-TPR-His
Bacterial	ICAT-3TPR-p27	His-ICAT-2TPR-p27-TPR
Bacterial	groove-4TPR-p27	TPR-groove-2TPR-p27-TPR-His
Bacterial	LRH-3TPR-p27	His-LRH-2TPR-p27-TPR
Bacterial	phospho-3TPR-p27	His-TPR-p27-2TPR-phospho-TPR
Mammalian	3TPR-p27	2TPR-p27-TPR-HA
Mammalian	LRH-2TPR	LRH-2TPR-HA
Mammalian	phospho-3TPR	TPR-phospho-2TPR-HA
Mammalian	axin-3TPR-p27	axin-2TPR-p27-TPR-HA
Mammalian	bcl9-3TPR-p27	bcl9-2TPR-p27-TPR-HA
Mammalian	ICAT-3TPR-p27	ICAT-2TPR-p27-TPR-HA
Mammalian	groove-4TPR-p27	TPR-groove-2TPR-p27-TPR-HA
Mammalian	LRH-3TPR-p27	LRH-2TPR-p27-TPR-HA
Mammalian	phospho-4TPR-p27	TPR-phospho-2TPR-p27-TPR-HA

Bi-functional TPR protein expression in *E. coli*

Expression of the bi-functional TPRs in *E. coli* was done using a mini-purification protocol established by Dr Albert Perez-Riba (Pereze-Riba A. *Sci Rep.* 2017).[256] All TPR scaffolds used the in degradation studies had lysines mutated to arginines. This was done to avoid potential attachment of ubiquitin on these lysines and subsequent degradation of the protein.

SDS-PAGE showing purifications of several TPRs containing grafted loops and helices are shown in Figure 6.9. In short, proteins were expressed in *E. coli* using IPTG induction for 3 hours at 37°C, cells were lysed using BugBuster and loaded on Ni-beads following elution with 300 mM imidazole. Proteins were further concentrated, flash frozen and stored at -80°C until further use.

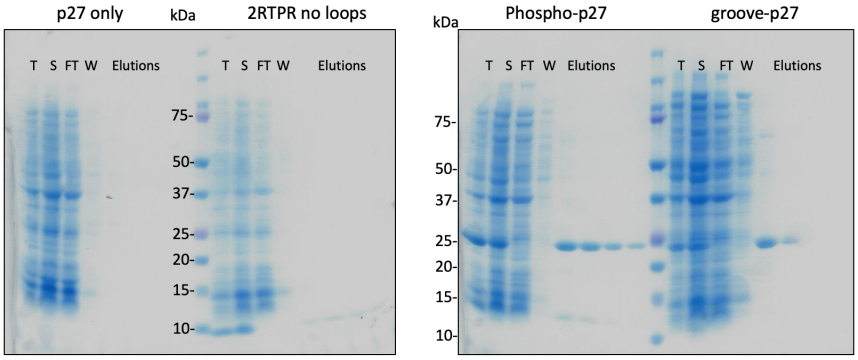

Figure 6.9: SDS-PAGE showing mini-purifications of His-tagged TPR proteins with no grafted loops, with p27 loop or bi-functional TPRs with β-catenin binder and p27 loops grafted in. T - total protein, S - soluble protein, FT - flow through, W -wash, elution with 350 mM imiadzole from HisTrap column.

From the gels it is clear that protein expression varied greatly. For example, when comparing expression of 3TPR-p27 (2TPR-p27-TPR-His) in Figure 6.9 to previously purified 5TPR-p27 (3TPR-p27-2TPR-His) in Figure 6.5, it is clear that 5TPR-p27 is produced in greater amounts. This is likely due to the higher stability of TPRs containing more repeats. Furthermore, bi-functional phospho-TPR-p27 had the highest yield in this expression. This could be due to the amino acid composition of the grafted loop. Other bi-functional TPRs, summarised in Table 6.1, were tested for bacterial expression but resulted in no or very little pure protein that could not be further tested in the biophysical assays. Only phospho-TPR-p27 was produced in sufficient quantities and was next tested in β-catenin ubiquitination assay.

β-catenin ubiquitination by SCF^{Skp2}

To further investigate the effects of bi-functional TPRs we designed a β-catenin ubiquitination assay similar to the previously described p27 assay. pcDNA3.1 plasmid containing HA-HA-HA-β-catenin was kindly donated by Dr Marc de la Roche (Department of Biochemistry). This β-catenin is full length in which the site that is phosphorylated and subsequently recognized by the natural E3 ligase is mutated to alanine. Therefore this β-catenin can not be recognised and subsequently degraded by its native ligase ($SCF^{\beta\text{-}TRCP}$). This allows us to study the degradation that is caused by hetero-bifunctional TPRs.

HEK293T cells were transfected using lipofectamine 2000 and 48 hours later 3HA-β-catenin was immuoprecipitated from cells with HA-beads and eluted of the HA-beads using HA peptide. This allowed production of a full-length β-catenin protein which otherwise is notoriously difficult to express in *E. coli*.

In the ubiquitination assay, *E. coli* purified phospho-TPR-p27 protein was added to samples containing β-catenin purified from mammalian cells, ubiquitination mix (E1, E2, ATP, Mg, ubiquitin and buffer), and SCF^{Skp2}. The results of this β-catenin ubiquitination assay are shown in Figure 6.10.

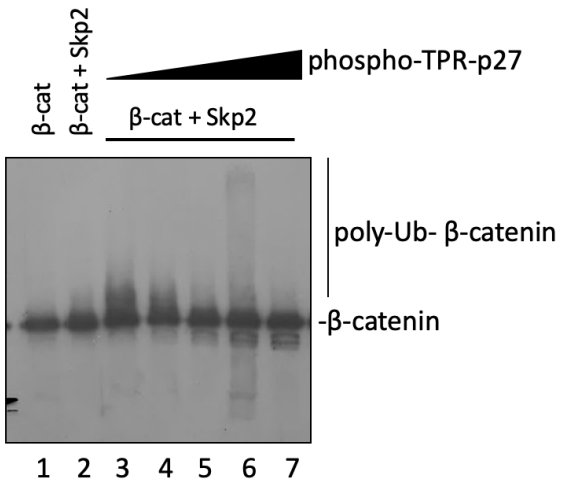

Figure 6.10: *In vitro* ubiquitination of β-catenin by SCF^{Skp2} by bi-functional TPRs. Phospho-TPR-p27 purified from *E. coli* was titrated into the ubiquitination assay (at concentrations of 4, 8, 16, 32 and 64 μM) resulting in poly-ubiquitinated β-catenin (lane 6).

This showed that by bringing β-catenin and SCF^{Skp2} in proximity using bi-functional TPRs we have achieved β-catenin ubiquitination by its non-natural ligase (compare lanes 2 and 6). Interestingly, poly-ubiquitination achieved with 32 μM concentration of phospho-TPR-p27 is greater than with 64 μM concentration (compare lanes 6 and 7). This type of effect is widely documented across the PROTACs community and is know as the Hook effect (see Introduction).[229,231] High concentrations of PROTAC molecules lead to preferential formation of unproductive binary complexes (PROTAC-ligase and or target-PROTAC) rather than the ternary complex (target-PROTAC-ligase).[234] However, this experiment was performed only once and needs repeating. The appearance of lower molecular weight smear in lane 6 cannot be explained, and thus is at odds with previously seen ubiquitination pattern. To understand the nature of the high and low molecular weight smears in lane 6 this blot should be probed for poly-ubiquitin chain specific antibodies to determine if these smears are caused by ubiquitin modification. Also, other E3 ligases should be tested to verify that these bi-functional TPRs are SCF^{Skp2} specific and the smear pattern is not caused by other protein interactions occurring *in vitro*.

Effects of bi-functional TPRs on β-catenin levels in HEK293T cells

We next moved to testing the polyproxins for their ability to degrade β-catenin. Mammalian expression constructs used in this study are summarised in Table 6.1.

The effects of the bi-functional TPRs on β-catenin levels were investigated by transiently transfecting bi-functional TPRs and performing Western blot analysis on β-catenin. First, the effects on endogenous levels of β-catenin were tested. However only poor quality western blot data were obtained using anti-β-catenin antibody, and therefore we started using transfected HA-HA-HA-β-catenin. The effects of bi-functional TPRs were tested with and without transfected Skp2/Cks1. The results are shown in Figure 6.11.

Cell lysates were blotted for HA to evaluate expression of TPRs and β-catenin levels, actin as a loading control. The analysis was performed using densitometry of the western blot bands corresponding to HA-tagged β-catenin (top band of β-catenin was used in this analysis) normalised to actin bands using ImageJ. The appearance of this double band of β-catenin is not fully understood and interestingly, the bi-functional TPRs can be seen to have an effect on both bands. We used the top band in quantification because it corresponds to the correct molecular weight of β-catenin protein.

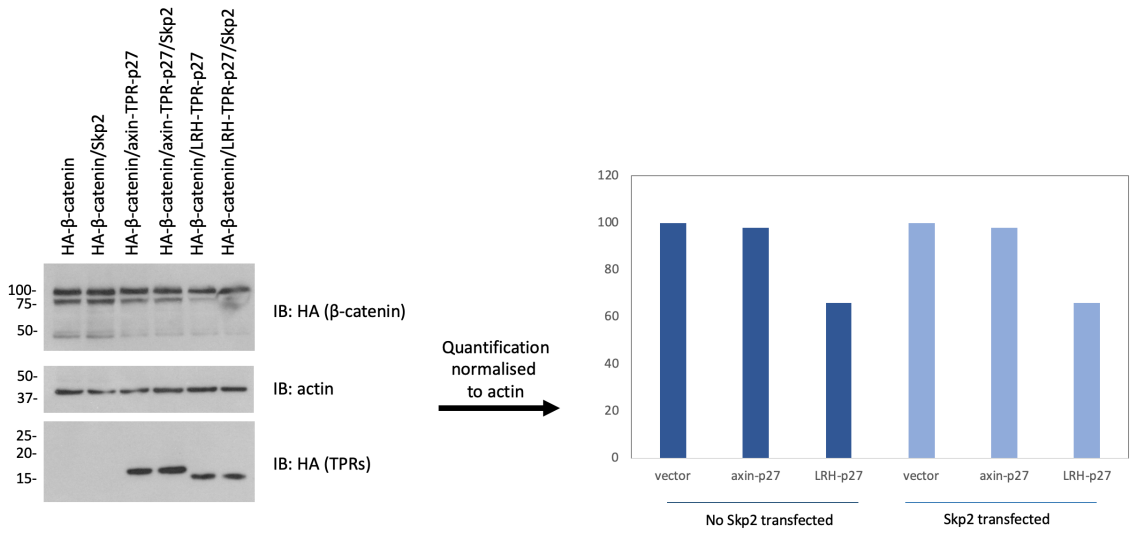

Figure 6.11: Effect of bi-functional TPRs on β-catenin levels. β-catenin levels in HEK293T cells transfected with either HA-tagged β-catenin plasmid alone or HA-tagged β-catenin plasmid together with bi-functional TPRs designed to bind simultaneously to β-catenin and E3 ligase $SCF^{Skp2/Cks1}$.

The analysis showed 34% reduction of β-catenin when LRH-TPR-p27 was transfected compared to the control cells (only β-catenin and vector control transfected). We have also tested whether the increased levels of Skp2 in the cell (Skp2 transfected together with the β-catenin and hetero-bifunctional TPRs) would result in higher levels of β-catenin degration. However, because no difference in levels was observed the future experiments were therefore performed without Skp2 transfections. Also, bi-functional TPRs were expressed and detected via the Western blot at the correct molecular weight, indicating that expression in mammalian cells of certain TPRs were better than compared to bacterial expression as difficult expression mentioned previously.

After all mammalian expression constructs were produced, we repeated this assay using an array of bi-functional TPRs as well as single function TPRs as controls. The results are shown in Figure 6.12.

This time, LRH-TPR-p27 reduced β-catenin levels by about 20% as compared to the previously observed 34%. The largest effect was observed with axin-TPR-p27, which showed almost 40% reduction. Furthermore, single-function TPRs (p27 loop only and LRH helix only) showed no effect on β-catenin levels. This result indicated that the effect on β-catenin levels is most likely due to its degradation induced by the bi-fucntional TPRs and not just a non-specific effect of TPR protein expression.

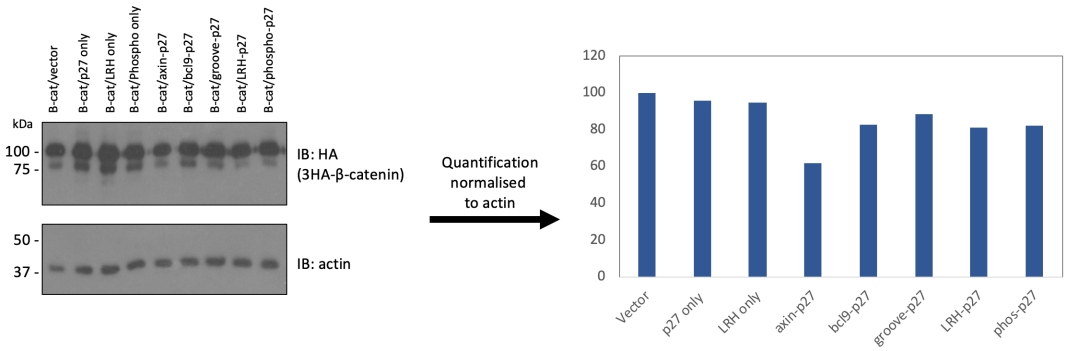

Figure 6.12: Effect of bi-functional TPRs on β-catenin levels using β-catenin-TPR-27. β-catenin levels in HEK293T cells transfected with either HA-tagged β-catenin plasmid alone or HA-tagged β-catenin plasmid together with bi-functional TPRs designed to bind simultaneously to β-catenin and E3 ligase $SCF^{Skp2/Cks1}$. The analysis was performed using densitometry of the western blot bands corresponding to HA-tagged β-catenin (top band of β-catenin was used in this analysis) normalised to actin bands using ImageJ. Single-function TPRs or pcDNA3.1 vector were used as controls. The experiment was performed once.

To further investigate the degradation of β-catenin we tested whether β-catenin is degraded by the proteasome after being ubiquitinated. We transfected HEK293T cells with β-catenin and mono- and bi-functional TPRs, and prior to cell lysis they were treated with a proteasome inhibitor MG132. The hypothesis was that if we inhibit the proteasome then the levels of β-catenin would increase relative to no treatment if degradation occurs via the proteasome. The results are shown in Figure 6.13.

Samples treated with proteasome inhibitor (10 μM MG132) for 6 hours prior to cell lysis showed increased levels of β-catenin and ubiquitination smear, indicating its degradation pathway via ubiquitin proteasome system. However, the reduction in β-catenin levels is somewhat variable in all these western blots assays, indicating that a more sensitive and reproducible method should be used (see later TOPflash dual-luciferase reporter assay).

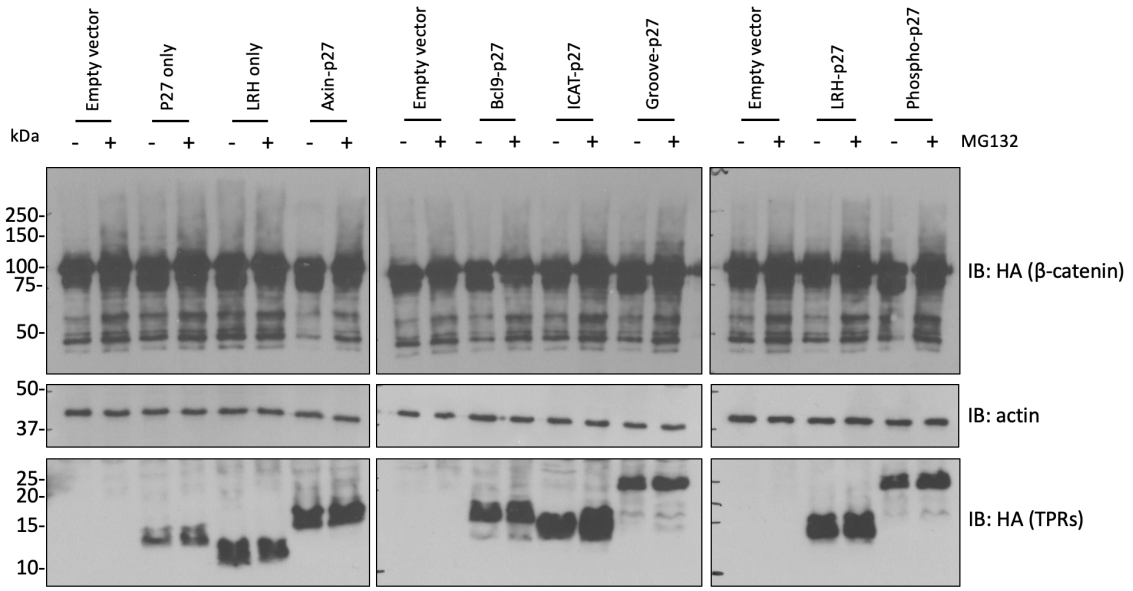

Figure 6.13: β-catenin degradation assay using transfected bi-functional TPRs in HEK293T cells. Levels of β-catenin are reduced in the presence of some bi-functional TPRs. Axin-TPR-p27 and bcl9-TPR-p27 resulted in reduction of β-catenin levels. Samples treated with proteasome inhibitor (10 μM MG132) for 6 hours show increased levels of β-catenin and ubiquitination smear thus indicating its degradation pathway via ubiquitin proteasome system. The experiment was performed once.

Furthermore, to test whether β-catenin is able to bind to various bi-functional TPRs we performed immnuprecipitation pull-downs. HA-tagged TPR constructs containing β-catenin binding helices and loops were transfected in HEK293T, cells were lysed 48 hours later and incubated with HA-beads for 4 hours. Beads were washed, laemmli buffer was added, and samples were analysed using western blot. None of the constructs appeared to pull down β-catenin. Unfortunately, the x-ray western blot film was damaged and is not shown here. Pull-downs were not investigated any further, but Dr Pam Rowling is currently working on biophysical analysis of grafted sequences binding to β-catenin.

In parallel, we also tested if TPR proteins containing MDM2-binding and β-catenin-binding sequences can result in reduced levels of β-catenin. HEK293T cells were transfected with various TPRs containing p53 helix and different β-catenin binding moieties. 48 hours after transfection, cells were lysed and samples blotted for actin (as sample loading control), HA (TPR-p53 expression control) and β-catenin. Western blots are shown in Figure 6.14.

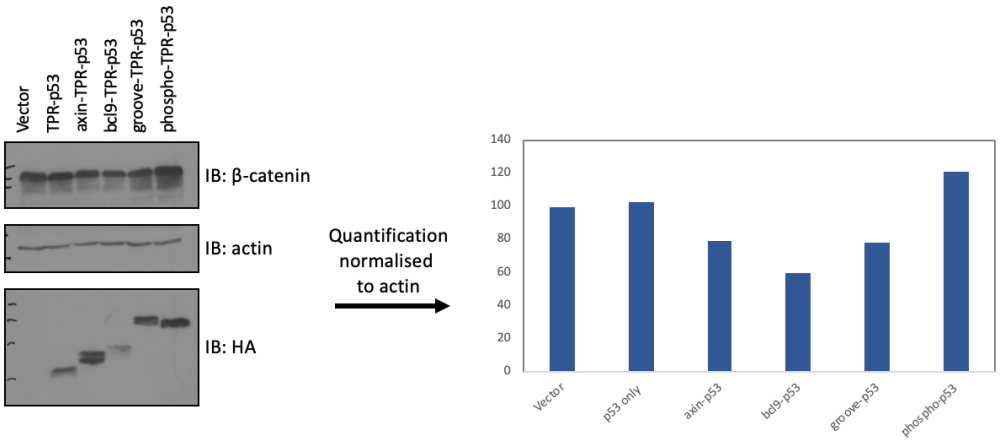

Figure 6.14: Effect of bi-functional TPRs on β-catenin levels using β-catenin-TPR-p53. β-catenin levels in HEK293T cells transfected with bi-functional TPRs designed to bind simultaneously to β-catenin and E3 ligase MDM2. The analysis was performed using densitometry of the western blot bands corresponding to β-catenin normalised to actin bands using ImageJ. Single-function TPRs or pcDNA3.1 vector were used as controls. The experiment was performed once.

From these data we can conclude that not all β-catenin-TPR-p53 constructs are expressed to the same level although they are all in the pcDNA3.1 vector with CMV promoter. When comparing expression levels of TPR-p53 to TPR-p27 proteins in mammalian cells, the TPR-p27 proteins are expressed in higher amounts and the expression levels are less variable. For example, we had to use highly sensitive western blot reagent to detect expression of TPR-p53 proteins versus a standard sensitivity reagent used for detection of TPR-p27. This suggests that grafting of the p53 helix impairs the expression of these proteins in cells or that they are very rapidly degraded. Furthermore, axin-TPR-p53 runs as a double band. When comparing the β-catenin levels with the transfected vector control it can be seen that levels are lower in presence of axin-TPR-p53 and bcl9-TPR-p53, even though bcl9-TPR-p53 expression is very low. The work using β-catenin-TPR-p53 was then continued by Dr Pam Rowling resulting in varying data as well. This indicated that assays used and the design of the TPR scaffold and of the p53-grafted helix potentially need additional improvements to obtain robust data which could be easily replicated. Since western blots were inconsistent we then transitioned to more biologically relevant assays using more sensitive methods. (Later studies carried out by Dr Pam Rowling focused on using HiBiT-tagged β-catenin.)

Effects of bi-functional TPRs on β-catenin function

Dual-luciferase assay (TOPflash)[257] was carried out to detect Wnt signalling in cells transfected with β-catenin-TPR-p27 constructs. This work was carried out in collaboration with Dr Marc de la Roche at the Department of Biochemistry. In the DLR Assay, the activities of firefly (Photinus pyralis) and Renilla (Renilla reniformis or sea pansy) luciferases are measured sequentially from a single sample. HEK293T cells were transfected with a firefly plasmid (as Wnt readout) and Renilla plasmid (as internal control), and β-catenin-TPR-p27 constructs. 6 hours after tranfection the media was changed to Wnt3A conditioned media for 16 hours (see Materials and Methods for Wnt3A media preparation). A DLR assay (Promega) was then performed to measure the levels of Wnt/β-catenin signalling in Wnt3A-activated HEK293T cells. The effects of transfected bi-functional TPRs on Wnt-activated HEK293T cells are shown in Figure 6.15. Relative luciferase values were obtained in triplicate samples from two independent experiments.

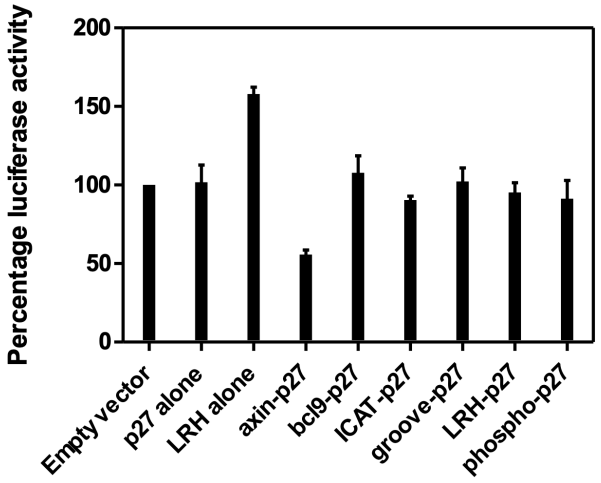

Figure 6.15: Effect of transfected bi-functional TPRs on Wnt-activated HEK293T cells. Error bars (SD) are obtained from triplicate sample measurements from two independent experiments.

The readout of the assay is correlated to the level of endogenous β-catenin in the cells, which is overexpressed under Wnt conditions. There was no observed change in activity of the Renilla control, indicating no general (non specific) effects of β-catenin-TPR-p27 constructs transfection on cell transcription and cell viability. Data in Figure 6.15 indicates that the transfection of HEK293T cells with axin-TPR-p27 polyproxin plasmid resulted in decreases in Wnt pathway reporter activity, indicating inhibition of Wnt signalling. The extent of Wnt inhibition induced axin-TPR-p27 broadly correlates with the extent

of degradation (see Figure 6.12). In contrast, single-function p27-TPRs showed no effects on Wnt inhibition. The increase in Wnt signaling with LRH-TPR was hypothesised to be due to a stabilising effect upon binding to LRH-TPR protein. However, this data cannot be fully interpreted without quantification (immuno blot) of the expressed mono- and bi-functional TPR constructs. As discussed previously, we have seen varying expression levels of these TPRs which would greatly affect their effects in cells. In the future experiments, the sample used in the TOPflash assay should be run for the immuno blot analysis as well.

This assay was also performed using colorectal cancer lines (SW480 and DLD-1) where Wnt signalling is always activated and the Wnt3A media is not needed for the pathway activation. This allows more biologically relevant data to be collected on the effects of bi-functional TPRs on cancerous β-catenin conditions. However, due to transfection difficulties of these colorectal cancer cells lines, reliable data could not be collected. Further studies will focus on improving transfection efficiency including the use of plasmid electroporation.

6.2.4 Taking a step back: p27 sequence effects on TPR

The clones used up to this point were provided by Dr Pam Rowling in the Itzhaki lab. Due to the repetitive nature of TPR protein repeats the expression was sometimes contaminated with several recombination products (despite different nucleotide sequences being use). To circumvent this problem Rohan Eapen, a PhD student in the Itzhaki lab has designed TPRs where each repeat (1 to 8) has a unique nucleotide sequence but still encoding the same amino acid sequences during translation. He incorporated these different TPR repeats into a modified pTriExMOD vector which allows protein expression in three different cell systems, namely bacterial, mammalian and insect cells.

We designed TPR proteins containing either the p27 sequence or a scrambled p27 sequence (p27 scramble) in the loop (see Table 6.2). A TPR without any grafted loops was also prepared. p27 sequences were grafted into the 3TPR and 6TPR scaffolds to maximise chances of successful expression. 3TPR was used to replicate previous experiments more closely since most bi-functional TPRs designed by Pam Rowling had either three or four repeats. We decided to also use a larger scaffold (6TPR comprising six repeats), as the longer the repeat array the higher its stability, and thus peptide grafting has a proportionately smaller destabilising effect and the grafted protein are expressed at higher levels and

have higher solubilities (shown by other Itzhaki lab members). This was important, as previous *E. coli* expression of 3TPR-p27 resulted in very low yields preventing any further characterisation (see previous Figure 6.9).

Table 6.2: p27 sequences used in TPR loop. Sequences in italics correspond to the linker region connecting inserted sequences to the TPR scaffold.

Name	Amino acid Sequence
p27	*DPNN* AGSNEQEPKK *RSPD*
p27 scramble	*DPNN* EPKEKGANSQ *RSPD*

In addition, the newly designed TPRs allowed rapid insertion of loops in between genetically different repeat sequences by altering the primers used. This allowed the cloning process to be done in one day without any requirement for restriction enzymes. In short, PCR was performed with specifically designed primers that were only able to anneal to specific repeats. The PCR product was then purified on agarose gel, DNA extracted and ligated using T4 Anza ligase following transformation. Agarose gels of the PCR products of 3TPR and 6TPR with the p27 inserts are shown in Figure 6.16. The constructs made in this way are summarised in Table 6.3. All of them contained a His_6 tag for bacterial expression and purification, and also an HA tag for immunoprecipitation experiments and western blotting.

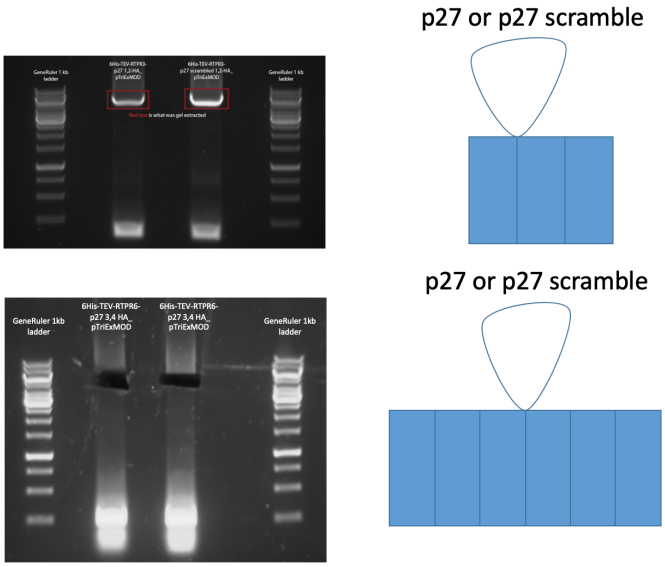

Figure 6.16: Cloning of 3TPR and 6TPR with the p27 loop grafted in either after the first repeat in case of 3TPR or after third repeat in 6TPR protein.

Table 6.3: 3TPR and 6TPR constructs in pTriExMOD vector.

Name	Binder positions within TPR
3TPR	3TPR-HA-His
3TPR-p27	2TPR-p27-TPR-HA-His
3TPR-p27 scramble	2TPR-p27 scramble-TPR-HA-His
6TPR	6TPR-HA-His
6TPR-p27	3TPR-p27-3TPR-HA-His
6TPR-p27-scramble	3TPR-p27 scramble-3TPR-HA-His

Purification of the TPR proteins expressed in *E. coli* are shown in Figures 6.17 and 6.18. Proteins were purified using a HisTrap column on the ÄKTA purification system. Elution profiles using 350 mM imidazole are shown next to SDS-PAGE analysis of protein expression and purity. The elution chromatogram in Figure 6.17 indicates that 3TPR without any grafted loop is expressed well, whereas expression levels of 3TPR-p27 and 3TPR with p27-scramble loop are low. This could potentially arise from a destabilising effect of p27 loop. In contrast, when p27 or p27 scramble loop was inserted into the larger 6TPR scaffold, it expressed well and even better than 6TPR without any loop (Figure 6.18).

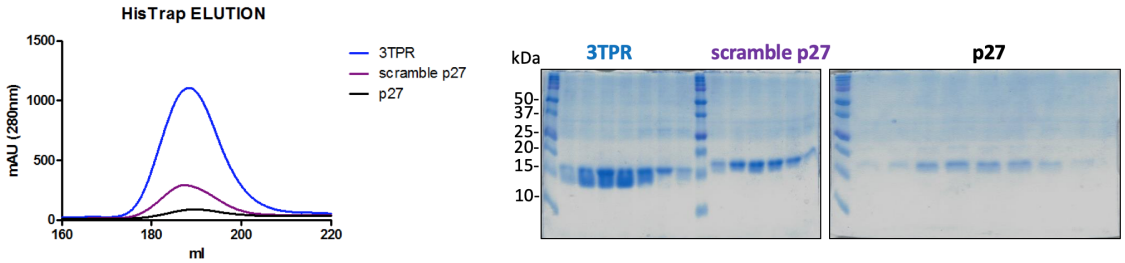

Figure 6.17: HisTrap purification of 3TPR with no loops, p27 and p27 scramble loops grafted in. All proteins were purified from 0.5 L *E. coli* culture. *Left* - elution profile from HisTrap column using 350 mM imidazole. *Right* - SDS-PAGE of eluted protein fractions.

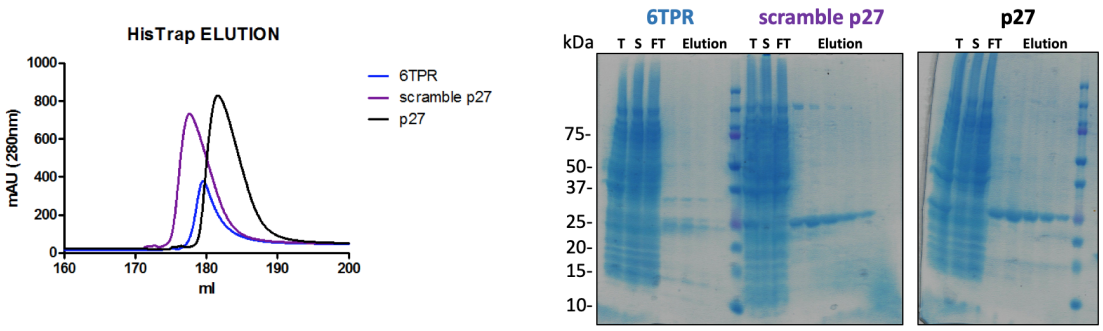

Figure 6.18: HisTrap purification of 6TPR with no loops, p27 and p27 scramble loops grafted in. All proteins were purified from 0.5 L *E. coli* culture. *Left* - elution profile from HisTrap column using 350 mM imidazole. *Right* - SDS-PAGE of protein purifications where T - total protein, S -soluble protein, FT - flow through.

6TPR-p27 and 6TPR-p27 scramble were produced in sufficient amounts to perform ITC experiments with the Skp1-Skp2-Cks1 complex by ITC (Figure 6.19). The results indicated that 6TPR-p27 and 6TPR-p27 scramble do not bind to Skp1-Skp2-Cks1 complex or bind with affinities that are weaker than the detection limit of ITC ($\sim$ hundreds of micromolar).

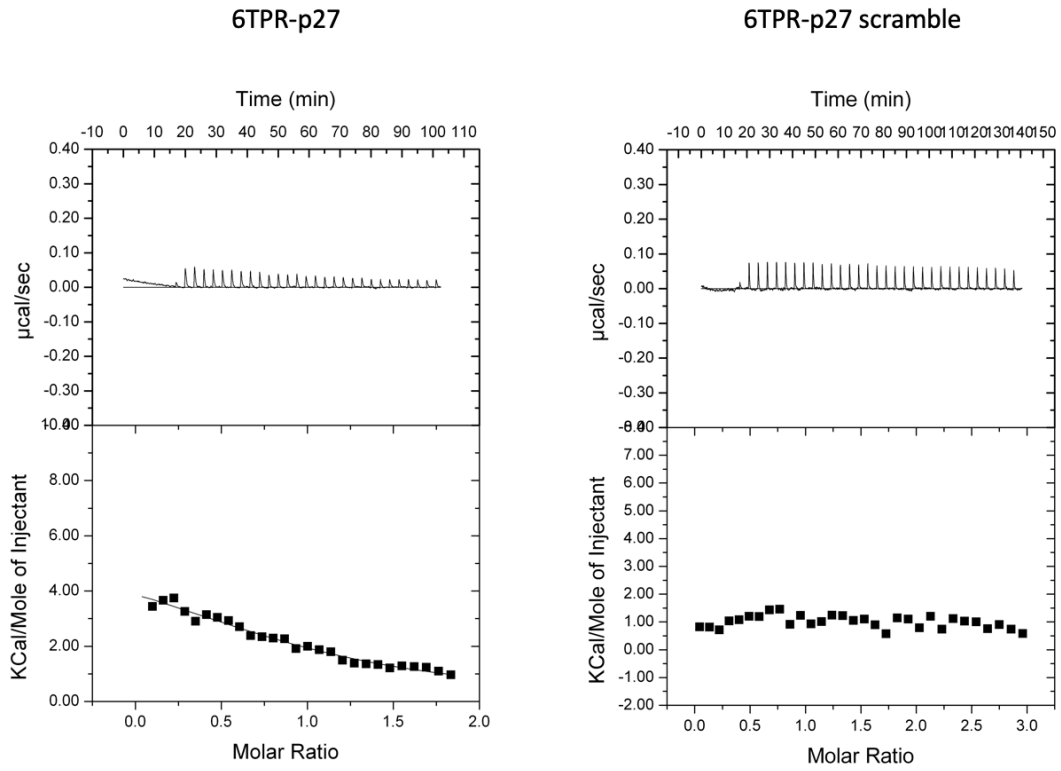

Figure 6.19: ITC traces showing titration of 6TPR-p27 or 6TPR-p27-scramble purified proteins into Skp1-Skp2-Cks1 complex.

Next, we performed p27 ubiquitination assays in the presence of the purified TPR constructs. Since the previous assay showed that a 5TPR containing grafted p27 loop was able to inhibit p27 ubiquitination (see Figure 6.6), it was important to reproduce these data with the necessary controls. This experiment would give us insights into whether the inhibition observed was caused by a non-specific effect of TPR protein or if it was due to the grafted p27 peptide interacting with SCF^{Skp2} ligase. 3TPR, 3TPR-p27 and 3TPR-p27 scramble were titrated into p27 ubiquitination assay, and the p27 ubiquitination was probed using the anti-HA antibody. Figure 6.20 shows that poly-ub-p27 bands are present in all samples with SCF^{Skp2}, including those containing 3TPR-p27. Bands of 3TPR proteins are also present since both p27 and TPR are HA-tagged. The polyubiquitination observed could therefore be arising from either p27 or TPR ubiquitination. In the future, this experiment should be repeated using TPRs without an HA tag to avoid mixed ubiquitination patterns.

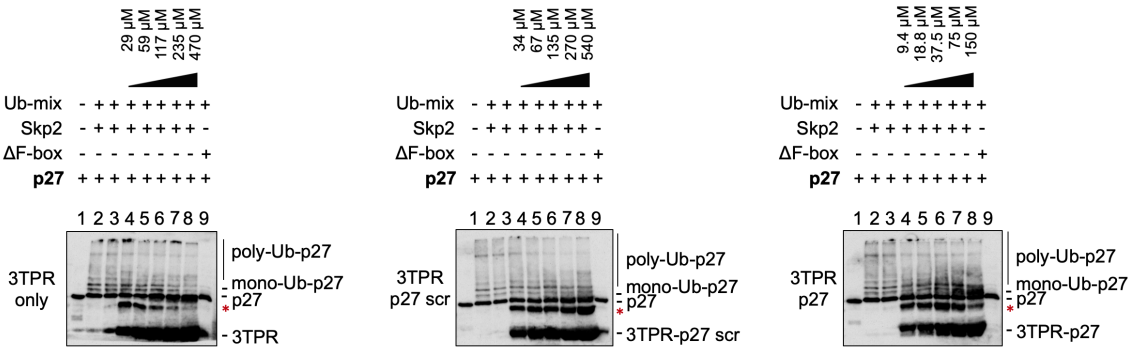

Figure 6.20: Titration of TPR proteins in a p27 ubiquitination assay. 'ΔF-box' indicates a truncated Skp2 that results in no ligase activity. The extent of ubiquitination was estimated from the intensity of the poly-ubiquitinated p27 bands. No effects on p27 ubiquitination were observed with TPR, TPR-p27 or TPR-p27 scramble. Blotting was using anti-HA antibody. Asterix marks a possible contamination band present in all TPR protein containing samples.

It is important to note that the p27 peptide contains two lysine residues, which could become ubiquitinated in this assay and lead to TPR-p27 degradation in cells. This was tested by performing a ubiquitination assay on the purified TPR proteins. All protein samples used in this assay were buffer exchanged into ubiquitination buffer (Boston Biochem) using Zeba spin columns to make sure only ubiquitination buffer was present in the assay and no other buffer components could interfere. The assay was performed in the same way as for p27 and samples analysed using the anti-HA antibody to detect any ubiquitination of HA-TPR proteins (Figure 6.21).

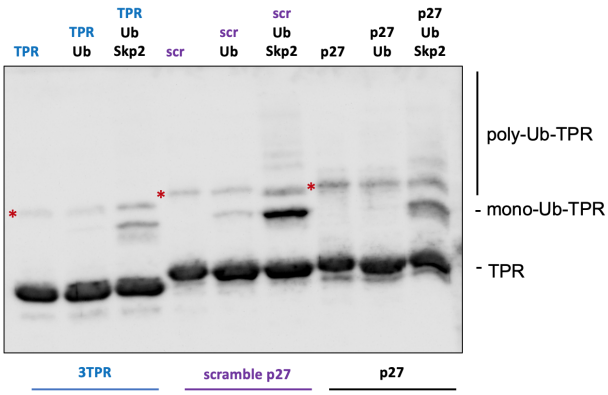

Figure 6.21: Western blot analysis of TPR protein ubiqutination by SCF^{Skp2} ligase. 50 µM concentration of each TPR was used. 3TPR, 3TPR-p27 and 3TPR-scramble p27 were tested for ubiquitination. Asterix marks a possible contamination band present in all TPR samples.

First sample - control sample - contained only the TPR protein; second sample - Ub sample contained protein and ubiquitination mix (comprising E1, E2, ATP, Mg, ubiquitin, ubiquitination buffer); third sample contained the protein of interest, the ubiquitination mix and SCF^{Skp2}. All proteins appear to have a higher molecular weight contaminant (marked with red asterix). In the presence of the ubiquitination mix and SCF^{Skp2} we can observe a mono-ub-TPR. Furthermore, when either p27 or p27 scramble is introduced in the loop poly-ub-TPR bands are also observed.

In summary, the experiments described show that the TPR proteins with grafted p27 loop can be ubiquitinated by SCF^{Skp2} *in vitro*. This could result in depletion of TPR protein designed for use in targeted degradation. Future work could replace the two lysine residues of the p27 sequence in the hope that this would prevent degradation of the TPRs when used for target degradation.

6.2.5 Analysis of constrained phosphomimetic p27 peptides

As mentioned previously, the p27 sequence inserted into the TPR loop has a glutamic acid as a phosphomimetic of the phospho-Thr. In order to understand whether this substitution has any detrimental effect on Skp2 binding, we synthesised a number of peptides containing the same substitution. This also allowed to compare these peptides with the phospho-Thr as discussed in previous chapters and also peptides containing phosphomimetic residue. Synthesised phosphomimetic p27 peptides were: linear (AGSVEQEPKK), and constrained

peptides CP1 E (AGS-X2-EQ**E**P-X4-K) and CP2 E (AGS-X2-EQ**E**P-X3-K) with the m7N linker. The phospho-Thr versions of these peptides, measured previously, had K_{d} values of 2.78 ± 0.19 μM, 356 ± 95 nM and 32 ± 8 nM, respectively. The phosphomimetic-containing peptides were then tested for binding to Skp1-Skp2-Cks1 using the competition FP assay (Figure 6.22). A control peptide, AGSVAQAPKA, showed no binding, as expected since all the key interacting residues were mutated to alanine. The linear and constrained phosphomimetic p27 peptides also showed no binding. A similar result was obtained for the linear phosphomimetic peptide when measured by ITC (Figure 6.23).

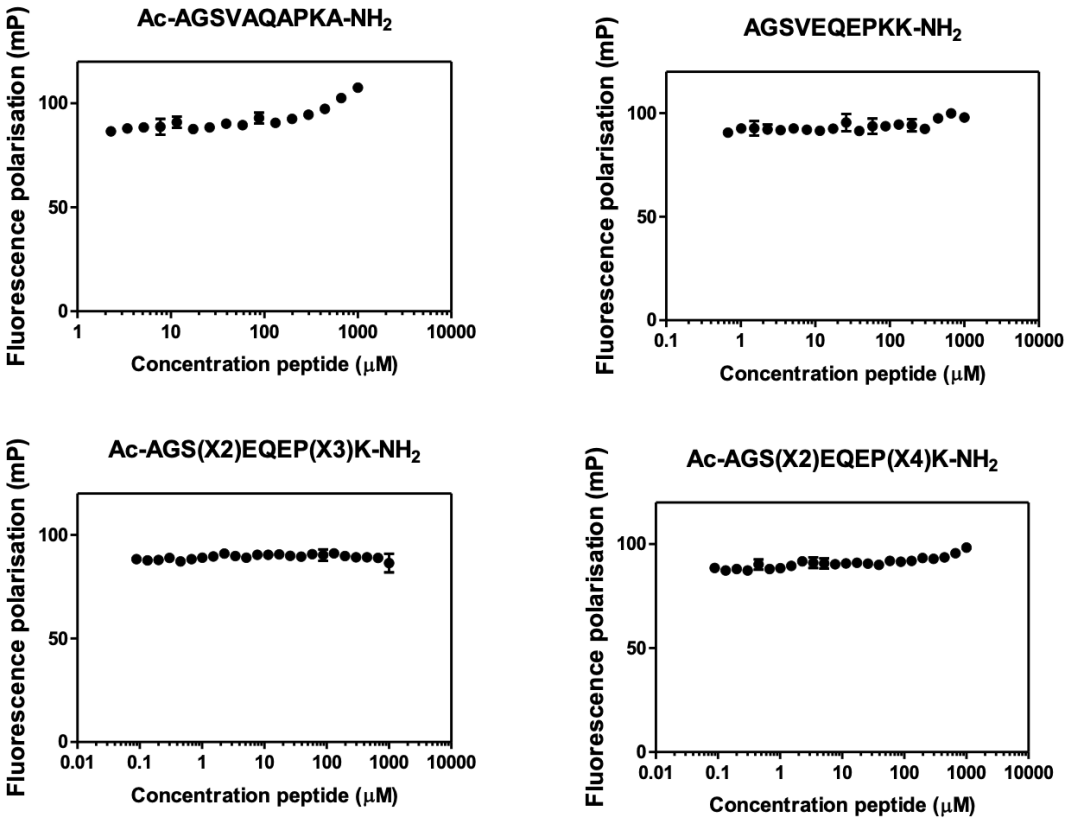

Figure 6.22: Competitive FP of displacement of TAMRA-AGSVEQT(phos)PKK peptide from Cks1-Skp2-Skp1 by titration of unlablled phosphomimetic p27 peptides. TAMRA-AGSVEQT(phos)PKK peptide (10 nM) and Cks1-Skp2-Skp1 (4 μM) were incubated for 15 min followed by addition of displacement peptide at varying concentrations and read after 30 min. The experiments were conducted in triplicate in a final volume of 25 μl.

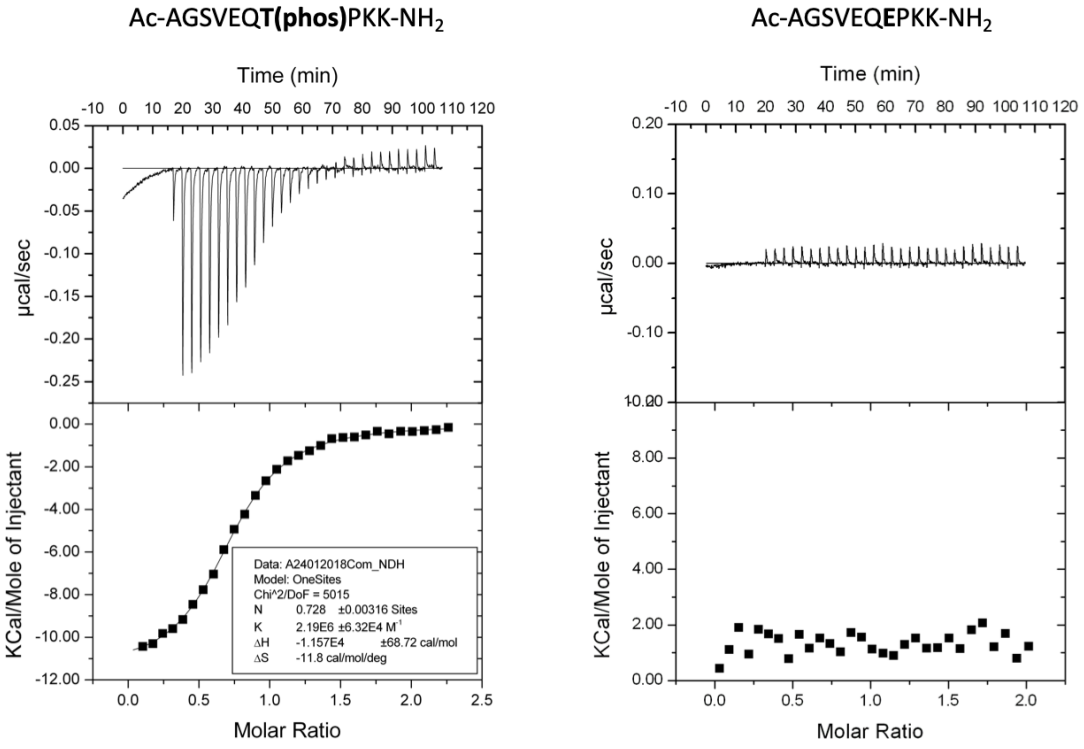

Figure 6.23: ITC traces showing titration of linear p27 peptide containing either phospho threonine or glutamic acid reside into Skp1-Skp2-Cks1 complex. Fitted to a one-site binding model.

As discussed in previous chapters, binding affinities and inhibitory effects on p27 ubiquitination did not directly correlate. Also, 5TPR-p27 was able to inhibit p27 ubiquitination in the *in vitro* assay. Therefore, we also looked at the inhibitory effects of the phosphomimetic peptides (both linear and constrained). The results are shown in Figure 6.24. The phosphomimetic peptides had similar effects on p27 ubiquitination as the linear peptide in that they only inhibited ubiquitination at 600 µM concentration. Compared to phosphorylated analogues of these peptides, CP1 and CP2 inhibited ubiquitination at 32.5 µM and 75 µM respectively. This further points to the essential role of the phosphothreonine for SCF^{Skp2} binding. This result suggests that 5TPR-p27 should not be able to inhibit p27 ubiquitination at the concentrations that it did (full inhibition was achieved at 150 µM, see Figure 6.6). This inhibition potentially could arise from TPR scaffold interacting sticking to p27 or the ligase or any other components of the *in vitro* assay and indirectly blocking Skp2 binding to p27. As mentioned previously, the ubiquitination assay using TPR with no grafted loops and with p27 scramble sequence should be performed to answer this question.

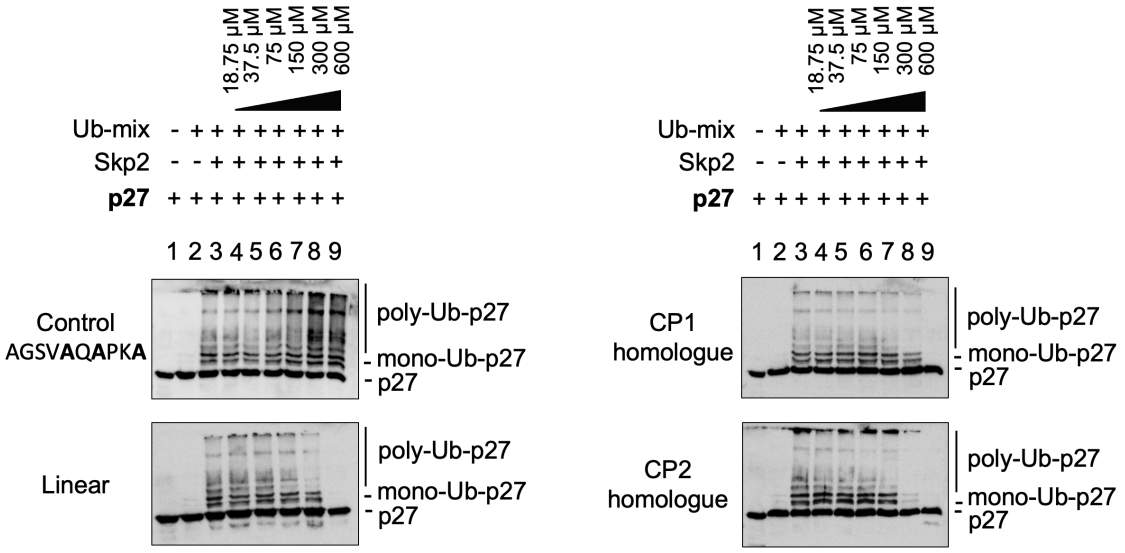

Figure 6.24: Titration of linear and constrained phosphomimetic peptides in a p27 ubiquitination assay. All experiments were repeated twice, and representative data are shown. The extent of ubiquitination was estimated from the intensity of the poly-ubiquitinated p27 bands. Control peptide with all binding residues mutated to alanines had no effect, the linear phospho Thr containing p27 peptide inhibited ubiquitnation at the highest 600 µM concentration. CP1 and CP2 homologues are the same sequence as CP1 and CP2 peptides but with glutamic acid instead of phospho Thr. Both of them had effects at 600 µM.

In summary, both competition FP and ubiquitination assays indicate that the phosphomimetic is not a good substitute for phosphor-Thr in binding to SCF^{Skp2}. These data appear inconsistent with the results obtained for the hetero-bifunctional TPRs containing the phosphomimetic p27 peptide showing their ability to induce degradation of β-catenin. Furthermore, members of the Itzhaki lab have observed degradation of another target (KRAS) using the phosphomimetic p27-grafted TPRs. We speculate that the phosphomimetic p27 peptide binds SCF^{Skp2} with a weak affinity that is below that required for detection by FP or ITC but that is sufficient to recruit to the target proteins and elicit their ubiquitination and subsequent degradation. Indeed, some studies have shown that the most potent PROTACs are those with relatively modest E3- and target-binding affinities.[224,236] It is thought that high-affinity PROTACs could saturate the E3 available in the cell and lead to more side effects. Moreover, testing single-function TPRs as inhibitors of ubiquitination of a natural substrate will not give us a good indication of the potency of the hetero-bifunctional TPRs as inducers of neosubstrate degradation. For example, the single-function TPRs may be ubiquitinated, but when used to recruit a neosubstrate to

the E3 the neosubstrate may be more easily ubiquitinated than the TPR due to its more favourable positioning on the E3.

Future work should explore further the effects of varying the TPR scaffold itself and of different scrambled p27 sequences to rule out any effects caused that might result in false positives. This is particularly important in cellular assays where transient transfection of unnatural proteins can have non-specific effects. Further work is underway to understand the relationship between the binding affinities of the grafted peptides and the degradation potencies of the hetero-bifunctional TPRs, and also the effect of varying the scaffold and thereby the relative display of the two functions on degradation. Our approach has the potential to give us access to a very large number of both E3 ligases and targets that cannot be addressed using small-molecule PROTACs. Furthermore, the ease with which they can be made (by cloning) compared with the difficult chemical synthesis required to make PROTACs means that we can rapidly build and test diverse combinatorial libraries of hetero-bifunctional TPRs (and other protein scaffolds) for target degradation.

Chapter 7

Ongoing Work

7.1 Crystallography

To understand the almost 100-fold increase in binding affinity upon p27 peptide macrocyclisation we decided to perform crystallography studies. A crystal structure of Skp1-Skp2-Cks1 in complex with stapled p27 peptide could then be directly compared with the structure of the complex with p27 linear peptide (PDB: 2AST). The structure could potential show new interactions contributing to the increased affinity between stapled peptide and the complex. Since the crystal structure of the complex is already solved and the crystallisation conditions known[72] we have decided to first replicate the crystals with the linear peptide. After crystals were obtained they would be soaked in solution containing stapled peptide. This would potentially allow exchange of weaker binding peptide with a stronger binder whilst keeping crystal packing intact. Crystallisation experiments were performed in the Crystallographic X-ray Facility at the Department of Biochemistry, University of Cambridge with assistance of Dr Paul Brear. The Skp1-Skp2-Cks1-p27 peptide complex, prepared by mixing a 20 mg/ml solution of Skp1-Skp2-Cks1 complex (prepared as described previously) with a 3-fold molar excess of the p27 peptide in a buffer of 50 mM TrisHCl, 150 mM NaCl, and 5 mM DTT, pH 7.6. First, we prepared a 96-well 2-drop crystallisation plates around the known condition (100 mM bis-tris-propane-HCl (BTP), 12% (w/v) PEG 8000, 5% (w/v) benzamidine, and 5 mM DTT, pH 8.5) using Dragonfly (TTPLabtech Ltd). We have varied concentration of PEG 8000, benzamidine and DTT. Protein drops were dispensed by Mosquito (TTPLabtech Ltd) at two different final concentrations (10 mg/ml and 15 mg/ml). Two plates were prepared and stored at 4°C

and 19°C incubators. Unfortunately, these plates did not yield any crystals in a 2-month period. Subsequently, we have used several commercial screens in further experiments at 19°C. Crystals obtained are shown in Figures 7.1 and 7.2.

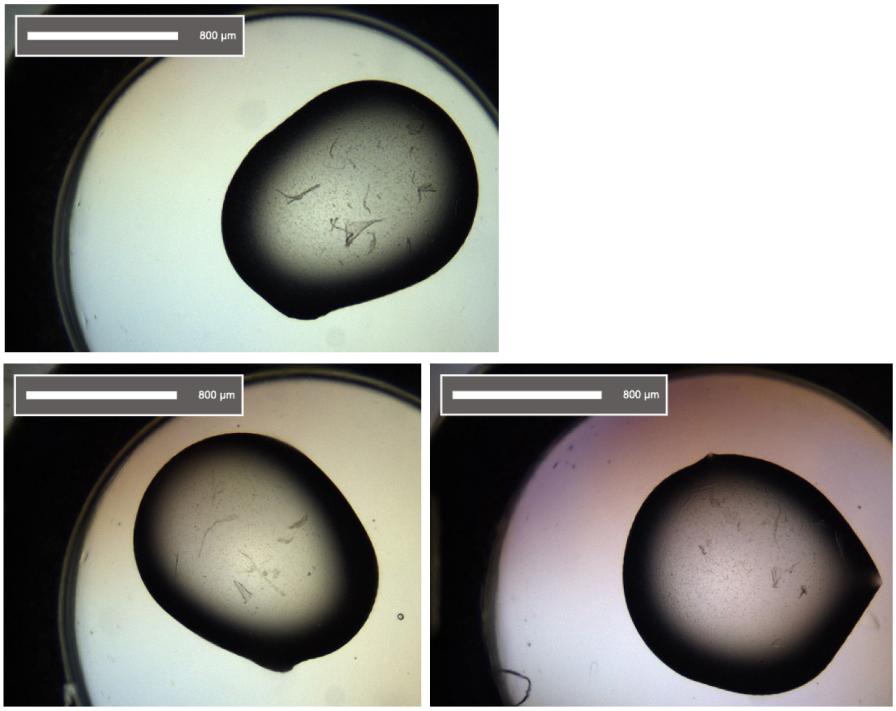

Figure 7.1: 2D plate crystals formed in several screens.

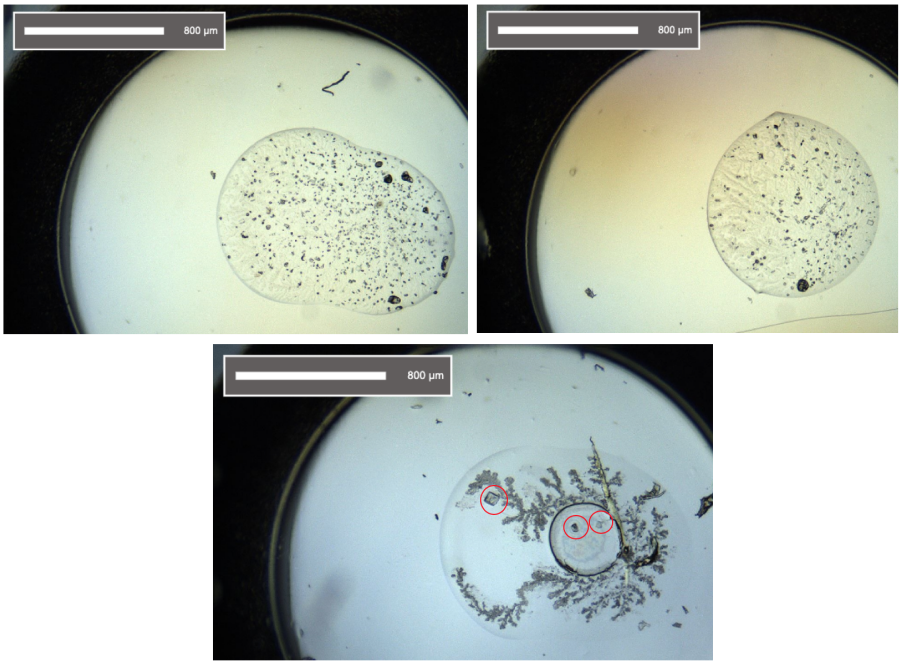

Figure 7.2: 3D micro crystals

Screens used in the crystallisation experiments were JCSG+ (Molecular Dimensions), Morpheus (Molecular Dimensions), PACT (Molecular Dimensions), Proplex (Molecular Dimensions), PEGS I and PEGS II (Qiagen), Wizard 1&2 and 3&4 (Emerald BioSystems). From the images it can be seen that several different kinds of crystals have formed. 2D plate crystals shown in Figure 7.1 were grown in 0.1 M MES 6.5 pH, 10% w/v PEG 4K, 0.2 M NaCl; 0.1 M TRIS 8 pH, 8% w/v PEG 20K, 0.1 M NaCl and 0.1 M MES 6.5 pH (Buffer), 15% v/v PEG MME 550. 3D crystals in Figure 7.2 formed in 30% v/v PEG 400, 0.1 M CAPS 10.5 pH and 30% v/v PEG 400, 0.1 M Na Cacod 6.5 pH, 0.2 M LiSO4. From this it can be concluded that PEG polymer is the key precipitant for Skp1-Skp2-Cks1-p27 peptide crystals.

The 2D plates were too thin to pick with the mounting loop. Furthermore due to their thinness they kept falling apart. The crystals shown in Figure 7.2 were more 3D in shape. However, the solution in the drop has severely dried out leading to the crystal sticking to the plate. This hindered mounting of the crystal on the loop. We are working on reproducing them and screening around these solution conditions to potentially grow bigger crystals. Once obtained, crystals will be soaked in concentrated stapled peptide solutions to allow peptide exchange. Potential obstacles might arise here if the crystals dissolve in the peptide solutions. If that happens, the best crystalliation conditions will be used to set up trials with the protein complex with stapled peptide. At the moment, due to having only small stocks of stapled peptides we are optimising crystal formation with linear peptide. We aim to solve structures of Skp1-Skp2-Cks1 in complex with our short 10-residue linear peptide and with CP2 also. These structures would be a valuable tool for designing even more potent inhibitor of Skp2 and could be even further used to design high affinity PROTACs.

7.2 Mouse xenograft models using MCF-7 breast cancer cells

To further study the effects of stapled peptides we are in a process of testing them in a mouse xenograft model. Stapled peptides were able to restore p27 levels associated with Skp2 increase as well as to reduce cellular proliferation of MCF-7 cells. Since MCF-7 cells successfully responded to peptide treatment we chose to use them in a xenograft model experiment. The workflow for xenograft experiment is shown in Figure 7.3.

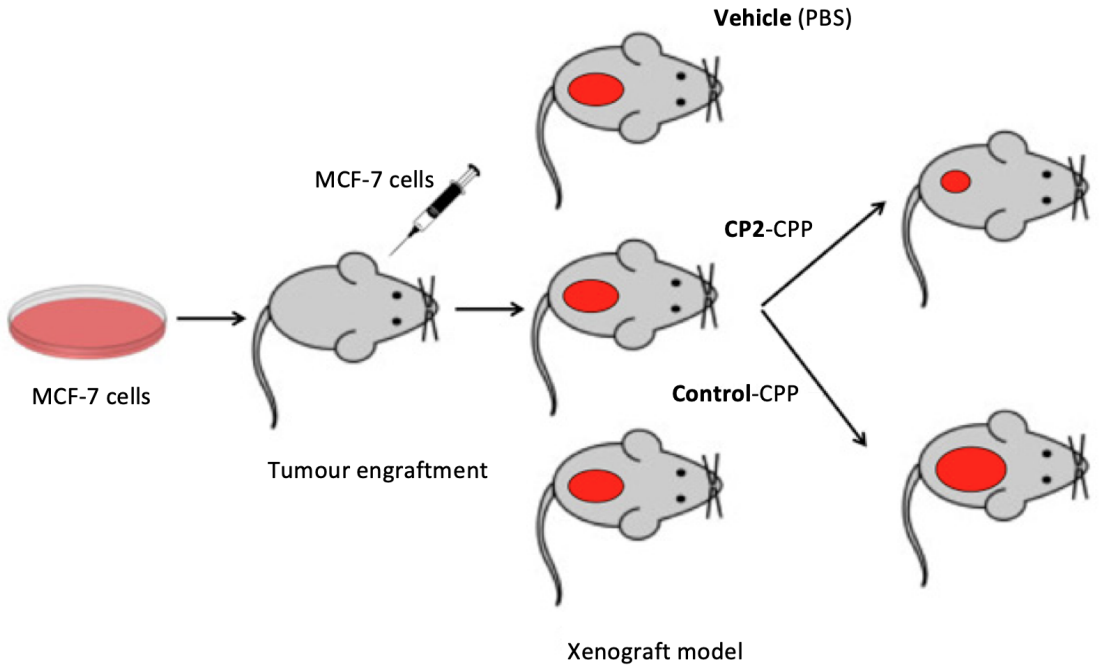

Figure 7.3: Workflow of mouse xenograft experiment.

Briefly, MCF-7 tumour cells resuspended in PBS and matrigel (to a maximum of 200 µL total volume) will be injected subcutaneously into the flank of Nod-Scid Gamma (NSG) immunodeficient mice. Once tumours reach 0.5-1 cm at their widest point, peptides will be injected intratumourally (maximum volume of 0.1 mL).

To this end, MCF-7 cells were checked for any mouse viruses using M-Level 1 testing (Surrey Diagnostics). No viruses were detected indicating that cell line can be used for mice work. Two peptides were selected for *in vivo* testing, CP2-CPP (Ac-AGS-X2-EQT(phos)P-X3-KRQIKIWFQNRR-Nle-KWKK-NH_2, 'click'ed' with m7N linker) and control-CPP (Ac-AGSVAQAPKARQIKIWFQNRR-Nle-KWKK-NH_2 with all ligase binding residues mutated to alanine) alongside vehicle control (PBS in this case, since these peptides do not require DMSO to dissolve). Peptides were synthesised as acetate salts to avoid residual TFA (Cambridge peptides Ltd).

Cellular proliferation and viability experiments will be performed to determine more accurately the amount of peptide to be used prior testing. The outcome of this work may determine whether stapled peptides can be used as a treatment for cancers that overexpress the oncogenic Skp2 ubiquitin ligase.

Chapter 8

Final Conclusions and Future Work

This project aimed to develop constrained peptides to inhibit the interaction between p27 and the SCF^{Skp2} E3 ubiquitin ligase as a potential anticancer agent. We have used a known Skp2-binding p27 peptide motif to design a short 10-residue peptide (amino acids 181-190 of p27) that was able to bind Skp1-Skp2-Cks1 with a K_d of 3 μM. This value was in agreement with previously published binding data for a 24-residue p27 peptide and for full-length p27 protein (~7 μM). Next, we identified positions on the peptide that are not involved in binding and that could therefore be substituted by unnatural amino acids (UAA) for cross-linking. The aim was to constrain the peptide in the turn-like conformation that it adopts in its bound form and thereby increase its binding affinity. We employed a two-component macrocyclization approach using 'click' chemistry between azido group-containing UAAs and an alkyne linker. We were able to generate several macrocyclic peptides of greatly enhanced binding affinities and one peptide, CP2, increased the binding affinity by almost two orders of magnitude (32 ± 8 nM). This result indicates that chemical constraint is a good strategy to produce much higher affinity peptides than the linear one for this particular system. To date, there are only a few constrained non-helical peptide inhibitors in the literature, and their affinities have generally only been marginally improved relative to their linear counterparts. Significantly, this is the first time that the constraint of a non-helical peptide has induced such a dramatic enhancement of binding affinity. We believe that the affinity increase arises due to p27 peptide being successfully constrained in its entropically unfavourable bioactive turn-like conformation. However, because such a large increase has not been seen previously in other systems, we are working on determining the structure of the Skp1-Skp2-Cks1-CP complex. A crystal

structure would show whether the process of macrocyclisation introduces new binding interactions, for example from the m7N linker or the triazole rings of the peptides. Some 2D and 3D crystals were produced, but due to their small size we were unable to collect X-ray data. A crystal structure would aid the further development of Skp2-binding peptides as well as provide a starting point for developing Skp2-specific, high-affinity small molecule ligands.

We have also investigated the possibility of constraining the p27 peptide using a triple staple, whereby three amino acids are changed to azido group containing unnatural amino acids and 'click'ed' with a triple alkyne linker. More work needs to be carried out to determine the most appropriate linker to use, and there are very few three alkyne group-containing linkers available to purchase. We have tried with a 1,3,5-triethynylbenzene linker, but only double-click products were produced. Furthermore, future work could focus on exploring other macrocyclisation chemistries such as hydrocarbon or cysteine stapling.

To evaluate the biological effects of the p27 peptides we have established an *in vitro* ubiquitination assay using SCF^{Skp2} E3 ligase. We used immunoprecipitation method to purify the SCF^{Skp2} complex from mammalian cells. The full complex includes five proteins, Skp2, Cks1, Skp1, Cul1 and Rbx1, co-immunoprecipitated using FLAG-tagged Skp2. We have also produced p21, p27 and β-catenin proteins in mammalian cells. This methods allows proteins to have all post-translational modifications needed for their activity. For example, p27 produced using IVT method cannot be ubiquitinated as it lacks the essential phosphorylated threonine. It should be noted that this complex dissociates over time and can only be kept for 2-3 months at -20°C before losing its ligase activity. The ubiquitination assay became invaluable during my PhD, mostly due to its versatility. First, we were able to study the effects of p27 peptide on the ubiquitination of various SCF^{Skp2} substrates like p27, p21 and N-myc. Moreover, the assay allowed us to further study target ubiquitination in the presence of bi-functional TPRs. In the ubiquitination assay, we found that the constrained peptides were able to inhibit p27 ubiquitination at much lower concentrations than the linear peptide, consistent with their enhanced Skp1-Skp2-Cks1-binding affinities. This result showed that these peptides are able to bind not only proteins purified from bacteria but also a full-length Skp2 protein as part of the full E3 ligase complex. Interestingly, the p27 peptides also inhibited the ubiqutination of other Skp2 substrates (p21 and N-myc). We believe that this arises due to the nature of the peptide inhibitor. It is tar-

geting an extended binding interface and is quite large in size, which could result in it also being able to block other Skp2 substrates from binding. Potentially, these peptides could be potent at inhibiting ubiquitination of most Skp2 substrates. To further understand their effects on Skp2 substrates it would be beneficial to perform a ProtoArrays Human Protein Microarrays v4.1 (Invitrogen) screen. This assay has been used successfully in the Laman lab by Dr F. Teixeira. The screen contains almost 10, 000 human proteins and will allow the rapid identification of proteins involved in the pathways mediated by E3 ligase (see Figure 8.1). Fluorophore-labeled streptavidin is used to detected biotinylated ubiqutin and thus identify the proteins ubiquitinated by the ligase. By using SCF^{Skp2} and $SCF^{Skp2\Delta Fbox}$ we could quickly identify pathways which are specifically targeted by constrained p27 peptides. This would be of high importance to start evaluating any potential side effects that could arise from using constrained p27 peptides as therapeutics.

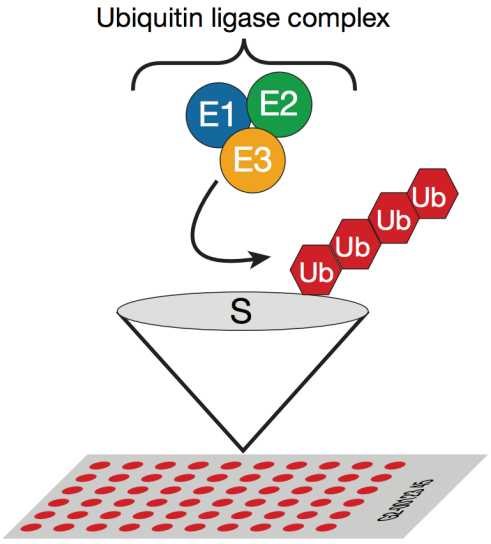

Figure 8.1: ProtoArrays Human Protein Microarrays v4.1 (Invitrogen) screen used to profile enzymatic activity of E3 ligases.

To understand the impact of p27 peptides on cancer cell proliferation, we explored the effects of different stapled peptides in cells. First, we investigated several methods to address intracellular delivery: conjugation of a cell penetrating peptide (Antp), electroporation and liposomal encapsulation. We demonstrated that p27 peptides can be delivered into several different cell lines using all three methods. However, when the Antp is used, an increased amount of endosomal encapsulation of the peptide is observed compared to the other delivery methods. The success of peptide delivery using liposomes was found to be highly dependent on the nature (charge) of the peptide as well as cell type used. And

thus was not pursued any further due to high variability in delivered amounts of different peptides. During my PhD we continued with Antp for cellular delivery, because it is well known in the literature including in xenograft mouse models. We showed that treatment of MCF-7 cells with CP2-Antp was able to restore p27 levels associated with increased $SCF^{Skp2/Cks1}$. Moreover, CP2-Antp decreased MCF-7 cellular proliferation by ∼35%. We are designing mouse xenograft model experiments that will be carried out using MCF-7 cells due to their responsiveness to CP2-Antp treatment.

In the future, the cell proliferation assays will be repeated using additional controls including control-peptide-Antp (non-binding peptide coupled to Antp), linear-Antp together with CP2-Antp to directly evaluate the affects of constrainment in cells. Future work should also focus on exploring the effects of these peptides in other cancer cell lines in which Skp2 over-expression and p27 degradation are the leading cause of cellular proliferation. These could include other breast cancer cell lines (MDA-MB-231, MDA-MB-468), as well as prostate cancer (LNCaP, PC-3, DU-145) and melanoma cell lines (MEL-HO,A375, IGR-37). These cell lines were investigated briefly during my PhD to determine the dependence of p27 levels on Skp2 expression. Preliminary results indicated troubles with transfection efficiency using lipid based methods but should be further explored using electroporation to deliver Skp2 plasmids. In addition, the effects of other stapled peptides will be evaluated using electroporation, as this delivery method resulted in good cytoplasmic distribution of the peptide. Moreover, electroporation will not only allow the comparison between different peptides without the need of cell penetrating peptide attachment, but will also allow us to bypass the effects that CPP has on cells. Namely, endosomal encapsulation of peptides as well as an effect on cellular proliferation, potentially due to endosome formation upon CPP uptake or any side effects that could arise from a large 16-residue long peptide. It should be noted that due to mechanically disruptive nature of electroporation appropriate precautions must be taken. It would be important to first assess the effects of electroporation itself on cellular proliferation before proceeding to evaluate constrained peptides.

Furthermore, it is important to evaluate the stability of the macrocyclic peptides. It is widely documented that the backbone of stapled peptides is much less accessible to proteases when compared to linear peptides. Furthermore, incorporation of unnatural amino acids make them less likely to be recognised by proteases. To explore the stability of our macrocyclic peptides we will perform assays to evaluate their resistance to proteases in

both plasma and blood serum. This would tell us whether these peptides could potentially be orally administered by patients. In addition, future work could focus on enhancing peptide stability even further e.g. by making a D-amino acid peptide (so-called a 'retro-inverso' peptide) of the best performing p27 peptide.[258]

During the course of this study, the work gradually transitioned towards exploring the use of these ligase binding peptides in targeted protein degradation. The work was a collaborative effort employing a scaffold developed by Dr Pam Rowling and Dr Albert Perez-Riba. First, we grafted a 10-residue p27 sequence into a loop between adjacent repeats of a TPR protein. It is worth noting that the key phosphothreonine of p27 peptide was changed to glutamic acid as a phosphomimetic for use in bacterial and mammalian expression systems. Immunoprecipitation experiments carried out using HEK293T cells showed that TPR-p27 was able to pull down Skp2, indicating that the p27 phosphomimetic sequence is still able to bind Skp2. We also tested the effects of TPR-p27 protein on p27 ubiquitination, which would be a key indicator of whether it can bind to Skp2 in SCF complex. TPR-p27 protein inhibited p27 ubiquitination at similar concentration as the constrained peptides demonstrating that p27 is successfully constrained in its bioactive conformation in the loop of the protein scaffold.

We then introduced a target binding protein sequence on the TPR-p27 to produce hetero-bifunctional molecules that could potentially act as PROTACs. We focused on β-catenin as the target. The preliminary experiments showed that hetero-bifunctional TPRs induced degradation of β-catenin and had an inhibitory effect on Wnt signaling, showing their potential in cells. We were also able to establish an *in vitro* β-catenin ubiquitination assay using full-length β-catenin protein purified from HEK293T cells. We showed that β-catenin ubiquitination by SCF^{Skp2} can be induced by bi-functional TPR.

Binding affinities of these TPR-p27 proteins to Skp1-Skp2-Cks1 complex could not be determined by ITC. We next synthesised several phosphomimetic peptides that are identical in sequence to the tightest binding peptides identified in the study but with glutamic acid instead of the phosphorylated threonine. No binding was observed to the Skp1-Skp2-Cks1 complex using FP and ITC. Furthermore, these peptides were unable to inhibit p27 ubiquitination *in vitro*. We hypothesise that the phosphomimetic peptides and TPR-p27 proteins might have too low Skp2-binding affinities to be measured using these methods, but that weak K_d values of 10s or 100s of μM could be enough to induce target degradation in the cellular environment. To explore this further, we are currently working to

produce the TPR-p27 protein containing a phosphorylated amino acid (instead of the phosphomimetic) using amber suppression system (Dr Marie Synakewicz, Itzhaki lab). The constructs have been successfully cloned, and we are currently working towards improving the yields of protein expression. Biophysical assays will be carried to investigate the binding of these phospho-containing TPR-p27 proteins to Skp1-Skp2-Cks1 complex as well as testing their performance in ubiquitination and β-catenin degradation assays.

The work in this study focused on detecting transiently expressed β-catenin, and data variability was observed. In the future, it will be important to generate stable cell lines expressing the target protein of interest (e.g. HiBiT-tagged β-catenin). This will circumvent the issue with variable transfection of target protein. We also observed that mammalian cell expression of the TPR constructs varied from very low to high, which complicates the evaluation of the grafted sequences. This could be the result of protein misfolding or of degradation. Therefore, the effects of non-functionilised, mono- and bifunctional TPRs on cells will be investigated using TPRs delivered directly into cells via electroporation or the liposomal methods rather than transfection. This would allow us to deliver only correctly folded proteins and we could also investigate dose-dependent effects. We have observed variable bacterial expression of these TPR proteins, most likely due to some of the grafted loops and helices causing destabilisation. Work currently is focused on improving the TPR protein scaffold to circumvent these issues. Nevertheless, repeat-protein scaffolds are widely used in protein engineering since the repetitive architectures can be utilised as building blocks for designing artificial proteins.[259] Their elongated surfaces are highly amenable for binding-specific protein targets, making them alternatives to antibodies. Binz and Plückthun et al. described an efficient way to generate consensus-designed ankyrin repeat proteins (DAPRins),[260] which are key emerging therapeutics for their designable high binding affinities and high specificity to target proteins.

Future work could focus on using a chemical linker to connect the binding peptide sequences that were identified using the TPR scaffold as a 'pre-screen'. This would allow the use of unnatural amino acids for stapling as well as incorporating phosphorylated amino acids were needed. Prior to linking, these peptides could even be made into a D-amino acid versions and could result in a much more stable PROTACs. Dr Wenshu Xu (Itzhaki lab) carried out preliminary work on this approach using different orthogonal cross-linking and conjugation methods. It could also be very interesting to link target-binding peptides (stapled loops or helices) to ligase-binding small molecules that are already widely used in

PROTACs to bind VHL or CRBN ligases. This would be a great way to compare protein degradation achieved using stapled peptides within an already established ligase system.

Overall, the TPR scaffold approach to target protein degradation provides a platform for rapid testing of different ligases and proteins of interest binding sequences that are deemed 'undruggable' by conventional small molecule approaches due to their extensive binding interfaces. When using a TriExMOD vector, a plasmid is generated which can be readily used in bacterial, insect and mammalian expression systems. This allows a high-throughput screen to quickly identify the best sequences for further study. Several other Itzhaki lab members, as well as scientists at PolyProx Therapeutics, are exploring degradation of other proteins using TPR-p27. The experiments carried out as part of this study along with future work will determine whether proteins like TPRs are viable scaffolds for targeted protein degradation.

References

[1] R. Schoenheimer, "The dynamic state of body constituents," *Cancer Research*, vol. 2, no. 11, p. 810, 1942.

[2] A. Hershko, A. Ciechanover, and I. A. Rose, "Resolution of the ATP dependent proteolytic system from reticulocytes: A component that interacts with ATP," *Proceedings of the National Academy of Sciences of the United States of America*, vol. 76, no. 7, pp. 3107–3110, 1979.

[3] A. Hershko, A. Ciechanover, H. Heller, A. L. Haas, and I. A. Rose, "Proposed role of ATP in protein breakdown: conjugation of protein with multiple chains of the polypeptide of ATP-dependent proteolysis," *Proceedings of the National Academy of Sciences of the United States of America*, vol. 77, no. 4, pp. 1783–1786, 1980.

[4] A. Hershko and A. Ciechanover, "The ubiquitin system," *Annual Review of Biochemistry*, vol. 67, no. 1, pp. 425–479, 1998.

[5] A. Hershko, H. Heller, S. Elias, and A. Ciechanover, "Components of ubiquitin-protein ligase system. Resolution, affinity purification, and role in protein breakdown," *Journal of Biological Chemistry*, vol. 258, no. 13, pp. 8206–8214, 1983.

[6] A. Ciechanover, S. Elias, H. Heller, and A. Hershko, "Covalent affinity purification of ubiquitin-activating enzyme," *Journal of Biological Chemistry*, vol. 257, no. 5, pp. 2537–2542, 1982.

[7] W. Baumeister, J. Walz, F. Zühl, and E. Seemüller, "The proteasome: Paradigm of a self-compartmentalizing protease," *Cell*, vol. 92, no. 3, pp. 367–380, 1998.

[8] D. H. Lee, "Proteasome inhibitors: Valuable new tools for cell biologists," *Trends in Cell Biology*, vol. 8, no. 10, pp. 397–403, 1998.

[9] M. Groll and R. Huber, "Inhibitors of the eukaryotic 20S proteasome core particle: A structural approach," *Biochimica et Biophysica Acta - Molecular Cell Research*, vol. 1695, no. 1-3, pp. 33–44, 2004.

[10] C. M. Pickart and R. E. Cohen, "Proteasomes and their kin: Proteases in the machine age," *Nature Reviews Molecular Cell Biology*, vol. 5, no. 3, pp. 177–187, 2004.

[11] D. H. Wolf and W. Hilt, "The proteasome: A proteolytic nanomachine of cell regulation and waste disposal," *Biochimica et Biophysica Acta - Molecular Cell Research*, vol. 1695, no. 1-3, pp. 19–31, 2004.

[12] M. Rechsteiner and C. P. Hill, "Mobilizing the proteolytic machine: Cell biological roles of proteasome activators and inhibitors," *Trends in Cell Biology*, vol. 15, no. 1, pp. 27–33, 2005.

[13] K. L. Rock, C. Gramm, L. Rothstein, K. Clark, R. Stein, L. Dick, D. Hwang, and A. L. Goldberg, "Inhibitors of the proteasome block the degradation of most cell proteins and the generation of peptides presented on MHC class I molecules," *Cell*, vol. 78, no. 5, pp. 761–771, 1994.

[14] J. Jin, X. Li, S. P. Gygi, and J. W. Harper, "Dual E1 activation systems for ubiquitin differentially regulate E2 enzyme charging," *Nature*, vol. 447, no. 7148, pp. 1135–1138, 2007.

[15] Y. Ye and M. Rape, "Building ubiquitin chains: E2 enzymes at work," *Nature Reviews Molecular Cell Biology*, vol. 10, no. 11, pp. 755–764, 2009.

[16] W. Li, M. H. Bengtson, A. Ulbrich, A. Matsuda, V. A. Reddy, A. Orth, S. K. Chanda, S. Batalov, and C. A. Joazeiro, "Genome-wide and functional annotation of human E3 ubiquitin ligases identifies MULAN, a mitochondrial E3 that regulates the organelle's dynamics and signaling," *PLoS ONE*, vol. 3, no. 1, p. e1487, 2008.

[17] R. J. Deshaies and C. A. Joazeiro, "RING domain E3 ubiquitin ligases," *Annual Review of Biochemistry*, vol. 78, no. 1, pp. 399–434, 2009.

[18] A. Ciechanover, "The ubiquitin-proteasome proteolytic pathway," *Cell*, vol. 79, no. 1, pp. 13–21, 1994.

[19] C. M. Pickart, "Back to the future with ubiquitin," *Cell*, vol. 116, no. 2, pp. 181–190, 2004.

[20] M. H. Glickman and A. Ciechanover, "The ubiquitin-proteasome proteolytic pathway: Destruction for the sake of construction," *Physiological Reviews*, vol. 82, no. 2, pp. 373–428, 2002.

[21] A. Y. Amerik and M. Hochstrasser, "Mechanism and function of deubiquitinating enzymes," *Biochimica et Biophysica Acta - Molecular Cell Research*, vol. 1695, no. 1-3, pp. 189–207, 2004.

[22] P. Xu, D. M. Duong, N. T. Seyfried, D. Cheng, Y. Xie, J. Robert, J. Rush, M. Hochstrasser, D. Finley, and J. Peng, "Quantitative proteomics reveals the function of unconventional ubiquitin chains in proteasomal degradation," *Cell*, vol. 137, no. 1, pp. 133–145, 2009.

[23] F. Tokunaga, S. I. Sakata, Y. Saeki, Y. Satomi, T. Kirisako, K. Kamei, T. Nakagawa, M. Kato, S. Murata, S. Yamaoka, M. Yamamoto, S. Akira, T. Takao, K. Tanaka, and K. Iwai, "Involvement of linear polyubiquitylation of NEMO in NF-κB activation," *Nature Cell Biology*, vol. 11, no. 2, pp. 123–132, 2009.

[24] D. Komander and M. Rape, "The ubiquitin code," *Annual Review of Biochemistry*, vol. 81, no. 1, pp. 203–229, 2012.

[25] R. Yau and M. Rape, "The increasing complexity of the ubiquitin code," *Nature Cell Biology*, vol. 18, no. 6, pp. 579–586, 2016.

[26] G. S. McDowell and A. Philpott, "Non-canonical ubiquitylation: Mechanisms and consequences," *International Journal of Biochemistry and Cell Biology*, vol. 45, no. 8, pp. 1833–1842, 2013.

[27] S. K. Olsen and C. D. Lima, "Structure of a ubiquitin E1-E2 complex: Insights to E1-E2 thioester transfer," *Molecular Cell*, vol. 49, no. 5, pp. 884–896, 2013.

[28] H. Walden, M. S. Podgorski, D. T. Huang, D. W. Miller, R. J. Howard, D. L. Minor, J. M. Holton, and B. A. Schulman, "The structure of the APPBP1-UBA3-NEDD8-ATP complex reveals the basis for selective ubiquitin-like protein activation by an E1," *Molecular Cell*, vol. 12, no. 6, pp. 1427–1437, 2003.

[29] L. M. Lois and C. D. Lima, "Structures of the SUMO E1 provide mechanistic insights into SUMO activation and E2 recruitment to E1," *EMBO Journal*, vol. 24, no. 3, pp. 439–451, 2005.

[30] D. T. Huang, H. W. Hunt, M. Zhuang, M. D. Ohi, J. M. Holton, and B. A. Schulman, "Basis for a ubiquitin-like protein thioester switch toggling E1-E2 affinity," *Nature*, vol. 445, no. 7126, pp. 394–398, 2007.

[31] I. Lee and H. Schindelin, "Structural insights into E1-catalyzed ubiquitin activation and transfer to conjugating enzymes," *Cell*, vol. 134, no. 2, pp. 268–278, 2008.

[32] M. W. Lake, M. M. Wuebbens, K. V. Rajagopalan, and H. Schindelin, "Mechanism of ubiquitin activation revealed by the structure of a bacterial MoeB-MoaD complex," *Nature*, vol. 414, no. 6861, pp. 325–329, 2001.

[33] S. K. Olsen, A. D. Capili, X. Lu, D. S. Tan, and C. D. Lima, "Active site remodelling accompanies thioester bond formation in the SUMO E1," *Nature*, vol. 463, no. 7283, pp. 906–912, 2010.

[34] S. Lipkowitz and A. M. Weissman, "RINGs of good and evil: RING finger ubiquitin ligases at the crossroads of tumour suppression and oncogenesis," *Nature Reviews Cancer*, vol. 11, no. 9, pp. 629–643, 2011.

[35] M. Scheffner and S. Kumar, "Mammalian HECT ubiquitin-protein ligases: Biological and pathophysiological aspects," *Biochimica et Biophysica Acta - Molecular Cell Research*, vol. 1843, no. 1, pp. 61–74, 2014.

[36] K. K. Dove, B. Stieglitz, E. D. Duncan, K. Rittinger, and R. E. Klevit, " Molecular insights into RBR E3 ligase ubiquitin transfer mechanisms ," *EMBO reports*, vol. 17, no. 8, pp. 1221–1235, 2016.

[37] A. Sarikas, T. Hartmann, and Z. Q. Pan, "The cullin protein family," *Genome Biology*, vol. 12, no. 4, p. 220, 2011.

[38] J. R. Skaar, J. K. Pagan, and M. Pagano, "Mechanisms and function of substrate recruitment by F-box proteins," *Nature Reviews Molecular Cell Biology*, vol. 14, no. 6, pp. 369–381, 2013.

[39] A. Ng and R. J. Xavier, "Leucine-rich repeat (LRR) proteins: Integrators of pattern recognition and signaling in immunity," *Autophagy*, vol. 7, no. 9, pp. 1082–1084, 2011.

[40] B. Kobe and A. V. Kajava, "The leucine-rich repeat as a protein recognition motif," *Current Opinion in Structural Biology*, vol. 11, no. 6, pp. 725–732, 2001.

[41] P. Enkhbayar, M. Kamiya, M. Osaki, T. Matsumoto, and N. Matsushima, "Structural Principles of Leucine-Rich Repeat (LRR) Proteins," *Proteins: Structure, Function and Genetics*, vol. 54, no. 3, pp. 394–403, 2004.

[42] B. A. Schulman, A. C. Carrano, P. D. Jeffrey, Z. Bowen, E. R. Kinnucan, M. S. Finnin, S. J. Elledge, J. W. Harper, M. Pagano, and N. P. Pavletich, "Insights into SCF ubiquitin ligases from the structure of the Skp1-Skp2 complex," *Nature*, vol. 408, no. 6810, pp. 381–386, 2000.

[43] N. Zheng, B. A. Schulman, L. Song, J. J. Miller, P. D. Jeffrey, P. Wang, C. Chu, D. M. Koepp, S. J. Elledge, M. Pagano, R. C. Conaway, J. W. Conaway, J. W. Harper, and N. P. Pavletich, "Structure of the Cul1-Rbx1-Skp1-F-box(Skp2) SCF ubiquitin ligase complex," *Nature*, vol. 416, no. 6882, pp. 703–709, 2002.

[44] M. Gstaiger, R. Jordan, M. Lim, C. Catzavelos, J. Mestan, J. Slingerland, and W. Krek, "Skp2 is oncogenic and overexpressed in human cancers," *Proceedings of the National Academy of Sciences of the United States of America*, vol. 98, no. 9, pp. 5043–5048, 2001.

[45] H. Inuzuka, D. Gao, L. W. Finley, W. Yang, L. Wan, H. Fukushima, Y. R. Chin, B. Zhai, S. Shaik, A. W. Lau, Z. Wang, S. P. Gygi, K. Nakayama, J. Teruya-Feldstein, A. Toker, M. C. Haigis, P. P. Pandolfi, and W. Wei, "Acetylation-dependent regulation of Skp2 function," *Cell*, vol. 150, no. 1, pp. 179–193, 2012.

[46] Z. Wang, P. Liu, H. Inuzuka, and W. Wei, "Roles of F-box proteins in cancer," *Nature Reviews Cancer*, vol. 14, no. 4, pp. 233–247, 2014.

[47] T. Cardozo and M. Pagano, "Wrenches in the works: Drug discovery targeting the SCF ubiquitin ligase and APC/C complexes," *BMC Biochemistry*, vol. 8, no. SUPPL. 1, p. S9, 2007.

[48] Andre M. Rosfelder, "A tubular spring valve used as a tight and thin-walled core-retainer," *SEPM Journal of Sedimentary Research*, vol. 36, no. 3, pp. 131–149, 1966.

[49] M. Malumbres and M. Barbacid, "Cell cycle, CDKs and cancer: A changing paradigm," *Nature Reviews Cancer*, vol. 9, no. 3, pp. 153–166, 2009.

[50] D. Frescas and M. Pagano, "Deregulated proteolysis by the F-box proteins SKP2 and β-TrCP: Tipping the scales of cancer," *Nature Reviews Cancer*, vol. 8, no. 6, pp. 438–449, 2008.

[51] S. J. Randle and H. Laman, "F-box protein interactions with the hallmark pathways in cancer," *Seminars in Cancer Biology*, vol. 36, pp. 3–17, 2016.

[52] S. Signoretti, L. D. Marcotullio, A. Richardson, S. Ramaswamy, B. Isaac, M. Rue, F. Monti, M. Loda, and M. Pagano, "Oncogenic role of the ubiquitin ligase subunit Skp2 in human breast cancer," *Journal of Clinical Investigation*, vol. 110, no. 5, pp. 633–641, 2002.

[53] H. Sonoda, H. Inoue, K. Ogawa, T. Utsunomiya, T. A. Masuda, and M. Mori, "Significance of Skp2 expression in primary breast cancer," *Clinical Cancer Research*, vol. 12, no. 4, pp. 1215–1220, 2006.

[54] M. Slotky, M. Shapira, O. Ben-Izhak, S. Linn, B. Futerman, M. Tsalic, and D. D. Hershko, "The expression of the ubiquitin ligase subunit Cks1 in human breast cancer," *Breast Cancer Research*, vol. 7, no. 5, pp. 737–744, 2005.

[55] F. Traub, M. Mengel, H. J. Lück, H. H. Kreipe, and R. Von Wasielewski, "Prognostic impact of Skp2 and p27 in human breast cancer," *Breast Cancer Research and Treatment*, vol. 99, no. 2, pp. 185–191, 2006.

[56] D. O. Morgan, "Principles of CDK regulation," *Nature*, vol. 374, no. 6518, pp. 131–134, 1995.

[57] C. J. Sherr and J. M. Roberts, "CDK inhibitors: Positive and negative regulators of G1-phase progression," *Genes and Development*, vol. 13, no. 12, pp. 1501–1512, 1999.

[58] E. R. Lacy, I. Filippov, W. S. Lewis, S. Otieno, L. Xiao, S. Weiss, L. Hengst, and R. W. Kriwacki, "p27 binds cyclin-CDK complexes through a sequential mechanism involving binding-induced protein folding," *Nature Structural and Molecular Biology*, vol. 11, no. 4, pp. 358–364, 2004.

[59] C. A. Galea, A. Nourse, Y. Wang, S. G. Sivakolundu, W. T. Heller, and R. W. Kriwacki, "Role of intrinsic flexibility in signal transduction mediated by the cell cycle regulator, p27Kip1," *Journal of Molecular Biology*, vol. 376, no. 3, pp. 827–838, 2008.

[60] M. Grimmler, Y. Wang, T. Mund, Z. Cilensek, E. M. Keidel, M. B. Waddell, H. Jäkel, M. Kullmann, R. Kriwacki, and L. Hengst, "Cdk-inhibitory activity and stability of p27Kip1 are directly regulated by oncogenic tyrosine kinases," *Cell*, vol. 128, no. 2, pp. 269–280, 2007.

[61] R. K. Das, Y. Huang, A. H. Phillips, R. W. Kriwacki, and R. V. Pappu, "Cryptic sequence features within the disordered protein p27Kip1 regulate cell cycle signaling," *Proceedings of the National Academy of Sciences of the United States of America*, vol. 113, no. 20, pp. 5616–5621, 2016.

[62] M. Pagano, S. W. Tam, A. M. Theodoras, P. Beer-Romero, G. Del Sal, V. Chau, P. R. Yew, G. F. Draetta, and M. Rolfe, "Role of the ubiquitin-proteasome pathway in regulating abundance of the cyclin-dependent kinase inhibitor p27," *Science*, vol. 269, no. 5224, pp. 682–685, 1995.

[63] A. C. Carrano, E. Eytan, A. Hershko, and M. Pagano, "SKP2 is required for ubiquitin-mediated degradation of the CDK inhibitor p27," *Nature Cell Biology*, vol. 1, no. 4, pp. 193–199, 1999.

[64] A. Montagnoli, F. Fiore, E. Eytan, A. C. Carrano, G. F. Draetta, A. Hershko, and M. Pagano, "Ubiquitination of p27 is regulated by Cdk-dependent phosphorylation and trimeric complex formation," *Genes and Development*, vol. 13, no. 9, pp. 1181–1189, 1999.

[65] H. Nguyen, D. M. Gitig, and A. Koff, "Cell-free degradation of p27Kip1, a G1 cyclin-dependent kinase inhibitor, is dependent on CDK2 activity and the proteasome," *Molecular and Cellular Biology*, vol. 19, no. 2, pp. 1190–1201, 1999.

[66] D. Patra and W. G. Dunphy, "Xe-p9, a Xenopus Suc1/Cks protein, is essential for the Cdc2-dependent phosphorylation of the anaphase-promoting complex at mitosis," *Genes and Development*, vol. 12, no. 16, pp. 2549–2559, 1998.

[67] C. Spruck, H. Strohmaier, M. Watson, A. P. Smith, A. Ryan, W. Krek, and S. I. Reed, "A CDK-independent function of mammalian Cks1: Targeting of SCF(Skp2) to the CDK inhibitor p27Kip1," *Molecular Cell*, vol. 7, no. 3, pp. 639–650, 2001.

[68] D. Ganoth, G. Bornstein, T. K. Ko, B. Larsen, M. Tyers, M. Pagano, and A. Hershko, "The cell-cycle regulatory protein Cks1 is required for SCF(Skp2)-mediated ubiquitinylation of p27," *Nature Cell Biology*, vol. 3, no. 3, pp. 321–324, 2001.

[69] J. Bartek and J. Lukas, "p27 destruction: Cks1 pulls the trigger," *Nature Cell Biology*, vol. 3, no. 4, pp. 95–98, 2001.

[70] D. Sitry, M. A. Seeliger, T. K. Ko, D. Ganoth, S. E. Breward, L. S. Itzhaki, M. Pagano, and A. Hershko, "Three different binding sites of Cks1 are required for p27-ubiquitin ligation," *Journal of Biological Chemistry*, vol. 277, no. 44, pp. 42233–42240, 2002.

[71] M. A. Seeliger, S. E. Breward, A. Friedler, O. Schon, and L. S. Itzhaki, "Cooperative organization in a macromolecular complex," *Nature Structural Biology*, vol. 10, no. 9, pp. 718–724, 2003.

[72] B. Hao, N. Zheng, B. A. Schulman, G. Wu, J. J. Miller, M. Pagano, and N. P. Pavletich, "Structural basis of the Cks1-dependent recognition of p27Kip1 by the SCF Skp2 ubiquitin ligase," *Molecular Cell*, vol. 20, no. 1, pp. 9–19, 2005.

[73] U. Kossatz, N. Dietrich, L. Zender, J. Buer, M. P. Manns, and N. P. Malek, "Skp2-dependent degradation of p27Kip1 is essential for cell cycle progression," *Genes and Development*, vol. 18, no. 21, pp. 2602–2607, 2004.

[74] J. Bloom and M. Pagano, "Deregulated degradation of the CDK inhibitor p27 and malignant transformation," *Seminars in Cancer Biology*, vol. 13, no. 1, pp. 41–47, 2003.

[75] R. Z. Orlowski and D. J. Kuhn, "Proteasome inhibitors in cancer therapy: Lessons from the first decade," *Clinical Cancer Research*, vol. 14, no. 6, pp. 1649–1657, 2008.

[76] W. Zhang and S. S. Sidhu, "Development of inhibitors in the ubiquitination cascade," *FEBS Letters*, vol. 588, no. 2, pp. 356–367, 2014.

[77] D. L. Buckley and C. M. Crews, "Small-molecule control of intracellular protein levels through modulation of the ubiquitin proteasome system," *Angewandte Chemie - International Edition*, vol. 53, no. 9, pp. 2312–2330, 2014.

[78] E. Bulatov and A. Ciulli, "Targeting Cullin-RING E3 ubiquitin ligases for drug discovery: Structure, assembly and small-molecule modulation," *Biochemical Journal*, vol. 467, no. 3, pp. 365–386, 2015.

[79] L. T. Vassilev, B. T. Vu, B. Graves, D. Carvajal, F. Podlaski, Z. Filipovic, N. Kong, U. Kammlott, C. Lukacs, C. Klein, N. Fotouhi, and E. A. Liu, "In Vivo activation of the p53 pathway by small-molecule antagonists of MDM2," *Science*, vol. 303, no. 5659, pp. 844–848, 2004.

[80] J. G. Allen, M. P. Bourbeau, G. E. Wohlhieter, M. D. Bartberger, K. Michelsen, R. Hungate, R. C. Gadwood, R. D. Gaston, B. Evans, L. W. Mann, M. E. Matison,

S. Schneider, X. Huang, D. Yu, P. S. Andrews, A. Reichelt, A. M. Long, P. Yakowec, E. Y. Yang, T. A. Lee, and J. D. Oliner, "Discovery and optimization of chromenotriazolopyrimidines as potent inhibitors of the mouse double minute 2-tumor protein 53 protein-protein interaction," *Journal of Medicinal Chemistry*, vol. 52, no. 22, pp. 7044–7053, 2009.

[81] C. J. Brown, S. Lain, C. S. Verma, A. R. Fersht, and D. P. Lane, "Awakening guardian angels: Drugging the p53 pathway," *Nature Reviews Cancer*, vol. 9, no. 12, pp. 862–873, 2009.

[82] J. Deng, R. Dayam, and N. Neamati, "Patented small molecule inhibitors of p53-MDM2 interaction," *Expert Opinion on Therapeutic Patents*, vol. 16, no. 2, pp. 165–188, 2006.

[83] L. Wu, A. V. Grigoryan, Y. Li, B. Hao, M. Pagano, and T. J. Cardozo, "Specific small molecule inhibitors of Skp2-mediated p27 degradation," *Chemistry and Biology*, vol. 19, no. 12, pp. 1515–1524, 2012.

[84] E. Rico-Bautista and D. A. Wolf, "Skipping cancer: Small molecule inhibitors of SKP2-mediated p27 degradation," *Chemistry and Biology*, vol. 19, no. 12, pp. 1497–1498, 2012.

[85] E. S. Fischer, K. Böhm, J. R. Lydeard, H. Yang, M. B. Stadler, S. Cavadini, J. Nagel, F. Serluca, V. Acker, G. M. Lingaraju, R. B. Tichkule, M. Schebesta, W. C. Forrester, M. Schirle, U. Hassiepen, J. Ottl, M. Hild, R. E. Beckwith, J. W. Harper, J. L. Jenkins, and N. H. Thomä, "Structure of the DDB1-CRBN E3 ubiquitin ligase in complex with thalidomide," *Nature*, vol. 512, no. 1, pp. 49–53, 2014.

[86] S. Orlicky, X. Tang, V. Neduva, N. Elowe, E. D. Brown, F. Sicheri, and M. Tyers, "An allosteric inhibitor of substrate recognition by the SCF(Cdc4) ubiquitin ligase," *Nature Biotechnology*, vol. 28, no. 7, pp. 733–737, 2010.

[87] M. Aghajan, N. Jonai, K. Flick, F. Fu, M. Luo, X. Cai, I. Ouni, N. Pierce, X. Tang, B. Lomenick, R. Damoiseaux, R. Hao, P. M. Del Moral, R. Verma, Y. Li, C. Li, K. N. Houk, M. E. Jung, N. Zheng, L. Huang, R. J. Deshaies, P. Kaiser, and J. Huang, "Chemical genetics screen for enhancers of rapamycin identifies a specific inhibitor of an SCF family E3 ubiquitin ligase," *Nature Biotechnology*, vol. 28, no. 7, pp. 738–742, 2010.

[88] H. Shen and C. G. Maki, "Pharmacologic activation of p53 by small-molecule MDM2 antagonists," *Current Pharmaceutical Design*, vol. 17, no. 6, pp. 560–568, 2011.

[89] C. H. Chan, J. K. Morrow, C. F. Li, Y. Gao, G. Jin, A. Moten, L. J. Stagg, J. E. Ladbury, Z. Cai, D. Xu, C. J. Logothetis, M. C. Hung, S. Zhang, and H. K. Lin, "Pharmacological inactivation of Skp2 SCF ubiquitin ligase restricts cancer stem cell traits and cancer progression," *Cell*, vol. 154, no. 3, pp. 556–568, 2013.

[90] D. Ungermannova, J. Lee, G. Zhang, H. G. Dallmann, C. S. McHenry, and X. Liu, "High-throughput screening alphascreen assay for identification of small-molecule inhibitors of ubiquitin E3 ligase SCF(Skp2-Cks1)," *Journal of Biomolecular Screening*, vol. 18, no. 8, pp. 910–920, 2013.

[91] C. R. Montgomery, *Protein-protein interactions (PPIs): Types, methods for detection and analysis*. 2016.

[92] T. A. Cardote and A. Ciulli, "Cyclic and macrocyclic peptides as chemical tools to recognise protein surfaces and probe protein-protein interactions," *ChemMedChem*, vol. 11, no. 8, pp. 787–794, 2016.

[93] D. J. Craik, D. P. Fairlie, S. Liras, and D. Price, "The future of peptide-based drugs," *Chemical Biology and Drug Design*, vol. 81, no. 1, pp. 136–147, 2013.

[94] D. E. Scott, A. R. Bayly, C. Abell, and J. Skidmore, "Small molecules, big targets: Drug discovery faces the protein-protein interaction challenge," *Nature Reviews Drug Discovery*, vol. 15, no. 8, pp. 533–550, 2016.

[95] M. M. Arkin and J. A. Wells, "Small-molecule inhibitors of protein-protein interactions: Progressing towards the dream," *Nature Reviews Drug Discovery*, vol. 3, no. 4, pp. 301–317, 2004.

[96] H. Jubb, A. P. Higueruelo, A. Winter, and T. L. Blundell, "Structural biology and drug discovery for protein-protein interactions," *Trends in Pharmacological Sciences*, vol. 33, no. 5, pp. 241–248, 2012.

[97] G. L. Verdine and G. J. Hilinski, "Stapled peptides for intracellular drug targets," *Methods in Enzymology*, vol. 503, pp. 3–33, 2012.

[98] A. C. L. Lee, J. L. Harris, K. K. Khanna, and J. H. Hong, "A comprehensive review on current advances in peptide drug development and design," *International Journal of Molecular Sciences*, vol. 20, no. 10, 2019.

[99] J. L. Lau and M. K. Dunn, "Therapeutic peptides: Historical perspectives, current development trends, and future directions," *Bioorganic and Medicinal Chemistry*, vol. 26, no. 10, pp. 2700–2707, 2018.

[100] K. Fosgerau and T. Hoffmann, "Peptide therapeutics: Current status and future directions," *Drug Discovery Today*, vol. 20, no. 1, pp. 122–128, 2015.

[101] L. Otvos and J. D. Wade, "Current challenges in peptide-based drug discovery," *Frontiers in Chemistry*, vol. 2, no. 62, pp. 1–4, 2014.

[102] T. Uhlig, T. Kyprianou, F. G. Martinelli, C. A. Oppici, D. Heiligers, D. Hills, X. R. Calvo, and P. Verhaert, "The emergence of peptides in the pharmaceutical business: From exploration to exploitation," *EuPA Open Proteomics*, vol. 4, pp. 58–69, 2014.

[103] L. B. Giebel, R. T. Cass, D. L. Milligan, D. C. Young, R. Arze, and C. R. Johnson, "Screening of cyclic peptide phage libraries identifies ligands that bind streptavidin with high affinities," *Biochemistry*, vol. 34, no. 47, pp. 15430–15435, 1995.

[104] M. Krook, C. Lindbladh, J. A. Eriksen, and K. Mosbach, "Selection of a cyclic nonapeptide inhibitor to α-chymotrypsin using a phage display peptide library," *Molecular Diversity*, vol. 3, no. 3, pp. 149–159, 1997.

[105] T. Czömpöly, Á. Lábadi, M. Balázs, P. Németh, and P. Balogh, "Use of cyclic peptide phage display library for the identification of a CD45RC epitope expressed on murine B cells and their precursors," *Biochemical and Biophysical Research Communications*, vol. 307, no. 4, pp. 791–796, 2003.

[106] S. C. Meyer, T. Gaj, and I. Ghosh, "Highly selective cyclic peptide ligands for neutravidin and avidin identified by phage display," *Chemical Biology and Drug Design*, vol. 68, no. 1, pp. 3–10, 2006.

[107] E. Valeur, S. M. Guéret, H. Adihou, R. Gopalakrishnan, M. Lemurell, H. Waldmann, T. N. Grossmann, and A. T. Plowright, "New modalities for challenging targets in drug discovery," *Angewandte Chemie - International Edition*, vol. 56, no. 35, pp. 10294–10323, 2017.

[108] D. S. Nielsen, N. E. Shepherd, W. Xu, A. J. Lucke, M. J. Stoermer, and D. P. Fairlie, "Orally absorbed cyclic peptides," *Chemical Reviews*, vol. 117, no. 12, pp. 8094–8128, 2017.

[109] T. A. Hill, N. E. Shepherd, F. Diness, and D. P. Fairlie, "Constraining cyclic peptides to mimic protein structure motifs," *Angewandte Chemie - International Edition*, vol. 53, no. 48, pp. 13020–13041, 2014.

[110] C. J. White and A. K. Yudin, "Contemporary strategies for peptide macrocyclization," *Nature Chemistry*, vol. 3, no. 7, pp. 509–524, 2011.

[111] J. Tang, Y. He, H. Chen, W. Sheng, and H. Wang, "Synthesis of bioactive and stabilized cyclic peptides by macrocyclization using C(sp3)-H activation," *Chemical Science*, vol. 8, no. 6, pp. 4565–4570, 2017.

[112] A. J. Wilson, "Inhibition of protein-protein interactions using designed molecules," *Chemical Society Reviews*, vol. 38, no. 12, pp. 3289–3300, 2009.

[113] Z. Fang, Y. Song, P. Zhan, Q. Zhang, and X. Liu, "Conformational restriction: An effective tactic in 'follow-on'-based drug discovery," *Future Medicinal Chemistry*, vol. 6, no. 8, pp. 885–901, 2014.

[114] C. E. Schafmeister, J. Po, and G. L. Verdine, "An all-hydrocarbon cross-linking system for enhancing the helicity and metabolic stability of peptides," *Journal of the American Chemical Society*, vol. 122, no. 24, pp. 5891–5892, 2000.

[115] G. H. Bird, N. Madani, A. F. Perry, A. M. Princiotto, J. G. Supko, X. He, E. Gavathiotis, J. G. Sodroski, and L. D. Walensky, "Hydrocarbon double-stapling remedies the proteolytic instability of a lengthy peptide therapeutic," *Proceedings of the National Academy of Sciences of the United States of America*, vol. 107, no. 32, pp. 14093–14098, 2010.

[116] S. M. Condon, I. Morize, S. Darnbrough, C. J. Burns, B. E. Miller, J. Uhl, K. Burke, N. Jariwala, K. Locke, P. H. Krolikowski, N. V. Kumar, and R. F. Labaudiniere, "The bioactive conformation of human parathyroid hormone. Structural evidence for the extended helix postulate," *Journal of the American Chemical Society*, vol. 122, no. 13, pp. 3007–3014, 2000.

[117] N. E. Shepherd, H. N. Hoang, G. Abbenante, and D. P. Fairlie, "Single turn peptide alpha helices with exceptional stability in water," *Journal of the American Chemical Society*, vol. 127, no. 9, pp. 2974–2983, 2005.

[118] N. E. Shepherd, H. N. Hoang, V. S. Desai, E. Letouze, P. R. Young, and D. P. Fairlie, "Modular α-helical mimetics with antiviral activity against respiratory syncitial virus," *Journal of the American Chemical Society*, vol. 128, no. 40, pp. 13284–13289, 2006.

[119] H. E. Blackwell and R. H. Grubbs, "Highly efficient synthesis of covalently cross-linked peptide helices by ring-closing metathesis," *Angewandte Chemie - International Edition*, vol. 37, no. 23, pp. 3281–3284, 1998.

[120] Y. Grigoryev, "Stapled peptide to enter human testing, but affinity questions remain," *Nature Medicine*, vol. 19, no. 2, p. 120, 2013.

[121] R. Huisgen, "1,3-Dipolar cycloadditions. Past and future," *Angewandte Chemie International Edition in English*, vol. 2, no. 10, pp. 565–598, 1963.

[122] V. V. Rostovtsev, L. G. Green, V. V. Fokin, and K. B. Sharpless, "A stepwise huisgen cycloaddition process: Copper(I)-catalyzed regioselective "ligation" of azides and terminal alkynes," *Angewandte Chemie - International Edition*, vol. 41, no. 14, pp. 2596–2599, 2002.

[123] S. Cantel, A. L. C. Isaad, M. Scrima, J. J. Levy, R. D. DiMarchi, P. Rovero, J. A. Halperin, A. M. D'Ursi, A. M. Papini, and M. Chorev, "Synthesis and conformational analysis of a cyclic peptide obtained via i to (i+4) intramolecular side-chain to side-chain azide-alkyne 1,3-dipolar cycloaddition," *Journal of Organic Chemistry*, vol. 73, no. 15, pp. 5663–5674, 2008.

[124] A. Le Chevalier Isaad, A. M. Papini, M. Chorev, and P. Rovero, "Side chain-to-side chain cyclization by click reaction," *Journal of Peptide Science*, vol. 15, no. 7, pp. 451–454, 2009.

[125] M. Scrima, A. Le Chevalier-Isaad, P. Rovero, A. M. Papini, M. Chorev, and A. M. D'Ursi, "Cu(I) catalyzed azide-alkyne intramolecular i to (i+4) side chain to side chain cyclization promotes the formation of helix-like secondary structures," *European Journal of Organic Chemistry*, no. 3, pp. 446–457, 2010.

[126] M. Larregola, O. Lequin, P. Karoyan, D. Guianvarc'h, and S. Lavielle, "β-Amino acids containing peptides and click-cyclized peptide as β-turn mimics: A comparative study with 'conventional' lactam- and disulfide-bridged hexapeptides," *Journal of Peptide Science*, vol. 17, no. 9, pp. 632–643, 2011.

[127] M. M. Madden, C. I. Rivera Vera, W. Song, and Q. Lin, "Facile synthesis of stapled, structurally reinforced peptide helices via a photoinduced intramolecular 1,3-dipolar cycloaddition reaction," *Chemical Communications*, no. 37, pp. 5588–5590, 2009.

[128] Y. S. Chang, B. Graves, V. Guerlavais, C. Tovar, K. Packman, K. H. To, K. A. Olson, K. Kesavan, P. Gangurde, A. Mukherjee, T. Baker, K. Darlak, C. Elkin, Z. Filipovic, F. Z. Qureshi, H. Cai, P. Berry, E. Feyfant, X. E. Shi, J. Horstick, D. A. Annis, A. M. Manning, N. Fotouhi, H. Nash, L. T. Vassilev, and T. K. Sawyer, "Stapled α-helical peptide drug development: A potent dual inhibitor of MDM2 and MDMX for p53-dependent cancer therapy," *Proceedings of the National Academy of Sciences of the United States of America*, vol. 110, no. 36, pp. E3445–E3454, 2013.

[129] W. Wolfson, "Aileron staples peptides," *Chemistry and Biology*, vol. 16, no. 9, pp. 910–912, 2009.

[130] T. L. Sun, Y. Sun, C. C. Lee, and H. W. Huang, "Membrane permeability of hydrocarbon-cross-linked peptides," *Biophysical Journal*, vol. 104, no. 9, pp. 1923–1932, 2013.

[131] F. Bernal, A. F. Tyler, S. J. Korsmeyer, L. D. Walensky, and G. L. Verdine, "Reactivation of the p53 tumor suppressor pathway by a stapled p53 peptide," *Journal of the American Chemical Society*, vol. 129, no. 9, pp. 2456–2457, 2007.

[132] R. E. Moellering, M. Cornejo, T. N. Davis, C. D. Bianco, J. C. Aster, S. C. Blacklow, A. L. Kung, D. G. Gilliland, G. L. Verdine, and J. E. Bradner, "Direct inhibition of the NOTCH transcription factor complex," *Nature*, vol. 462, no. 7270, pp. 182–188, 2009.

[133] M. L. Stewart, E. Fire, A. E. Keating, and L. D. Walensky, "The MCL-1 BH3 helix is an exclusive MCL-1 inhibitor and apoptosis sensitizer," *Nature Chemical Biology*, vol. 6, no. 8, pp. 595–601, 2010.

[134] H. Andersson, H. Demaegdt, A. Johnsson, G. Vauquelin, G. Lindeberg, M. Hallberg, M. Erdélyi, A. Karlén, and A. Hallberg, "Potent macrocyclic inhibitors of insulin-regulated aminopeptidase (IRAP) by olefin ring-closing metathesis," *Journal of Medicinal Chemistry*, vol. 54, no. 11, pp. 3779–3792, 2011.

[135] T. N. Grossmann, J. T. Yeh, B. R. Bowman, Q. Chu, R. E. Moellering, and G. L. Verdine, "Inhibition of oncogenic Wnt signaling through direct targeting of β-catenin,"

Proceedings of the National Academy of Sciences of the United States of America, vol. 109, no. 44, pp. 17942–17947, 2012.

[136] S. A. Kawamoto, A. Coleska, X. Ran, H. Yi, C. Y. Yang, and S. Wang, "Design of triazole-stapled BCL9 α-helical peptides to target the β-catenin/B-cell CLL/lymphoma 9 (BCL9) protein-protein interaction," *Journal of Medicinal Chemistry*, vol. 55, no. 3, pp. 1137–1146, 2012.

[137] S. Ingale and P. E. Dawson, "On resin side-chain cyclization of complex peptides using CuAAC," *Organic Letters*, vol. 13, no. 11, pp. 2822–2825, 2011.

[138] J. Rivier, S. L. Lahrichi, J. Gulyas, J. Erchegyi, S. C. Koerber, A. G. Craig, A. Corrigan, C. Rivier, and W. Vale, "Minimal-size, constrained corticotropin-releasing factor agonists with i-(i+3) Glu-Lys and Lys-Glu bridges," *Journal of Medicinal Chemistry*, vol. 41, no. 14, pp. 2614–2620, 1998.

[139] B. Yang, D. Liu, and Z. Huang, "Synthesis and helical structure of lactam bridged BH3 peptides derived from pro-apoptotic Bcl-2 family proteins," *Bioorganic and Medicinal Chemistry Letters*, vol. 14, no. 6, pp. 1403–1406, 2004.

[140] H. Guo, F. Gallazzi, and Y. Miao, "Design and evaluation of new Tc-99m-labeled lactam bridge-cyclized alpha-MSH peptides for melanoma imaging," *Molecular Pharmaceutics*, vol. 10, no. 4, pp. 1400–1408, 2013.

[141] J. C. Serrano, J. Sipthorp, W. Xu, L. S. Itzhaki, and S. V. Ley, "A new methodology for incorporating chiral linkers into stapled peptides," *ChemBioChem*, vol. 18, no. 12, pp. 1066–1071, 2017.

[142] L. Nevola, A. Martín-Quirõs, K. Eckelt, N. Camarero, S. Tosi, A. Llobet, E. Giralt, and P. Gorostiza, "Light-regulated stapled peptides to inhibit protein-protein interactions involved in clathrin-mediated endocytosis," *Angewandte Chemie - International Edition*, vol. 52, no. 30, pp. 7704–7708, 2013.

[143] J. C. Phelan, N. J. Skelton, A. C. Braisted, and R. S. McDowell, "A general method for constraining short peptides to an α-helical conformation," *Journal of the American Chemical Society*, vol. 119, no. 3, pp. 455–460, 1997.

[144] D. P. Fairlie and A. Dantas de Araujo, "Review stapling peptides using cysteine crosslinking," *Biopolymers*, vol. 106, no. 6, pp. 843–852, 2016.

[145] E. Y. Hui, B. Rout, Y. S. Tan, C. S. Verma, K. P. Chan, and C. W. Johannes, "An intramolecular tryptophan-condensation approach for peptide stapling," *Organic and Biomolecular Chemistry*, vol. 16, no. 3, pp. 389–392, 2018.

[146] R. Hueisgen, "1,3-Dipolar cycloadditions," *Proceedings of the Chemical Society*, no. Centenary lecture, pp. 356–396, 1961.

[147] O. Torres, D. Yüksel, M. Bernardina, K. Kumar, and D. Bong, "Peptide tertiary structure nucleation by side-chain crosslinking with metal complexation and double "Click" cycloaddition," *ChemBioChem*, vol. 9, no. 11, pp. 1701–1705, 2008.

[148] P. T. Tran, C. Ø. Larsen, T. Røndbjerg, M. De Foresta, M. B. Kunze, A. Marek, J. H. Løper, L. E. Boyhus, A. Knuhtsen, K. Lindorff-Larsen, and D. S. Pedersen, "Diversity-oriented peptide stapling: A third generation copper-catalysed azide–alkyne cycloaddition stapling and functionalisation strategy," *Chemistry - A European Journal*, vol. 23, no. 14, pp. 3490–3495, 2017.

[149] L. Zhang, T. Navaratna, J. Liao, and G. M. Thurber, "Dual-purpose linker for alpha helix stabilization and imaging agent conjugation to glucagon-like peptide-1 receptor ligands," *Bioconjugate Chemistry*, vol. 26, no. 2, pp. 329–337, 2015.

[150] Y. H. Lau, P. De Andrade, S. T. Quah, M. Rossmann, L. Laraia, N. Sköld, T. J. Sum, P. J. Rowling, T. L. Joseph, C. Verma, M. Hyvönen, L. S. Itzhaki, A. R. Venkitaraman, C. J. Brown, D. P. Lane, and D. R. Spring, "Functionalised staple linkages for modulating the cellular activity of stapled peptides," *Chemical Science*, vol. 5, no. 5, pp. 1804–1809, 2014.

[151] Y. H. Lau, Y. Wu, P. de Andrade, W. R. J. D. Galloway, and D. R. Spring, "A two-component 'double-click' approach to peptide stapling," *Nature Protocols*, vol. 10, no. 4, pp. 585–594, 2015.

[152] J. Iegre, J. S. Gaynord, N. S. Robertson, H. F. Sore, M. Hyvönen, and D. R. Spring, "Two-component stapling of biologically active and conformationally constrained peptides: Past, present, and future," *Advanced Therapeutics*, vol. 1, no. 7, p. 1800052, 2018.

[153] Y. H. Lau and D. R. Spring, "Efficient synthesis of Fmoc-protected azido amino acids," *Synlett*, no. 13, pp. 1917–1919, 2011.

[154] Y. H. Lau, P. De Andrade, Y. Wu, and D. R. Spring, "Peptide stapling techniques based on different macrocyclisation chemistries," *Chemical Society Reviews*, vol. 44, no. 1, pp. 91–102, 2015.

[155] Y. H. Lau, Y. Wu, M. Rossmann, B. X. Tan, P. De Andrade, Y. S. Tan, C. Verma, G. J. McKenzie, A. R. Venkitaraman, M. Hyvönen, and D. R. Spring, "Double strain-promoted macrocyclization for the rapid selection of cell-active stapled peptides," *Angewandte Chemie - International Edition*, vol. 54, no. 51, pp. 15410–15413, 2015.

[156] N. J. Agard, J. A. Prescher, and C. R. Bertozzi, "A strain-promoted [3+2] azide-alkyne cycloaddition for covalent modification of biomolecules in living systems," *Journal of the American Chemical Society*, vol. 126, no. 46, pp. 15046–15047, 2004.

[157] J. Dommerholt, F. P. Rutjes, and F. L. van Delft, "Strain-promoted 1,3-dipolar cycloaddition of cycloalkynes and organic azides," *Topics in Current Chemistry*, vol. 374, no. 2, pp. 1–20, 2016.

[158] A. M. Leduc, J. O. Trent, J. L. Wittliff, K. S. Bramlett, S. L. Briggs, N. Y. Chirgadze, Y. Wang, T. P. Burris, and A. F. Spatola, "Helix-stabilized cyclic peptides as selective inhibitors of steroid receptor - coactivator interactions," *Proceedings of the National Academy of Sciences of the United States of America*, vol. 100, no. 20, pp. 11273–11278, 2003.

[159] F. Giordanetto, J. D. Revell, L. Knerr, M. Hostettler, A. Paunovic, C. Priest, A. Janefeldt, and A. Gill, "Stapled vasoactive intestinal peptide (VIP) derivatives improve VPAC 2 agonism and glucose-dependent insulin secretion," *ACS Medicinal Chemistry Letters*, vol. 4, no. 12, pp. 1163–1168, 2013.

[160] L. Frankiewicz, C. Betti, K. Guillemyn, D. Tourwé, Y. Jacquot, and S. Ballet, "Stabilisation of a short α-helical VIP fragment by side chain to side chain cyclisation: A comparison of common cyclisation motifs by circular dichroism," *Journal of Peptide Science*, vol. 19, no. 7, pp. 423–432, 2013.

[161] A. D. De Araujo, H. N. Hoang, W. M. Kok, F. Diness, P. Gupta, T. A. Hill, R. W. Driver, D. A. Price, S. Liras, and D. P. Fairlie, "Comparative α-helicity of cyclic pentapeptides in water," *Angewandte Chemie - International Edition*, vol. 53, no. 27, pp. 6965–6969, 2014.

[162] M. Guharoy and P. Chakrabarti, "Secondary structure based analysis and classification of biological interfaces: Identification of binding motifs in protein-protein interactions," *Bioinformatics*, vol. 23, no. 15, pp. 1909–1918, 2007.

[163] A. Glas, D. Bier, G. Hahne, C. Rademacher, C. Ottmann, and T. N. Grossmann, "Constrained peptides with target-adapted cross-links as inhibitors of a pathogenic protein-protein interaction," *Angewandte Chemie - International Edition*, vol. 53, no. 9, pp. 2489–2493, 2014.

[164] W. Xu, Y. H. Lau, G. Fischer, Y. S. Tan, A. Chattopadhyay, M. De La Roche, M. Hyvönen, C. Verma, D. R. Spring, and L. S. Itzhaki, "Macrocyclized extended peptides: Inhibiting the substrate-recognition domain of tankyrase," *Journal of the American Chemical Society*, vol. 139, no. 6, pp. 2245–2256, 2017.

[165] M. M. Wiedmann, Y. S. Tan, Y. Wu, S. Aibara, W. Xu, H. F. Sore, C. S. Verma, L. Itzhaki, M. Stewart, J. D. Brenton, and D. R. Spring, "Development of cell-permeable, non-helical constrained peptides to target a key protein–protein interaction in ovarian cancer," *Angewandte Chemie - International Edition*, vol. 56, no. 2, pp. 524–529, 2017.

[166] B. Gupta, T. S. Levchenko, and V. P. Torchilin, "Intracellular delivery of large molecules and small particles by cell-penetrating proteins and peptides," *Advanced Drug Delivery Reviews*, vol. 57, no. 4, pp. 637–651, 2005.

[167] G. P. Dietz and M. Bähr, "Delivery of bioactive molecules into the cell: The Trojan horse approach," *Molecular and Cellular Neuroscience*, vol. 27, no. 2, pp. 85–131, 2004.

[168] M. Mäe and Ü. Langel, "Cell-penetrating peptides as vectors for peptide, protein and oligonucleotide delivery," *Current Opinion in Pharmacology*, vol. 6, no. 5, pp. 509–514, 2006.

[169] P. Jarver, K. Langel, S. El Andaloussi, and U. Langel, "Applications of cell-penetrating peptides in regulation of gene expression," *Biochemical Society Transactions*, vol. 35, no. 4, pp. 770–774, 2007.

[170] B. R. Meade and S. F. Dowdy, "Enhancing the cellular uptake of siRNA duplexes following noncovalent packaging with protein transduction domain peptides," *Advanced Drug Delivery Reviews*, vol. 60, no. 4-5, pp. 530–536, 2008.

[171] W. L. Munyendo, H. Lv, H. Benza-Ingoula, L. D. Baraza, and J. Zhou, "Cell penetrating peptides in the delivery of biopharmaceuticals," *Biomolecules*, vol. 2, no. 2, pp. 187–202, 2012.

[172] A. Bolhassani, "Potential efficacy of cell-penetrating peptides for nucleic acid and drug delivery in cancer," *Biochimica et biophysica acta*, vol. 1816, no. 2, pp. 232–246, 2011.

[173] D. Raucher and J. S. Ryu, "Cell-penetrating peptides: Strategies for anticancer treatment," *Trends in Molecular Medicine*, vol. 21, no. 9, pp. 560–570, 2015.

[174] S. W. Jones, R. Christison, K. Bundell, C. J. Voyce, S. M. Brockbank, P. Newham, and M. A. Lindsay, "Characterisation of cell-penetrating peptide-mediated peptide delivery," *British Journal of Pharmacology*, vol. 145, no. 8, pp. 1093–1102, 2005.

[175] C. Bechara and S. Sagan, "Cell-penetrating peptides: 20 years later, where do we stand?," *FEBS Letters*, vol. 587, no. 12, pp. 1693–1702, 2013.

[176] P. Agrawal, S. Bhalla, S. S. Usmani, S. Singh, K. Chaudhary, G. P. Raghava, and A. Gautam, "CPPsite 2.0: A repository of experimentally validated cell-penetrating peptides," *Nucleic Acids Research*, vol. 44, no. D1, pp. D1098–D1103, 2016.

[177] A. Gräslund, F. Madani, S. Lindberg, Ü. Langel, and S. Futaki, "Mechanisms of cellular uptake of cell-penetrating peptides," *Journal of Biophysics*, vol. 2011, pp. 1–10, 2011.

[178] F. Milletti, "Cell-penetrating peptides: Classes, origin, and current landscape," *Drug Discovery Today*, vol. 17, no. 15-16, pp. 850–860, 2012.

[179] K. Fujimoto, R. Hosotani, Y. Miyamoto, R. Doi, T. Koshiba, A. Otaka, N. Fujii, R. D. Beauchamp, and M. Imamura, "Inhibition of pRb phosphorylation and cell cycle progression by an antennapedia-p16(INK4A) fusion peptide in pancreatic cancer cells," *Cancer Letters*, vol. 159, no. 2, pp. 151–158, 2000.

[180] M. A. Lindsay, "Peptide-mediated cell delivery: Application in protein target validation," *Current Opinion in Pharmacology*, vol. 2, no. 5, pp. 587–594, 2002.

[181] D. Derossi, A. H. Joliot, G. Chassaing, and A. Prochiantz, "The third helix of the Antennapedia homeodomain translocates through biological membranes," *Journal of Biological Chemistry*, vol. 269, no. 14, pp. 10444–10450, 1994.

[182] M. Green and P. M. Loewenstein, "Autonomous functional domains of chemically synthesized human immunodeficiency virus tat trans-activator protein," *Cell*, vol. 55, no. 6, pp. 1179–1188, 1988.

[183] M. Pooga, M. Hällbrink, M. Zorko, and U. Langel, "Cell penetration by transportan," *The FASEB Journal*, vol. 12, no. 1, pp. 67–77, 1998.

[184] Ü. Langel, M. Pooga, C. Kairane, M. Zilmer, and T. Bartfai, "A galanin-mastoparan chimeric peptide activates the Na+,K+-ATPase and reverses its inhibition by ouabain," *Regulatory Peptides*, vol. 62, no. 1, pp. 47–52, 1996.

[185] P. A. Wender, D. J. Mitchell, K. Pattabiraman, E. T. Pelkey, L. Steinman, and J. B. Rothbard, "The design, synthesis, and evaluation of molecules that enable or enhance cellular uptake: Peptoid molecular transporters," *Proceedings of the National Academy of Sciences of the United States of America*, vol. 97, no. 24, pp. 13003–13008, 2000.

[186] A. Elmquist, M. Lindgren, T. Bartfai, and Ü. Langel, "Ve-cadherin-derived cell-penetrating peptide, pVEC with carrier functions," *Experimental Cell Research*, vol. 269, no. 2, pp. 237–244, 2001.

[187] J. Oehlke, A. Scheller, B. Wiesner, E. Krause, M. Beyermann, E. Klauschenz, M. Melzig, and M. Bienert, "Cellular uptake of an α-helical amphipathic model peptide with the potential to deliver polar compounds into the cell interior non-endocytically," *Biochimica et Biophysica Acta - Biomembranes*, vol. 1414, no. 1-2, pp. 127–139, 1998.

[188] H. J. Johansson, S. El-Andaloussi, T. Holm, M. Mäe, J. Jänes, T. Maimets, and Ü. Langel, "Characterization of a novel cytotoxic cell-penetrating peptide derived from p14ARF protein," *Molecular Therapy*, vol. 16, no. 1, pp. 115–123, 2008.

[189] J. C. Mai, H. Shen, S. C. Watkins, T. Cheng, and P. D. Robbins, "Efficiency of protein transduction is cell type-dependent and is enhanced by dextran sulfate," *The Journal of biological chemistry*, vol. 277, no. 33, pp. 30208–30218, 2002.

[190] M. J. May, F. D'Acquisto, L. A. Madge, J. Glockner, J. S. Pober, and S. Ghosh, "Selective inhibition of NF-κB activation by a peptide that blocks the interaction of NEMO with the IκB kinase complex," *Science*, vol. 289, no. 5484, pp. 1550–1554, 2000.

[191] J. A. Gomez, J. Chen, J. Ngo, D. Hajkova, I. J. Yeh, V. Gama, M. Miyagi, and S. Matsuyama, "Cell-penetrating penta-peptides (CPP5s): Measurement of cell entry

and protein-transduction activity," *Pharmaceuticals*, vol. 3, no. 12, pp. 3594–3613, 2010.

[192] P. L. Leopold, "Endosomal escape pathways for delivery of biologics," *Lysosomes: Biology, Diseases, and Therapeutics*, pp. 383–407, 2016.

[193] A. El-Sayed, S. Futaki, and H. Harashima, "Delivery of macromolecules using arginine-rich cell-penetrating peptides: Ways to overcome endosomal entrapment," *AAPS Journal*, vol. 11, no. 1, pp. 13–22, 2009.

[194] G. Guidotti, L. Brambilla, and D. Rossi, "Cell-penetrating peptides: From basic research to clinics," *Trends in Pharmacological Sciences*, vol. 38, no. 4, pp. 406–424, 2017.

[195] S. Pujals, J. Fernández-Carneado, M. D. Ludevid, and E. Giralt, "D-SAP: A new, noncytotoxic, and fully protease resistant cell-penetrating peptide," *ChemMedChem*, vol. 3, no. 2, pp. 296–301, 2008.

[196] M. J. Klein, S. Schmidt, P. Wadhwani, J. Bürck, J. Reichert, S. Afonin, M. Berditsch, T. Schober, R. Brock, M. Kansy, and A. S. Ulrich, "Lactam-stapled cell-penetrating peptides: Cell uptake and membrane binding properties," *Journal of Medicinal Chemistry*, vol. 60, no. 19, pp. 8071–8082, 2017.

[197] Q. Chu, R. E. Moellering, G. J. Hilinski, Y. W. Kim, T. N. Grossmann, J. T. Yeh, and G. L. Verdine, "Towards understanding cell penetration by stapled peptides," *MedChemComm*, vol. 6, no. 1, pp. 111–119, 2015.

[198] M. P. Stewart, A. Sharei, X. Ding, G. Sahay, R. Langer, and K. F. Jensen, "In vitro and ex vivo strategies for intracellular delivery," *Nature*, vol. 538, no. 7624, pp. 183–192, 2016.

[199] V. J. Bruce and B. R. McNaughton, "Inside job: Methods for delivering proteins to the interior of mammalian cells," *Cell Chemical Biology*, vol. 24, no. 8, pp. 924–934, 2017.

[200] S. R. Sarker, R. Hokama, and S. Takeoka, "Intracellular delivery of universal proteins using a lysine headgroup containing cationic liposomes: Deciphering the uptake mechanism," *Molecular Pharmaceutics*, vol. 11, no. 1, pp. 164–174, 2014.

[201] M. Furuhata, H. Kawakami, K. Toma, Y. Hattori, and Y. Maitani, "Intracellular delivery of proteins in complexes with oligoarginine-modified liposomes and the effect of oligoarginine length," *Bioconjugate Chemistry*, vol. 17, no. 4, pp. 935–942, 2006.

[202] J. Heuts, E. M. Varypataki, K. van der Maaden, S. Romeijn, J. W. Drijfhout, A. T. van Scheltinga, F. Ossendorp, and W. Jiskoot, "Cationic liposomes: A flexible vaccine delivery system for physicochemically diverse antigenic peptides," *Pharmaceutical Research*, vol. 35, no. 11, 2018.

[203] S. Van Meirvenne, L. Straetman, C. Heirman, M. Dullaers, C. De Greef, V. Van Tendeloo, and K. Thielemans, "Efficient genetic modification of murine dendritic cells by electroporation with mRNA," *Cancer Gene Therapy*, vol. 9, no. 9, pp. 787–797, 2002.

[204] G. Freund, A. P. Sibler, D. Desplancq, M. Oulad-Abdelghani, M. Vigneron, J. Gannon, M. H. Van Regenmortel, and E. Weiss, "Targeting endogenous nuclear antigens by electrotransfer of monoclonal antibodies in living cells," *mAbs*, vol. 5, no. 4, pp. 518–522, 2013.

[205] D. Clift, W. A. McEwan, L. I. Labzin, V. Konieczny, B. Mogessie, L. C. James, and M. Schuh, "A method for the acute and rapid degradation of endogenous proteins," *Cell*, vol. 171, no. 7, pp. 1692–1706, 2017.

[206] S. Movahed and D. Li, "Microfluidics cell electroporation," *Microfluidics and Nanofluidics*, vol. 10, no. 4, pp. 703–734, 2011.

[207] T. Geng, Y. Zhan, H. Y. Wang, S. R. Witting, K. G. Cornetta, and C. Lu, "Flow-through electroporation based on constant voltage for large-volume transfection of cells," *Journal of Controlled Release*, vol. 144, no. 1, pp. 91–100, 2010.

[208] Y. Zhan, J. Wang, N. Bao, and C. Lu, "Electroporation of cells in microfluidic droplets," *Analytical Chemistry*, vol. 81, no. 5, pp. 2027–2031, 2009.

[209] P. E. Boukany, A. Morss, W. C. Liao, B. Henslee, H. Jung, X. Zhang, B. Yu, X. Wang, Y. Wu, L. Li, K. Gao, X. Hu, X. Zhao, O. Hemminger, W. Lu, G. P. Lafyatis, and L. J. Lee, "Nanochannel electroporation delivers precise amounts of biomolecules into living cells," *Nature Nanotechnology*, vol. 6, no. 11, pp. 747–754, 2011.

[210] A. A. Adjei, "What is the right dose? The elusive optimal biologic dose in phase I clinical trials," *Journal of Clinical Oncology*, vol. 24, no. 25, pp. 4054–4055, 2006.

[211] C. Holohan, S. Van Schaeybroeck, D. B. Longley, and P. G. Johnston, "Cancer drug resistance: An evolving paradigm," *Nature Reviews Cancer*, vol. 13, no. 10, pp. 714–726, 2013.

[212] J. M. Blair, M. A. Webber, A. J. Baylay, D. O. Ogbolu, and L. J. Piddock, "Molecular mechanisms of antibiotic resistance," *Nature Reviews Microbiology*, vol. 13, no. 1, pp. 42–51, 2015.

[213] I. Churcher, "Protac-induced protein degradation in drug discovery: Breaking the rules or just making new ones?," *Journal of Medicinal Chemistry*, vol. 61, no. 2, pp. 444–452, 2018.

[214] K. G. Coleman and C. M. Crews, "Proteolysis-targeting chimeras: Harnessing the ubiquitin-proteasome system to induce degradation of specific target proteins," *Annual Review of Cancer Biology*, vol. 2, no. 1, pp. 41–58, 2018.

[215] K. M. Sakamoto, K. B. Kim, A. Kumagai, F. Mercurio, C. M. Crews, and R. J. Deshaies, "Protacs: Chimeric molecules that target proteins to the Skp1-Cullin-F box complex for ubiquitination and degradation," *Proceedings of the National Academy of Sciences of the United States of America*, vol. 98, no. 15, pp. 8554–8559, 2001.

[216] G. M. Burslem and C. M. Crews, "Small-molecule modulation of protein homeostasis," *Chemical Reviews*, vol. 117, no. 17, pp. 11269–11301, 2017.

[217] P. M. Cromm and C. M. Crews, "Targeted protein degradation: From chemical biology to drug discovery," *Cell Chemical Biology*, vol. 24, no. 9, pp. 1181–1190, 2017.

[218] K. Raina and C. M. Crews, "Targeted protein knockdown using small molecule degraders," *Current Opinion in Chemical Biology*, vol. 39, pp. 46–53, 2017.

[219] S. L. Fisher and A. J. Phillips, "Targeted protein degradation and the enzymology of degraders," *Current Opinion in Chemical Biology*, vol. 44, pp. 47–55, 2018.

[220] D. P. Bondeson, A. Mares, I. E. Smith, E. Ko, S. Campos, A. H. Miah, K. E. Mulholland, N. Routly, D. L. Buckley, J. L. Gustafson, N. Zinn, P. Grandi, S. Shimamura, G. Bergamini, M. Faelth-Savitski, M. Bantscheff, C. Cox, D. A. Gordon, R. R. Willard, J. J. Flanagan, L. N. Casillas, B. J. Votta, W. Den Besten, K. Famm, L. Kruidenier, P. S. Carter, J. D. Harling, I. Churcher, and C. M. Crews, "Catalytic in vivo protein knockdown by small-molecule PROTACs," *Nature Chemical Biology*, vol. 11, no. 8, pp. 611–617, 2015.

[221] S. L. Paiva and C. M. Crews, "Targeted protein degradation: elements of PROTAC design," *Current Opinion in Chemical Biology*, vol. 50, pp. 111–119, 2019.

[222] G. M. Burslem, B. E. Smith, A. C. Lai, S. Jaime-Figueroa, D. C. McQuaid, D. P. Bondeson, M. Toure, H. Dong, Y. Qian, J. Wang, A. P. Crew, J. Hines, and C. M. Crews, "The advantages of targeted protein degradation over inhibition: An RTK case study," *Cell Chemical Biology*, vol. 25, no. 1, pp. 67–77, 2018.

[223] H. T. Huang, D. Dobrovolsky, J. Paulk, G. Yang, E. L. Weisberg, Z. M. Doctor, D. L. Buckley, J. H. Cho, E. Ko, J. Jang, K. Shi, H. G. Choi, J. D. Griffin, Y. Li, S. P. Treon, E. S. Fischer, J. E. Bradner, L. Tan, and N. S. Gray, "A chemoproteomic approach to query the degradable kinome using a multi-kinase degrader," *Cell Chemical Biology*, vol. 25, no. 1, pp. 88–99, 2018.

[224] D. P. Bondeson, B. E. Smith, G. M. Burslem, A. D. Buhimschi, J. Hines, S. Jaime-Figueroa, J. Wang, B. D. Hamman, A. Ishchenko, and C. M. Crews, "Lessons in PROTAC design from selective degradation with a promiscuous warhead," *Cell Chemical Biology*, vol. 25, no. 1, pp. 78–87, 2018.

[225] T. K. Neklesa, L. B. Snyder, M. Bookbinder, X. Chen, A. P. Crew, C. M. Crews, H. Dong, D. A. Gordon, K. Raina, A. K. Rossi, I. Taylor, N. Vitale, J. Wang, R. R. Willard, and K. Zimmermann, "An oral androgen receptor PROTAC degrader for prostate cancer," *Journal of Clinical Oncology*, vol. 35, no. 6, pp. 273–273, 2017.

[226] E. F. Douglass, C. J. Miller, G. Sparer, H. Shapiro, and D. A. Spiegel, "A comprehensive mathematical model for three-body binding equilibria," *Journal of the American Chemical Society*, vol. 135, no. 16, pp. 6092–6099, 2013.

[227] C. Lu and Z. X. Wang, "Quantitative analysis of ligand induced heterodimerization of two distinct receptors," *Analytical Chemistry*, vol. 89, no. 13, pp. 6926–6930, 2017.

[228] S. J. Hughes and A. Ciulli, "Molecular recognition of ternary complexes: A new dimension in the structure-guided design of chemical degraders," *Essays in Biochemistry*, vol. 61, no. 5, pp. 505–516, 2017.

[229] L. E. Miles, "Properties, variants, and applications of the immunoradiometric assay method," *La Ricerca in Clinica e in Laboratorio*, vol. 5, no. 1, pp. 59–72, 1975.

[230] X. Huang and V. M. Dixit, "Drugging the undruggables: Exploring the ubiquitin system for drug development," *Cell Research*, vol. 26, no. 4, pp. 484–498, 2016.

[231] R. D. Roy, C. Rosenmund, and M. I. Stefan, "Cooperative binding mitigates the high-dose hook effect," *BMC Systems Biology*, vol. 11, no. 74, 2017.

[232] M. S. Gadd, A. Testa, X. Lucas, K. H. Chan, W. Chen, D. J. Lamont, M. Zengerle, and A. Ciulli, "Structural basis of PROTAC cooperative recognition for selective protein degradation," *Nature Chemical Biology*, vol. 13, no. 5, pp. 514–521, 2017.

[233] S. An and L. Fu, "Small-molecule PROTACs: An emerging and promising approach for the development of targeted therapy drugs," *EBioMedicine*, vol. 36, pp. 553–562, 2018.

[234] M. Pettersson and C. M. Crews, "PROteolysis TArgeting Chimeras (PROTACs) — Past, present and future," *Drug Discovery Today: Technologies*, vol. 31, pp. 15–27, 2019.

[235] K. H. Chan, M. Zengerle, A. Testa, and A. Ciulli, "Impact of target warhead and linkage vector on inducing protein degradation: Comparison of bromodomain and extra-terminal (BET) degraders derived from triazolodiazepine (JQ1) and tetrahydroquinoline (I-BET726) BET inhibitor scaffolds," *Journal of Medicinal Chemistry*, vol. 61, no. 2, pp. 504–513, 2018.

[236] A. P. Crew, K. Raina, H. Dong, Y. Qian, J. Wang, D. Vigil, Y. V. Serebrenik, B. D. Hamman, A. Morgan, C. Ferraro, K. Siu, T. K. Neklesa, J. D. Winkler, K. G. Coleman, and C. M. Crews, "Identification and characterization of von Hippel-Lindau-recruiting proteolysis targeting chimeras (PROTACs) of TANK-binding kinase 1," *Journal of Medicinal Chemistry*, vol. 61, no. 2, pp. 583–598, 2018.

[237] R. P. Nowak, S. L. Deangelo, D. Buckley, Z. He, K. A. Donovan, J. An, N. Safaee, M. P. Jedrychowski, C. M. Ponthier, M. Ishoey, T. Zhang, J. D. Mancias, N. S. Gray, J. E. Bradner, and E. S. Fischer, "Plasticity in binding confers selectivity in ligand-induced protein degradation article," *Nature Chemical Biology*, vol. 14, no. 7, pp. 706–714, 2018.

[238] L. N. Gechijian, D. L. Buckley, M. A. Lawlor, J. M. Reyes, J. Paulk, C. J. Ott, G. E. Winter, M. A. Erb, T. G. Scott, M. Xu, H. S. Seo, S. Dhe-Paganon, N. P. Kwiatkowski, J. A. Perry, J. Qi, N. S. Gray, and J. E. Bradner, "Functional TRIM24 degrader via conjugation of ineffectual bromodomain and VHL ligands article," *Nature Chemical Biology*, vol. 14, no. 4, pp. 405–412, 2018.

[239] J. Arrowsmith and P. Miller, "Trial watch: Phase II and phase III attrition rates 2011-2012," *Nature Reviews Drug Discovery*, vol. 12, no. 8, p. 569, 2013.

[240] B. Nabet, J. M. Roberts, D. L. Buckley, J. Paulk, S. Dastjerdi, A. Yang, A. L. Leggett, M. A. Erb, M. A. Lawlor, A. Souza, T. G. Scott, S. Vittori, J. A. Perry, J. Qi, G. E. Winter, K. K. Wong, N. S. Gray, and J. E. Bradner, "The dTAG system for immediate and target-specific protein degradation," *Nature Chemical Biology*, vol. 14, no. 5, pp. 431–441, 2018.

[241] M. A. Erb, T. G. Scott, B. E. Li, H. Xie, J. Paulk, H. S. Seo, A. Souza, J. M. Roberts, S. Dastjerdi, D. L. Buckley, N. E. Sanjana, O. Shalem, B. Nabet, R. Zeid, N. K. Offei-Addo, S. Dhe-Paganon, F. Zhang, S. H. Orkin, G. E. Winter, and J. E. Bradner, "Transcription control by the ENL YEATS domain in acute leukaemia," *Nature*, vol. 543, no. 7644, pp. 270–274, 2017.

[242] K. M. Riching, S. Mahan, C. R. Corona, M. McDougall, J. D. Vasta, M. B. Robers, M. Urh, and D. L. Daniels, "Quantitative live-cell kinetic degradation and mechanistic profiling of PROTAC mode of action," *ACS Chemical Biology*, vol. 13, no. 9, pp. 2758–2770, 2018.

[243] J. Porath, J. Carlsson, I. Olsson, and G. Belfrage, "Metal chelate affinity chromatography, a new approach to protein fractionation," *Nature*, vol. 258, no. 5536, pp. 598–599, 1975.

[244] J. Porath and P. Flodin, "Gel filtration: a method for desalting and group separation," *Nature*, vol. 183, no. 4676, pp. 1657–1659, 1959.

[245] D. S. King, C. G. Fields, and G. B. Fields, "A cleavage method which minimizes side reactions following Fmoc solid phase peptide synthesis," *International Journal of Peptide and Protein Research*, vol. 36, no. 3, pp. 255–266, 1990.

[246] M. H. A. Roehrl, J. Y. Wang, and G. Wagner, "A general framework for development and data analysis of competitive high-throughput screens for small-molecule inhibitors of protein-protein interactions by fluorescence polarization," *Biochemistry*, vol. 43, no. 51, pp. 16056–16066, 2004.

[247] L. D. Walensky, A. L. Kung, I. Escher, T. J. Malia, S. Barbuto, R. D. Wright, G. Wagner, G. L. Verdine, and S. J. Korsmeyer, "Activation of apoptosis in vivo by a hydrocarbon-stapled BH3 helix," *Science*, vol. 305, no. 5689, pp. 1466–1470, 2004.

[248] A. M. Gilles, P. Marliere, T. Rose, R. Sarfati, R. Longin, A. Meier, S. Fermandjian, M. Monnot, G. N. Cohen, and O. Barzu, "Conservative replacement of methionine by norleucine in Escherichia coli adenylate kinase," *Journal of Biological Chemistry*, vol. 263, no. 17, pp. 8204–8209, 1988.

[249] G. Bornstein, J. Bloom, D. Sitry-Shevah, K. Nakayama, M. Pagano, and A. Hershko, "Role of the SCF(Skp2) ubiquitin ligase in the degradation of p21Cip1 in S phase," *Journal of Biological Chemistry*, vol. 278, no. 28, pp. 25752–25757, 2003.

[250] S. Y. Kim, A. Herbst, K. A. Tworkowski, S. E. Salghetti, and W. P. Tansey, "Skp2 regulates Myc protein stability and activity," *Molecular Cell*, vol. 11, no. 5, pp. 1177–1188, 2003.

[251] N. Von Der Lehr, S. Johansson, S. Wu, F. Bahram, A. Castell, C. Cetinkaya, P. Hydbring, I. Weidung, K. Nakayama, K. I. Nakayama, O. Söderberg, T. K. Kerppola, and L. G. Larsson, "The F-box protein Skp2 participates in c-Myc proteosomal degradation and acts as a cofactor for c-Myc-regulated transcription," *Molecular Cell*, vol. 11, no. 5, pp. 1189–1200, 2003.

[252] A. S. Farrell and R. C. Sears, "MYC degradation," *Cold Spring Harbor Perspectives in Medicine*, vol. 4, no. 3, p. a014365, 2014.

[253] G. Bretones, J. C. Acosta, J. M. Caraballo, N. Ferrándiz, M. T. Gómez-Casares, M. Albajar, R. Blanco, P. Ruiz, W. C. Hung, M. P. Albero, I. Perez-Roger, and J. León, "SKP2 oncogene is a direct MYC target gene and MYC down-regulates p27 KIP1 through SKP2 in human leukemia cells," *Journal of Biological Chemistry*, vol. 286, no. 11, pp. 9815–9825, 2011.

[254] B. E. Smith, S. L. Wang, S. Jaime-Figueroa, A. Harbin, J. Wang, B. D. Hamman, and C. M. Crews, "Differential PROTAC substrate specificity dictated by orientation of recruited E3 ligase," *Nature Communications*, vol. 10, no. 1, pp. 131–144, 2019.

[255] A. H. Huber, W. J. Nelson, and W. I. Weis, "Three-dimensional structure of the armadillo repeat region of β-catenin," *Cell*, vol. 90, no. 5, pp. 871–882, 1997.

[256] A. Perez-Riba and L. S. Itzhaki, "A method for rapid high-throughput biophysical analysis of proteins," *Scientific Reports*, vol. 7, no. 9071, 2017.

[257] V. Korinek, N. Barker, P. J. Morin, D. Van Wichen, R. De Weger, K. W. Kinzler, B. Vogelstein, and H. Clevers, "Constitutive transcriptional activation by a β-catenin-

Tcf complex in APC(-/-) colon carcinoma," *Science*, vol. 275, no. 5307, pp. 1784–1787, 1997.

[258] Z. Feng and B. Xu, "Inspiration from the mirror: D-amino acid containing peptides in biomedical approaches," *Biomolecular Concepts*, vol. 7, no. 3, pp. 179–187, 2016.

[259] E. R. Main, S. E. Jackson, and L. Regan, "The folding and design of repeat proteins: Reaching a consensus," *Current Opinion in Structural Biology*, vol. 13, no. 4, pp. 482–489, 2003.

[260] H. K. Binz, M. T. Stumpp, P. Forrer, P. Amstutz, and A. Plückthun, "Designing repeat proteins: Well-expressed, soluble and stable proteins from combinatorial libraries of consensus ankyrin repeat proteins," *Journal of Molecular Biology*, vol. 332, no. 2, pp. 489–503, 2003.

Biochemical Journal (2016) **473** 3563–3580
DOI: 10.1042/BCJ20160387

PORTLAND PRESS

Research Article

Gsk3β and Tomm20 are substrates of the SCFFbxo7/PARK15 ubiquitin ligase associated with Parkinson's disease

Felipe Roberti Teixeira[1,2,3,*], Suzanne J. Randle[2,*], Shachi P. Patel[2,*], Tycho E.T. Mevissen[4], Grasilda Zenkeviciute[2], Tie Koide[3], David Komander[4] and Heike Laman[2]

[1]Department of Genetics and Evolution, Federal University of São Carlos, São Carlos, Brazil; [2]Department of Pathology, University of Cambridge, Tennis Court Road, Cambridge CB2 1QP, U.K.; [3]Department of Biochemistry and Immunology, Ribeirão Preto Medical School, University of São Paulo, Ribeirão Preto, Brazil; and [4]MRC Laboratory of Molecular Biology, Francis Crick Avenue, Cambridge Biomedical Campus, Cambridge CB2 0QH, U.K.

Correspondence: Heike Laman (hl316@cam.ac.uk)

Fbxo7 is a clinically relevant F-box protein, associated with both cancer and Parkinson's disease (PD). Additionally, SNPs within *FBXO7* are correlated with alterations in red blood cell parameters. Point mutations within *FBXO7* map within specific functional domains, including near its F-box domain and its substrate recruiting domains, suggesting that deficiencies in $SCF^{Fbxo7/PARK15}$ ubiquitin ligase activity are mechanistically linked to early-onset PD. To date, relatively few substrates of the ligase have been identified. These include HURP (hepatoma up-regulated protein), whose ubiquitination results in proteasome-mediated degradation, and c-IAP1 (inhibitor of apoptosis protein 1), TNF receptor-associated factor 2 (TRAF2), and NRAGE, which are not destabilized as a result of ubiquitination. None of these substrates have been linked directly to PD, nor has it been determined whether they would directly engage neuronal cell death pathways. To discover ubiquitinated substrates of SCF^{Fbxo7} implicated more directly in PD aetiology, we conducted a high-throughput screen using protein arrays to identify new candidates. A total of 338 new targets were identified and from these we validated glycogen synthase kinase 3β (Gsk3β), which can phosphorylate α-synuclein, and translocase of outer mitochondrial membrane 20 (Tomm20), a mitochondrial translocase that, when ubiquitinated, promotes mitophagy, as SCF^{Fbxo7} substrates both *in vitro* and *in vivo*. Ubiquitin chain restriction analyses revealed that Fbxo7 modified Gsk3β using K63 linkages. Our results indicate that Fbxo7 negatively regulates Gsk3β activity, rather than its levels or localization. In addition, Fbxo7 ubiquitinated Tomm20, and its levels correlated with Fbxo7 expression, indicating a stabilizing effect. None of the PD-associated mutations in Fbxo7 impaired Tomm20 ubiquitination. Our findings demonstrate that SCF^{Fbxo7} has an impact directly on two proteins implicated in pathological processes leading to PD.

Introduction

F-box proteins assemble with Skp1, Cullin 1 and Rbx1 to form SCF-type E3 ubiquitin ligases [1–3]. These enzymes act in a cascade with a ubiquitin-activating enzyme (E1) and a ubiquitin-carrier enzyme (E2) to mediate the ubiquitination of their substrates, the consequences of which range from promoting proteasomal degradation to changing the localization or activity of the modified protein. Individual substrates are thought to be targeted for ubiquitination by E3 ligases by factors such as post-translational modifications (PTMs), such as phosphorylation, glycosylation, or the phase of the cell cycle and cellular localization of the substrate and/or the ligase [4]. The biological importance of F-box proteins stems from their involvement in the regulation of many core processes such as cell

*Equal first authors.

Received: 27 April 2016
Revised: 2 August 2016
Accepted: 8 August 2016

Accepted Manuscript online: 8 August 2016
Version of Record published: 11 October 2016

PORTLAND PRESS

Biochemical Journal (2016) **473** 3563–3580
DOI: 10.1042/BCJ20160387

cycle (Fbxl1, Fbxw5, Fbxw7, and Fbxw1), differentiation and development (Fbxw1, Fbxl14, Fbxo11, Fbxo32, and Fbxw7), cell death (Fbxw1 and Fbxw7), intracellular signaling (Fbxo25), and others (reviewed in ref. [5–8]).

Fbxo7 is a multi-functional F-box protein, with both SCF-dependent and -independent functions that are capable of impacting on many core cellular processes, and is associated with human diseases (reviewed in ref. [9]). For example, the effects of Fbxo7 on the cell cycle are independent of its ubiquitin ligase activity and are mediated instead through its interactions with cell cycle proteins, Cdk6 and p27 [10,11]. Remarkably, Fbxo7's functional effects on cell proliferation and transformation, for example, are dependent on cell type. For example, Fbxo7 overexpression transforms immortalized fibroblasts and imparts tumorigenic properties to p53 null hematopoietic stem and progenitor cells [10,12]. In contrast, in pro-B cells and pro-erythroblasts, Fbxo7 negatively regulates cell proliferation and differentiation [11]. Within other cell types, altered Fbxo7 activity may be linked to pathological changes. For example, four studies reported on many SNPs in *FBXO7* that correlated with changes in human red blood cell traits such as mean cell volume and mean cell hemoglobin, which are associated with adverse health outcomes such as anemia, cardiovascular diseases, and cancer [13–16].

Recessive mutations in *FBXO7*, also designated *PARK15*, have been identified in patients with phenotypes of idiopathic Parkinson's disease (PD) and an early-onset form of PD [17–20]. Pathological point mutations are located within specific domains which hint at Fbxo7 function(s) that might be compromised. In addition to its F-box domain, which enables incorporation into an SCF complex via Skp1 binding, Fbxo7 contains an Ubl (ubiquitin-like) domain (aa 1–79), which interacts with Parkin and PINK1; a 40 amino acid linker (aa 129–169), which binds to Cdk6; a dimerization domain (aa 182–325), which enables homo-dimerization and hetero-dimerization with PI31; and a PRR (proline-rich region) (aa 423–522), which mediates protein–protein interactions with hepatoma up-regulated protein (HURP) and Cdk6 (reviewed in ref. [9]). One PD-associated mutation, T22M, lies within the N-terminal Ubl domain and compromises its ability to interact with Parkin and to promote mitophagy [21]. A second missense mutation R378G abuts the F-box domain and compromises its ability to interact with Skp1 [22]. Finally, a point mutation R498X within the PRR truncates the final 24 aa [17]. The loss of interaction with Skp1 and a substrate-interacting domain resulting from the R378G and R498X mutations suggests that SCF^{Fbxo7}-mediated ubiquitination is compromised in PD patients. However, the identity of critical targets and the functional effect of their ubiquitination are not known.

To date, there are only a handful of ubiquitinated proteins reported for SCF^{Fbxo7}. These include HURP/DLG7 (hepatoma up-regulated protein), a regulator of mitotic spindle assembly, which is up-regulated in hepatocellular carcinoma, colon cancer, breast cancer, and transitional cell carcinoma [23,24]. SCF^{Fbxo7} also promotes ubiquitination of c-IAP1 (inhibitor of apoptosis) and TRAF2 resulting in decreased NF-κB signaling activity [25,26]. Most recently, NRAGE (neurotrophin receptor-interacting MAGE) was reported to be ubiquitinated by SCF^{Fbxo7}, which positively regulated bone morphogenic protein (BMP) signaling [27]. Interestingly, Fbxo7 increased formation of a BMP receptor–NRAGE–TAK1–TAB1 complex and up-regulated NF-κB activity. The contrasting effects of Fbxo7 expression on NF-κB signaling may reflect cell-type-specific effects of Fbxo7 on this pathway, or alternatively, reflect the influence of other signaling inputs, like cellular stresses. There is a potential relationship between NF-κB signaling, long-term neuroinflammation and PD, as suggested, for example, by the symptoms demonstrated by the c-Rel knockout mouse [28]; however, evidence for the role of NF-κB signaling in PD remains controversial (as reviewed in ref. [29]).

There are currently no studies that define ubiquitination substrates for SCF^{Fbxo7} at a proteome-wide scale, which would greatly assist in clarifying its function(s) in its multiple clinically relevant settings. Given the contrasting biological effects of Fbxo7 expression in different cellular environments, we sought to bypass considerations of cell-type specificity, cell cycle phase, or subcellular localization, which might limit the interaction of Fbxo7 with its substrates. We undertook an *in vitro* high-throughput experimental approach utilizing a human protein microarray that displays ∼9500 individual proteins on a slide, to identify mammalian substrates for ubiquitination by SCF^{Fbxo7}. This powerful approach has been used to identify substrates for ubiquitin ligases, such as yeast Rsp5 [30] and human NEDD4/NEDD4L [31], SCF^{Fbxo25} [32], and SMURF1 [33]. Our *in vitro* ubiquitination screen identified 338 unique, high-confidence Fbxo7 substrates distributed across different cellular compartments, and which are involved in many biological processes. To validate this screen, we assessed individually the *in vitro* and *in vivo* ubiquitination of two candidate proteins, Gsk3β (glycogen synthase kinase 3β) and Tomm20 (translocase of outer mitochondrial membrane 20). In addition, the type of ubiquitin chain linkages introduced by Fbxo7 onto these substrates was investigated using ubiquitin chain restriction analysis, [34] and the functional effects of their ubiquitination were tested.

Biochemical Journal (2016) **473** 3563–3580
DOI: 10.1042/BCJ20160387

PORTLAND PRESS

Experimental materials and methods

Purification of SCF complexes

The SCF components such as human influenza hemagglutinin (HA)-Skp1, Cul1, Myc-Rbx1, and FLAG-Fbxo7 or FLAG-Fbxo7(ΔF-box) were transfected in HEK293T cells by using polyethylenimine. After 48 h of transfection, the cells were harvested and resuspended in lysis buffer (LB) (25 mM Tris–HCl, pH 7.5, 225 mM KCl and 1% NP-40) containing a protease inhibitor cocktail (Sigma-Aldrich, St. Louis, MO) and phosphatase inhibitors (10 mM NaF and 1 mM Na_3VO_4). The lysates were incubated with agarose anti-FLAG M2 beads (Sigma-Aldrich, St. Louis, MO) for 6 h at 4°C with rocking. Beads were washed with LB and the SCF complexes eluted with FLAG elution buffer (300 μg/ml of peptide FLAG in 10 mM HEPES pH 7.9, 225 mM KCl, 1.5 mM $MgCl_2$, and 0.1% NP-40) for 1 h at 4°C with rocking. The eluates were stored in 15% glycerol at −20°C until use. To evaluate the purification of SCF complexes, immunoblotting was performed and probed using anti-Fbxo7 (ABN1038, Merck Millipore, Watford, UK), anti-HA (Abcam, Cambridge, UK), anti-Gsk3β (Santa Cruz Biotechnologies, CA, USA), anti-Tomm20 (Abcam, Cambridge, UK), or anti-myc (Cell Signaling Technologies, MA, USA). The concentration of the complexes was determined against known concentrations of BSA by Coomassie blue staining of the gel. The densitometry of the bands was determined by ImageJ.

In vitro ubiquitination assays

The plasmids encoding human Gsk3β-HA and Tomm20 were purchased from Addgene (14 753 and 40 291, respectively). Human cIAP-1-myc was kindly provided by Dr Yasuko Matsuzawa (Sanford-Burnhan Medical Research Institute, La Jolla, CA, USA). Tomm20 was cloned into pcDNA3 in fusion with HA at the C-terminus. cIAP was truncated (183–570) and cloned in fusion with HA at the C-terminus. The substrates cIAP-1(183–570)-HA, Gsk3β-HA, and Tomm20-HA were produced by *in vitro* transcription/translation (IVT), and the crude programmed reticulocyte lysates were added to *in vitro* ubiquitination reactions. For the ubiquitination reactions, purified SCF complexes were used at the indicated concentrations in combination with ubiquitin mix [ubiquitination buffer, E1(100 nM), E2(500 nM), biotin-ubiquitin (20 μM), Mg-ATP (2 mM; Boston Biochem)], and the purified substrates and incubated for 90 min at 30°C. Proteins were resolved by SDS–PAGE and immunoblotting was performed using anti-Gsk3β, anti-Tomm20, or anti-HA antibodies. To determine which E2(s) enabled SCF^{Fbxo7} ligase activity, an *in vitro* E2 screening with 10 different E2 enzymes, each at 500 nM was performed. Auto-ubiquitination was observed with UBE2D1 (UbcH5a), UBE2D2 (UbcH5b), and UBE2D3 (UbcH5c; Supplementary Figure S1), and UBE2D1 (UbcH5a) was used in further experiments. Reactions were resolved by SDS–PAGE and detected by probing with streptavidin–HRP (Thermo Pierce, MA, USA).

Analysis of ligases

Samples were resolved ∼1 cm into a pre-cast SDS–polyacrylamide gel, and the entire lane was excised and cut into four equal slices. Proteins were reduced and alkylated, then digested in-gel using trypsin. The resulting peptides were analyzed by LC–MS/MS using an Orbitrap XL (Thermo) coupled to a nanoAcquity UPLC (Waters). Data were acquired in a DDA fashion with MS/MS in the LTQ triggered at 1000 counts. Raw files were converted into mzML using MSconvert (ProteoWizard) and submitted to MASCOT 2.3.0 to search a human Uniprot database (20 264 entries, downloaded on 09 June 14). Carbamidomethyl cysteine was set as a fixed modification with oxidized methionine and deamidation of asparagine and glutamine as potential variable modifications. Peptide and protein validation were performed using Scaffold 4.3.2. Peptides required a minimum of 95% probability and proteins required a minimum of 90% probability and two peptides in order to be counted.

In vitro ubiquitination assays of protein arrays

Protoarray® v5.0 was obtained from Life Technologies (catalog number PAH0525101). Supplementary Table S1 contains an Excel file of Protoarray® v5.0 protein content. Protocols were followed according to the manufacturer's instructions (Protoarray® v5.0, Invitrogen, MA, USA). Slides were incubated in Protoarray® Synthetic Block for 1 h at 4°C with shaking at 50 rpm. During this time, reactions were prepared in a volume of 120 μl as follows: 25 or 50 nM of the purified SCF^{Fbxo7} or Fbxo7(ΔF-box) in combination with ubiquitin mix [E1 (100 nM), UbcH5a (500 nM), Mg-ATP (2 mM), and biotin-ubiquitin 0.1 mg/ml in ubiquitination buffer; Boston Biochem]. The slides were washed with assay buffer (AB; 50 mM Tris, pH 7.5, 50 mM NaCl, 5 mM

PORTLAND PRESS

Biochemical Journal (2016) **473** 3563–3580
DOI: 10.1042/BCJ20160387

$MgSO_4$, 0.1% Tween 20, 1% BSA, and 1 mM DTT) and 110 μl of the reaction was added to the slide and overlaid with a coverslip followed by incubation for 1.5 h at 30°C in a humidified chamber. Slides were washed in 0.5% SDS and AB and then incubated with 1 μg/μl of streptavidin–AlexaFluor 647 for 45 min at 4°C with shaking. The arrays were washed with AB, once with distilled water, and finally dried by centrifugation at $1000 \times \boldsymbol{g}$ for 2 min, before being scanned on a GenePix Personal 4100A (Axon–Molecular Devices).

Data acquisition and analysis

Software used for Protoarray® image acquisition was GenePix Pro 4.1 (Molecular Devices). The experimental design comprised two biological replicates [25 or 50 nM ligase of wild type (WT) or mutant F-box protein, ΔF] with two intraslide technical replicates. Each slide has 3004 negative control spots (Supplementary Table S2) and 576 positive control spots (Supplementary Table S3).

The intensity value of each array feature was considered as the average raw intensity of all pixels in the delimited spot region minus the median intensity of pixels immediately surrounding the spot region (local background). Background-subtracted intensities were subjected to normalization to make them directly comparable among different Protoarray® slides (replicates and conditions). Assuming that the manufacturer-produced positive controls should present the same theoretical intensities among replicates, their background-corrected values were obtained and a single centering (normalization) value per slide was defined as the average of all known positive control spots. An interslide, study-wide overall positive control value was obtained by averaging all the intraslide centering/normalization factors. Finally, all array features had their background-subtracted intensities corrected by this overall factor to end up with comparable normalized intensities ($I_{WT,25\ nM}$, $I_{WT,50\ nM}$, $I_{\Delta F,25\ nM}$, and $I_{\Delta F,50\ nM}$).

To determine spots with statistically significant signals, we used all the negative control spots to estimate non-parametrically the null density distribution (*NC*) for each slide using a Gaussian kernel density estimator [35]. The intensity value that encompasses the vast majority of null probability mass was chosen as cutoff (c) for each slide: $\mathbf{P}(NC > c) = 0.005$. This yielded four cutoff values: $c_{WT,25\ nM}$; $c_{WT,50\ nM}$; $c_{\Delta F,25\ nM}$, and $c_{\Delta F,50\ nM}$.

Selected spots presented intensities $I_{WT} > c_{WT}$ and $I_{\Delta F} < c_{\Delta F}$ for each concentration and log fold change [FC = $\log_2(I_{WT}/I_{\Delta F})$] greater than 5-fold: $\log_2(I_{WT}/I_{\Delta F}) > \log_2(5)$. To increase stringency, only proteins which met these criteria simultaneously on both concentrations were defined as possible substrates. Mean FC values of possible substrates were calculated and used to rank the proteins (Supplementary Table S4).

The selected list of proteins was subjected to Gene Enrichment analysis using DAVID Bioinformatics Resources v6.7 [36] using Protoarray® v5.0 content (Supplementary Table S1) or the human proteome as the background. DAVID's *P*-values up to 0.05 were considered significant (Supplementary Table S4).

In vivo ubiquitination assays and co-immunoprecipitation assays

HEK293T cells were transfected with empty vector, FLAG-Fbxo7 or FLAG-Fbxo7-ΔF-box, or truncated FLAG-Fbxo7 alleles where indicated, in combination with Gsk3β-HA or Tomm20-HA, with or without ubiquitin-6xHis-myc. Where indicated, cells were treated with 10 μM of MG132 prior to lysis with LB for 30 min on ice. Cells were centrifuged and supernatants were subjected to immunoprecipitation (IP) with agarose-anti-HA or agarose-anti-FLAG. The proteins were eluted by Laemmli buffer and the eluates were resolved by SDS–PAGE. The ubiquitinated proteins were visualized using antibodies to HA, the substrates, or anti-myc antibody.

In vitro binding assays

HEK293T cells were transfected with empty vector or various FLAG-Fbxo7 truncation mutants. Cells were lysed in NETN lysis buffer [NB; 10 mM Tris–HCl, pH 7.5, 150 mM NaCl, 1 mM EDTA, and 0.2% NP-40 containing a protease inhibitor cocktail and phosphatase inhibitors (10 mM NaF and 1 mM Na_3VO_4)], and clarified lysates were subjected to IP with anti-FLAG antibodies immobilized on agarose beads. Gsk3β-HA protein was IP from transfected HEK293T cells by anti-HA antibodies immobilized on agarose beads and eluted using HA peptide. Gsk3β-HA protein was added to immobilized FLAG-Fbxo7 proteins and rotated for 3 h at 4°C. Beads were washed twice in NB and twice in RIPA buffer, then eluted by Laemmli buffer and the eluates resolved by SDS–PAGE.

Biochemical Journal (2016) **473** 3563–3580
DOI: 10.1042/BCJ20160387

PORTLAND PRESS

Fbxo7 protein knockdown

Cells were infected with miR30-based retroviruses encoding independent human *FBXO7*-specific shRNAs and selected using puromycin (2 μg/ml), as described previously [11]. Transient knockdown (KD) of Fbxo7 was performed by transfecting dsRNA targeting Fbxo7 into cells using Effectene (Invitrogen) as described previously [10].

Gsk3β activity reporter

The Gsk3β reporter pCS2-GFP-Gsk3-MAPK and mutant version pCS2-GFP-Gsk3mut-MAPK described in ref. [37] were purchased from Addgene (29 689 and 29 690, respectively). U2OS cells were transfected with empty vector, FLAG-Fbxo7, or FLAG-Fbxo7(ΔF-box) and 24 h later transfected with pCS2-GFP-Gsk3-MAPK or pCS2-GFP-Gsk3mut-MAPK, in quadruplicate. After a further 24 h, cells were trypsinized and analyzed by flow cytometry using a Cytek analyzer. The GFP mean fluorescence intensity was determined and levels were expressed as a percentage of the mutant GFP-Gsk3mut-MAPK-expressing cells.

Ubiquitin chain restriction analysis

Ubiquitin chain restriction (UbiCRest) analyses were performed as described recently [34]. *In vivo* expressed substrates were IP from HEK293T cells transfected with FLAG-Fbxo7 and the tagged-HA substrates using agarose-anti-HA. Cell lysates were obtained as mentioned above and the *in vivo* polyubiquitinated substrates were eluted by HA peptide at 300 μg/ml in FLAG elution buffer and stored at −80°C. Deubiquitinating enzymes (DUBs) were diluted with 2× dilution buffer (50 mM Tris, pH 7.4, 300 mM NaCl, and 20 mM DTT) and added to the samples for 30 min at 37°C, and reactions were stopped by Laemmli buffer. Samples were run on SDS–PAGE, and the blots were probed for anti-polyubiquitin (Santa Cruz Biotechnologies, CA, USA).

Immunofluorescence

U2OS cells were plated onto glass coverslips, transfected with FLAG-Fbxo7, and 24 h later fixed in 4% paraformaldehyde in PBS for 15 min. Cells were permeabilized in 0.2% Triton X-100 in PBS, blocked for 1 h in 10% donkey serum, and incubated overnight with anti-FLAG and anti-Gsk3β antibodies. Cells were repeatedly washed in PBS, incubated with anti-rabbit AlexaFluor 488 and anti-mouse AlexaFluor 647 for 1 h, washed again, and then counterstained with Hoechst 33342 to visualize nuclei. Cells were visualized using a Zeiss ApoTome microscope.

Luciferase assays

U20S cells, seeded at 5000 cells per well of a 96-well plate, were transfected in quintuplicate with 1.5 ng pCMV-Renilla luciferase control plasmid, 75 ng minimal promotor firefly luciferase (pTA-luc) or LEF/TCF responsive firefly luciferase reporters (TOP-FLASH), and 75 ng empty, FLAG-Fbxo7 or FLAG-Fbxo7(ΔF-box) vectors. Where stated, cells were treated after 24 h with 50 mM LiCl or NaCl and 24 h later, luciferase levels were assayed using the Dual Glo luciferase assay system (Promega, Southampton, UK).

Statistical analysis

Statistical differences in normalized protein levels in shRNA lines were compared with vector control levels using Student's *t*-tests. For Gsk3β reporter assays, normalized data were analyzed by one-way ANOVA, with a *post hoc* Dunnett's multiple comparisons test to determine statistical significance compared with control cells. For luciferase assays, one-way ANOVA with a *post hoc* Tukey's multiple comparisons test was used to determine differences between samples.

Results

Purified SCF^{Fbxo7} complexes are active *in vitro*

SCF complexes were purified from mammalian HEK293T cells using mild conditions to maintain activity and structure. WT Fbxo7, but not a mutant with a deletion of the F-box domain (denoted ΔF-box, lacking amino acids 335–367), co-purified with other SCF components: Skp1, Cullin1, and Rbx1 (Figure 1A,B). To test for ligase activity, we performed *in vitro* ubiquitination assays using SCF^{Fbxo7} or the mutant Fbxo7(ΔF-box) in conjunction with both E1 and E2 enzymes. We found UBE2D1 (UbcH5a), UBE2D2 (UbcH5b), UBE2D3 (UbcH5c), and UBE2E1 (UbcH6), all promoted robust levels of auto-ubiquitination in a screen of E2 enzymes

PORTLAND PRESS

Biochemical Journal (2016) 473 3563–3580
DOI: 10.1042/BCJ20160387

(Supplementary Figure S1A,B). To test the ability of SCF^{Fbxo7} to ubiquitinate one of its known substrates, we used cIAP-1 [25,26]. This protein contains a RING box domain that can bind independently to E2 enzymes, promoting auto-ubiquitination. As this would obscure the ubiquitination signal generated by SCF^{Fbxo7}, this RING domain was deleted, creating cIAP-1(183–570)-HA, for these assays. cIAP-1(183–570)-HA was synthesized by IVT using reticulocyte lysates, and the programmed lysates were added to *in vitro* ubiquitination reactions. A smear of higher molecular weight (MW) ubiquitinated species of cIAP-1, which intensified with increasing concentration of ligase, was seen in the presence of the WT SCF^{Fbxo7}, but not mutant Fbxo7 (ΔF-box; Figure 1C). These experiments established that the purified SCF^{Fbxo7} ligase showed robust ligase activity and could ubiquitinate itself and one of its known substrates.

In addition to probing for known subunits of an SCF-type E3 ligase (Figure 1B), we also conducted an unbiased mass spectrometry (MS)-based screen on the purified WT ligase and the mutant Fbxo7(ΔF-box). Alongside expected SCF components, NEDD8, two proteasome subunits (PSMB3 and PSMB6), EIF4A2, FBL, HDLBP, and DNAJB6, appeared exclusively associated with SCF^{Fbxo7} and not the vector control or the mutant F-box protein made from transfection with Fbxo7(ΔF-box; Supplementary Table S4). A longer list of 107 proteins that interacted with both the WT SCF^{Fbxo7} ligases and the mutant Fbxo7 protein, included the proteasome inhibitor, PI31, a previously identified dimerization partner of Fbxo7 [38]. The association of PI31 with the ligases was confirmed by immunoblotting, where an Fbxo7(V253E) mutant that prevents binding to PI31 served as a negative control (Figure 1D). Analysis of the longer list using KEGG databases for data enrichment identified proteins from the ribosome, proteasome, and spliceosome as being significantly represented (Supplementary Table S4).

Identification of novel SCF^{Fbxo7} substrates using a protein array

We next optimized the SCF E3 ligase to perform a large-scale *in vitro* ubiquitination experiment using a protein microarray. The commercially available Protoarray® v5.0 (Invitrogen) contained over 9000 unique, full-length native proteins purified and spotted in duplicate under non-denaturing conditions onto a nitrocellulose slide. Ligase activity was first titrated, and a 50 nM concentration, which demonstrated robust auto-ubiquitination activity, was chosen for use on the array (Supplementary Figure S1C). Ligase (25 nM) was used in a replicate experiment, where more overall signal was seen on the array with the WT than the mutant ligase (Figure 2A,B). Overviews of the experimental design (Figure 2A) and the data analysis (Supplementary Figure S2, Materials and Methods) are provided. To increase the stringency of our screen, only proteins which met defined criteria for statistically significant intensities at both 25 and 50 nM of ligase were categorized as possible substrates. This analysis yielded 338 unique proteins as substrates of SCF^{Fbxo7} (Supplementary Table S5).

Candidate substrates were next grouped in accordance with their cellular compartment and their biological pathway using the Gene Onthology and KEGG databases for data enrichment (Supplementary Table S5) [39,40]. Forty-six candidate substrates were localized to the nuclear lumen, 39 to the cytosol, 13 to the ribosome, and 10 to the microtubule-organizing centre. This wide distribution pattern of candidate substrates is in agreement with the reported localization of Fbxo7 [10,22], and with the analyses of Fbxo7 ligases (Supplementary Table S4). Consistent with the presence of a mitochondrial-targeting sequence (MTS) at the N-terminus of Fbxo7, 29 candidates were localized to mitochondria, where Fbxo7 interacts with Parkin and PINK1 to mediate stress-induced mitophagy [21]. Such candidates represent potential Fbxo7 substrates that may be important for this process. In addition, although PINK1 is present on the Protoarray® (Supplementary Table S1), it was not ubiquitinated by SCF^{Fbxo7}, suggesting that their reported interaction does not result in PINK1 ubiquitination. An analysis of the substrates using Enrichment by Biological Process indicated that Fbxo7 ubiquitinates multiple proteins that have an impact on ErbB2 (10 substrates), Wnt (10 substrates), and MAPK (13 substrates) signalling, ribosomes (9 substrates), axonal guidance (10 substrates), and pathways in cancer (16 substrates). We reported that Fbxo7 regulated cyclin D/Cdk6/p27 complexes which transformed cells, via an ubiquitin-independent mechanism [10], and in agreement with this, cyclin D3, Cdk6, and p27 were present on the Protoarray® v5.0 (Supplementary Table S1), but not ubiquitinated. Our dataset further indicates that SCF^{Fbxo7} also ubiquitinates proteins important in cancer progression. With regard to concordance with known SCF^{Fbxo7} substrates, cIAP-1, HURP, and NRAGE were not present on the protein arrays, and although TRAF2 was, it did not make the final list of substrates due to high levels of signal with the negative control Fbxo7(ΔF-box). We speculate that as TRAF2 is also an E3 ligase, it catalyzed auto-ubiquitination in the

Biochemical Journal (2016) **473** 3563–3580
DOI: 10.1042/BCJ20160387

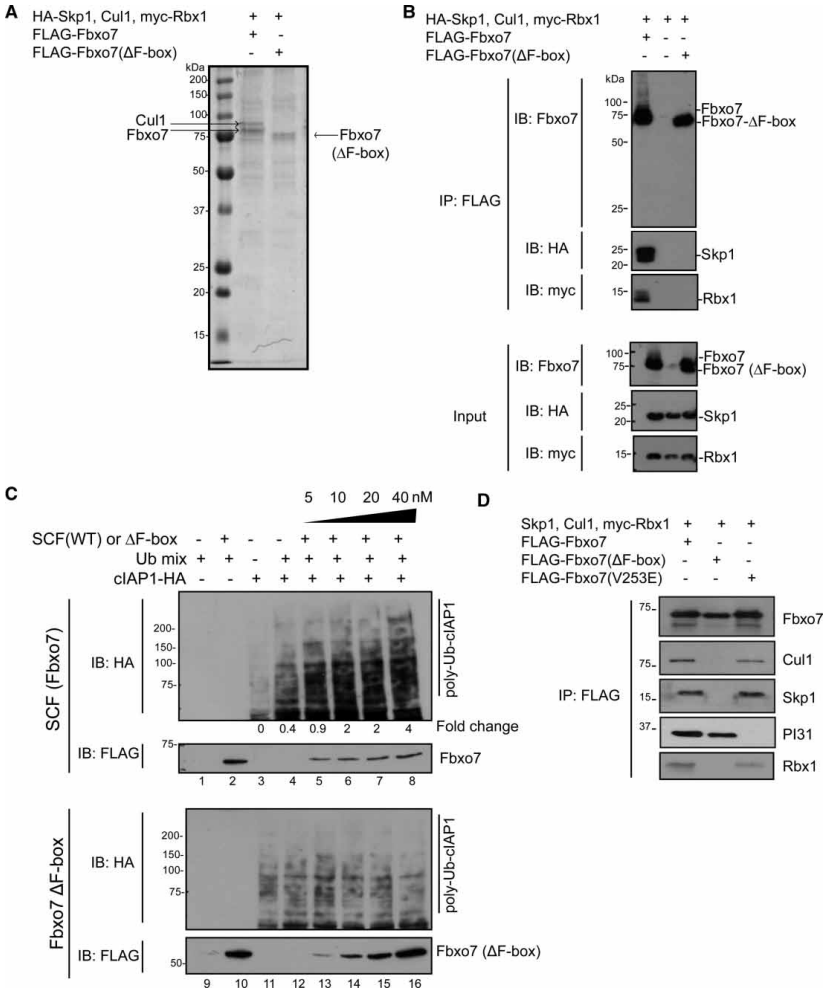

Figure 1. Fbxo7, but not a mutant version Fbxo7(ΔF-box), forms an active SCF complex.

(**A**) Purified SCF ligases resolved by SDS–PAGE and visualized with Coomassie brilliant blue stain ($n = 3$). (**B**) Immunoblots for components of SCF holoenzyme that co-immunoprecipitate with FLAG-Fbxo7 or FLAG-Fbxo7-ΔF-box ($n = 2$). (**C**) Titration of the ligase activity of purified SCF^{Fbxo7} complexes or mutant Fbxo7(ΔF-box) protein on cIAP-1(183–570)-HA. A concentration gradient (5, 10, 20, and 40 nM) of SCF^{Fbxo7} or Fbxo7(ΔF-box) protein was used for *in vitro* ubiquitination assays in combination with ubiquitin mix (ubiquitin buffer, E1, UBE2D1, and ATP) and purified cIAP-1(183–570). Membranes were probed with anti-HA antibodies to visualize the ubiquitination profile and anti-FLAG antibodies to evaluate the amount of E3 ligase ($n = 2$). (**D**) Immunoblot for proteins that co-immunoprecipitate with FLAG-tagged SCF Fbxo7 ligases (WT, ΔF-box, or V253E).

presence of the ubiquitin mix used in this experiment, hence the high background observed in the negative control.

These data demonstrate the robust ligase activity of the SCF^{Fbxo7} ligase and its potential to ubiquitinate a large number of proteins. Importantly, there was no overlap between the SCF^{Fbxo7} substrates with those identified in a previously reported SCF^{Fbxo25} Protoarray® screen [41], arguing that this methodology identifies specific candidate substrates for individual SCF-type E3 ligases.

Biochemical Journal (2016) 473 3563–3580
DOI: 10.1042/BCJ20160387

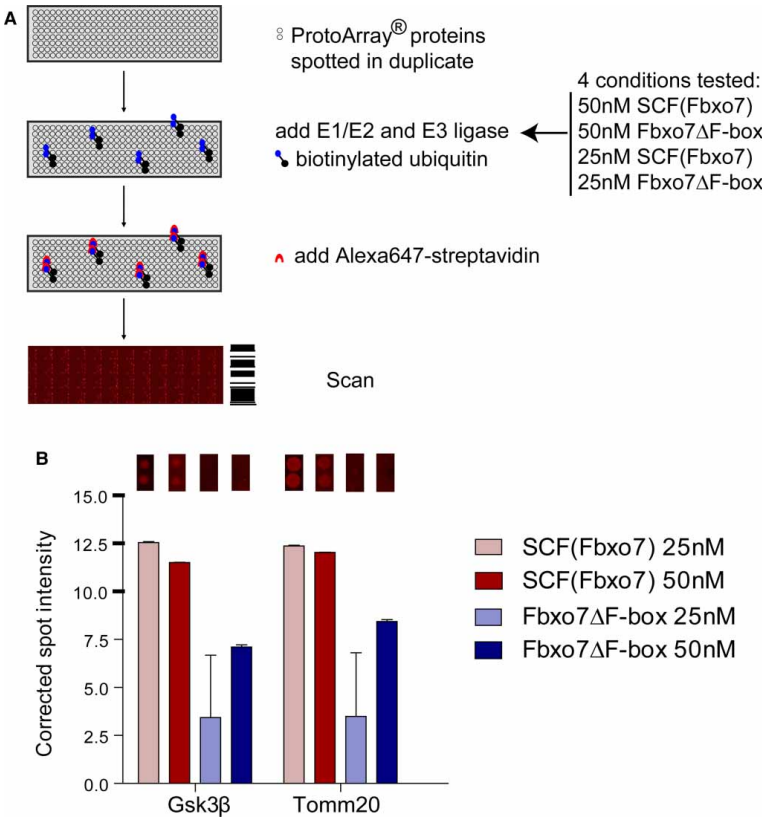

Figure 2. Identification of new Fbxo7 ubiquitinated substrates using protein arrays.

(**A**) Schematic of the experimental design. Two concentrations of SCF^{Fbxo7} or Fbxo7(ΔF-box) protein were used for the ubiquitination of Protoarrays®. Unique substrates were grouped according to the Gene Ontology Cell Compartment or Biological Process through the use of Cytoscape (plugin ClueGO + CluePedia; Supplementary Table S4). (**B**) Both concentrations of the SCF^{Fbxo7}, but not Fbxo7(ΔF-box) protein, promoted ubiquitination of Gsk3β and Tomm20. Quantification of the fluorescence intensity of individual spots.

Gsk3β and Tomm20 were ubiquitinated *in vitro* and *in vivo* by SCF^{Fbxo7}

One caveat inherent in using protein arrays is that the full-length proteins spotted on the arrays are purified from insect cells in fusion with both His and GST tags, which may affect ubiquitination. Also, these proteins would lack the posited PTMs and/or cofactors, which may be needed for ligase recruitment within cells. We therefore wished to retest our findings from the arrays using independent methodologies. To take this forward, we selected Gsk3β, ranked 38th, and Tomm20, ranked 44th (Supplementary Table S5), because of the existing literature arguing that they act within pathways that are potentially involved in the pathobiology of PD, and because inhibitors of these pathways are being pursued as potential therapeutics [21,42–47]. Their ubiquitination signal on the arrays is shown in Figure 2B. We produced these potential substrates by *in vitro* transcription/translation in reticulocyte lysates using plasmids encoding C-terminally HA-tagged substrates, Gsk3β-HA or Tomm20-HA, and used these programmed lysates for *in vitro* ubiquitination assays (Figure 3A,B and Supplementary Figure S3A,C). We also used purified Gsk3β-HA or Tomm20-HA isolated by immunoprecipitation from cells and eluated with HA peptide as the substrates for *in vitro* ubiquitination assays (Supplementary Figure S3B,D). In the case of Gsk3β, a smear of higher MW bands was seen in crude reticulocyte lysates when no exogenous ligase was added to the reaction, suggesting that Gsk3β modification occurred in reticulocyte

Biochemical Journal (2016) **473** 3563–3580
DOI: 10.1042/BCJ20160387

lysates (Figure 3A and Supplementary Figure S3A). However, there was an increased intensity of higher MW bands in the presence of WT SCF^{Fbxo7} ligase, which was dependent on the F-box domain (Figure 3A and Supplementary Figure S3A,B). For Tomm20, the addition of WT SCF^{Fbxo7} ligase promoted discrete laddering, suggesting mono- or multi-mono-ubiquitination, and was also dependent on the F-box domain of Fbxo7 (Figure 3B, arrows). In addition, higher MW bands, dependent on Fbxo7 ligase activity, were also detectable using antibodies to Tomm20 (Supplementary Figure S3C,D, arrows). Taken together, these data support the idea that SCF^{Fbxo7} catalyzed ubiquitination of these proteins.

To further test whether these candidate targets are substrates for SCF^{Fbxo7}, we carried out ubiquitination assays in HEK293T cells co-transfected with plasmids encoding C-terminally HA-tagged substrates including Gsk3β-HA or Tomm20-HA and N-terminally FLAG-tagged Fbxo7 or Fbxo7(ΔF-box). Substrates were IP via their HA tag, and immunoblotted with antibodies to the protein (Gsk3β or Tomm20; Figure 3C,D). In the samples co-transfected with WT Fbxo7, a smear of higher MW proteins was seen for Gsk3β (Figure 3C), while discrete laddering was observed for Tomm20 (Figure 3D). Similar results were obtained when experiments were performed with endogenous ubiquitin (Supplementary Figure S3E,F). In addition, in *in vivo* ubiquitination assays performed with exogenous myc-tagged ubiquitin, Tomm20 showed discrete laddering, and both proteins showed robust smears of high-MW polyubiquitinated proteins over 100 kDa (Supplementary Figure S3G,H). These data support the idea that Fbxo7 promoted ubiquitination of both Gsk3β and Tomm20, and taken together, with the *in vitro* ubiquitination assays indicate that these two candidates identified on the protein arrays are ubiquitinated substrates of SCF^{Fbxo7}.

The N-terminus of Fbxo7 can mediate an interaction with Gsk3β

To determine the region within Fbxo7 required for interacting with these substrates in cells, co-immunoprecipitation assays were conducted. HEK293T cells were co-transfected with plasmids encoding C-terminally HA-tagged Gsk3β and various N-terminally FLAG-tagged Fbxo7 constructs: WT or Fbxo7 constructs wherein the Ubl domain (1–88), a linker region (89–128), the PRR (399–522), or the last 24 aa at the C-terminus (R498X) was deleted either singly or in combination. The R498X mutation is a naturally occurring pathogenic mutation causing an early-onset PD. For Gsk3β, the loss of either the C-terminal 24 aa (R498X) or the PRR (1–398) did not substantially affect binding (Figure 4A). Loss of the N-terminal Ubl domain, as tested with the 89–522 construct, also did not affect Fbxo7 interaction with Gsk3β. However, loss of both the Ubl domain and the linker, as seen with a 129–522 construct, ablated their interaction. At the Fbxo7 C-terminus, loss of the PRR alone, 1–398, weakened binding, but the additional loss of the Ubl domain, as tested with the 89–398 construct, ablated Gsk3β binding altogether. These data suggest that the PRR, together with the Ubl/linker sequences, contributes to the interaction of Fbxo7 with Gsk3β in cells, but is not sufficient to mediate binding (Figure 4A). These experiments indicate multiple binding sites and/or a bipartite interaction for Gsk3β with Fbxo7. These interaction experiments are summarized in Figure 4B. To further validate the binding sites of Gsk3β on Fbxo7, we performed *in vitro* binding assays using FLAG-Fbxo7 deletion mutants immunopurified from cells and immobilized on agarose, in binding assays with purified Gsk3β (Figure 4C). In support of the *in vivo* co-immunoprecipitation studies, Fbxo7 constructs lacking the first 129 amino acids, deleting the Ubl and linker of Fbxo7 were unable to interact with Gsk3β. Fbxo7 1–398 lacking only the PRR could still bind to Gsk3β, as could ΔF-box in this *in vitro* setting. To test this further, we created a ligase lacking the N-terminal 128 amino acids for its ability to ubiquitinate Gsk3β. We found that $SCF^{Fbxo7(129–522)}$ was an E3 ubiquitin ligase with equivalent activity to SCF^{Fbxo7} (Supplementary Figure S4A), which showed reduced activity against Gsk3β tested in *in vitro* ubiquitination assays (Figure 4D). These data argue for the N-terminus of Fbxo7 being the domain through which Gsk3β can be recruited for ubiquitination.

Similar experiments to map the interaction of Fbxo7 with Tomm20 were conducted in cells (Figure 4E) and by *in vitro* binding assays, although the latter were unsuccessful. In cells, the interaction of Tomm20 with Fbxo7 was substantially weakened when the N-terminus was deleted, see 89–522 and 129–522, suggesting that amino acids 1–128 also mediated the interaction of Fbxo7 and Tomm20. However, unlike Gsk3β, which is reported to localize in the cytosol, nucleus, and mitochondria, Tomm20 is part of a tranlocation complex and resident in the outer membrane of mitochondria. Therefore, an alternative explaination for this loss of binding could be the deletion of the MTS of Fbxo7, which lies at the start of isoform 1 (Figure 4B) and is essential for its recruitment to mitochondria [21]. To test this directly, an *in vitro* ubiquitination assay with $SCF^{Fbxo7(129–522)}$ against Tomm20 was performed and showed that the ligase lacking the N-terminus of Fbxo7 was still able to mono-ubiquitinate Tomm20, and that there was only minor loss of ubiqutinated higher MW species

Biochemical Journal (2016) **473** 3563–3580
DOI: 10.1042/BCJ20160387

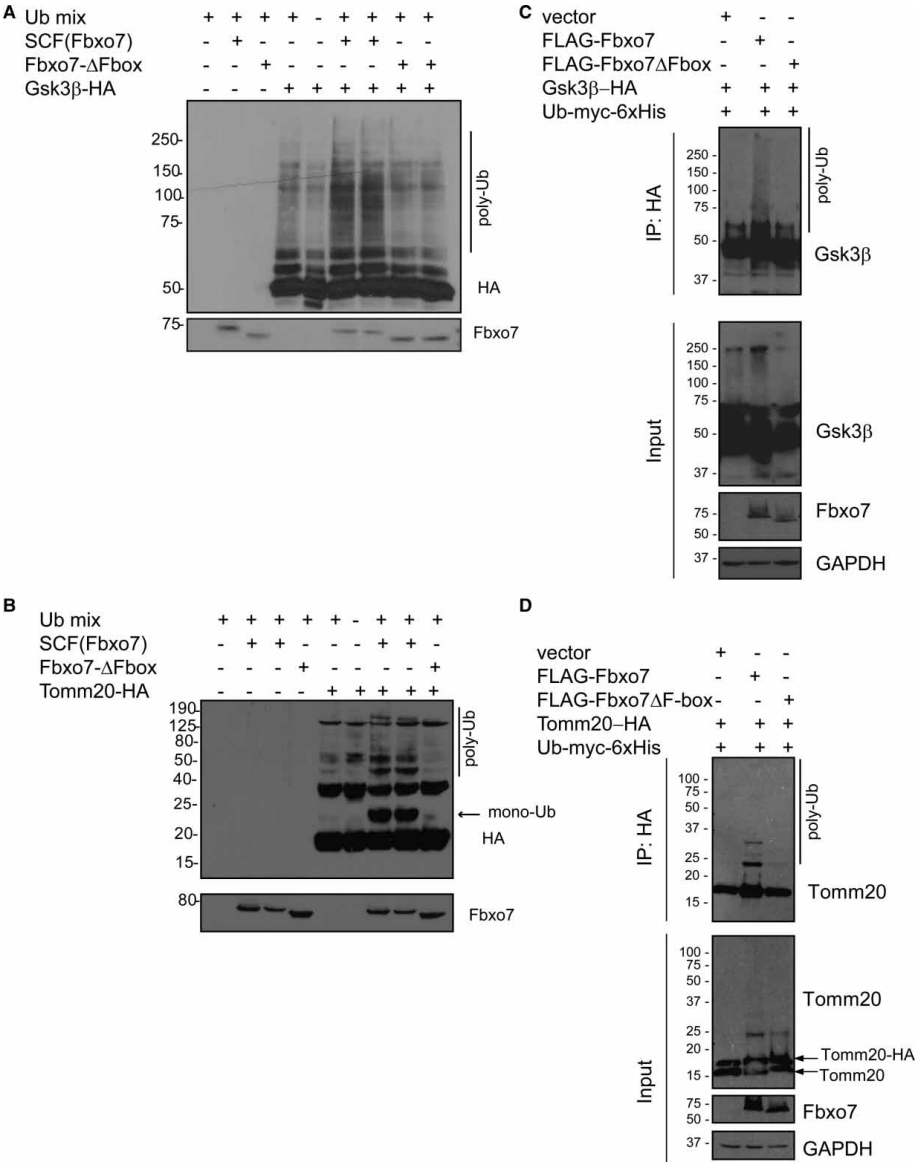

Figure 3. Fbxo7 promotes ubiquitination of Gsk3β and Tomm20 *in vitro* and in cells.

In vitro ubiquitination reactions contained purified SCF^{Fbxo7} ligase or Fbxo7(ΔF-box) protein and ubiquitin mix (E1, UBE2D1, ubiquitin, and ATP) in combination with HA-tagged substrates Gsk3β ($n = 2$) (**A**) or Tomm20 ($n = 2$) (**B**). The proteins were resolved by SDS–PAGE, and immunoblots were performed with the indicated antibodies. (**C** and **D**) HEK293T cells were transfected with the indicated plasmids and the substrates were IP with anti-HA beads; Gsk3β ($n = 3$) (**C**) and Tomm20 ($n = 3$) (**D**). Proteins were separated by SDS–PAGE, and immunoblots were probed with antibodies to the substrates.

(Figure 4F). These data argue that other sites downstream of amino acid 128 in Fbxo7 bind to Tomm20. Deletion of the PRR at the C-terminus of the Fbxo7 (1–398) did not compromise binding to Tomm20, but suprisingly, deletion of the PRR restored Tomm20 binding to Fbxo7 lacking the MTS/Ubl domain (Figure 4,

Biochemical Journal (2016) **473** 3563–3580
DOI: 10.1042/BCJ20160387

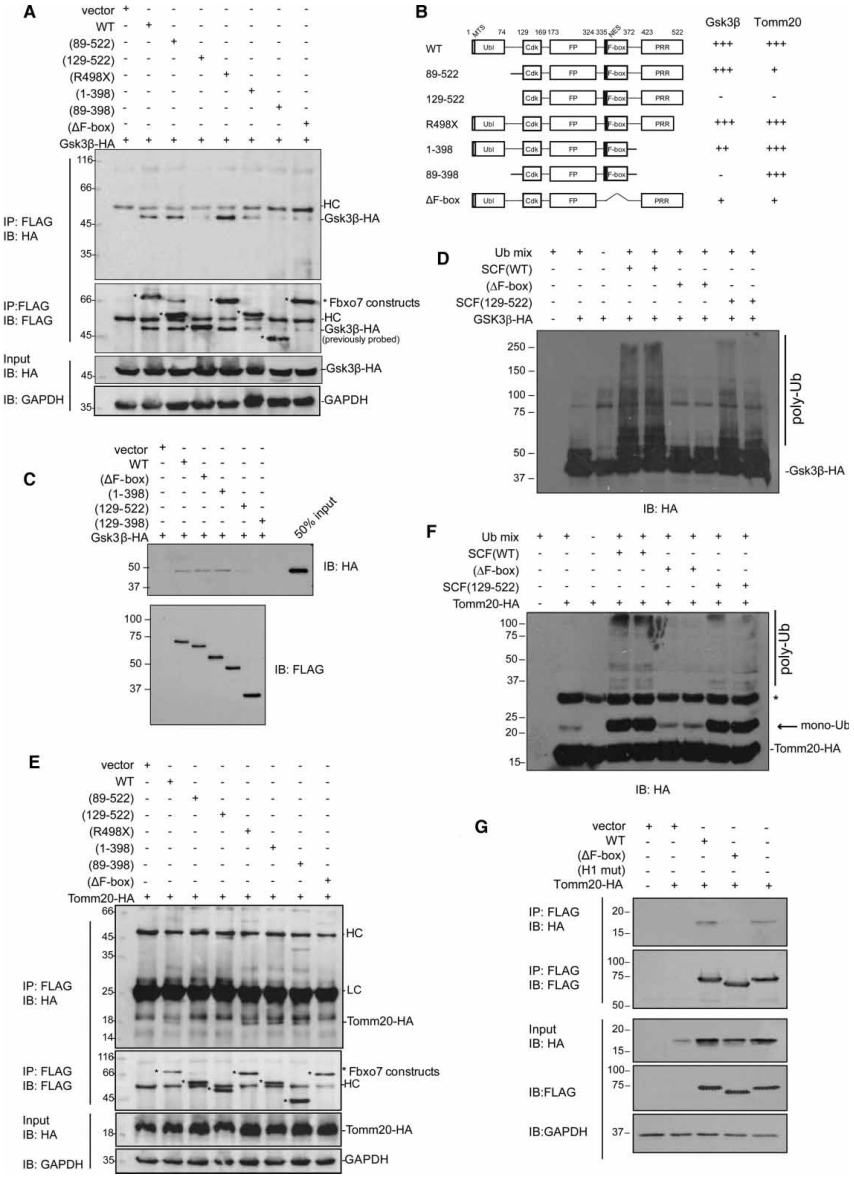

Figure 4. The N-terminus of Fbxo7 mediates its interaction with Gsk3β.

(**A**) HEK293T cells were transfected with the indicated FLAG-Fbxo7 plasmids and Gsk3β-HA and the lysates were IP with anti-FLAG beads. Proteins were resolved by SDS–PAGE, and immunoblots were probed with the indicated antibodies. (**B**) Summary of the interaction mapping for Gsk3β and Tomm20 with various Fbxo7 constructs. (**C**) *In vitro* binding assays using immunopurified and eluted Gsk3β-HA protein added to various Fbxo7 proteins lacking N- and C-terminal domains immobilized on anti-FLAG antibodies on agarose. (**D**) *In vitro* ubiquitination assay using an $SCF^{Fbxo7(129–522)}$ ligase lacking the N-terminus against immunopurified and eluted Gsk3β-HA protein as the substrate. (**E**) HEK293T cells were transfected with the indicated FLAG-Fbxo7 plasmids and Tomm20-HA and the lysates were IP with anti-FLAG beads, as in (**A**). (**F**) *In vitro* ubiquitination assay using an $SCF^{Fbxo7(129–522)}$ ligase lacking the N-terminus against immunopurified and eluted Tomm20-HA protein as the substrate. (**G**) *In vivo* co-immunoprecipitation assays conducted as in (**E**).

Biochemical Journal (2016) **473** 3563–3580
DOI: 10.1042/BCJ20160387

compare 89–522 binding with 89–398). Potential reasons for this include that the PRR inhibits Fbxo7 interaction with Tomm20 or the smaller 89–398 construct can localize to the mitochondria. Combined, these data indicate that sequences between 89 and 398 of Fbxo7 can bind to Tomm20 in cells. These sequences include the F-box domain (335–372), and we also noted a diminished interaction of Tomm20 with an Fbxo7 construct lacking the F-box domain similar to Gsk3β (Figure 4A,E). However, this was likely to be due to a change in the localization of Fbxo7 as a result of a deletion of an NES embedded within the first helix of the F-box domain [22]. We previously demonstrated that the NES of Fbxo7 is important for its cell cycle-dependent cytoplasmic/nuclear shuttling, and if mutated, Fbxo7 becomes a predominantly nuclear protein. To test whether the ΔF-box mutant does not interact with Tomm20 because of its localization to the nucleus, we utilized an Fbxo7 quadruple point mutant, called H1, which mutates the F-box domain such that it does not bind to Skp1 but leaves a functional NES. The H1 mutant localizes similarly to WT, predominantly cytoplasmic with nuclear shuttling [22]. We directly compared the H1 mutant with the ΔF-box mutant for their interaction with Tomm20 using co-immunoprecipitation studies, and found the H1 mutant can bind to Tomm20, whereas the ΔF-box mutant does not (Figure 4G), supporting the nuclear localization of the NES/ΔF-box mutant is the likely cause for the lack of interaction with Tomm20. Both mutants do not bind to Skp1, which also indicates that Fbxo7 can bind to Tomm20 independent of it being part of an E3 ligase.

SCF^{Fbxo7} promotes non-degradative chain formation on Gsk3β and Tomm20

The type of polyubiquitin chain linkages catalyzed by an E3 ligase on a substrate induces different functional consequences [48]. To investigate the types of ubiquitin chains ligated by SCF^{Fbxo7} onto Gsk3β, we carried out UbiCRest analyses by using DUBs as described in ref. [34]. The source of the ubiquitinated protein used in DUB assays was obtained by immunoprecipitating Gsk3β-HA from cells also transfected with Fbxo7 as in Figure 3A, where Fbxo7 expression enhanced a smear of ubiquitination. Ubiquitinated Gsk3β was subjected to cleavage using a panel of DUBs, including as a positive control, USP21, a non-specific DUB which cleaves all types of ubiquitin chains (Figure 5A). Only increasing amounts of the K63-specific OTUD1 concentration diminished the intensity of the smear of polyubiquitinated Gsk3β (Figure 5A, lanes 6 and 7), indicating that Fbxo7 catalyzed predominantly K63-linked ubiquitin chains. To independently test for the presence of Fbxo7-enhanced K63 chains on Gsk3β, HEK293T cells were co-transfected with Gsk3β-HA and Fbxo7 or ΔF-box domain. Immunoprecipitates of Gsk3β-HA were probed for the presence of K63 chains, and these were detected when Fbxo7, but not ΔF-box, was overexpressed (Figure 5B).

To test the effect of SCF^{Fbxo7} ubiquitination on Gsk3β and Tomm20, their total levels were assayed by immunoblotting of HEK293T cell lysates where constitutive knockdown (KD) of Fbxo7 expression was achieved by stable expression of two independent short hairpin miRNA constructs. Consistent with the identification of mainly K63 polyubiquitination by SCF^{Fbxo7} from UbiCRest analyses, reducing Fbxo7 expression did not alter Gsk3β levels (Figure 5C). These results were also confirmed by similar experiments in SHSY-5Y KD cells (data not shown) and in experiments where cells were transiently transfected with dsRNA targeting Fbxo7 in U2OS cells (Supplementary Figure S4B). These findings suggest that ubiquitination may modulate its localization or function. Gsk3β is an upstream regulator of β-catenin, which has roles both in transcription through activation of TCF/LEF-binding sites and in adhesion through its binding to cadherins. We first tested whether Fbxo7 affected transcriptional activation using a TCF/LEF luciferase reporter, which is responsive to β-catenin, in U2OS cells. We found that the overexpression of Fbxo7 increased transactivation from this reporter, and this was dependent on the F-box domain (Figure 5D). We also show that inhibition of Gsk3β upon LiCl treatment strongly activates the TCF/LEF reporter, and no further induction of reporter activity is seen with Fbxo7 expression, arguing for its effect being via Gsk3β inhibition (Supplementary Figure S4C). We also tested whether Gsk3β localization was changed as a result of Fbxo7 expression, but no significant differences were observed by immunofluorescence assays, neither when Fbxo7 was overexpressed nor when its levels were reduced (Supplementary Figure S4D,E). Gsk3β levels were also not significantly altered by Fbxo7 overexpression (Supplementary Figure S4F). To determine if Fbxo7 affected Gsk3β activity, we utilized a GFP reporter with a degron that is sensitive to levels of Gsk3β activity [37]. For comparison, a GFP reporter with alanine substitutions of the Gsk3β phosphoacceptors in the degron was used. The co-expression of Fbxo7, but not the ΔF-box mutant, with the GFP reporter significantly increased the mean fluorescence intensity of the cells compared with vector only expressing cells, indicating a decrease in Gsk3β kinase activity (Figure 5E). Taken together, these data argue for a repressive effect of SCF^{Fbxo7} ubiquitination on Gsk3β activity.

Biochemical Journal (2016) **473** 3563–3580
DOI: 10.1042/BCJ20160387

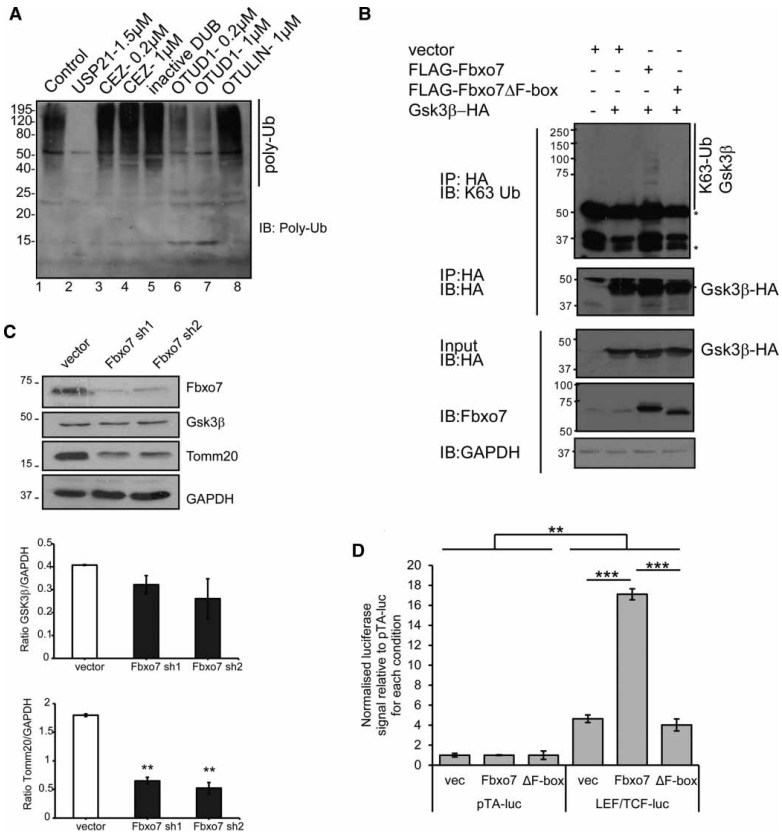

Figure 5. Analysis of ubiquitin chain linkages catalyzed on SCF^{Fbxo7} substrates Gsk3β and Tomm20.
(**A**) UbiCRest analyses using DUBs for polyubiquitinated Gsk3β purified from cells ($n = 2$). The non-specific DUB (USP21) cleaved all ubiquitin chains from polyubiquitinated Gsk3β, and K63-specific DUB, OTUD1, showed concentration-dependent activity against polyubiquitinated protein. (**B**) Immunoprecipitation of Gsk3β from cells and detecting the presence of K63 polyubiquitin chains using a K63-specific antibody ($n = 2$). Asterisk indicates heavy or light chains. (**C**) Effect of reducing Fbxo7 expression on expression of Gsk3β and Tomm20. HEK293T cell lines expressing two independent shRNAs for Fbxo7 (Fbxo7 sh1 and sh2) or vector control were used. Immunoblotting with the indicated antibodies was performed and protein levels were determined relative to GAPDH. The ratio of the densitometry value for each substrate relative to GAPDH is graphed ($n = 3$). (**D**) U2OS cells were co-transfected with an empty luciferase vector (pTA-luc) or a β-catenin-responsive TCF/LEF luciferase reporter, along with a Renilla luciferase reporter as a transfection control. Cells were also co-transfected with an empty vector (vec), Fbxo7 or Fbxo7(ΔF-box). After 48 h, cells were harvested and luciferase expression was assayed in quintuplicate from cell lysates using the Dual Glo kit according to the manufacturer's instructions (Promega), and luciferase levels were normalized to Renilla levels and expressed relative to pTA-luc control levels ($n = 3$). (**E**) U2OS cells were transfected with MAPK-Gsk3β-GFP or MAPK-Gsk3βmut-GFP reporters with empty vector, Fbxo7 or Fbxo7(ΔF-box), and GFP expression was determined by flow cytometry. GFP mean fluorescence intensity (MFI) was expressed as a percentage of MAPK-Gsk3βmut-GFP levels ($n = 6$). (**F**) U2OS cells were co-transfected with Tomm20-HA and the indicated plasmids bearing Fbxo7 WT or PD-associated mutant alleles, and immunoblots on total cell lysates were performed for the transfected proteins as indicated, and GAPDH used as a loading control. ***P-value is <0.001, **P-value is <0.01.

In the case of Tomm20, there was a significant decrease in its endogenous levels when Fbxo7 was knocked down constitutively or by transient transfection of siRNA (Figure 5C and Supplementary Figure S4B), suggesting that Fbxo7 stabilizes Tomm20 levels. Conversely, a small and reproducible 50% increase was observed in

Biochemical Journal (2016) **473** 3563–3580
DOI: 10.1042/BCJ20160387

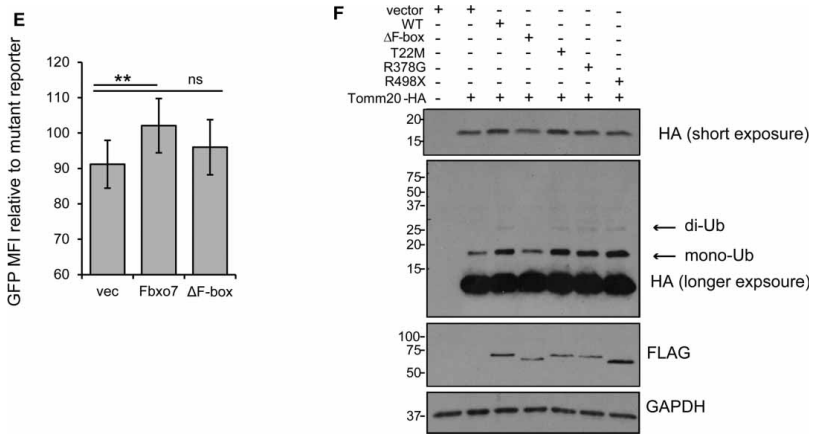

Figure 5. Continued

endogenous Tomm20 levels when Fbxo7 was overexpressed, (Supplementary Figure S4F). These data indicate a direct correlation between endogenous Fbxo7 and Tomm20 expression levels. However, results in Figure 4G argue that stabilization of Tomm20 occurred independently of Fbxo7 being part of an SCF complex. As can be seen in Figure 4G, overexpression of WT Fbxo7 and the H1 mutant both caused increased Tomm20-HA levels (Input, IB: HA, lanes 3 and 5), even though H1 does not recruit Skp1. These data suggest that the stabilization of Tomm20 does not require ubiquitination by SCF^{Fbxo7}.

We also tested whether the mutants in Fbxo7 associated with early-onset PD affected the ubiquitination of Tomm20 by co-transfecting cells with the mutant Fbxo7 alleles (T22M, R378G, and R498X) and Tomm20-HA (Figure 5F). The presence the higher MW mono- and di-ubiquitinated Tomm20 were not altered by co-transfection of mutant alleles of Fbxo7 when compared with WT Fbxo7. Importantly, as the T22M Fbxo7 mutant cannot bind to Parkin, these data strongly argue that the ubiquitination detected was not due to Parkin-mediated ubiquitination, but rather mediated by Fbxo7. These data indicate that mutant Fbxo7 alleles were capable of enhancing Tomm20 ubiquitination, and suggest that defects in Tomm20 ubiquitination do not contribute to the aetiology of the Fbxo7 cases of early-onset PD.

Discussion

In a study of the Cullin interactome using MS and where the abundance of the cullin-associated proteins was calculated based on peptide recovery, Fbxo7 was the fifth most abundant F-box protein identified (behind Skp2, Fbxl18, Fbxo21, and Fbxo22), suggesting that SCF^{Fbxo7} is a stable, abundant E3 ligase in a modified 293 cell line [49]. In agreement with this prediction, we found that the purified SCF^{Fbxo7} ligase from HEK293T cells was indeed abundant, stable and robustly active when used for *in vitro* assays. A total of 338 unique proteins, or about 3.6% of the proteins on the array, were defined as putative substrates of SCF^{Fbxo7} ubiquitination using a cell-independent methodology to obtain a global view of its activity. Approximately 123 (36%) of the Fbxo7 ubiquinome are listed as ubiquitinated proteins in either HEK293T and/or U2OS cells [50,51], with 17% of this subset affected by treatment with a proteasomal inhibitor MG132. In comparison, the number of substrates identified in the present study is about four times those for SCF^{Fbxo25} and SMURF1 where 89 and 75 substrates, respectively, were identified using a similar experimental approach [33,41]. The substrates for SCF^{Fbxo7} do not overlap with these other screens, arguing for the specificity of these ligases in comparable settings. We hypothesize that within specific cell types, SCF^{Fbxo7} activity and the chain linkages assembled will be refined and dictated by the expression levels of Fbxo7, the abundance and potential PTM of its substrates, and the E2 ligases with which it engages.

An enrichment analysis of KEGG pathways revealed that several proteins directly involved in the Wnt signaling pathway, including Csnk1E, Gsk3β, Prickle2, and Nkd2, were ubiquitinated by SCF^{Fbxo7} on the Protoarray®. Gsk3β phosphorylates proteins like β-catenin, Snail, and Smad, which creates a degron for E3 ligases $SCF^{β\text{-}TRCP}$

and SMURF1 that ubiquitinates them to promote their proteasomal degradation [52–55]. The deregulation of this pathway is associated with several types of cancer [56,57]. In addition to its function in the Wnt pathway, Gsk3β phosphorylates a large number of proteins located throughout the cell and is involved in many cellular processes such as cell proliferation, differentiation, microtubule dynamics, cell cycle, and apoptosis [58]. With such pleiotropic function, Gsk3β is linked with many different diseases including diabetes, cancer, Alzheimer's disease, osteoporosis, and cardiac hypertrophy, and also with PD [59]. Investigations into the role of Gsk3β in PD have uncovered many associations including a high level of kinase activity within the striatum and also the finding that a phosphorylated form of Gsk3β is found surrounding Lewy bodies, which may stem from the fact that Gsk3β can directly phosphorylate α-synuclein [60–62]. Gsk3β is also an interesting therapeutic target, and several small-molecule inhibitors have already been described [63]. We find that SCF^{Fbxo7} can ubiquitinate Gsk3β and promote K63 linkages. Fbxo7 did not affect Gsk3β endogenous levels or localization, but instead repressed its activity leading to increased expression of a Gsk3β-sensitive GFP reporter and increased β-catenin transactivation in cells. Our data place Fbxo7 in the complex regulatory landscape of Gsk3β function and activity, and indicate that the consequences of Gsk3β ubiquitination by SCF^{Fbxo7} warrant further investigation in the context of neurodegenerative PD model systems.

Fbxo7 has a reported role in mitophagy through its direct association with two other PD associated proteins, PINK1/*PARK6* and Parkin/*PARK2* [21]. Upon depolarization, Tomm20 is one of the mitochondrial proteins that is ubiquitinated by Parkin [64,65]. Tomm20 is a core component of the mitochondrial translocase complex, and its overexpression alone can promote mitophagy [44]. We demonstrate here that under normal conditions, WT Fbxo7 and the mutant alleles of Fbxo7 stabilized its levels, which did not depend on SCF formation, and promoted Tomm20 mono-, multi-mono-, or di-ubiquitination. The overexpression of human Fbxo7, but not the PD-associated alleles, rescues the phenotypes of *parkin* loss in a *Drosophila* model of neurodegeneration [21]. However, the WT and mutant alleles tested have a similar ability to ubiquitinate Tomm20, indicating that improper ubiquitination of Tomm20 by Fbxo7 is unlikely to be the pathological deficiency. These included a T22M mutant of Fbxo7, which cannot recruit Parkin, indicating Parkin was not catalyzing Tomm20 ubiquitination in these experiments. An enrichment analysis of the substrates by GO Cellular Compartment revealed a further 29 mitochondrial proteins, which may indicate a more general role of Fbxo7 in mitochondrial biology, and suggests that Fbxo7 may affect other activities through ubiquitination of substrates, like ATP5C1, CHCHD2, and MTIF3, mitochondrial translation initiation factor 3 (Supplementary Table S5). We note that the only reported polymorphism within *MTIF3*, rs7669, has been reported to show a significant association with risk of PD [66], and CHCHD2 also has been reported to be associated with cases of autosomal dominant PD [67–69]. These substrates indicate a connected network among the genes mutated in familial PD data and are an area for future study.

In summary, we identified 338 new targets of SCF^{Fbxo7} using a high-throughput, cell-independent proteomic approach and validated Gsk3β and Tomm20 as new substrates, and argue against defective regulation of Tomm20 by Fbxo7 as an underlying mechanism in PD. On the basis of our findings, we predict that Fbxo7 will impact on multiple biological functions, and this potentially explains why this F-box protein is of clinical importance in pathologies affecting many different tissue and cell types. Our dataset opens new perspectives and avenues for investigation in determining the role of SCF^{Fbxo7} ligase activity in the biology of human diseases, including PD and cancer.

Abbreviations

AB, assay buffer; BMP, bone morphogenic protein; BSA, bovine serum albumin; c-IAP1, inhibitor of apoptosis protein 1; DDA, data-dependent acquisition; DTT, dithiothreitol; DUBs, deubiquitinating enzymes; E1, ubiquitin-activating enzyme; E2, ubiquitin-carrier enzyme; FC, fold change; Gsk3β, glycogen synthase kinase 3β; HA, human influenza hemagglutinin; HRP, horseradish peroxidase; HURP, hepatoma up-regulated protein; IVT, *in vitro* transcription/translation; LB, lysis buffer; LEF/TCF, lymphoid enhancer factor/T-cell factor; LQT, linear trap quadrupole; MTS, mitochondrial-targeting sequence; MW, molecular weight; NB, NETN lysis buffer; NES, nuclear export signal; NRAGE, neurotrophin receptor-interacting MAGE; PD, Parkinson's disease; PTMs, post-translational modifications; SCF, Skp1-Cul1-F box protein; SNP, single nucleotide polymorphism; Tomm20, translocase of outer mitochondrial membrane 20; TRAF2, TNF receptor-associated factor 2; UbiCRest, ubiquitin chain restriction; WT, wild type.

Biochemical Journal (2016) **473** 3563–3580
DOI: 10.1042/BCJ20160387

Author Contribution

F.R.T., S.J.R., S.P.P., T.E.T.M., G.Z., and T.K. conducted experiments and analyzed data. D.K. and H.L. designed experiments, analyzed data and wrote the manuscript. All authors read and edited the manuscript.

Funding

F.R.T. was funded by a BEPE-FAPESP Fellowship [2010/16464-8, 2012/09241-8]. S.J.R. and H.L. are funded by the Biotechnology and Biological Science Research Council [BB/J007846/1]. D.K. is funded by the European Research Council [309756], Medical Research Council [U105192732] and the Lister Institute for Preventive Medicine. T.E.T.M. was funded by the Marie Curie ITN 'UPStream'.

Acknowledgements

We thank Dr Marcelo D. Gomes from the Department of Biochemistry and Immunology, Faculty of Medicine of Ribeirão Preto, University of São Paulo, Ribeirão Preto, Brazil for enabling the research exchange of FRT to the University of Cambridge. We also thank Dr Yasuko Matsuzawa, Sanford-Burnhan Medical Research Institute, La Jolla, CA, USA for kindly providing the human cIAP-1 plasmid. We thank Robin Antrobus and Yagnesh Umrania for expert technical help with LC/MS-MS.

Competing Interests

The Authors declare that there are no competing interests associated with the manuscript.

References

1 Cenciarelli, C., Chiaur, D.S., Guardavaccaro, D., Parks, W., Vidal, M. and Pagano, M. (1999) Identification of a family of human F-box proteins. *Curr. Biol.* **9**, 1177–1179 doi:10.1016/S0960-9822(00)80020-2
2 Winston, J.T., Koepp, D.M., Zhu, C., Elledge, S.J. and Harper, J.W. (1999) A family of mammalian F-box proteins. *Curr. Biol.* **9**, 1180–1182 doi:10.1016/S0960-9822(00)80021-4
3 Skowyra, D., Craig, K.L., Tyers, M., Elledge, S.J. and Harper, J.W. (1997) F-box proteins are receptors that recruit phosphorylated substrates to the SCF ubiquitin-ligase complex. *Cell* **91**, 209–219 doi:10.1016/S0092-8674(00)80403-1
4 Skaar, J.R., Pagan, J.K. and Pagano, M. (2013) Mechanisms and function of substrate recruitment by F-box proteins. *Nat. Rev. Mol. Cell. Biol.* **14**, 369–381 doi:10.1038/nrm3582
5 Lee, E.K. and Diehl, J.A. (2014) SCFs in the new millennium. *Oncogene* **33**, 2011–2018 doi:10.1038/onc.2013.144
6 Hermand, D. (2006) F-box proteins: more than baits for the SCF? *Cell Div.* **1**, 30 doi:10.1186/1747-1028-1-30
7 Wang, Z., Liu, P., Inuzuka, H. and Wei, W. (2014) Roles of F-box proteins in cancer. *Nat. Rev. Cancer.* **14**, 233–247 doi:10.1038/nrc3700
8 Ho, M.S., Ou, C., Chan, Y.-r., Chien, C.-T. and Pi, H. (2008) The utility F-box for protein destruction. *Cell. Mol. Life Sci.* **65**, 1977–2000 doi:10.1007/s00018-008-7592-6
9 Nelson, D.E., Randle, S.J. and Laman, H. (2013) Beyond ubiquitination: the atypical functions of Fbxo7 and other F-box proteins. *Open. Biol.* **3**, 130131 doi:10.1098/rsob.130131
10 Laman, H., Funes, J.M., Ye, H., Henderson, S., Galinanes-Garcia, L., Hara, E. et al. (2005) Transforming activity of Fbxo7 is mediated specifically through regulation of cyclin D/cdk6. *EMBO J.* **24**, 3104–3116 doi:10.1038/sj.emboj.7600775
11 Meziane, E.K., Randle, S.J., Nelson, D.E., Lomonosov, M. and Laman, H. (2011) Knockdown of Fbxo7 reveals its regulatory role in proliferation and differentiation of haematopoietic precursor cells. *J. Cell. Sci.* **124**(Pt 13), 2175–2186 doi:10.1242/jcs.080465
12 Lomonosov, M., Meziane, E.K., Ye, H., Nelson, D.E., Randle, S.J. and Laman, H. (2011) Expression of Fbxo7 in haematopoietic progenitor cells cooperates with p53 loss to promote lymphomagenesis. *PLoS ONE* **6**, e21165 doi:10.1371/journal.pone.0021165
13 Ganesh, S.K., Zakai, N.A., van Rooij, F.J.A, Soranzo, N., Smith, A.V., Nalls, M.A. et al. (2009) Multiple loci influence erythrocyte phenotypes in the CHARGE Consortium. *Nat. Genet.* **41**, 1191–1198 doi:10.1038/ng.466
14 Soranzo, N., Spector, T.D., Mangino, M., Kühnel, B., Rendon, A., Teumer, A. et al. (2009) A genome-wide meta-analysis identifies 22 loci associated with eight hematological parameters in the HaemGen consortium. *Nat. Genet.* **41**, 1182–1190 doi:10.1038/ng.467
15 Ding, K., Shameer, K., Jouni, H., Masys, D.R., Jarvik, G.P., Kho, A.N. et al. (2012) Genetic loci implicated in erythroid differentiation and cell cycle regulation are associated with red blood cell traits. *Mayo Clin. Proc.* **87**, 461–474 doi:10.1016/j.mayocp.2012.01.016
16 van der Harst, P., Zhang, W., Mateo Leach I., Rendon, A., Verweij, N., Sehmi, J. et al. (2012) Seventy-five genetic loci influencing the human red blood cell. *Nature* **492**, 369–375 doi:10.1038/nature11677
17 Di Fonzo, A., Dekker, M.C.J, Montagna, P., Baruzzi, A., Yonova, E.H., Correia Guedes, L. et al. (2009) FBXO7 mutations cause autosomal recessive, early-onset parkinsonian-pyramidal syndrome. *Neurology* **72**, 240–245 doi:10.1212/01.wnl.0000338144.10967.2b
18 Lohmann, E., Coquel, A.-S., Honoré, A., Gurvit, H., Hanagasi, H., Emre, M. et al. (2015) A new F-box protein 7 gene mutation causing typical Parkinson's disease. *Mov. Disord.* **30**, 1130–1133 doi:10.1002/mds.26266
19 Paisán-Ruiz, C., Guevara, R., Federoff, M., Hanagasi, H., Sina, F., Elahi, E. et al. (2010) Early-onset L-DOPA-responsive Parkinsonism with pyramidal signs due to ATP13A2, PLA2G6, FBXO7 and spatacsin mutations. *Mov. Disord.* **25**, 1791–1800 doi:10.1002/mds.23221
20 Shojaee, S., Sina, F., Banihosseini, S.S., Kazemi, M.H., Kalhor, R., Shahidi, G.-A. et al. (2008) Genome-wide linkage analysis of a Parkinsonian-pyramidal syndrome pedigree by 500 K SNP arrays. *Am. J. Hum. Genet.* **82**, 1375–1384 doi:10.1016/j.ajhg.2008.05.005
21 Burchell, V.S., Nelson, D.E., Sanchez-Martinez, A., Delgado-Camprubi, M., Ivatt, R.M., Pogson, J.H. et al. (2013) The Parkinson's disease-linked proteins Fbxo7 and Parkin interact to mediate mitophagy. *Nat. Neurosci.* **16**, 1257–1265 doi:10.1038/nn.3489

22 Nelson, D.E. and Laman, H. (2011) A competitive binding mechanism between Skp1 and exportin 1 (CRM1) controls the localization of a subset of F-box proteins. *J. Biol. Chem.* **286**, 19804–19815 doi:10.1074/jbc.M111.220079
23 Hsu, J.-M., Lee, Y.-C., Yu, C.-T.R. and Huang, C.-Y.F. (2004) Fbx7 functions in the SCF complex regulating Cdk1-cyclin B-phosphorylated hepatoma up-regulated protein (HURP) proteolysis by a proline-rich region. *J. Biol. Chem.* **279**, 32592–32602 doi:10.1074/jbc.M404950200
24 Tsou, A.-P., Yang, C.-W., Huang, C.-Y.F, Yu, R.C.-T, Lee, Y.-C.G, Chang, C.-W. et al. (2003) Identification of a novel cell cycle regulated gene, HURP, overexpressed in human hepatocellular carcinoma. *Oncogene* **22**, 298–307 doi:10.1038/sj.onc.1206129
25 Chang, Y.-F., Cheng, C.-M., Chang, L.-K., Jong, Y.-J. and Yuo, C.-Y. (2006) The F-box protein Fbxo7 interacts with human inhibitor of apoptosis protein cIAP1 and promotes cIAP1 ubiquitination. *Biochem. Biophys. Res. Commun.* **342**, 1022–1026 doi:10.1016/j.bbrc.2006.02.061
26 Kuiken, H.J., Egan, D.A., Laman, H., Bernards, R., Beijersbergen, R.L. and Dirac, A.M. (2012) Identification of F-box only protein 7 as a negative regulator of NF-kappaB signalling. *J. Cell. Mol. Med.* **16**, 2140–2149 doi:10.1111/j.1582-4934.2012.01524.x
27 Kang, J. and Chung, K.C. (2015) The F-box protein FBXO7 positively regulates bone morphogenetic protein-mediated signaling through Lys-63-specific ubiquitination of neurotrophin receptor-interacting MAGE (NRAGE). *Cell. Mol. Life Sci.* **72**, 181–195 doi:10.1007/s00018-014-1665-5
28 Baiguera, C., Alghisi, M., Pinna, A., Bellucci, A., De Luca, M.A., Frau, L. et al. (2012) Late-onset Parkinsonism in NFκB/c-Rel-deficient mice. *Brain* **135** (Pt 9), 2750–2765 doi:10.1093/brain/aws193
29 Mincheva-Tasheva, S. and Soler, R.M. (2013) NF-κB signaling pathways: role in nervous system physiology and pathology. *Neuroscientist* **19**, 175–194 doi:10.1177/1073858412444007
30 Lu, J.Y., Lin, Y.Y., Qian, J., Tao, S.C., Zhu, J., Pickart, C. et al. (2008) Functional dissection of a HECT ubiquitin E3 ligase. *Mol. Cell Proteomics* **7**, 35–45 doi:10.1186/s12864-015-2239-0
31 Persaud, A., Alberts, P., Amsen, E.M., Xiong, X., Wasmuth, J., Saadon, Z. et al. (2009) Comparison of substrate specificity of the ubiquitin ligases Nedd4 and Nedd4-2 using proteome arrays. *Mol. Syst. Biol.* **5**, 333 doi:10.1038/msb.2009.85
32 Teixeira, F.R., Manfiolli, A.O., Soares, C.S., Baqui, M.M.A, Koide, T. and Gomes, M.D. (2013) The F-box protein FBXO25 promotes the proteasome-dependent degradation of ELK-1 protein. *J. Biol. Chem.* **288**, 28152–28162 doi:10.1074/jbc.M113.504308
33 Andrews, P.S., Schneider, S., Yang, E., Michaels, M., Chen, H., Tang, J. et al. (2010) Identification of substrates of SMURF1 ubiquitin ligase activity utilizing protein microarrays. *Assay Drug Dev. Technol.* **8**, 471–487 doi:10.1089/adt.2009.0264
34 Hospenthal, M.K., Mevissen, T.E. and Komander, D. (2015) Deubiquitinase-based analysis of ubiquitin chain architecture using ubiquitin chain restriction (UbiCRest). *Nat. Protoc.* **10**, 349–361 doi:10.1038/nprot.2015.018
35 Silverman, B.W. (1986) *Density Estimation for Statistics and Data Analysis*, Chapman & Hall, New York
36 Huang, D.W., Sherman, B.T. and Lempicki, R.A. (2009) Systematic and integrative analysis of large gene lists using DAVID bioinformatics resources. *Nat. Protoc.* **4**, 44–57 doi:10.1038/nprot.2008.211
37 Taelman, V.F., Dobrowolski, R., Plouhinec, J.-L., Fuentealba, L.C., Vorwald, P.P., Gumper, I. et al. (2010) Wnt signaling requires sequestration of glycogen synthase kinase 3 inside multivesicular endosomes. *Cell* **143**, 1136–1148 doi:10.1016/j.cell.2010.11.034
38 Kirk, R., Laman, H., Knowles, P.P., Murray-Rust, J., Lomonosov, M., Meziane, E.K. et al. (2008) Structure of a conserved dimerization domain within the F-box protein Fbxo7 and the PI31 proteasome inhibitor. *J. Biol. Chem.* **283**, 22325–22335 doi:10.1074/jbc.M709900200
39 Bindea, G., Mlecnik, B., Hackl, H., Charoentong, P., Tosolini, M., Kirilovsky, A. et al. (2009) ClueGO: a cytoscape plug-in to decipher functionally grouped gene ontology and pathway annotation networks. *Bioinformatics* **25**, 1091–1093 doi:10.1093/bioinformatics/btp101
40 Bindea, G., Galon, J. and Mlecnik, B. (2013) Cluepedia Cytoscape plugin: pathway insights using integrated experimental and in silico data. *Bioinformatics* **29**, 661–663 doi:10.1093/bioinformatics/btt019
41 Teixeira, F.R., Yokoo, S., Gartner, C.A., Manfiolli, A.O., Baqui, M.M., Assmann, E.M. et al. (2010) Identification of FBXO25-interacting proteins using an integrated proteomics approach. *Proteomics* **10**, 2746–2757 doi:10.1002/pmic.200900419
42 Golpich, M., Amini, E., Hemmati, F., Ibrahim, N.M., Rahmani, B., Mohamed, Z. et al. (2015) Glycogen synthase kinase-3 beta (GSK-3β) signaling: implications for Parkinson's disease. *Pharmacol. Res.* **97**, 16–26 doi:10.1016/j.phrs.2015.03.010
43 Li, D.W., Liu, Z.Q., Chen, W., Yao, M. and Li, G.R. (2014) Association of glycogen synthase kinase-3β with Parkinson's disease (review). *Mol. Med. Rep.* **9**, 2043–2050 doi:10.3892/mmr.2014.2080
44 Bingol, B., Tea, J.S., Phu, L., Reichelt, M., Bakalarski, C.E., Song, Q. et al. (2014) The mitochondrial deubiquitinase USP30 opposes parkin-mediated mitophagy. *Nature* **510**, 370–375 doi:10.1038/nature13418
45 Cunningham, C.N., Baughman, J.M., Phu, L., Tea, J.S., Yu, C., Coons, M. et al. (2015) USP30 and parkin homeostatically regulate atypical ubiquitin chains on mitochondria. *Nat. Cell. Biol.* **17**, 160–169 doi:10.1038/ncb3097
46 Zhou, Z.D., Sathiyamoorthy, S., Angeles, D.C. and Tan, E.K. (2016) Linking F-box protein 7 and parkin to neuronal degeneration in Parkinson's disease (PD). *Mol. Brain.* **9**, 41 doi:10.1186/s13041-016-0218-2
47 Rugarli, E.I. and Langer, T. (2012) Mitochondrial quality control: a matter of life and death for neurons. *EMBO J.* **31**, 1336–1349 doi:10.1038/emboj.2012.38
48 Komander, D. and Rape, M. (2012) The ubiquitin code. *Annu. Rev. Biochem.* **81**, 203–229 doi:10.1146/annurev-biochem-060310-170328
49 Lee, J.E., Sweredoski, M.J., Graham, R.L., Kolawa, N.J., Smith, G.T., Hess, S. et al. (2011) The steady-state repertoire of human SCF ubiquitin ligase complexes does not require ongoing Nedd8 conjugation. *Mol. Cell Proteomics* **10**, M110 doi:10.1074/mcp.M110.006460
50 Wagner, S.A., Beli, P., Weinert, B.T., Nielsen, M.L., Cox, J., Mann, M. et al. (2011) A proteome-wide, quantitative survey of in vivo ubiquitylation sites reveals widespread regulatory roles. *Mol. Cell Proteomics* **10**, M111 doi:10.1074/mcp.M111.013284
51 Danielsen, J.M.R, Sylvestersen, K.B., Bekker-Jensen, S., Szklarczyk, D., Poulsen, J.W., Horn, H. et al. (2011) Mass spectrometric analysis of lysine ubiquitylation reveals promiscuity at site level. *Mol. Cell Proteomics* **10**, M110 doi:10.1074/mcp.M110.003590
52 Fuentealba, L.C., Eivers, E., Ikeda, A., Hurtado, C., Kuroda, H., Pera, E.M. et al. (2007) Integrating patterning signals: Wnt/GSK3 regulates the duration of the BMP/Smad1 signal. *Cell* **131**, 980–993 doi:10.1016/j.cell.2007.09.027
53 Zhou, B.P. and Hung, M.-C. (2005) Wnt, hedgehog and snail: sister pathways that control by GSK-3β and β-Trcp in the regulation of metastasis. *Cell Cycle* **4**, 772–776 doi:10.4161/cc.4.6.1744
54 Aberle, H., Bauer, A., Stappert, J., Kispert, A. and Kemler, R. (1997) β-catenin is a target for the ubiquitin-proteasome pathway. *EMBO J.* **16**, 3797–3804 doi:10.1093/emboj/16.13.3797

Biochemical Journal (2016) **473** 3563–3580
DOI: 10.1042/BCJ20160387

55 Latres, E., Chiaur, D.S. and Pagano, M. (1999) The human F box protein β-Trcp associates with the Cul1/Skp1 complex and regulates the stability of β-catenin. *Oncogene* **18**, 849–854 doi:10.1038/sj.onc.1202653
56 Lucero, O.M., Dawson, D.W., Moon, R.T. and Chien, A.J. (2010) A re-evaluation of the 'oncogenic' nature of Wnt/β-catenin signaling in melanoma and other cancers. *Curr. Oncol. Rep.* **12**, 314–318 doi:10.1007/s11912-010-0114-3
57 Polakis, P. (2007) The many ways of Wnt in cancer. *Curr. Opin. Genet. Dev.* **17**, 45–51 doi:10.1016/j.gde.2006.12.007
58 Cohen, P. and Frame, S. (2001) The renaissance of GSK3. *Nat. Rev. Mol. Cell Biol.* **2**, 769–776 doi:10.1038/35096075
59 Morales-García, J.A., Susín, C., Alonso-Gil, S., Pérez, D.I., Palomo, V., Pérez, C. et al. (2013) Glycogen synthase kinase-3 inhibitors as potent therapeutic agents for the treatment of Parkinson disease. *ACS Chem. Neurosci.* **4**, 350–360 doi:10.1021/cn300182g
60 Wills, J., Jones, J., Haggerty, T., Duka, V., Joyce, J.N. and Sidhu, A. (2010) Elevated tauopathy and alpha-synuclein pathology in postmortem Parkinson's disease brains with and without dementia. *Exp. Neurol.* **225**, 210–218 doi:10.1016/j.expneurol.2010.06.017
61 Khandelwal, P.J., Dumanis, S.B., Feng, L.R., Maguire-Zeiss, K., Rebeck, G., Lashuel, H.A. et al. (2010) Parkinson-related parkin reduces α-synuclein phosphorylation in a gene transfer model. *Mol. Neurodegener.* **5**, 47 doi:10.1186/1750-1326-5-47
62 Nagao, M. and Hayashi, H. (2009) Glycogen synthase kinase-3β is associated with Parkinson's disease. *Neurosci. Lett.* **449**, 103–107 doi:10.1016/j.neulet.2008.10.104
63 Phukan, S., Babu, V.S., Kannoji, A., Hariharan, R. and Balaji, V.N. (2010) GSK3β: role in therapeutic landscape and development of modulators. *Br. J. Pharmacol.* **160**, 1–19 doi:10.1111/j.1476-5381.2010.00661.x
64 Sarraf, S.A., Raman, M., Guarani-Pereira, V., Sowa, M.E., Huttlin, E.L., Gygi, S.P. et al. (2013) Landscape of the PARKIN-dependent ubiquitylome in response to mitochondrial depolarization. *Nature* **496**, 372–376 doi:10.1038/nature12043
65 Chan, N.C., Salazar, A.M., Pham, A.H., Sweredoski, M.J., Kolawa, N.J., Graham, R.L. et al. (2011) Broad activation of the ubiquitin-proteasome system by Parkin is critical for mitophagy. *Hum. Mol. Genet.* **20**, 1726–1737 doi:10.1093/hmg/ddr048
66 Behrouz, B., Vilariño-Guell, C., Heckman, M.G., Soto-Ortolaza, A.I., Aasly, J.O., Sando, S. et al. (2010) Mitochondrial translation initiation factor 3 polymorphism and Parkinson's disease. *Neurosci. Lett.* **486**, 228–230 doi:10.1016/j.neulet.2010.09.059
67 Funayama, M., Ohe, K., Amo, T., Furuya, N., Yamaguchi, J., Saiki, S. et al. (2015) CHCHD2 mutations in autosomal dominant late-onset Parkinson's disease: a genome-wide linkage and sequencing study. *Lancet Neurol.* **14**, 274–282 doi:10.1016/S1474-4422(14)70266-2
68 Ogaki, K., Koga, S., Heckman, M.G., Fiesel, F.C., Ando, M., Labbé, C. et al. (2015) Mitochondrial targeting sequence variants of the CHCHD2 gene are a risk for Lewy body disorders. *Neurology* **85**, 2016–2025 doi:10.1212/WNL.0000000000002170
69 Shi, C.H., Mao, C.Y., Zhang, S.Y., Yang, J., Song, B., Wu, P. et al. (2016) CHCHD2 gene mutations in familial and sporadic Parkinson's disease. *Neurobiol. Aging* **38**, 217e9–13

